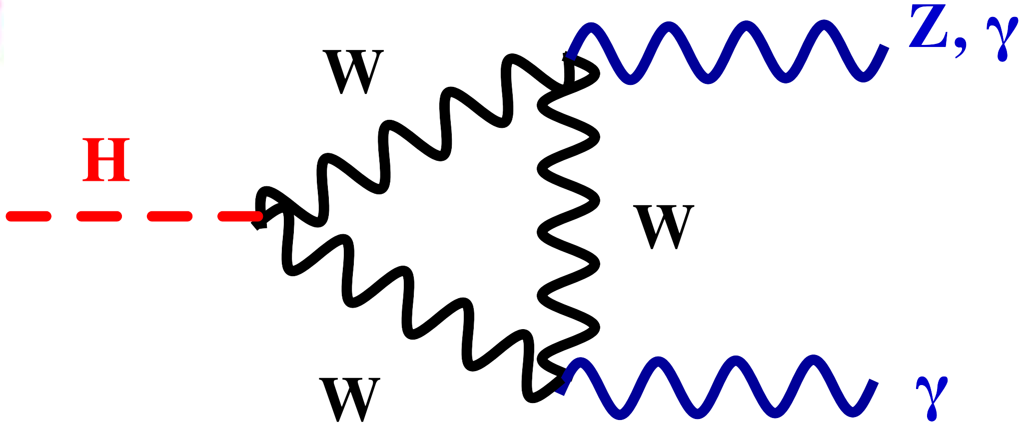

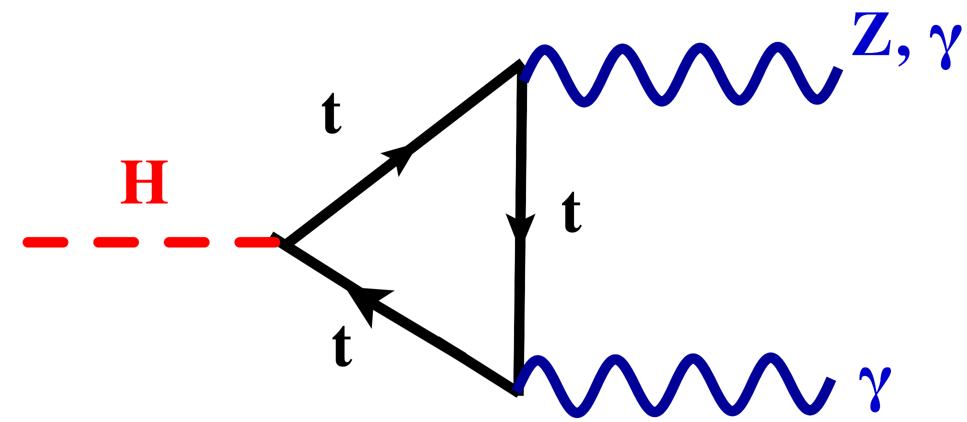

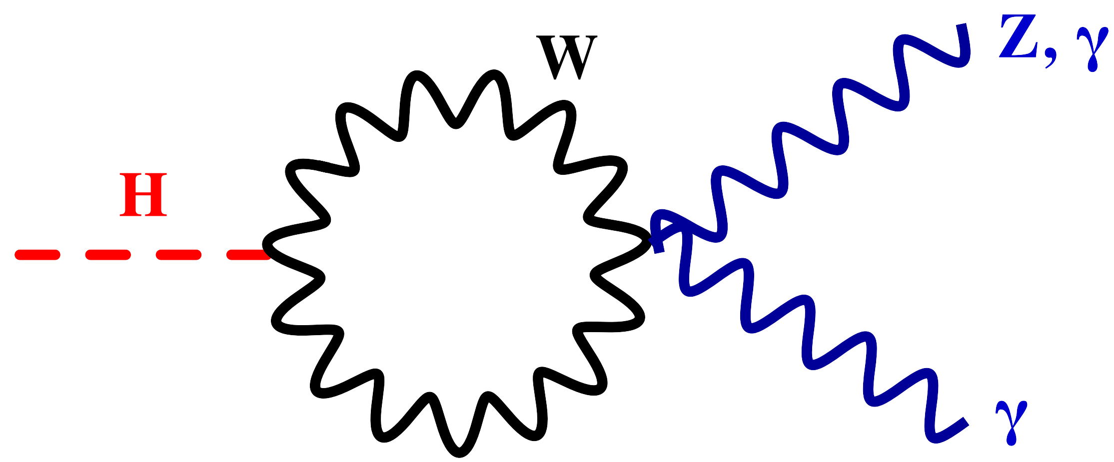

Étude des performances de photons avec les desintégrations radiatives du Z, et recherche du boson de Higgs dans les modes H→$\gamma\gamma$ et H→Zγ auprès du détecteur ATLAS au LHC

Camila Rangel Smith

Soutenance de thèse

27 septembre 2013

LPNHE Paris

université PARIS DIDEROT PARIS

October 2010: Higgs?

- Just 5 months after the first 7 TeV collisions occurred.
- The peak instantaneous luminosity at that year was $2\times 10^{32}\ cm^{-2}s^{-1}$.

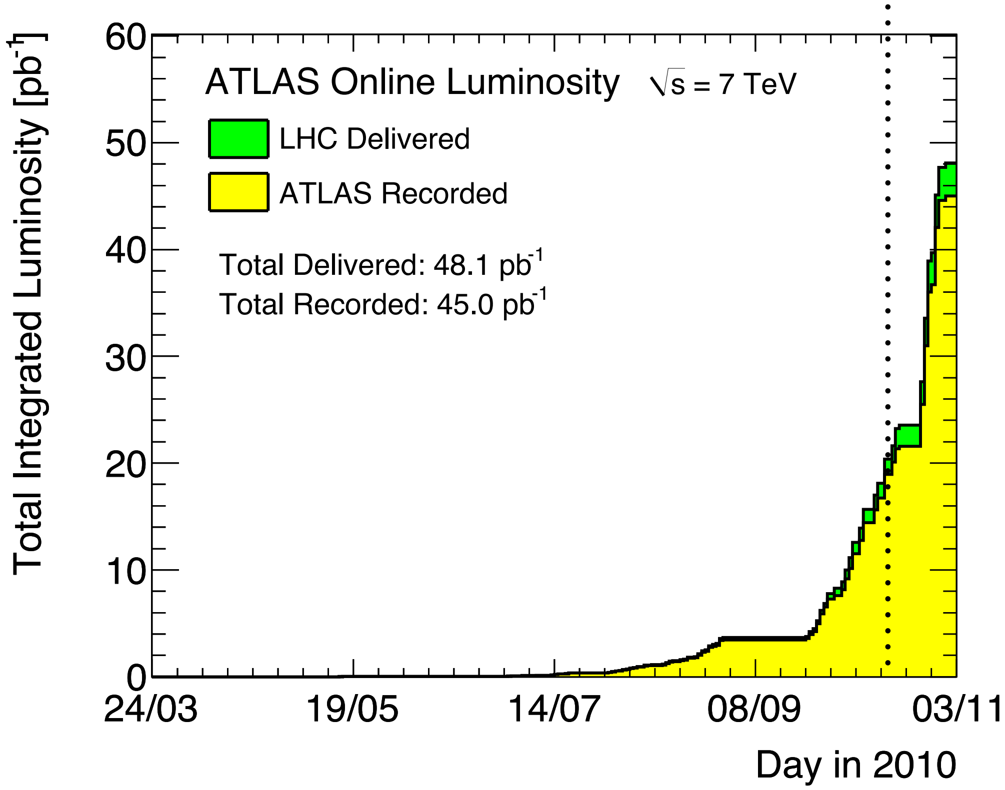

? ? ??

September 2013: Higgs!

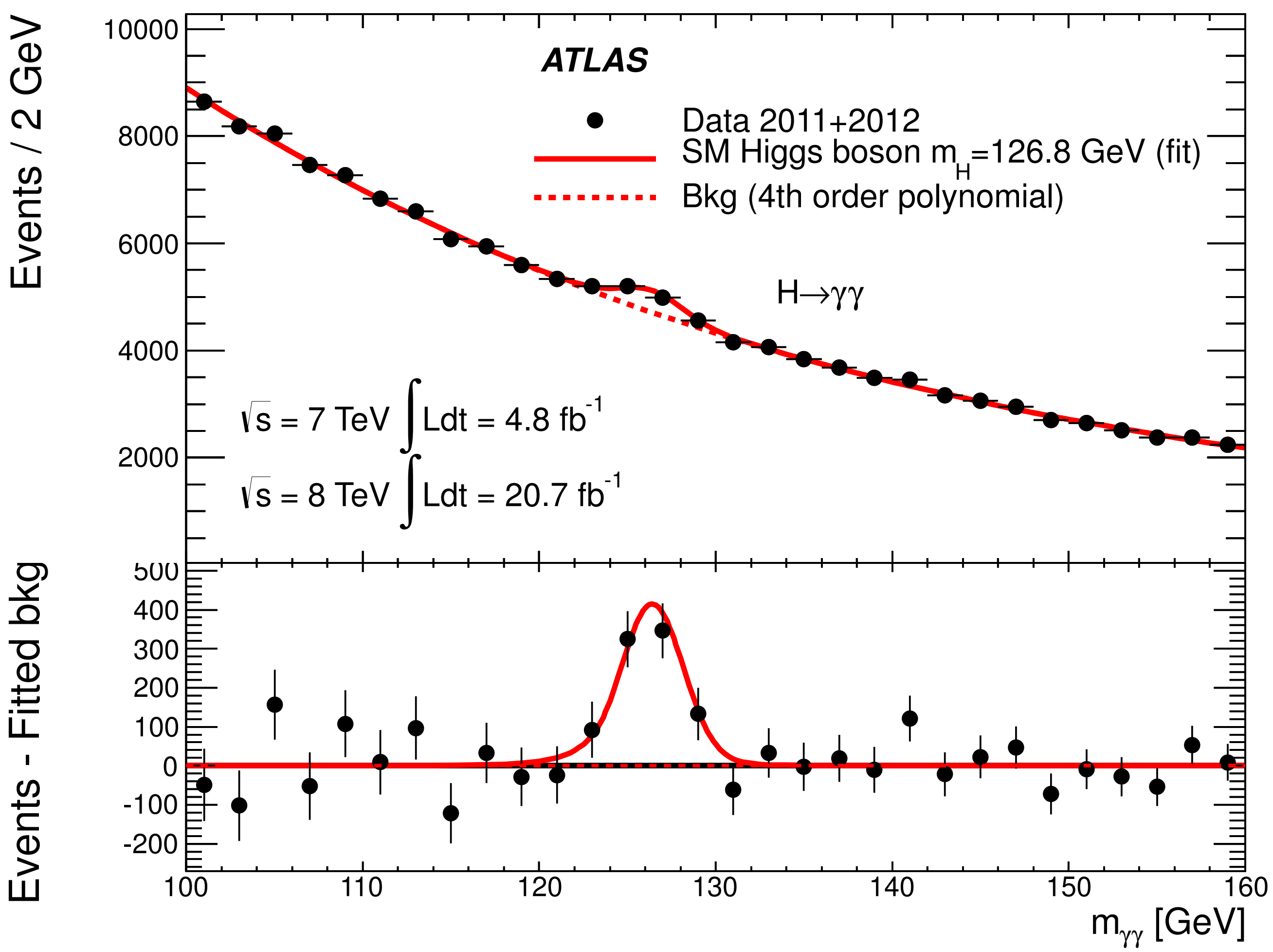

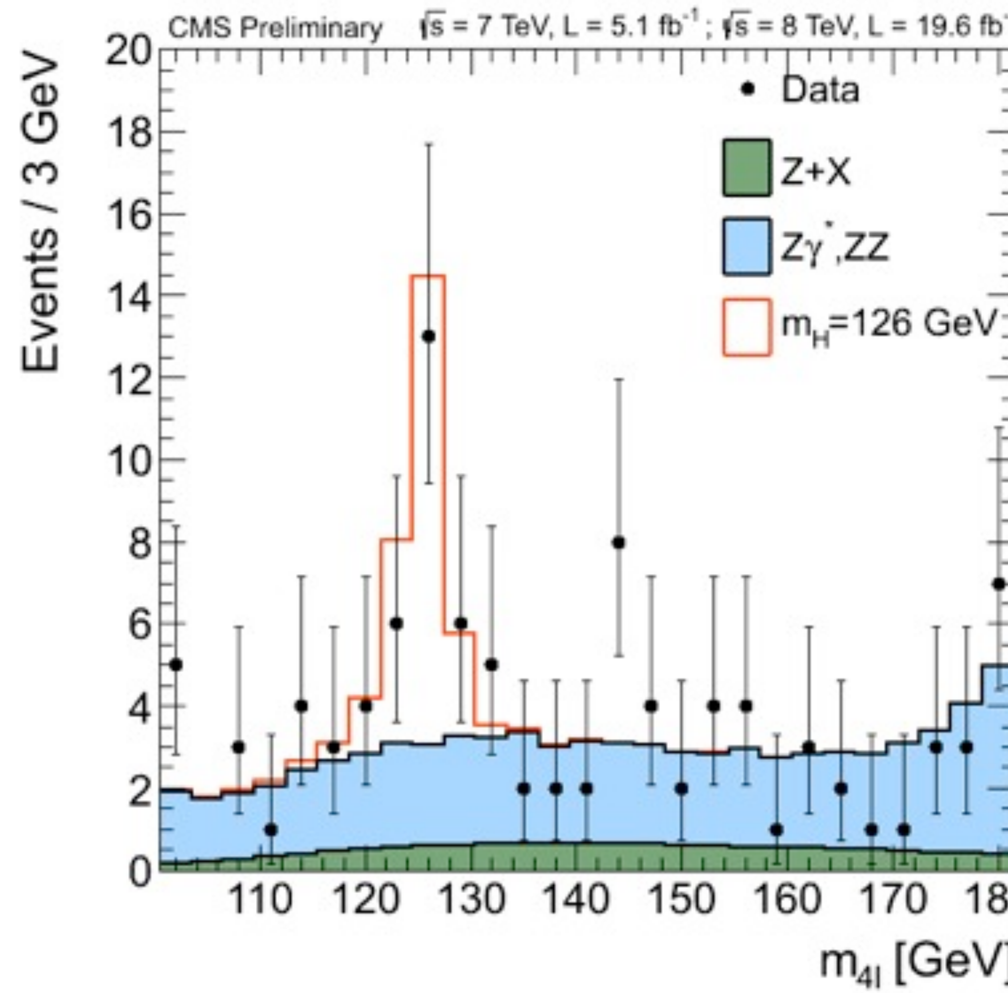

H➡γγ and H➡Zγ channels

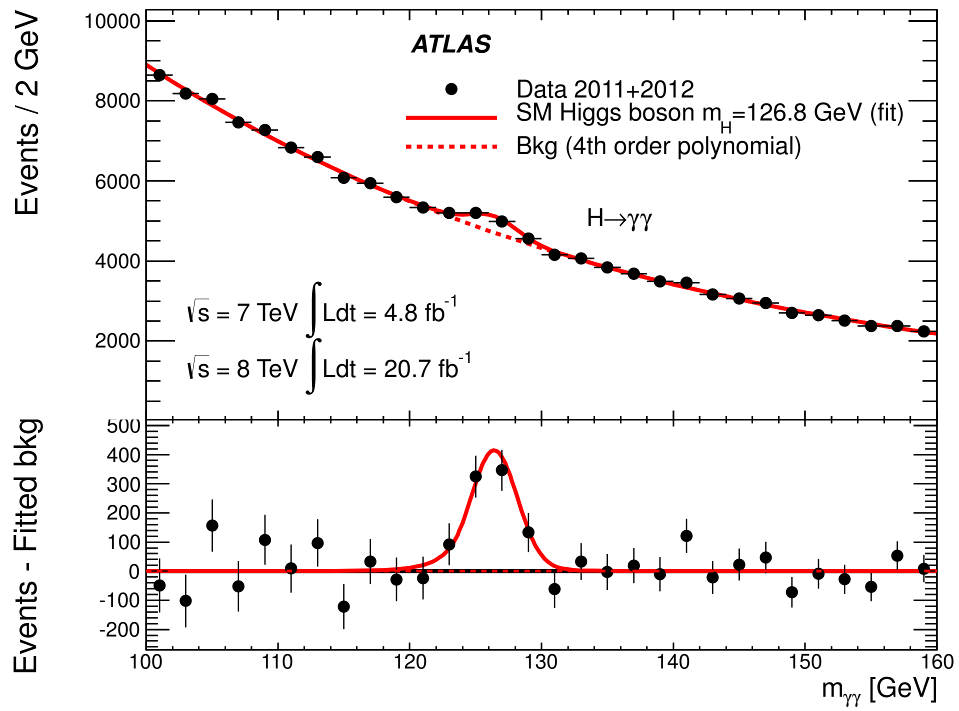

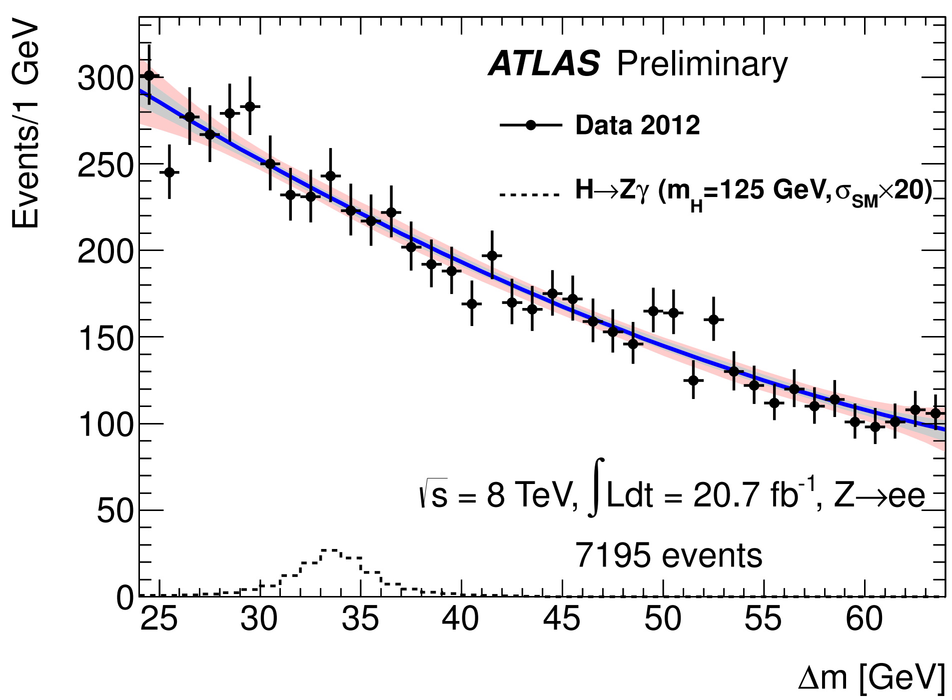

H➔γγ and H➔Zγ channels

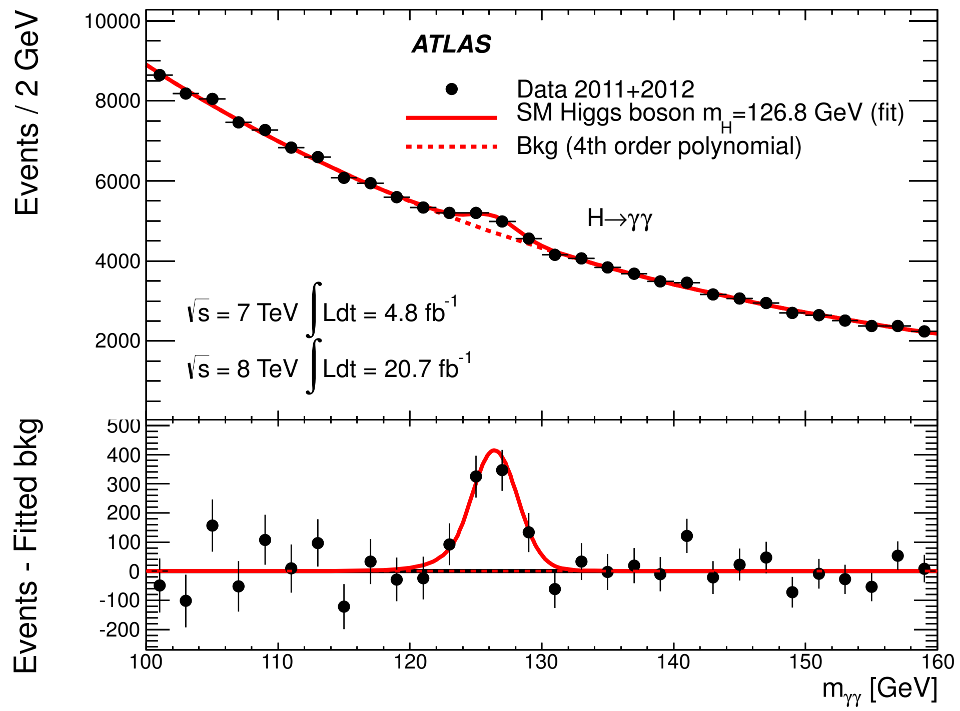

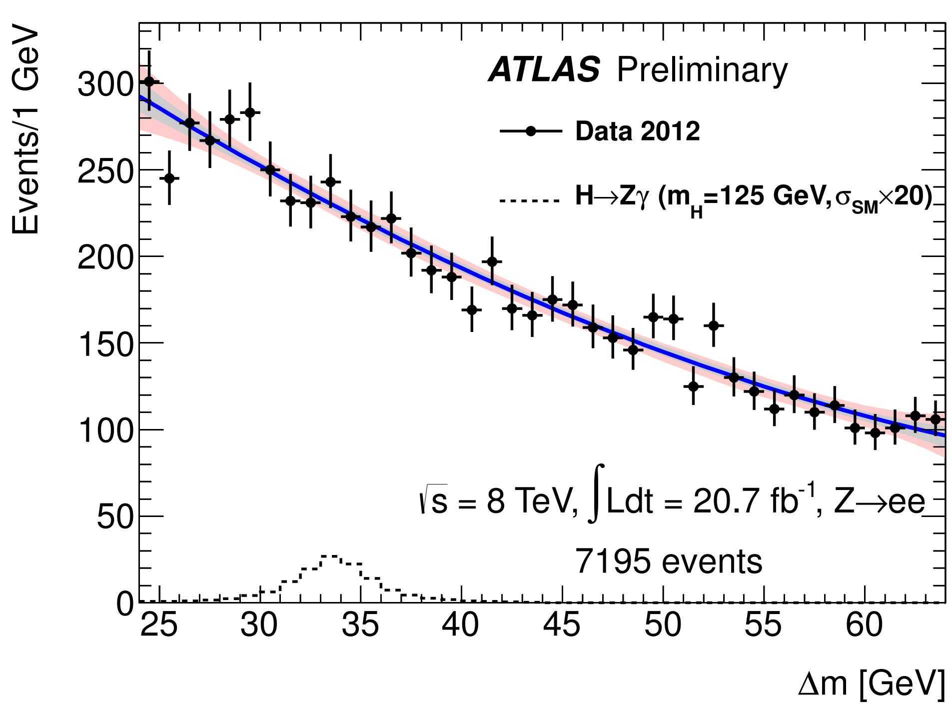

1. The SM and the Higgs boson

H→γγ and H→Zγ channels

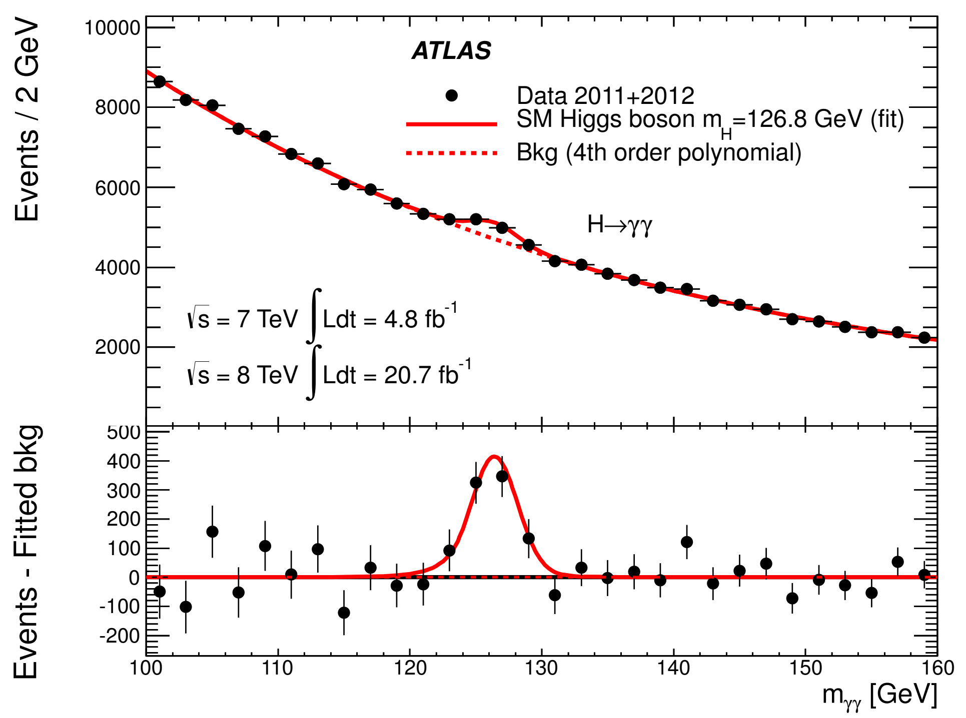

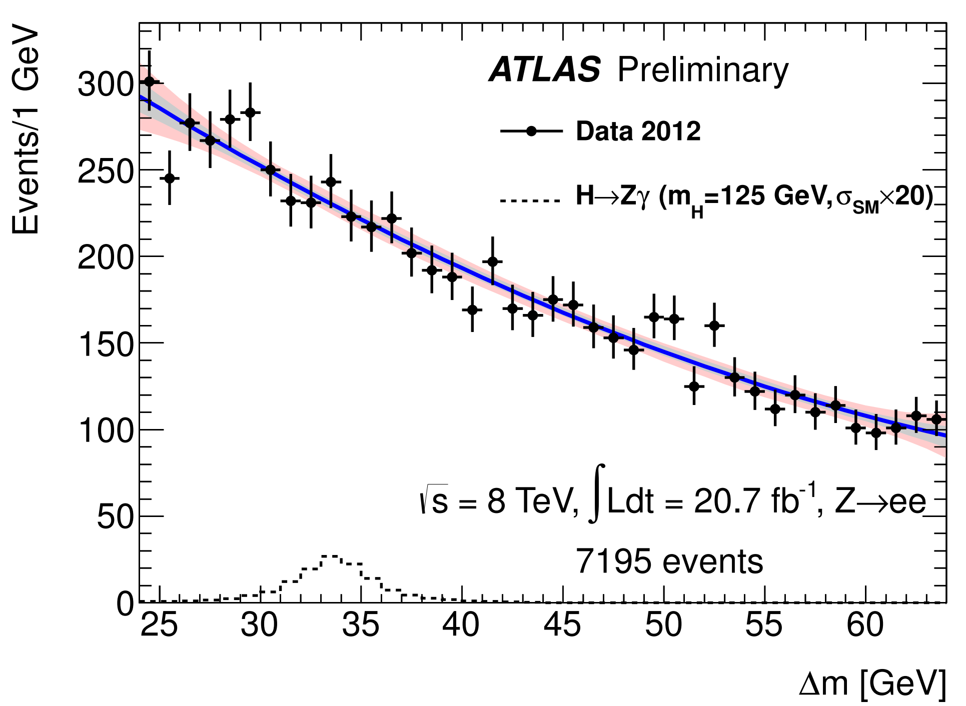

1. The SM and the Higgs boson

2. The LHC and the ATLAS experiment

H➛$\gamma\gamma$ and H➛Zγ channels

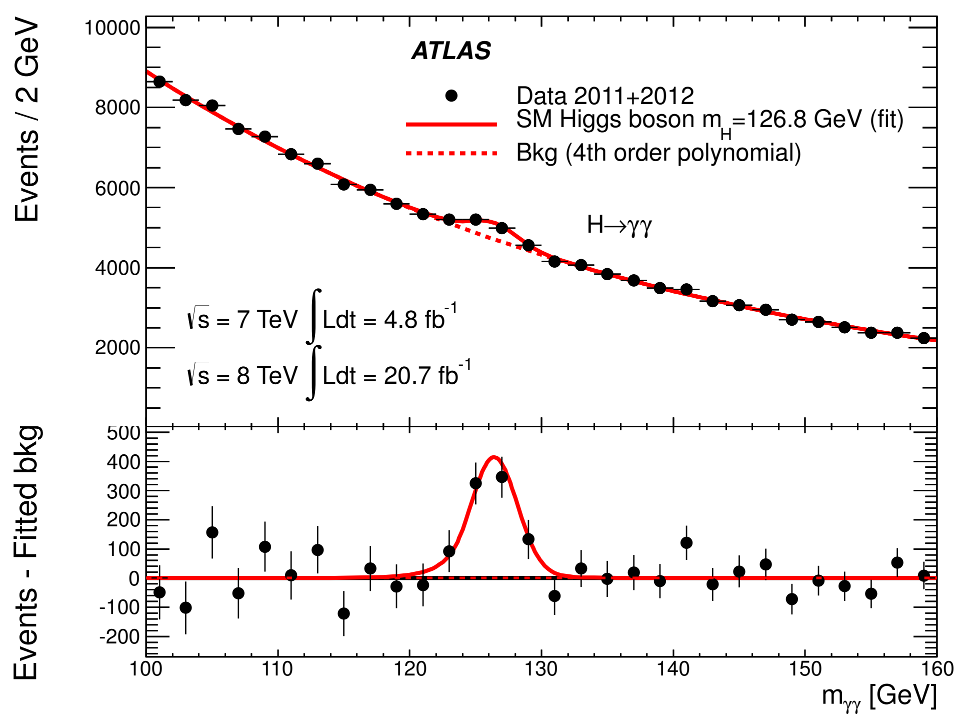

1. The SM and the Higgs boson

2. The LHC and the ATLAS experiment

3. The H➛$\gamma\gamma$ analysis in ATLAS (personal contributions)

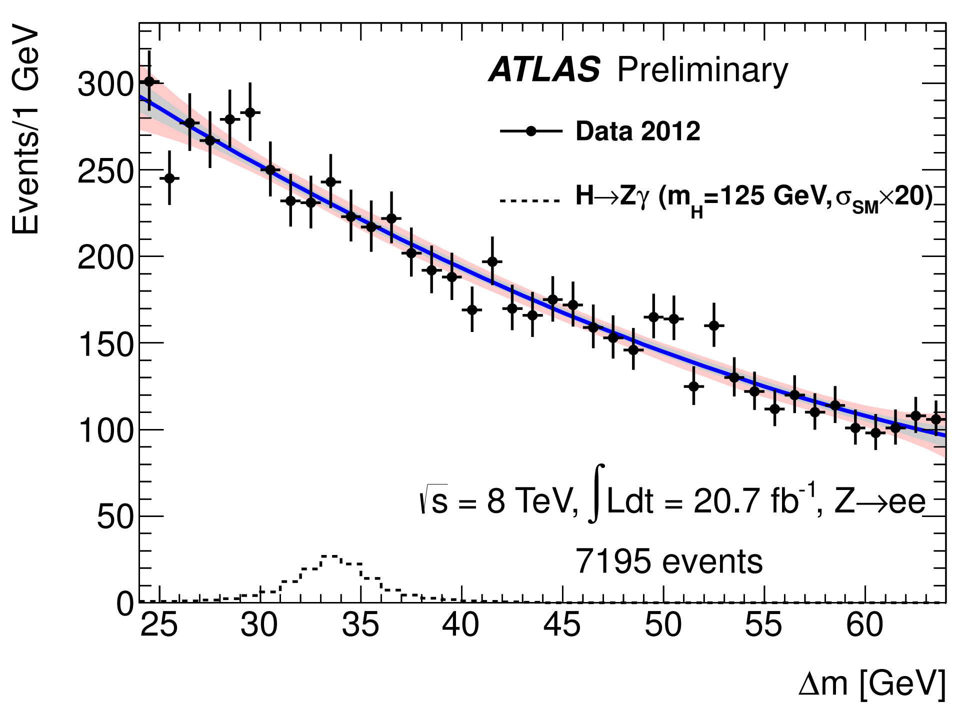

H➙$\gamma\gamma$ and H➙Zγ channels

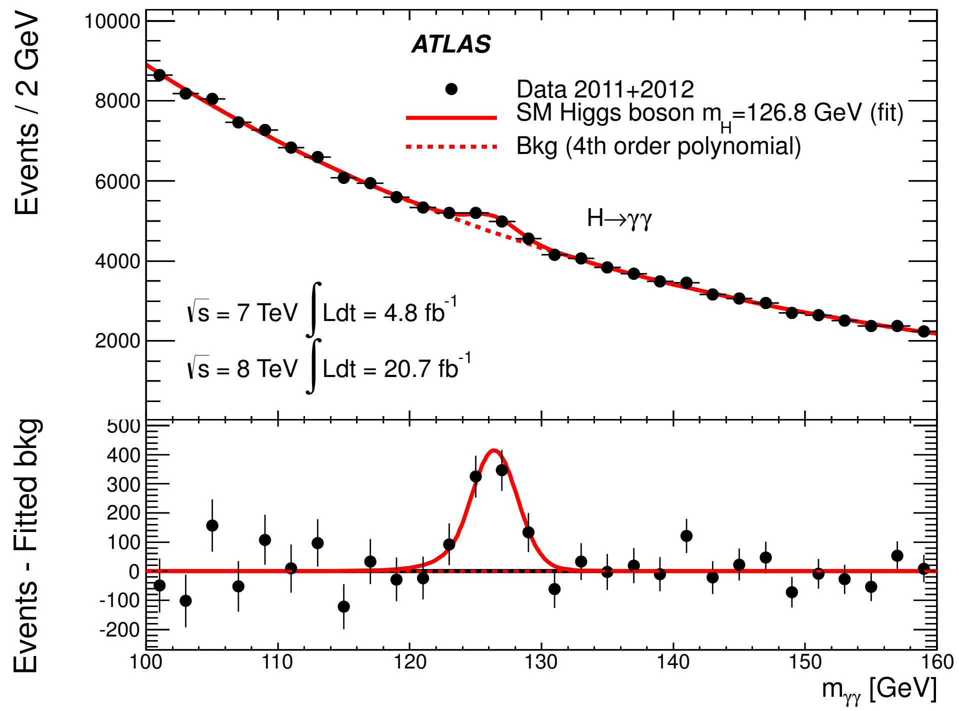

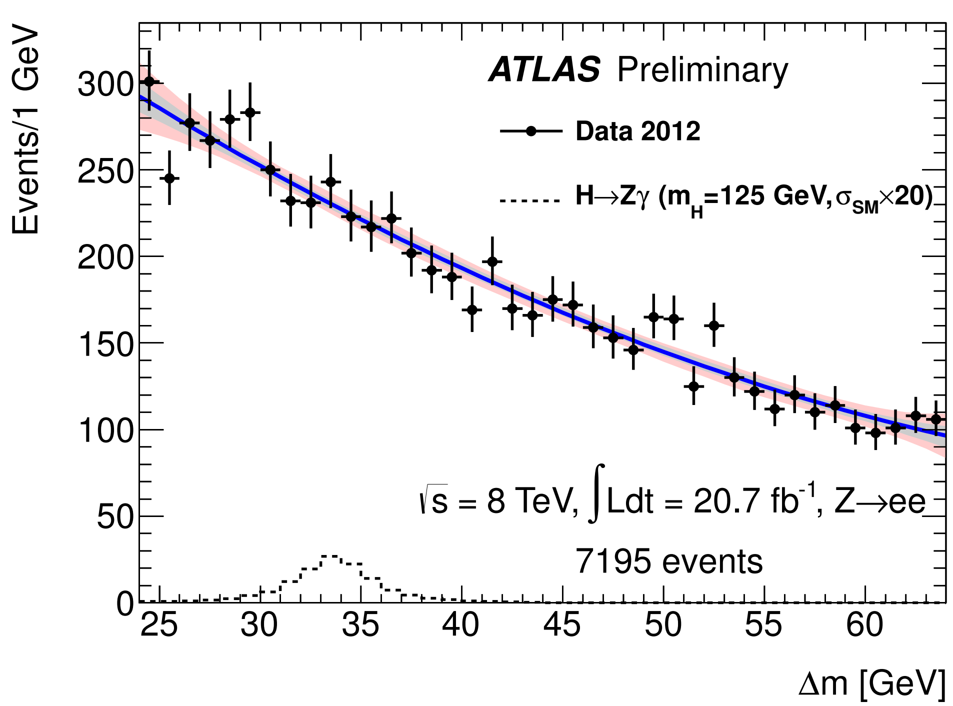

1. The SM and the Higgs boson
2. The LHC and the ATLAS experiment
3. The H➙$\gamma\gamma$ analysis in ATLAS (personal contributions)
4. Measurement of the photon energy scales using Radiative Z decays

H➞$\gamma\gamma$ and H➞Zγ channels

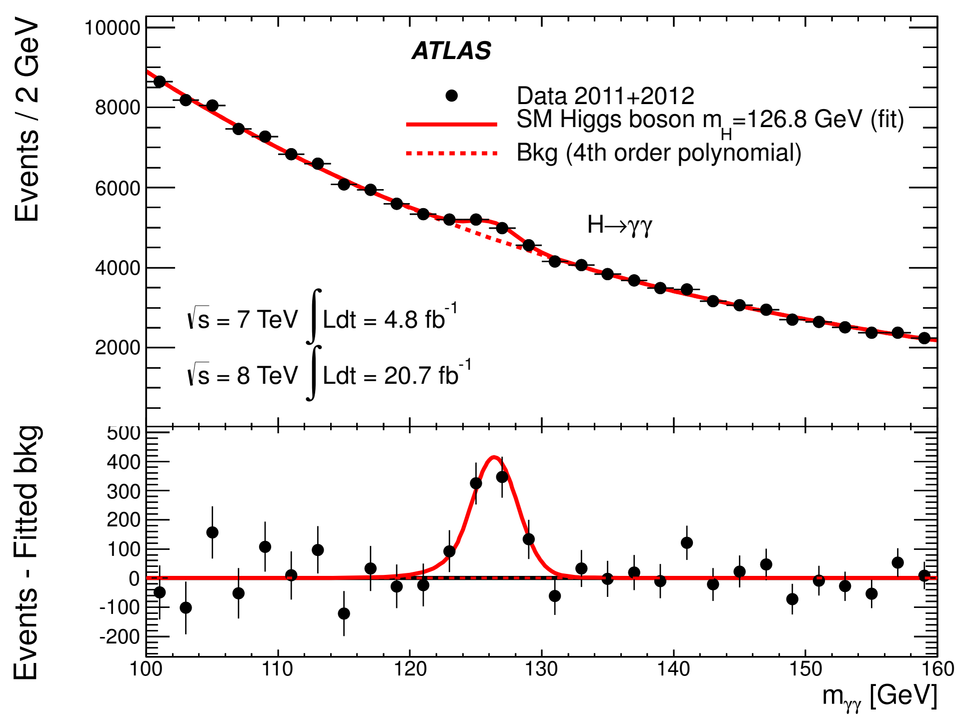

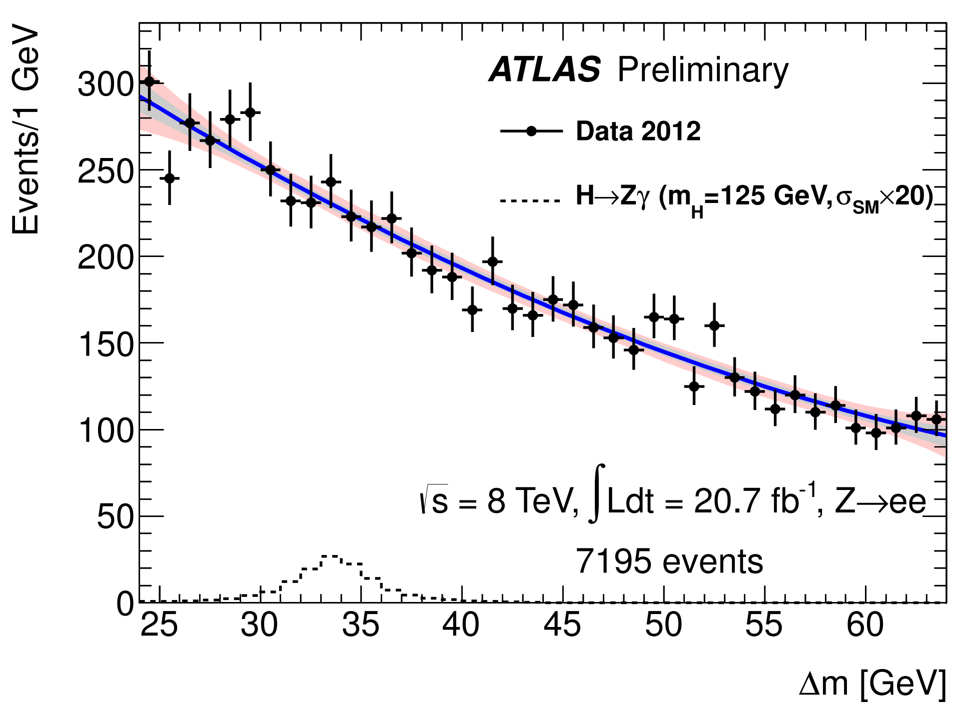

1. The SM and the Higgs boson
2. The LHC and the ATLAS experiment
3. The H➞$\gamma\gamma$ analysis in ATLAS (personal contributions)
4. Measurement of the photon energy scales using Radiative Z decays
5. The search for the Higgs boson in the H➞Zγ channel

H➙γγ and H➙Zγ channels

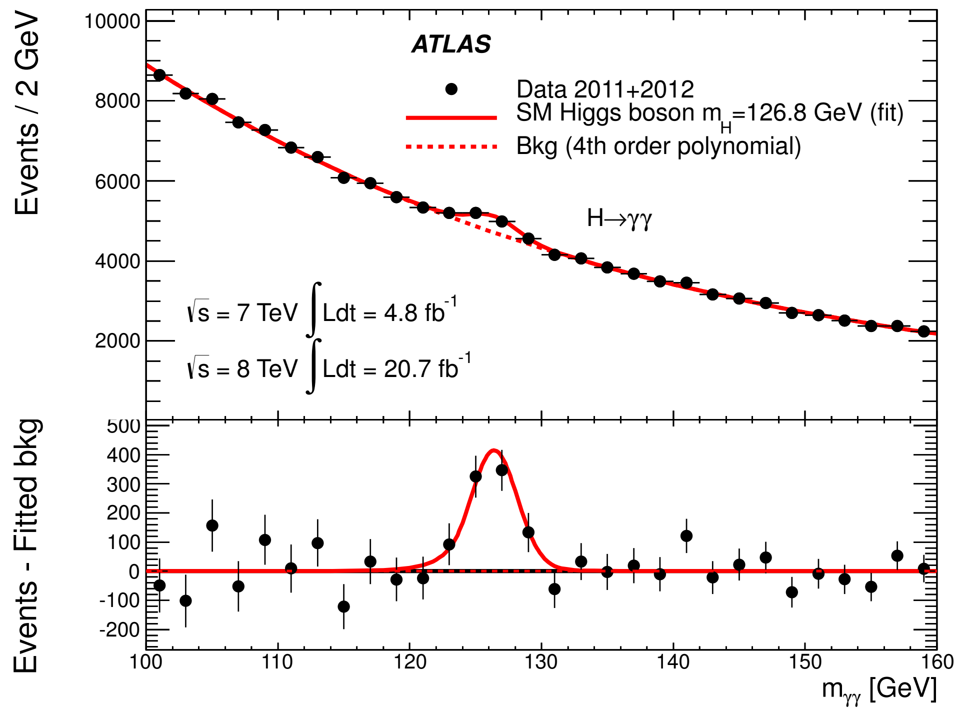

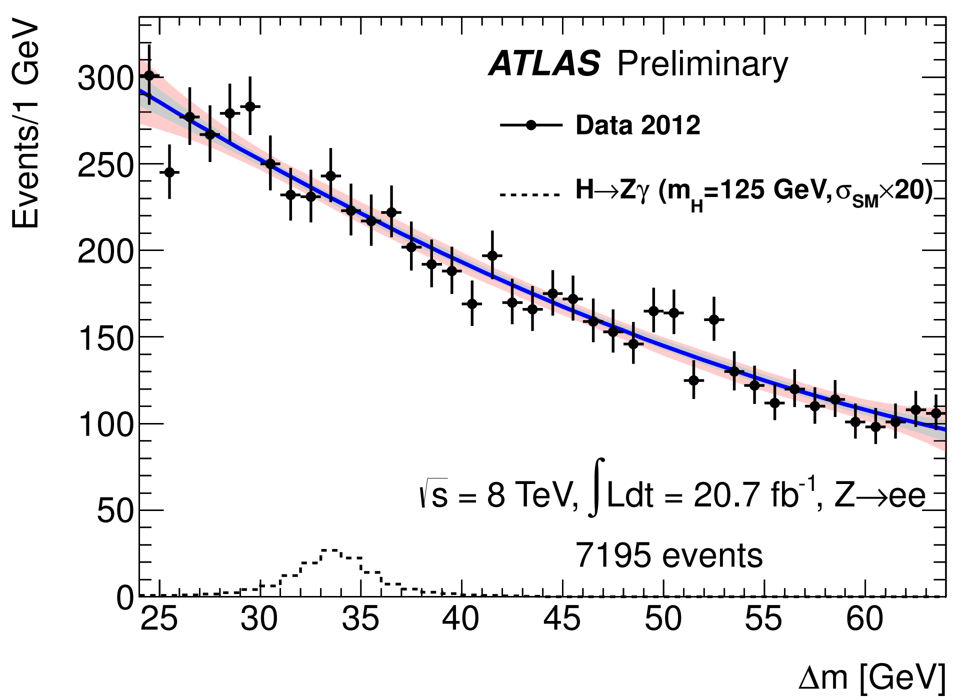

1. The SM and the Higgs boson
2. The LHC and the ATLAS experiment
3. The H➙γγ analysis in ATLAS (personal contributions)
4. Measurement of the photon energy scales using Radiative Z decays
5. The search for the Higgs boson in the H➙Zγ channel
6. Outlook

H➛$\gamma\gamma$ and H➛Zγ channels

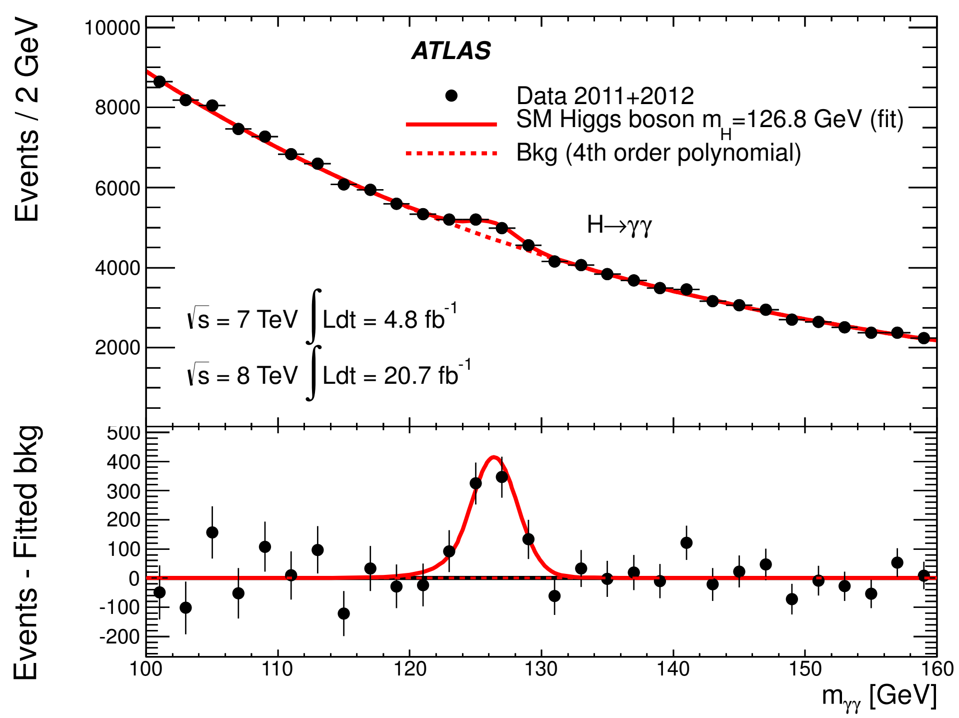

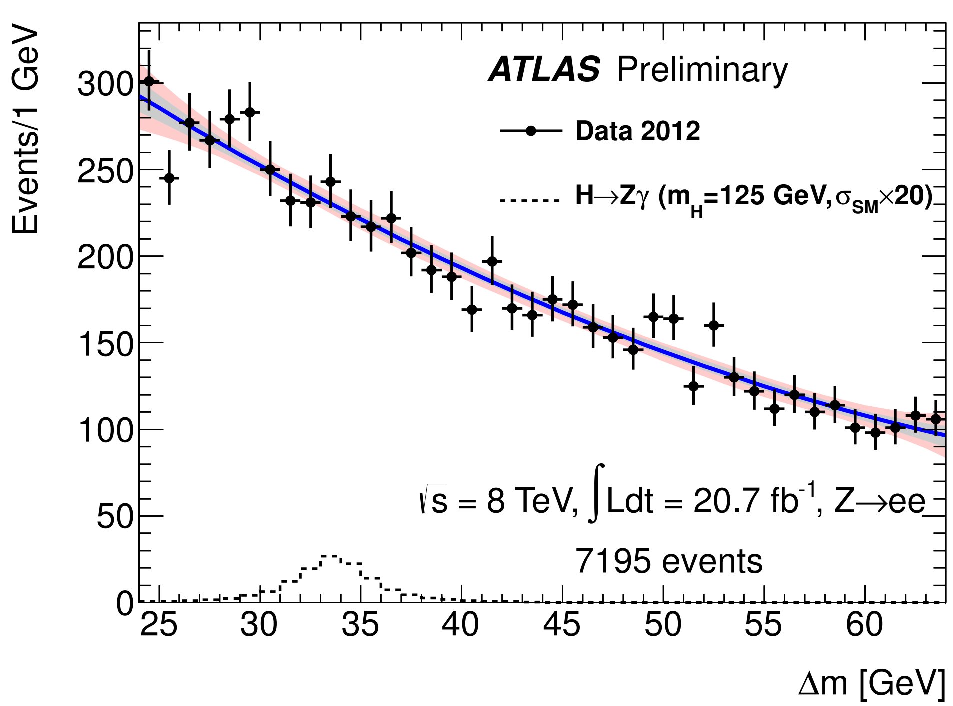

1. The SM and the Higgs boson
2. The LHC and the ATLAS experiment
3. The H➛$\gamma\gamma$ analysis in ATLAS (personal contributions)
4. Measurement of the photon energy scales using Radiative Z decays
5. The search for the Higgs boson in the H➛Zγ channel
6. Outlook

The Standard Model of particle physics

The building blocks of matter and their interactions through fundamental forces are described by the Standard Model of particle physics:

- The SM describes the strong, weak and electromagnetic interactions in terms of local gauge symmetries
- All interactions are mediated by exchanges of particles
- Matter is described in terms of fermions and forces in terms of bosons
- In the SM, the weak and the electromagnetic interactions are unified into a single electroweak gauge symmetry

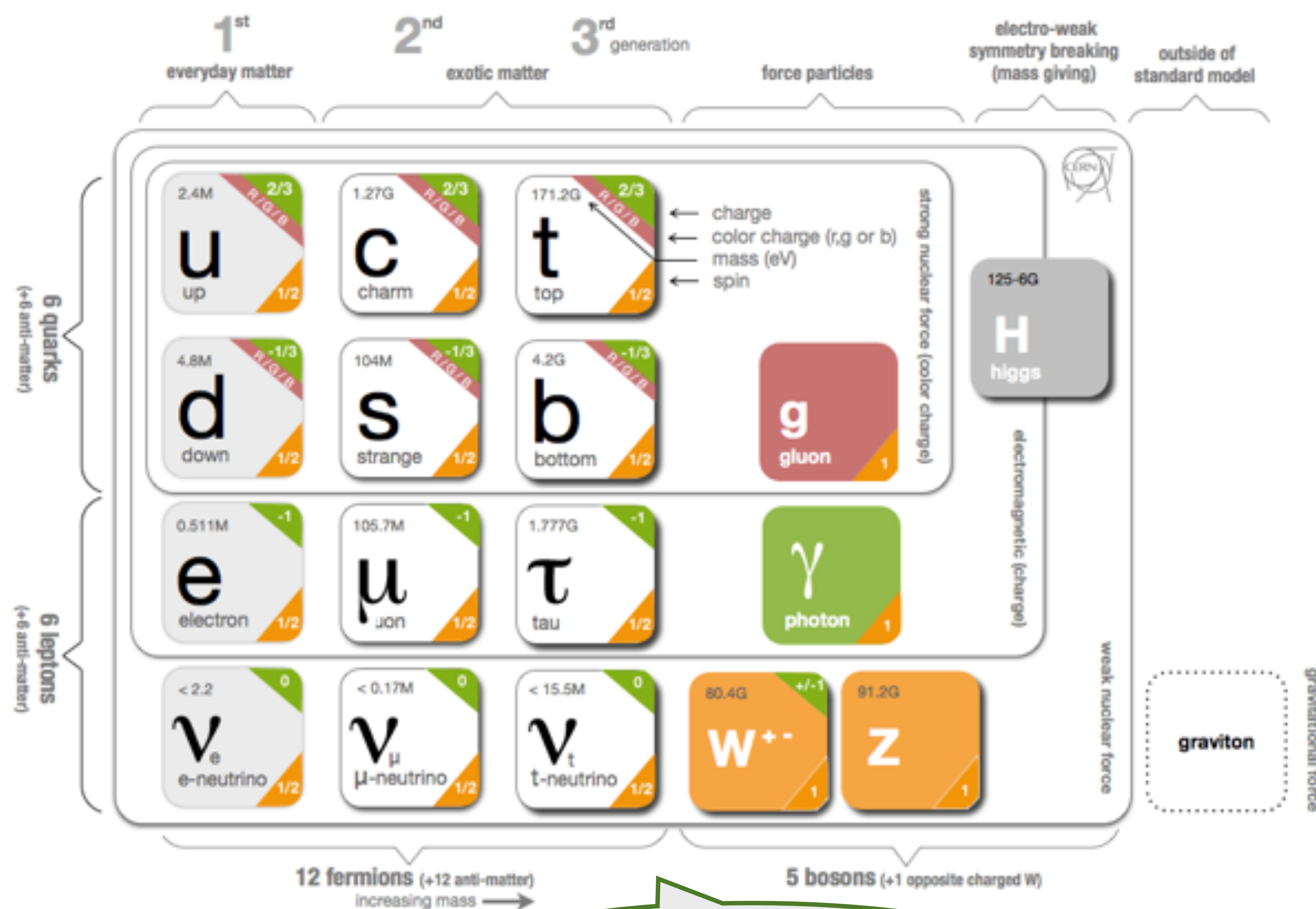

The SM has been rigorously tested agreeing exceptionally well with results of experiments

The BEH mechanism and the Higgs boson

The BEH mechanism was proposed in 1964 (Higgs, Brout + Englert....)

- A scalar field is introduced in the SM, to generate a spontaneous breaking of the EW symmetry. Through this mechanism, the W and Z bosons acquire mass
- The scalar field also couples to fermions generating the fermion masses

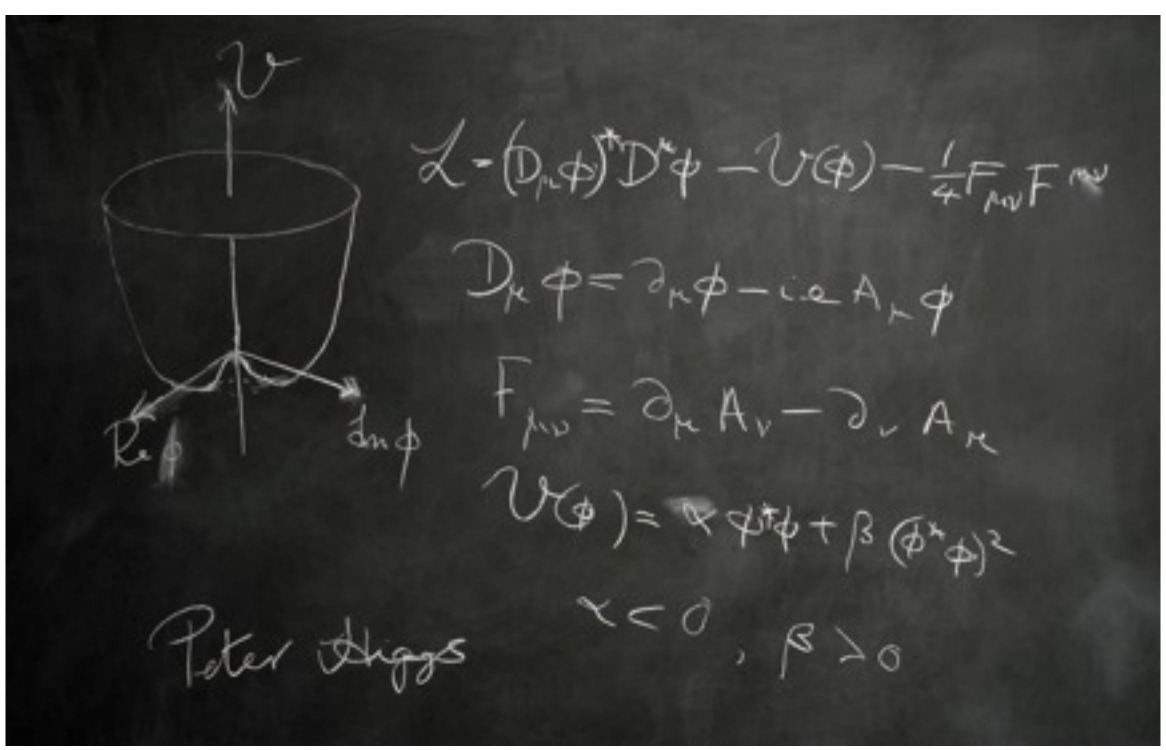

- A single neutral scalar particle so-called **Higgs boson** remains after the symmetry breaking
- Before observation, all Higgs properties (production, decay rates and couplings) were a function of its own yet unknown mass (mH).

Experimental constraints on the Higgs mass

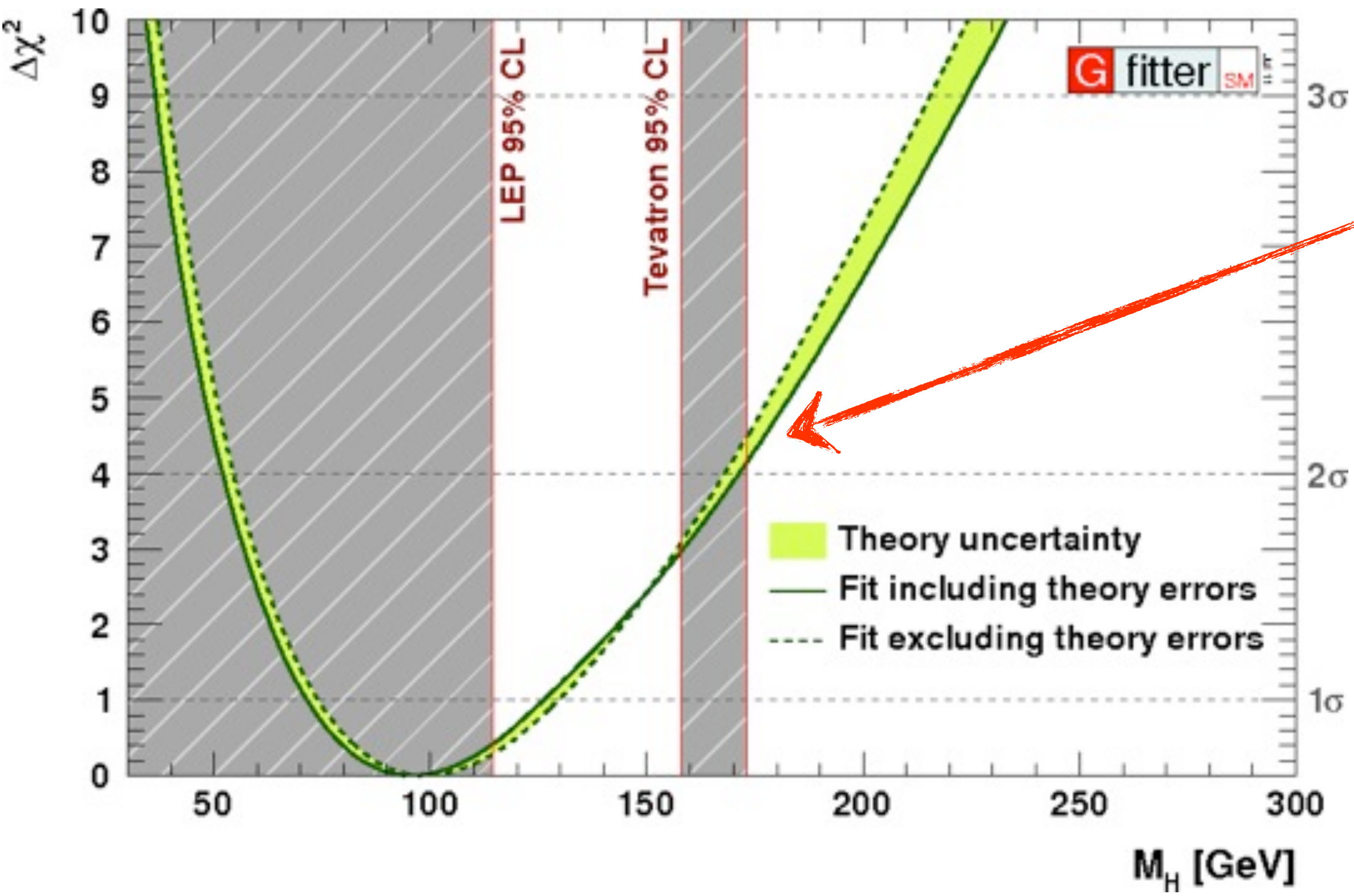

Indirect constraints on mH from a fit to precision EW measurements

Status of LHC direct searches by end 2011

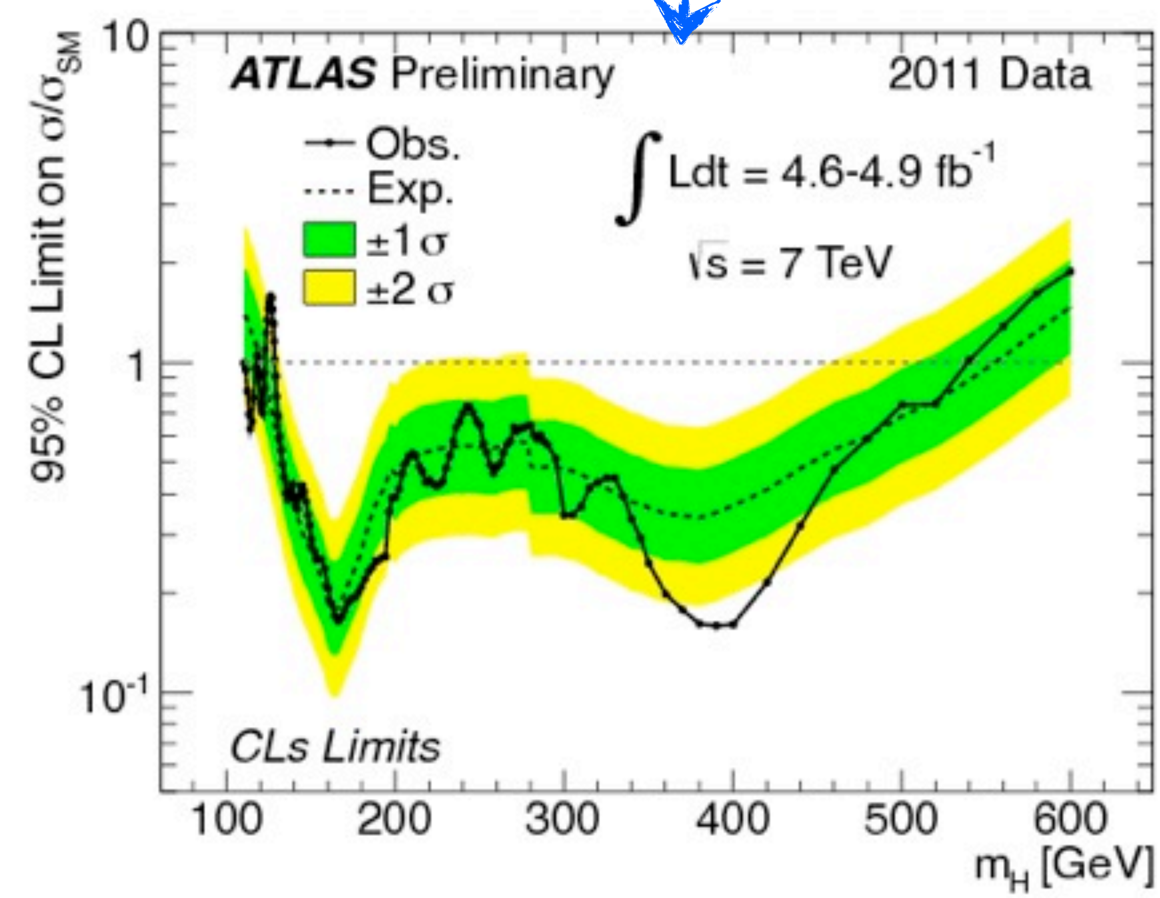

Indirect constrains and direct searches left only two regions for the search:

- Low mass region (in agreement with EW fit)
- High mass region (quickly excluded by the LHC)

The Higgs at the LHC

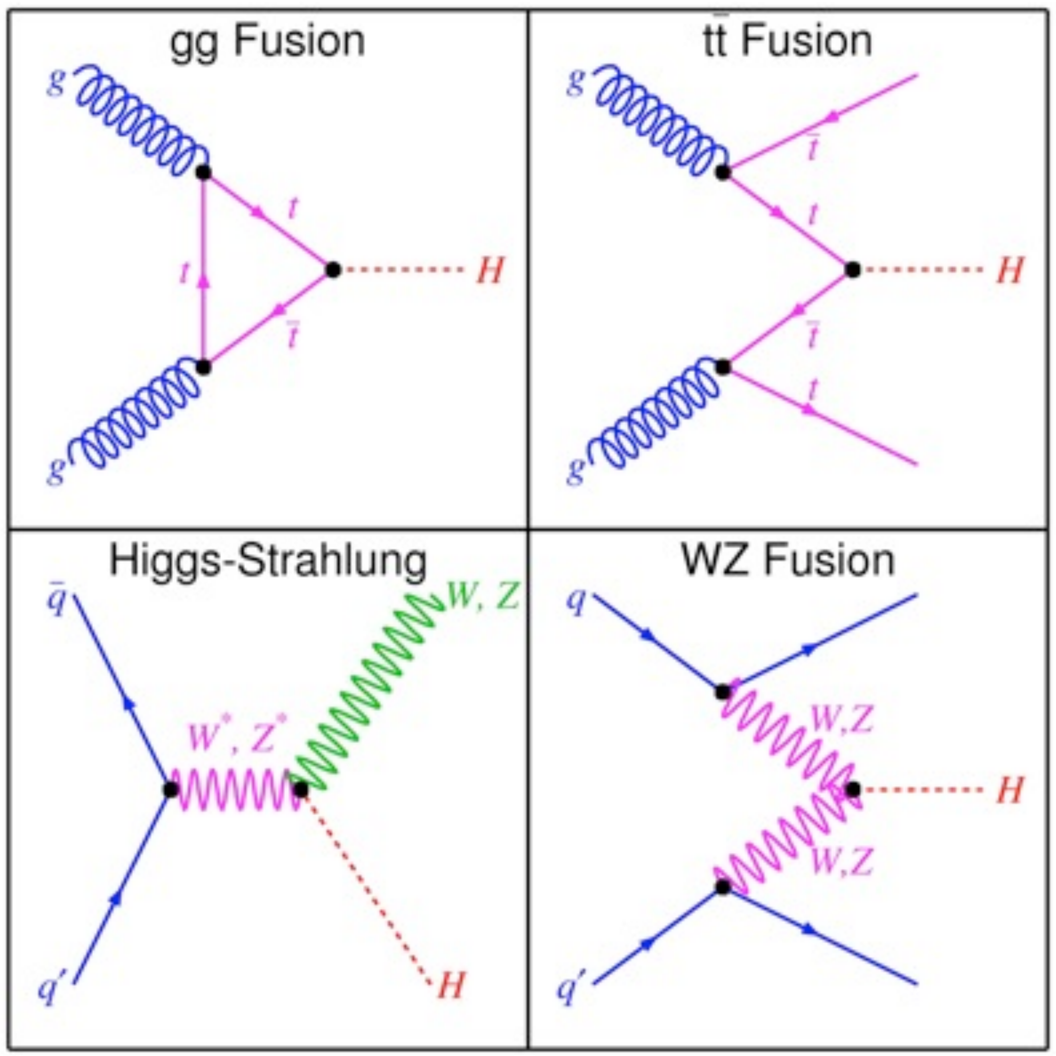

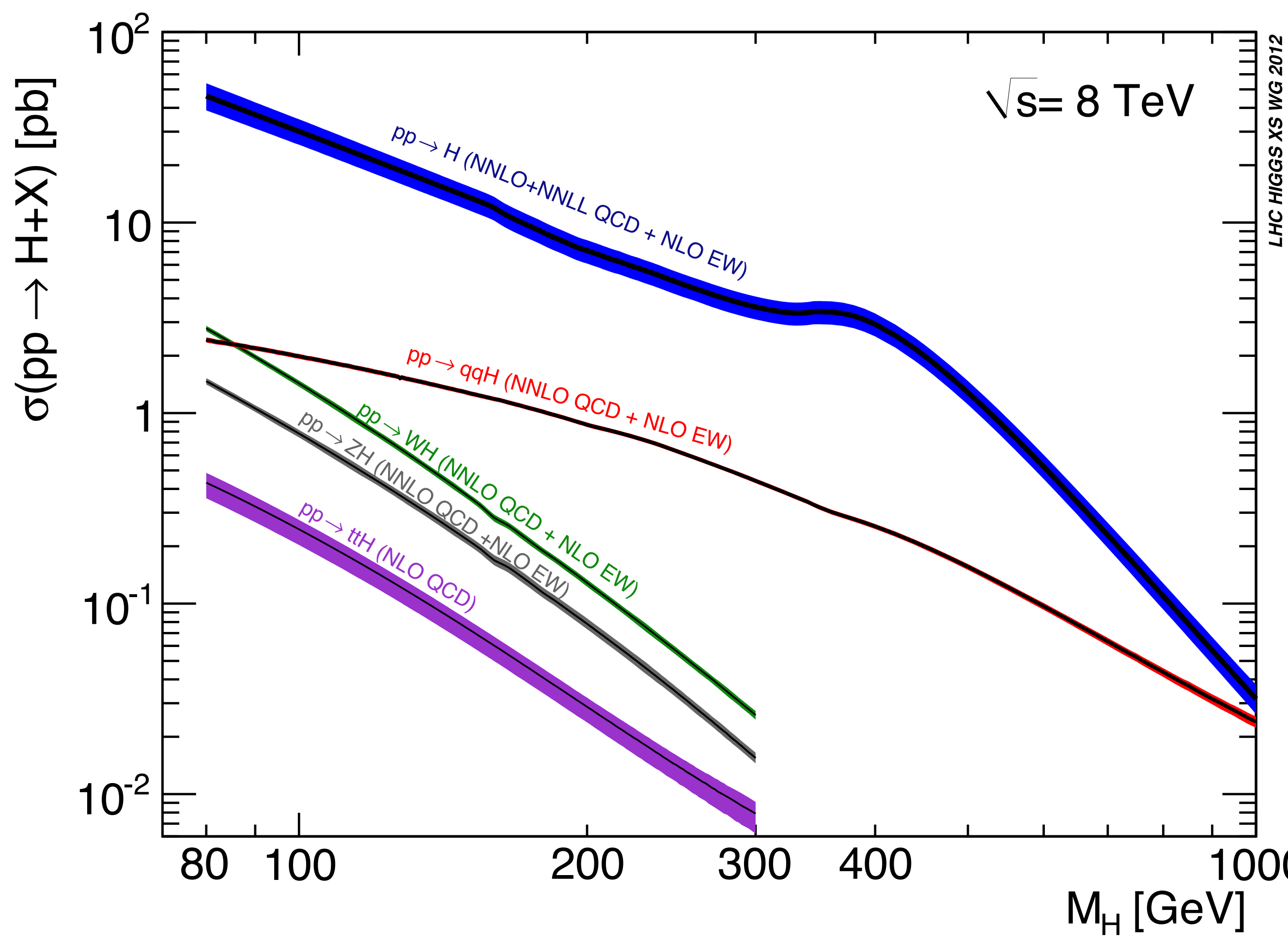

- Main production through gluon fusion (mainly proceeds through top quark).

- VBF, WH, ZH and ttH, follow in order.

Higgs decays

- In the low mass range the H➛$\gamma\gamma$ and H➛Zγ decays have a small BR in the order of 10^{-3}.
- H➛$\gamma\gamma$ was one of the most promising for Higgs search in the low mass range, due to a clean signature to discriminate QCD backgrounds.

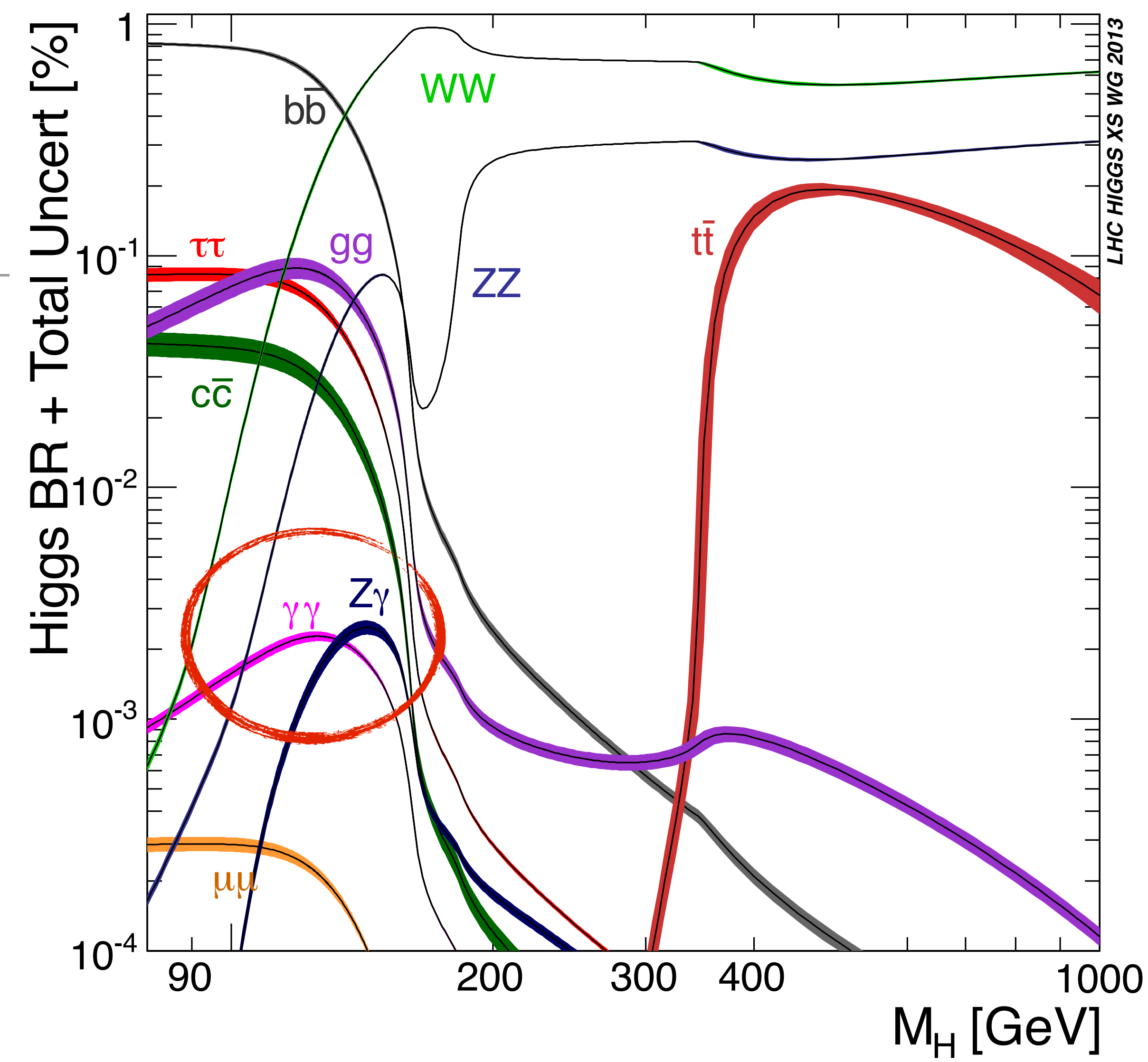

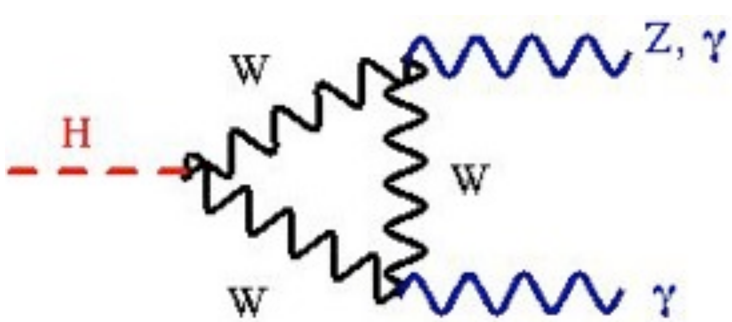

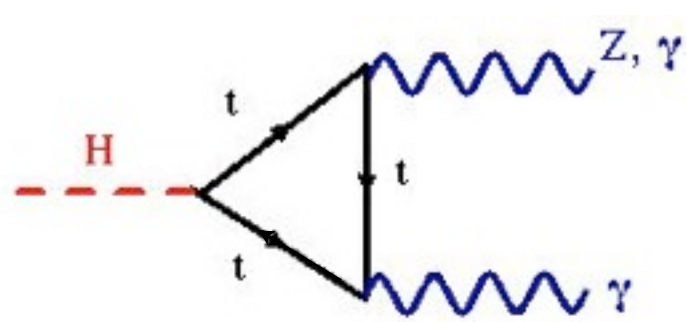

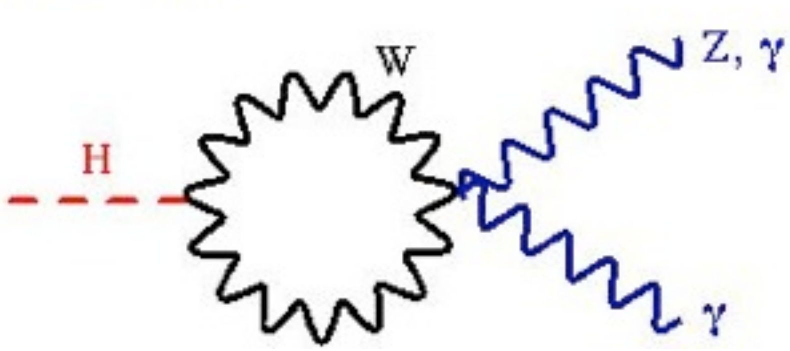

H➛$\gamma\gamma$ and H➛Zγ, a window to new physics:

Decay via loop processes, any new charged particle coupling to the Higgs could contribute to the loops and change their relative decay rate magnitudes.

H➙γγ and H➙Zγ channels

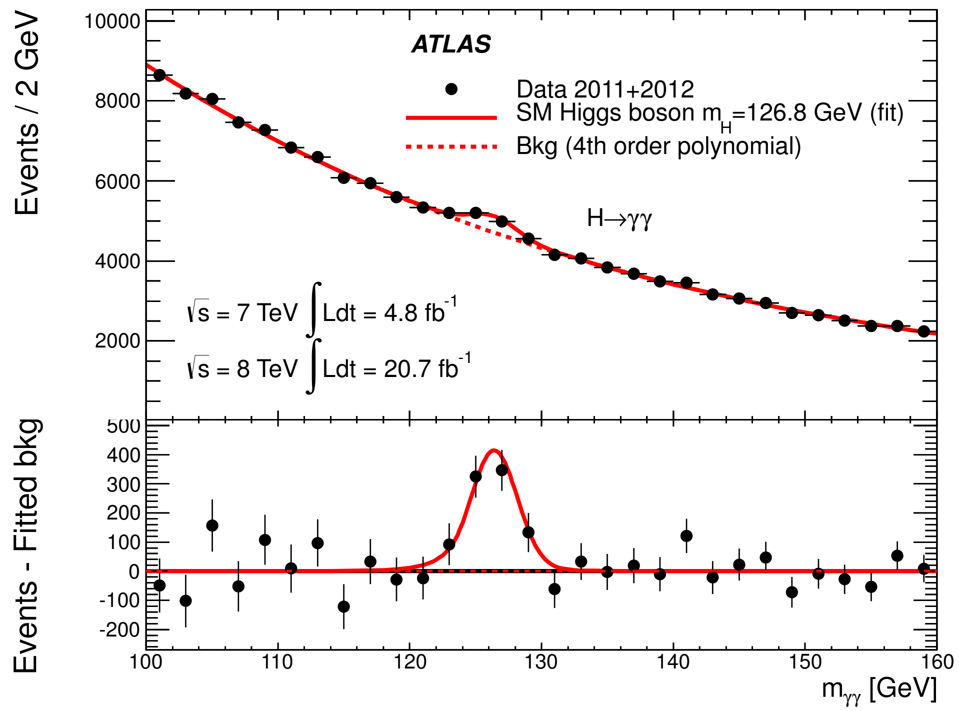

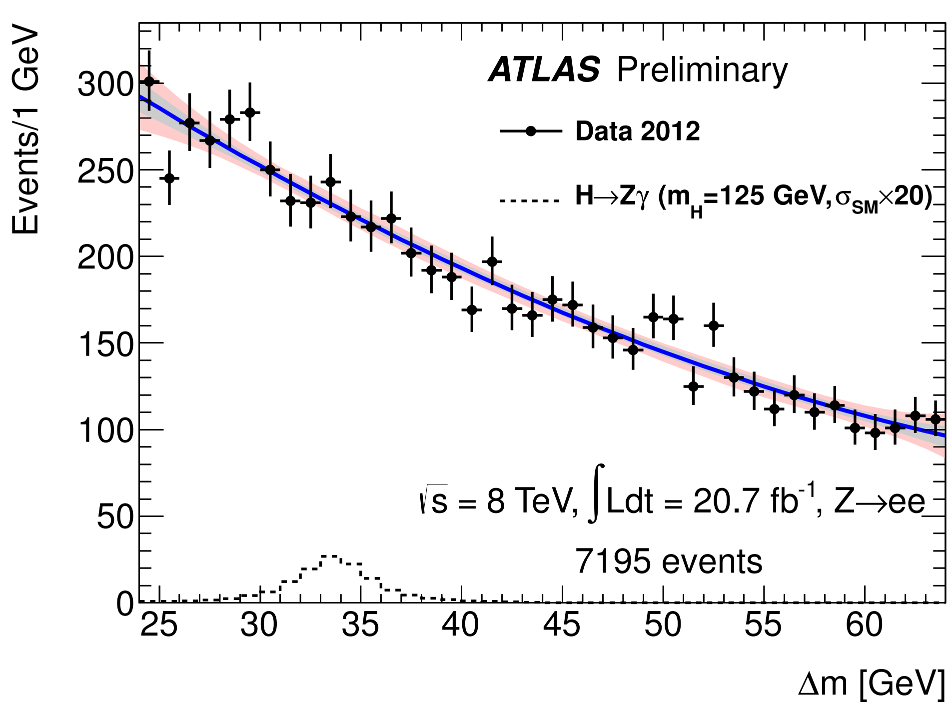

1. The SM and the Higgs boson
2. The LHC and the ATLAS experiment
3. The H➙γγ analysis in ATLAS (personal contributions)
4. Measurement of the photon energy scales using Radiative Z decays
5. The search for the Higgs boson in the H➙Zγ channel
6. Outlook

The LHC

- Circular tunnel 27 km circumference located on the Franco-Swiss border.

- Proton - proton collisions at a center of mass energy of 7 TeV (2010-2011) and 8 TeV (2012).

- Two general purpose detectors (ATLAS and CMS) with the main task of searching for the Higgs boson and new physics.

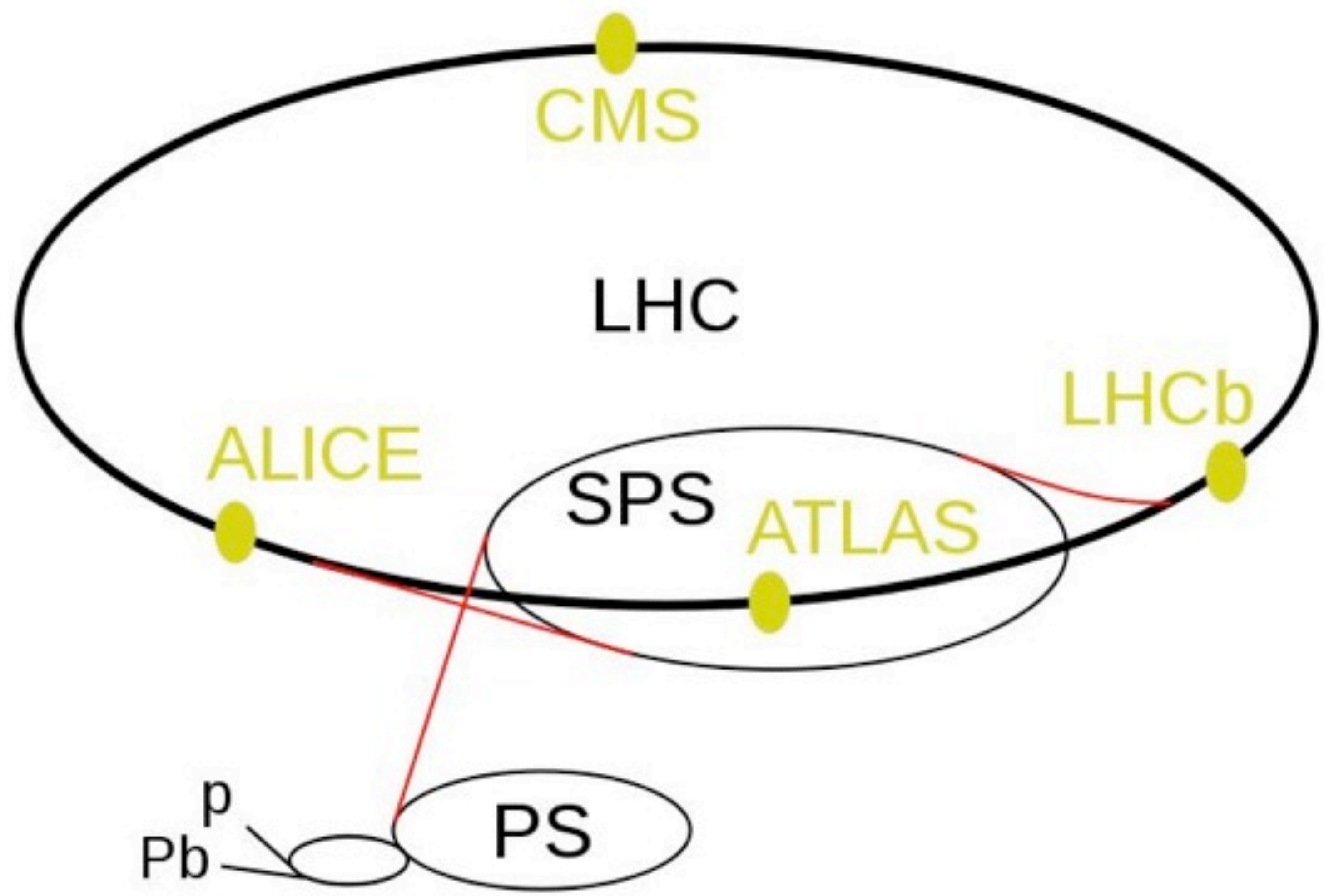

The ATLAS detector

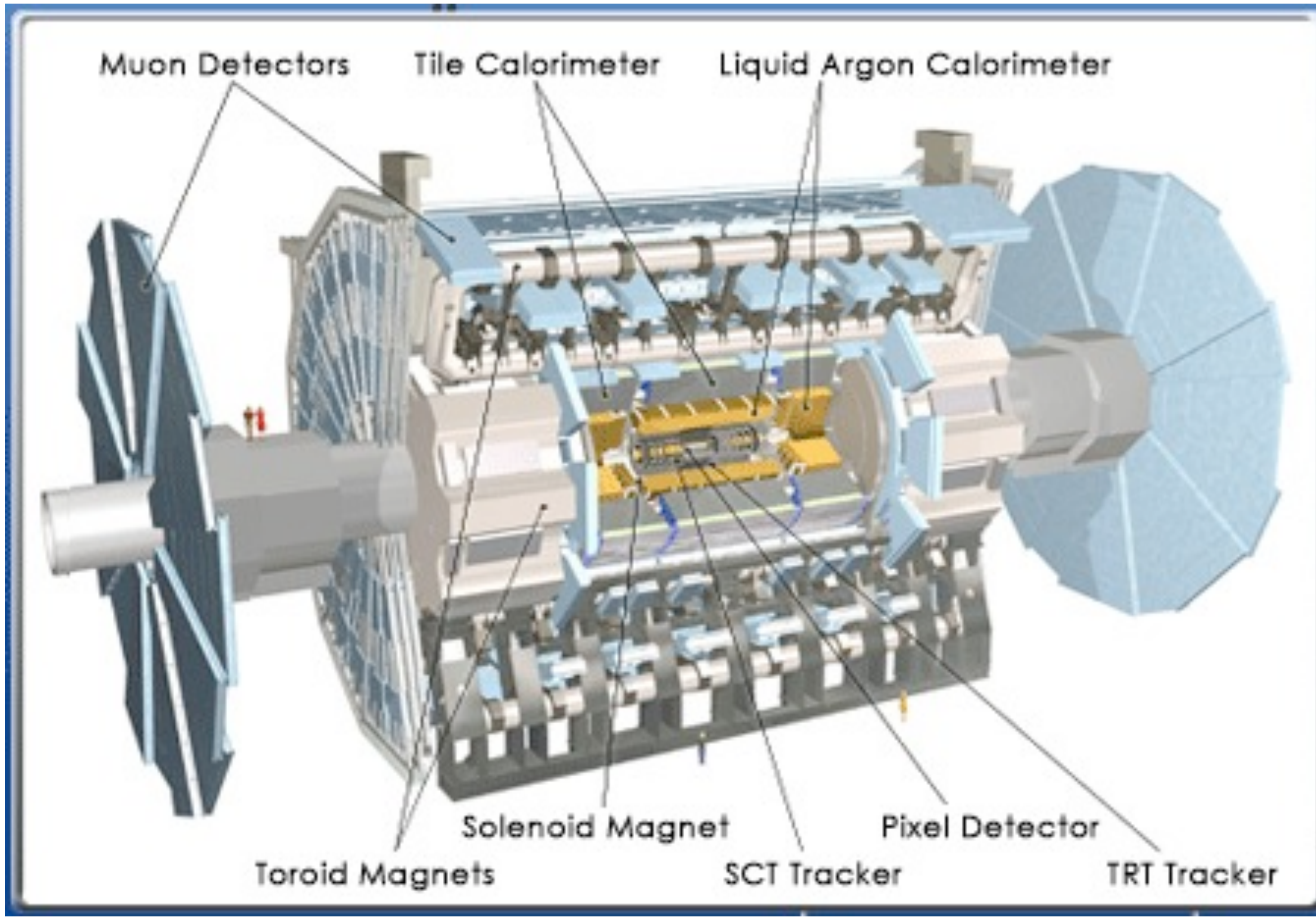

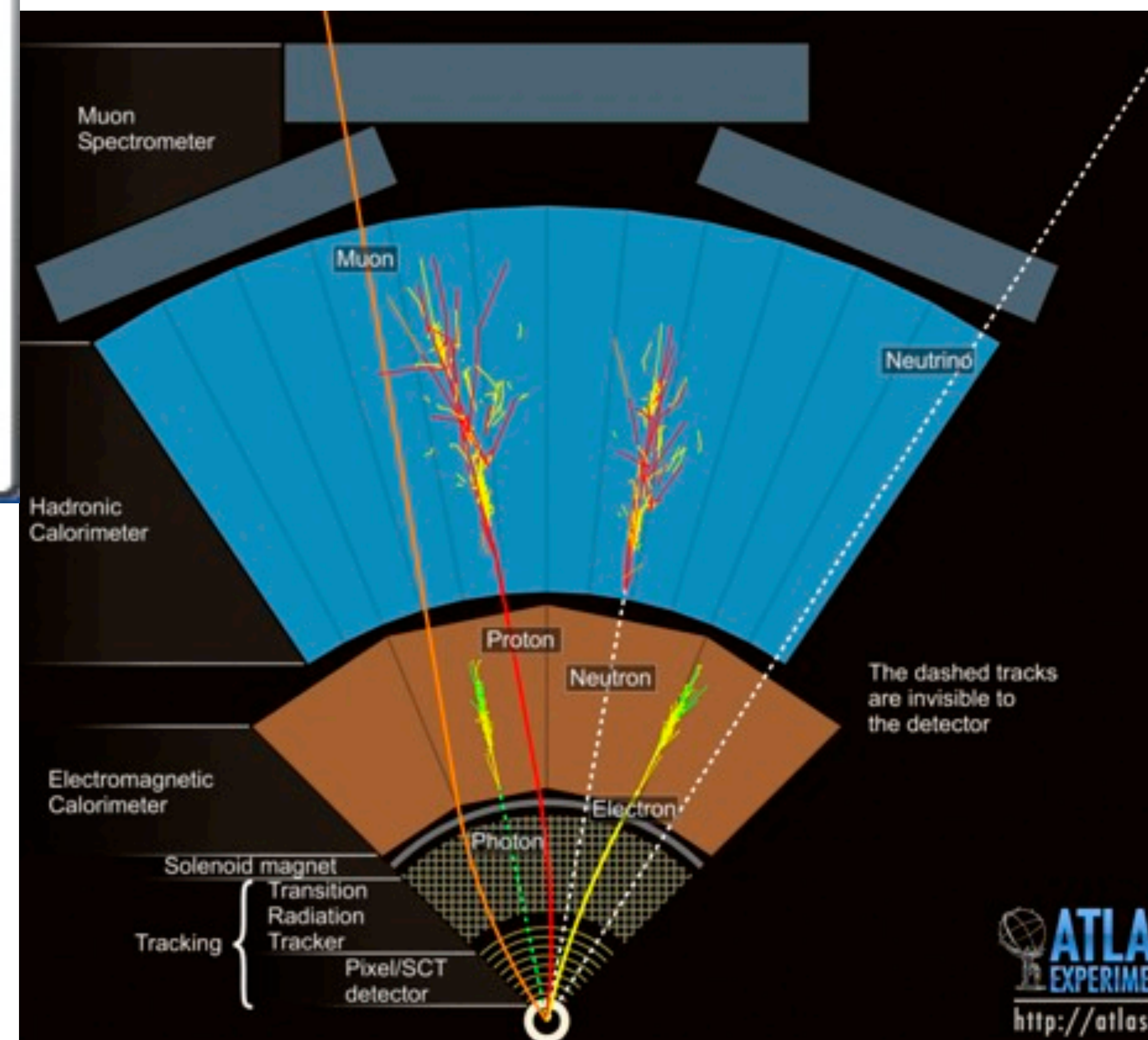

EMCAL, ID and MS are relevant for the analyses of this thesis, I'll focus on the EMCAL.

ATLAS data-taking in the LHC Run I

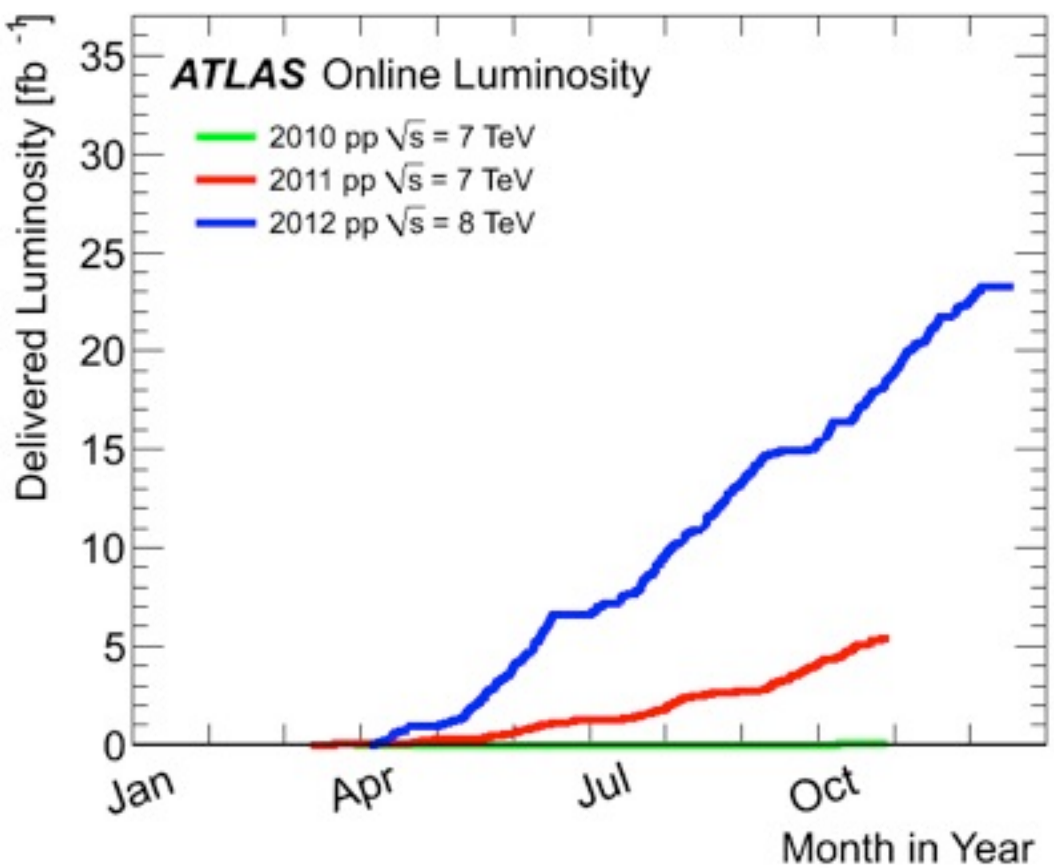

- LHC Run I finished after 3 years in February 2013.

Very good LHC performance:
– Integrated luminosity delivered in 2012: 23.3 fb^{-1}
– Peak luminosity achieved: 7.73 x 10^{33} cm^{-2} s^{-1}

At the cost of:
-Larger probability of producing separated events in a single bunch crossing (so-called pile-up events).

The ATLAS detector operated producing very high data quality.

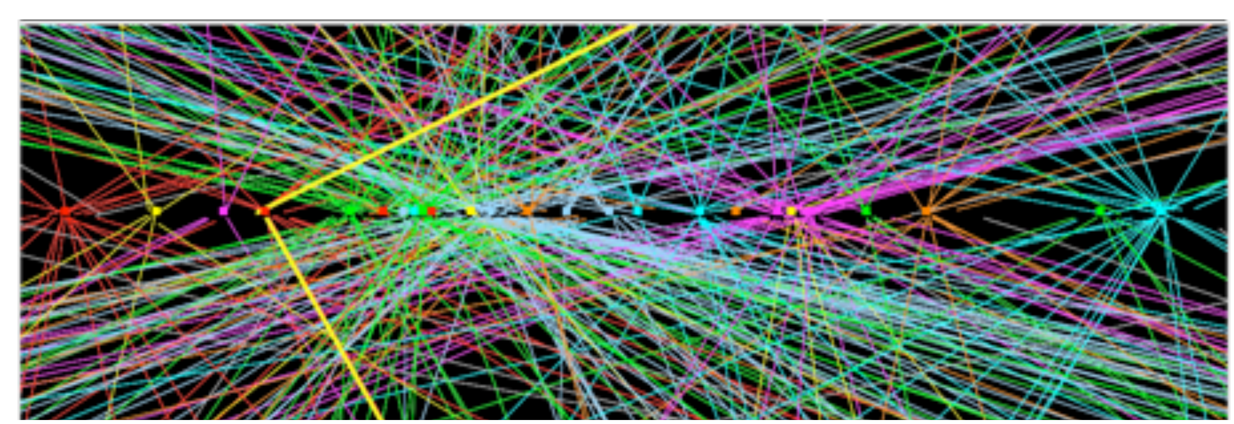

Z ➝μμ event candidate with 25 reconstructed vertices

H➙$\gamma\gamma$ and H➙Zγ channels

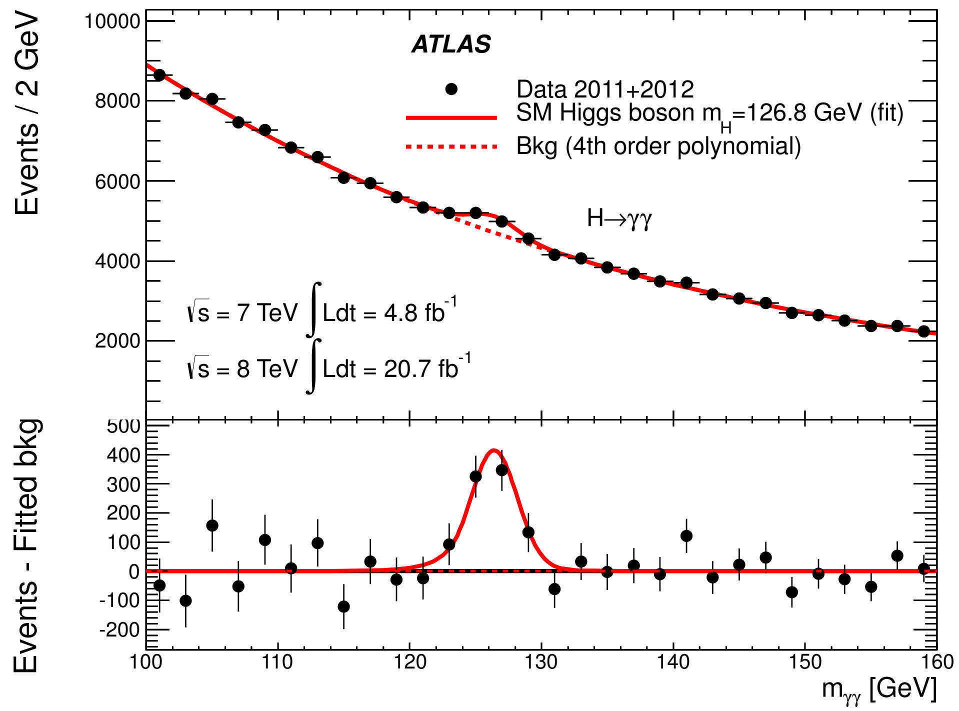

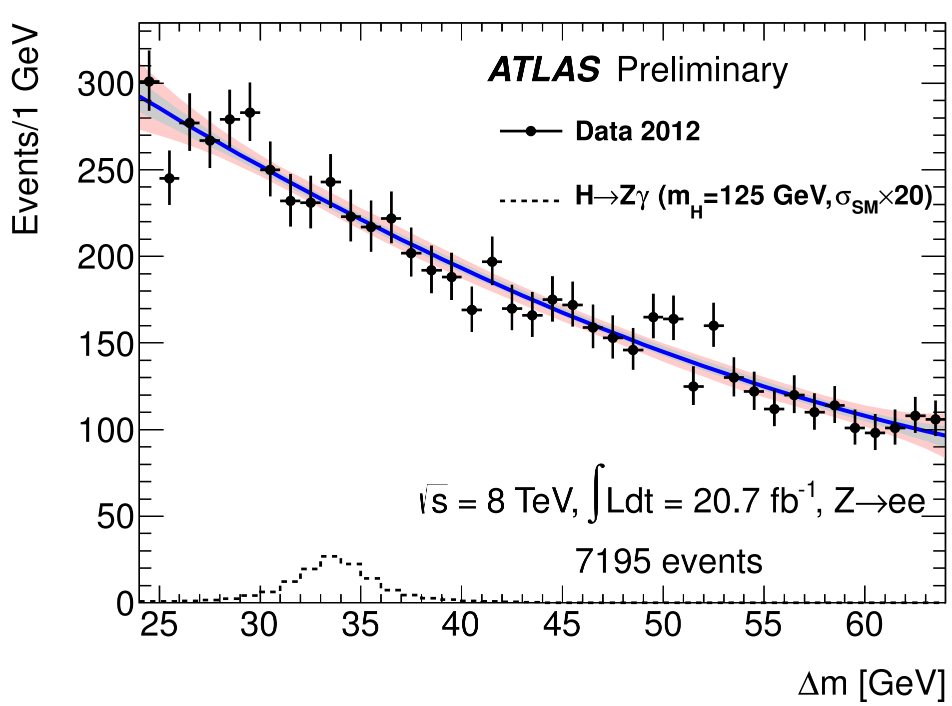

1. The SM and the Higgs boson
2. The LHC and the ATLAS experiment
3. **The H➙$\gamma\gamma$ analysis in ATLAS (personal contributions)**
4. Measurement of the photon energy scales using Radiative Z decays
5. The search for the Higgs boson in the H➙Zγ channel
6. Outlook

The H➙$\gamma\gamma$ analysis strategy

- Based on the diphoton invariant mass ($m_{\gamma\gamma}$) as the main discriminating variable, which is built with a photon pair with well measured energies and directions.
- The $m_{\gamma\gamma}$ spectrum is scanned from 110 to 150 GeV, looking for a narrow resonance over a large smooth monotonically decreasing QCD background.
- The background is mainly composed of QCD diphoton production $\gamma\gamma$ (irreducible ~75%), followed by reducible γ-jet and di-jet (~25% combined).

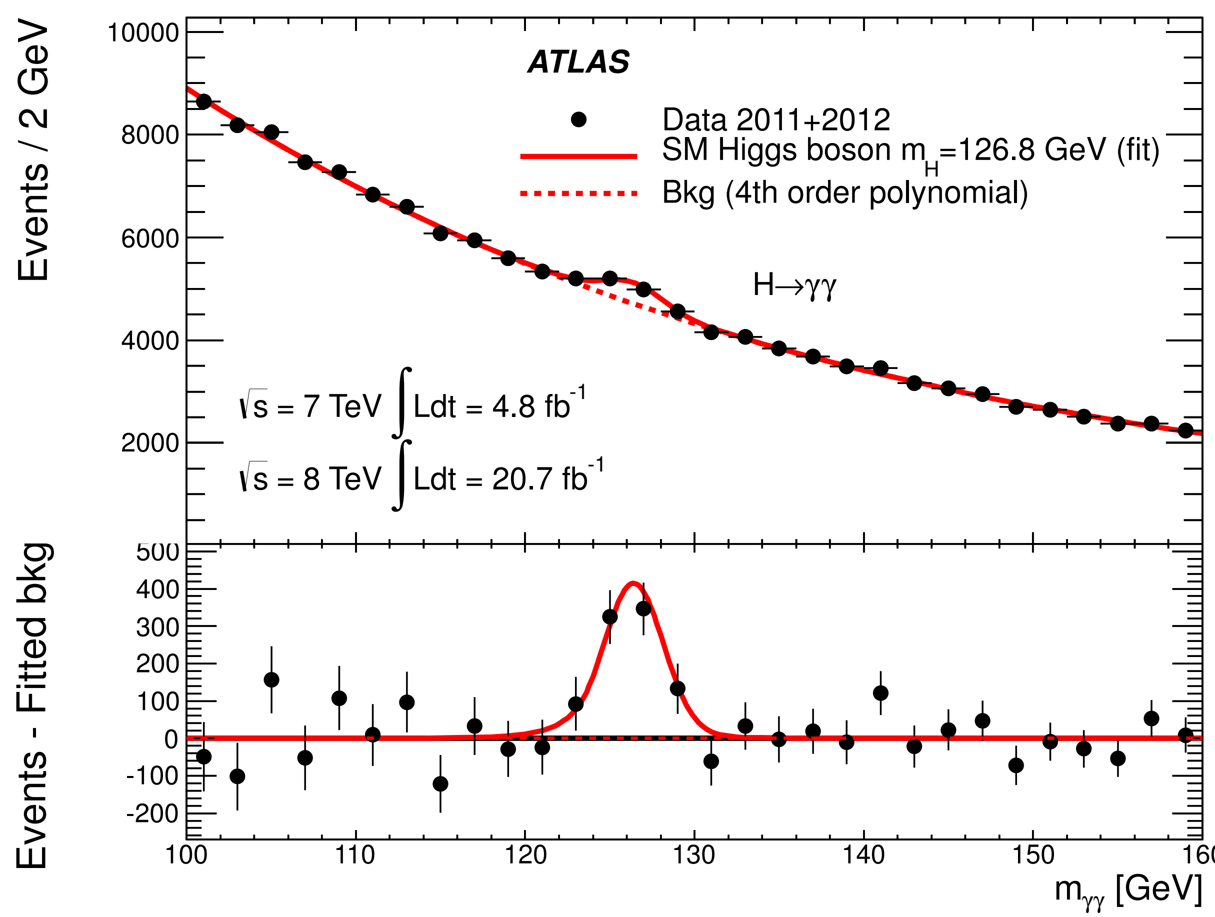

The H➙$\gamma\gamma$ analysis strategy

- Based on the diphoton invariant mass (m$\gamma\gamma$) as main the main discriminating variable, which is built with a **photon pair with well measured energies and directions**

- The m$\gamma\gamma$ spectrum is scanned from 110 to 150 GeV, looking for a narrow resonance over a large smooth monotonically decreasing QCD background.

- The background is mainly composed of irreducible $\gamma\gamma$ (~75%), followed by reducible γ-jet ...%).

how?

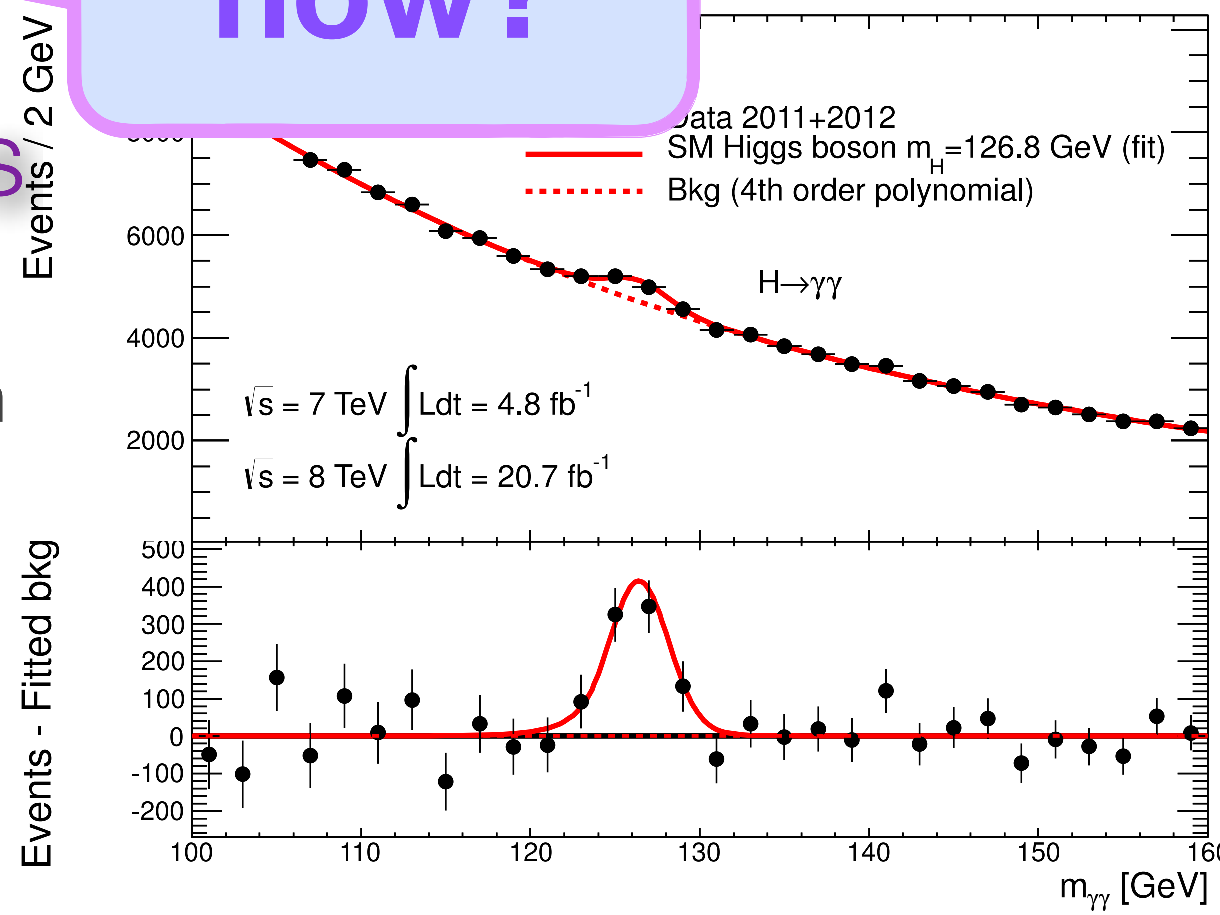

Inner detector and EM calorimeter

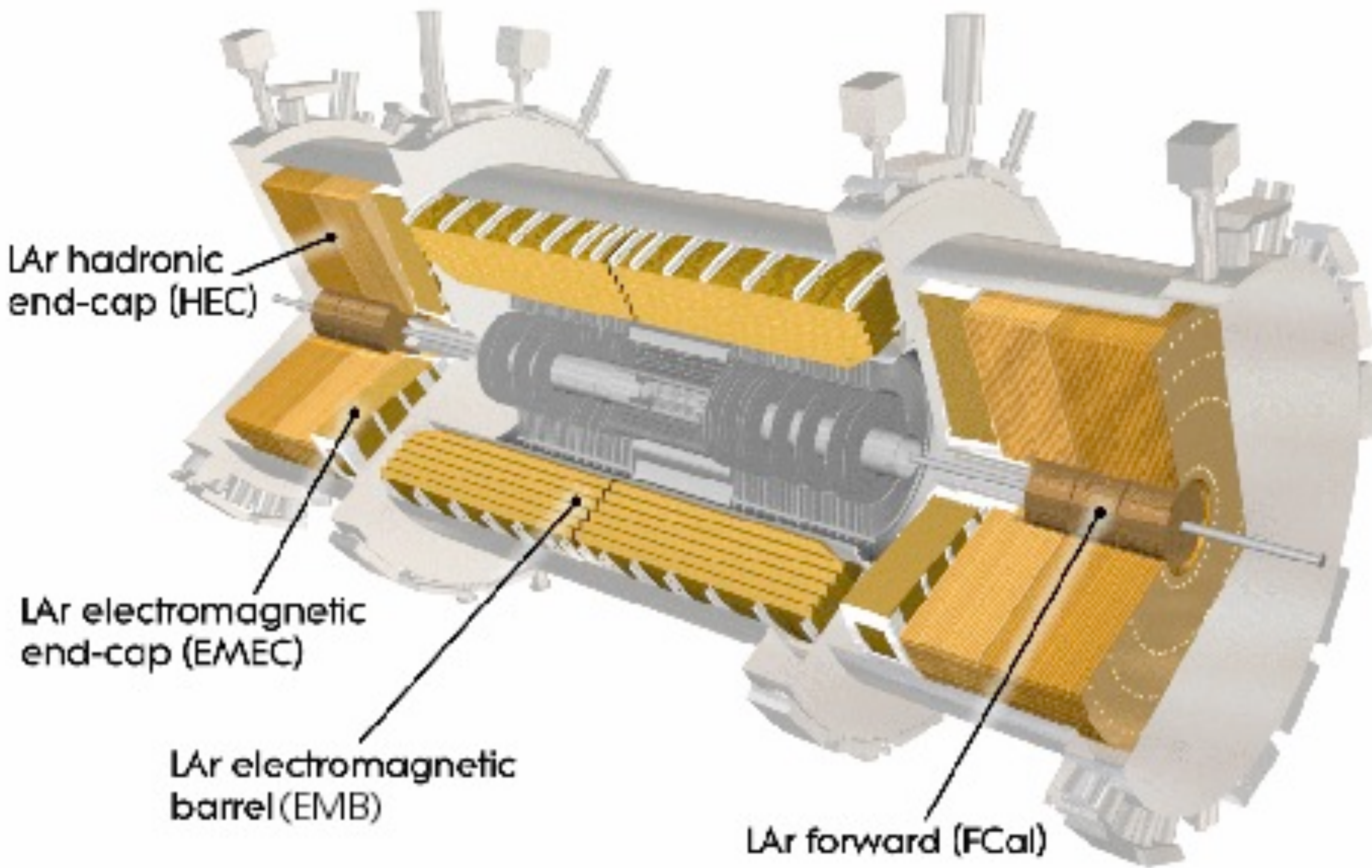

Inner detector

The coordinate system

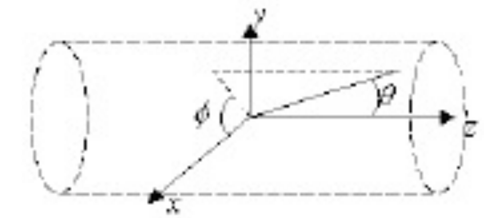

$$\eta = -\ln(\tan(\theta/2))$$

$$\Delta R = \sqrt{\Delta\eta^2 + \Delta\phi^2}$$

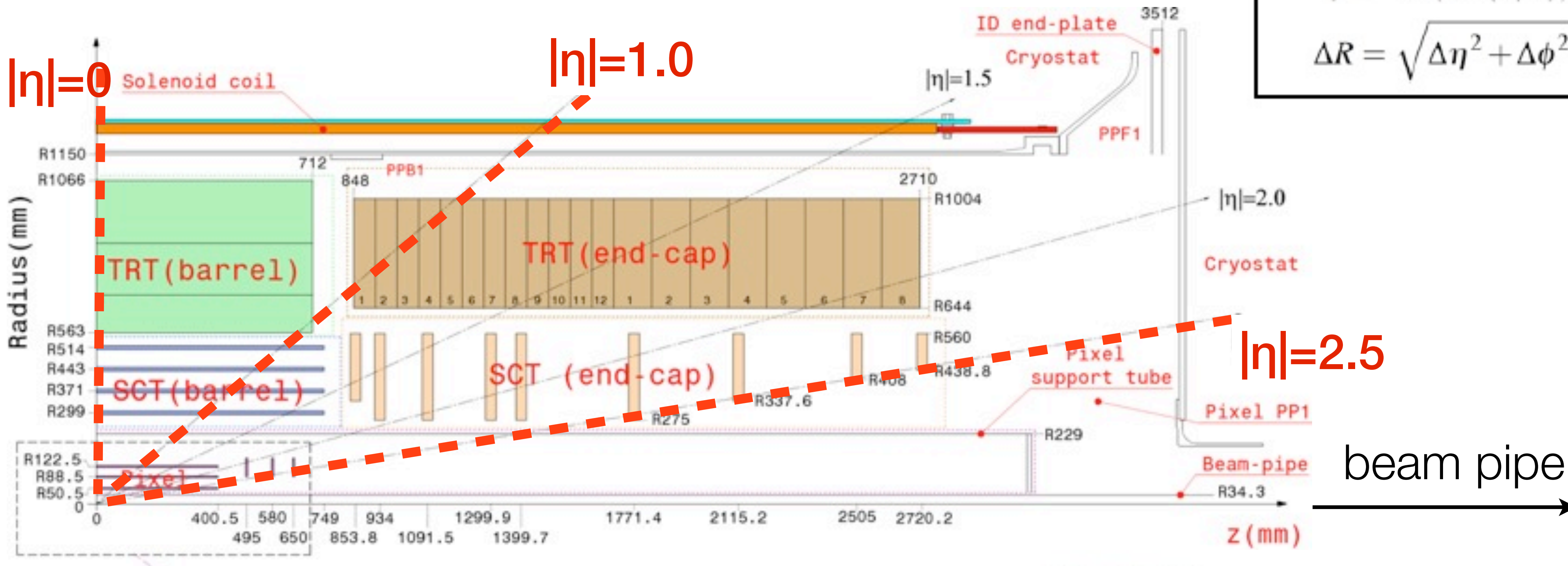

ID 3 sub-detectors

- *Transition Radiation Tracker: straw tubes, |η|<2.0*
- *SemiConductor Tracker: silicon micro-strip detector |η|<2.5*
- *Pixels: 3 layers, |η|<2.5*

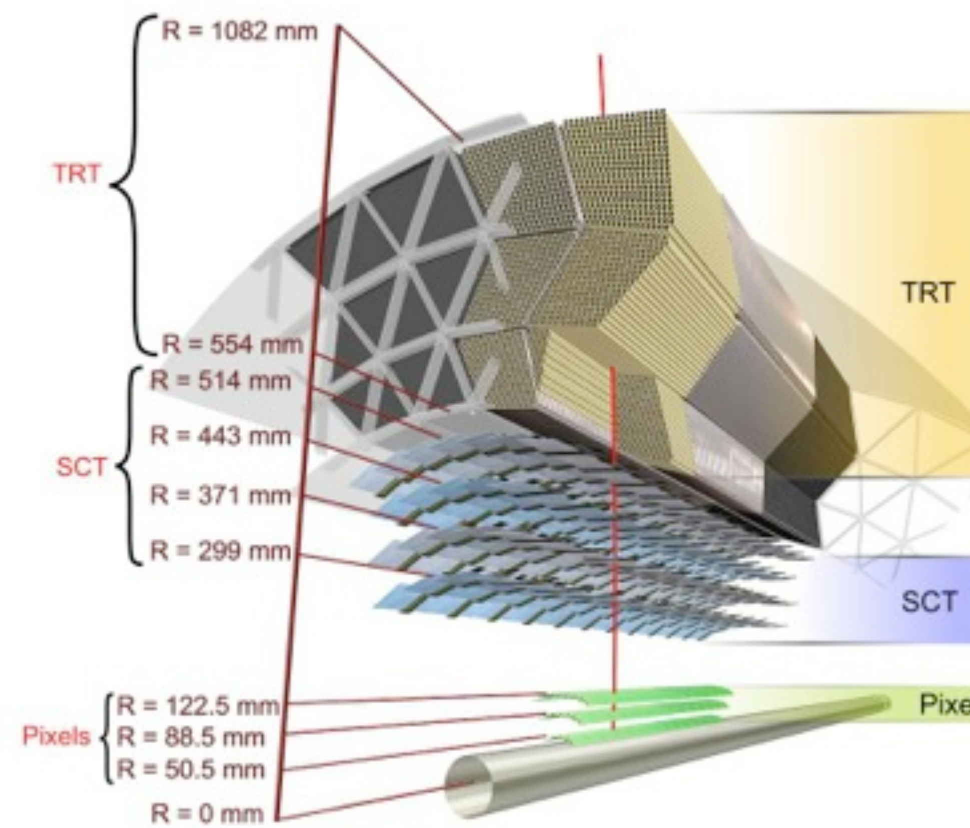

The EM calorimeter

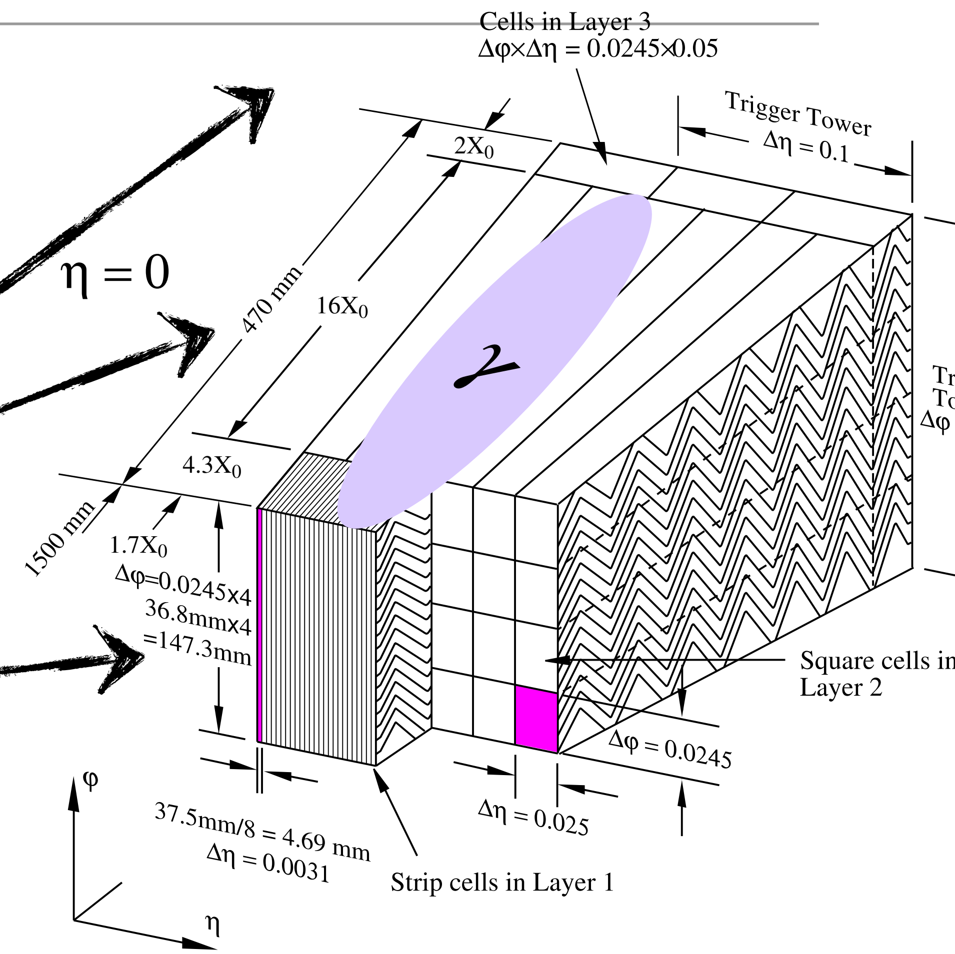

EMCAL: Sampling calorimeter

- Lead absorbers + liquid argon as ionising medium
- Accordion structure : excellent uniformity

Back : correct for shower energy leakage beyond calorimeter
Middle : collect most of shower energy,
Front : precise η measurement, γ-π0 separation
Pre-sampler: (|η|<1.8) : flat, no absorber control energy losses before calorimeter

$$\sigma/E = a/\sqrt{E} \oplus b/E \oplus c$$

a : Stochastic term: fluctuations related to the development of the shower (around 10% in the barrel).
b: Noise term:Negligible at high E.
c: Constant term: contributions that degrade the energy measurement and are independent of the energy of the incoming particle. Dominates at high E. Expected to be 0.7% in the barrel.

The EM calorimeter

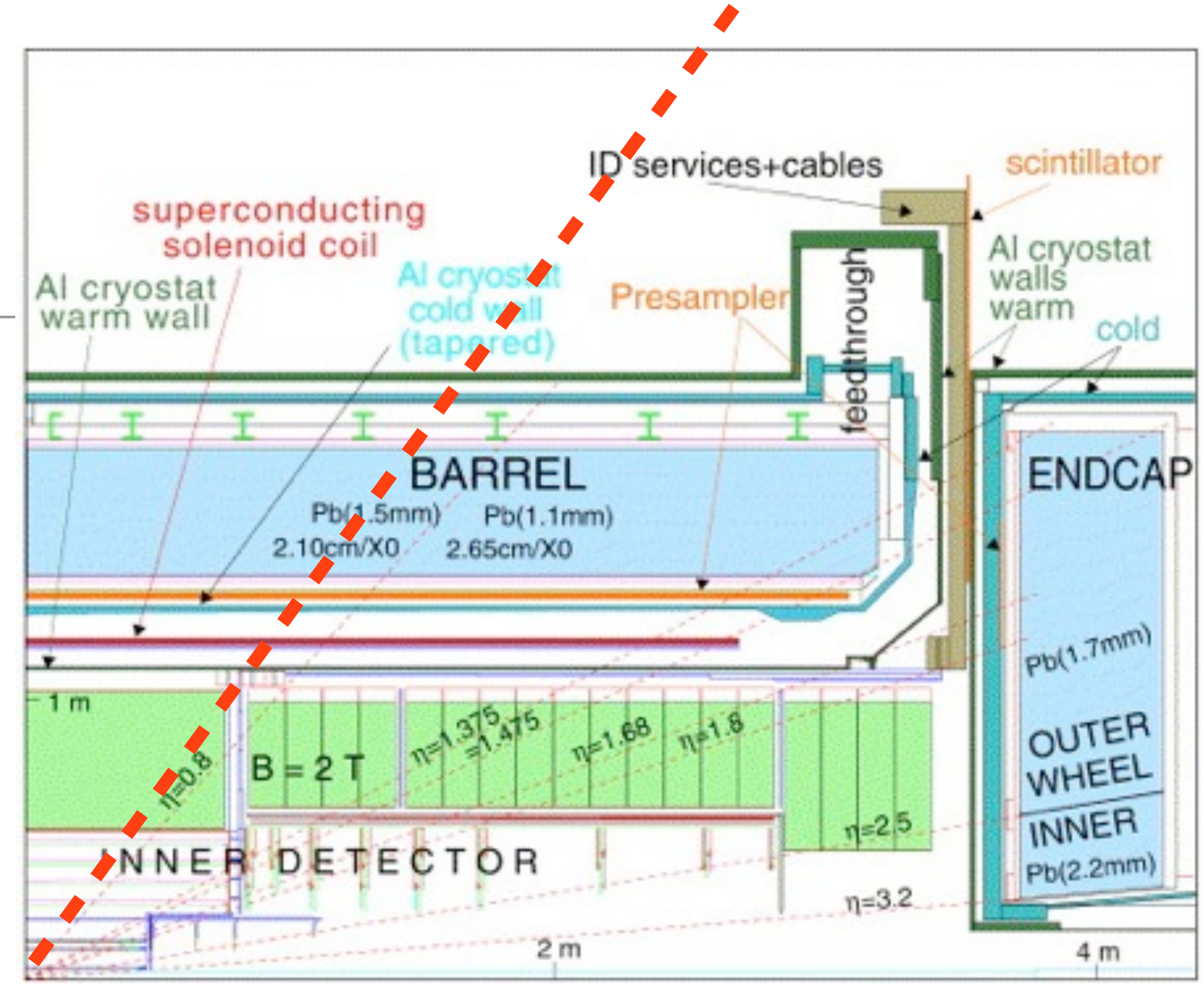

Amount of material upstream of the calorimeter (radiation length X_0) depends on η:

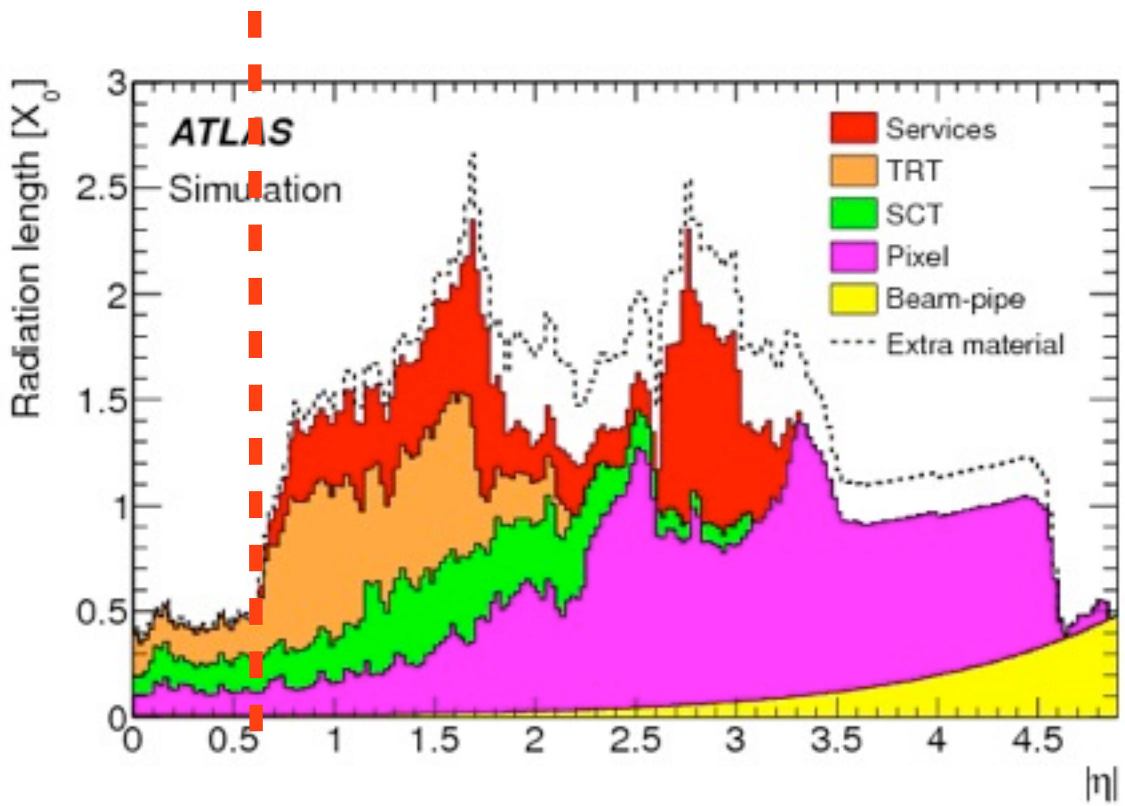

Affects directly the energy resolution.
From MC, in |η|<0.6 range:
- Better than 1% for high energy photons.
- ~2% for a 25 GeV photon

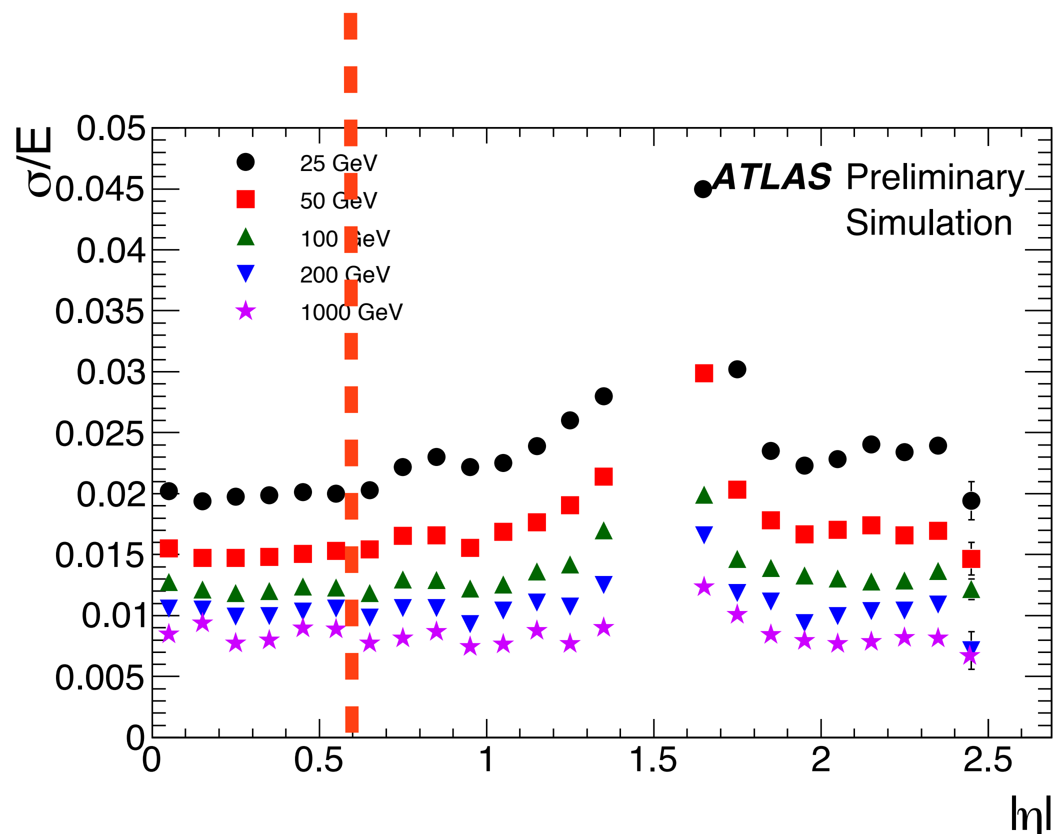

Photon reconstruction

✓ Photon and electron reconstructions use a sliding window algorithm:

Find seeds with Et > 2.5 GeV

✓There are three types of photons:

- No ID track matched to EM cluster: **Unconverted photon ("Unconv")**.

- EM cluster matched to two ID tracks from a common conversion vertex: **Converted photon with two reconstructed tracks ("2-track")**.

- One single track with no hit in the first ID layer is matched to the cluster: **Converted photon with one reconstructed track ("1-track")**.

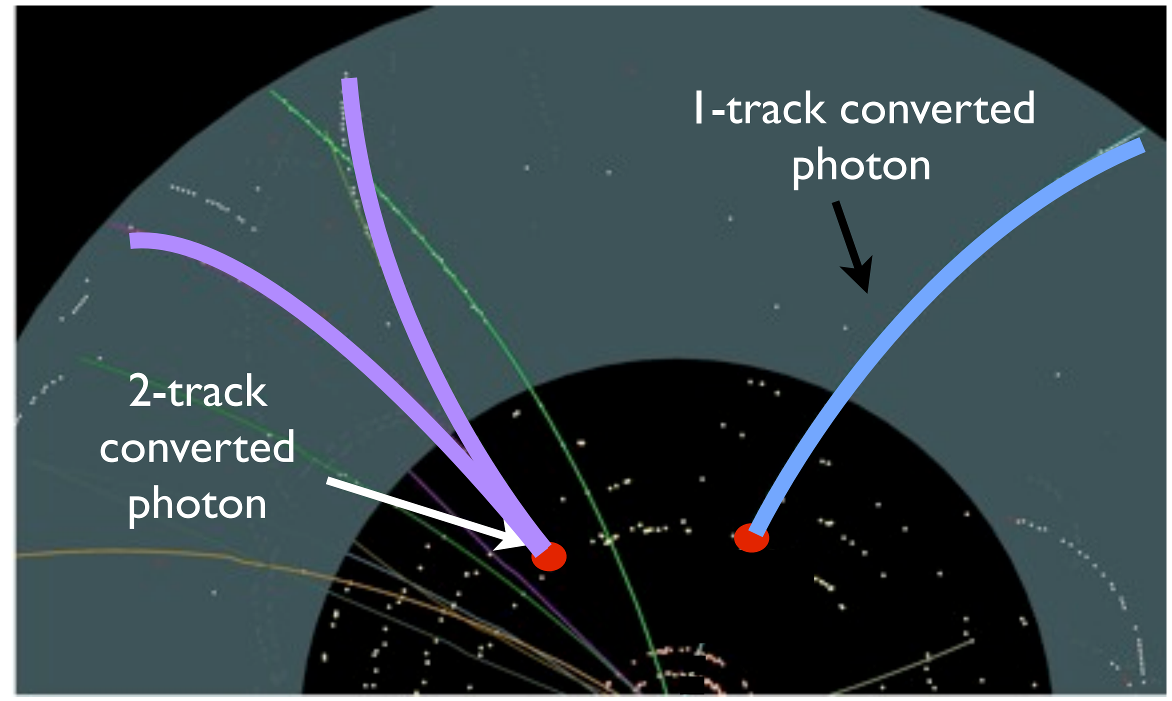

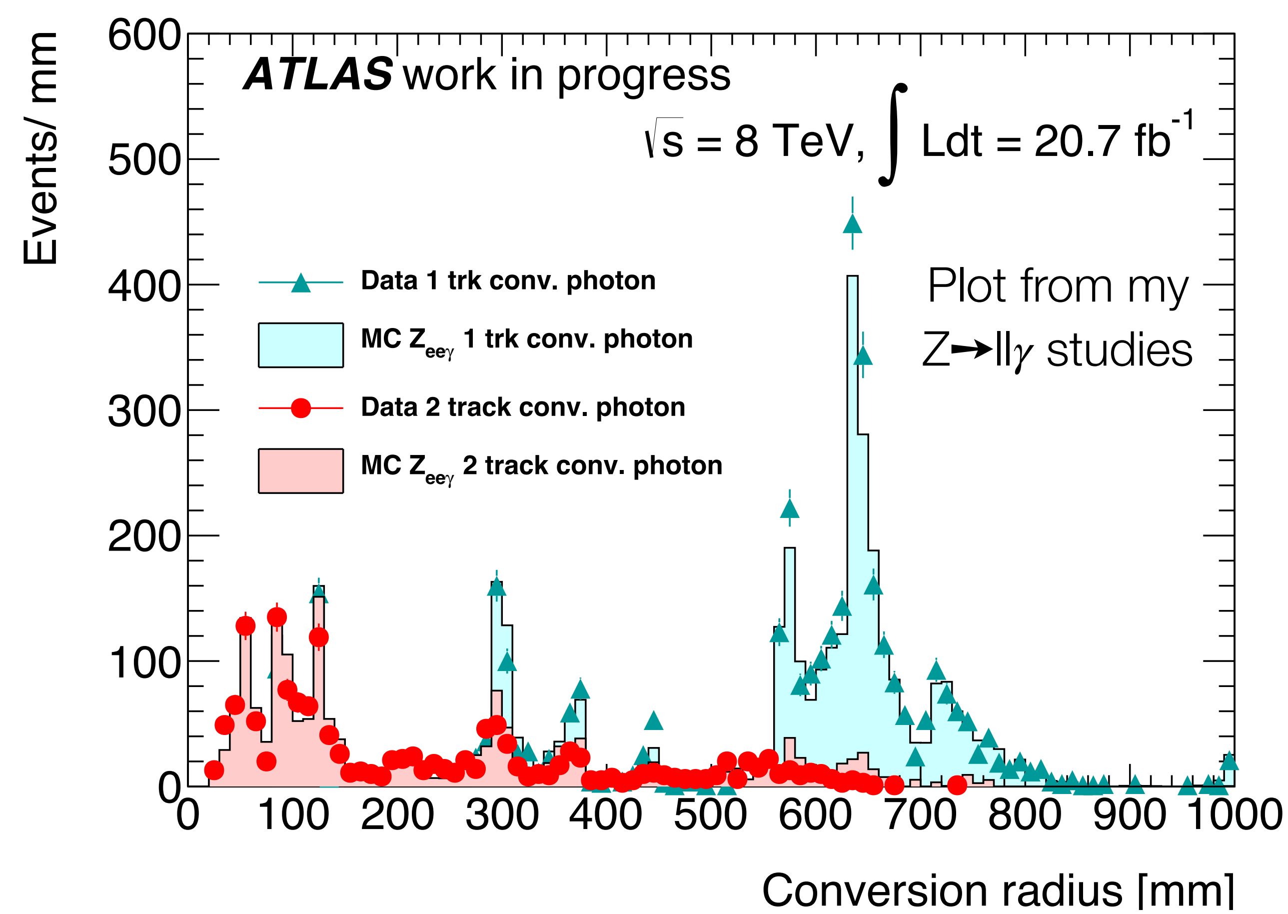

Photon reconstruction

✓ Photo
a sliding
F

✓There
- No ID
Unconv
- EM cl
common
Converte
tracks (“
- One sin
is matche
Convert
track (“2

Due to the amount of upstream material the probability of conversion depends on η.

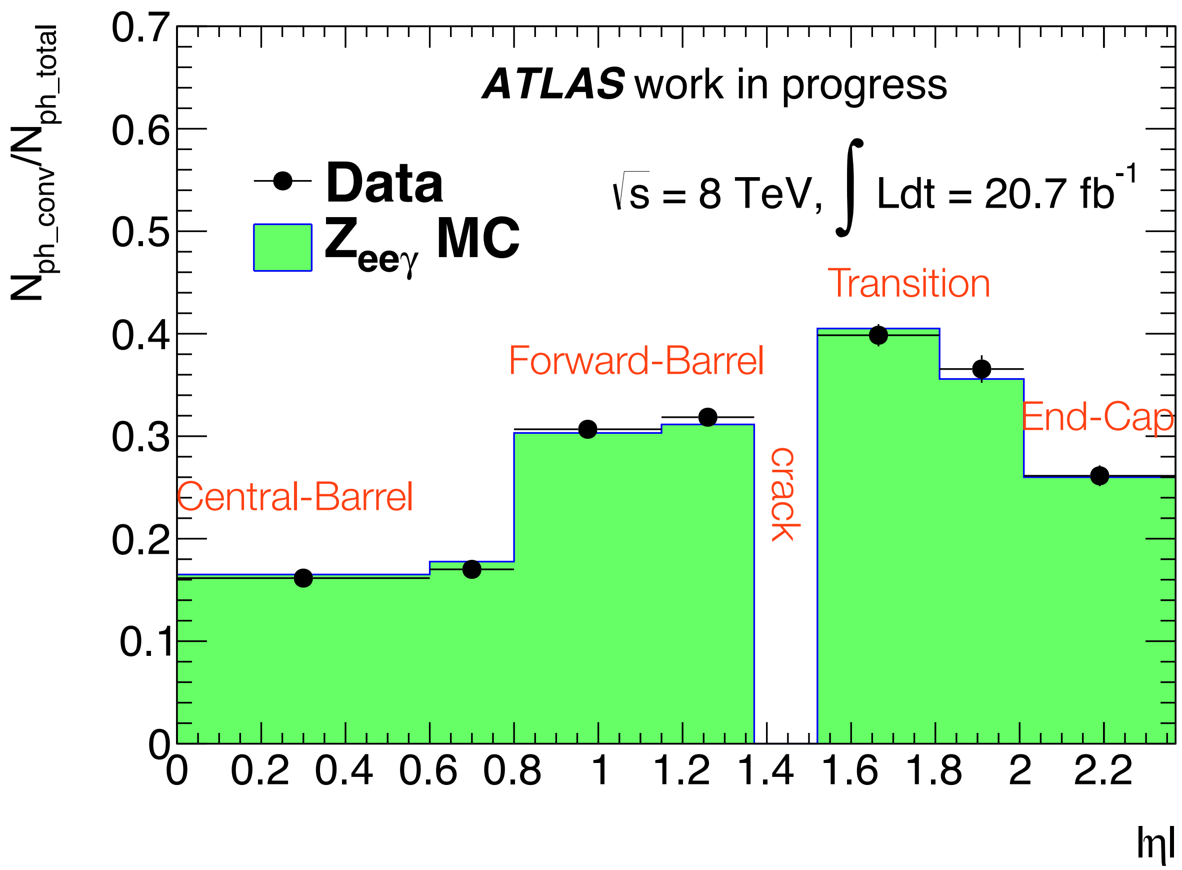

Plot from my $Z \rightarrow ll\gamma$ studies

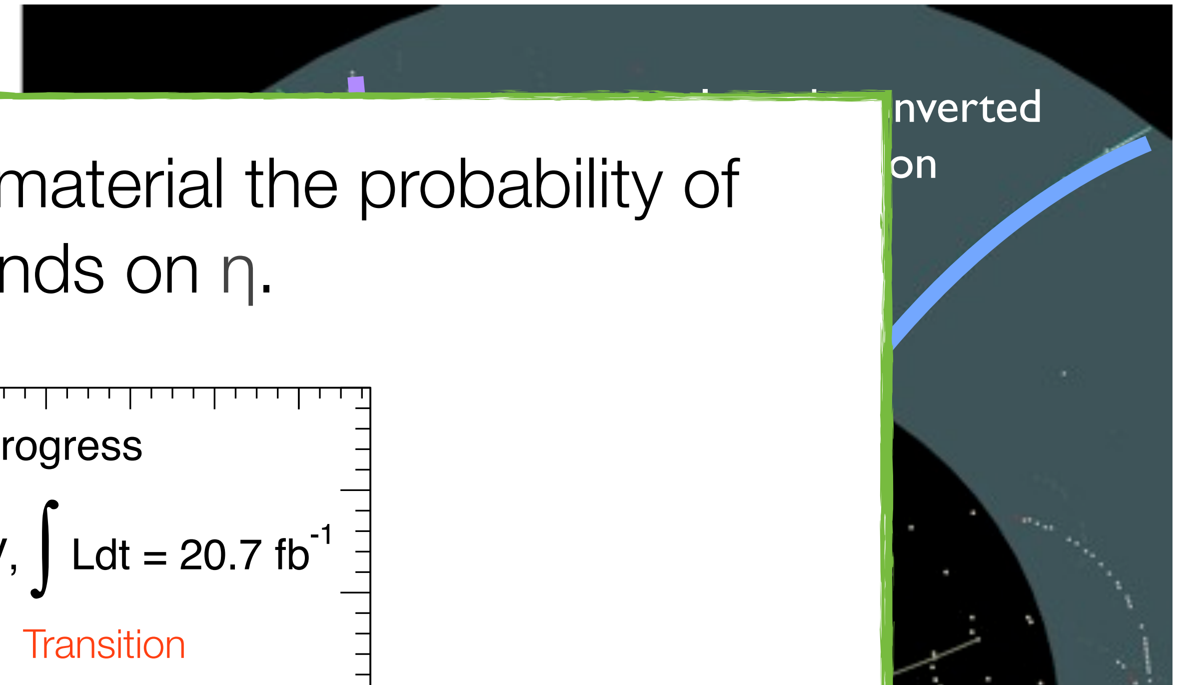

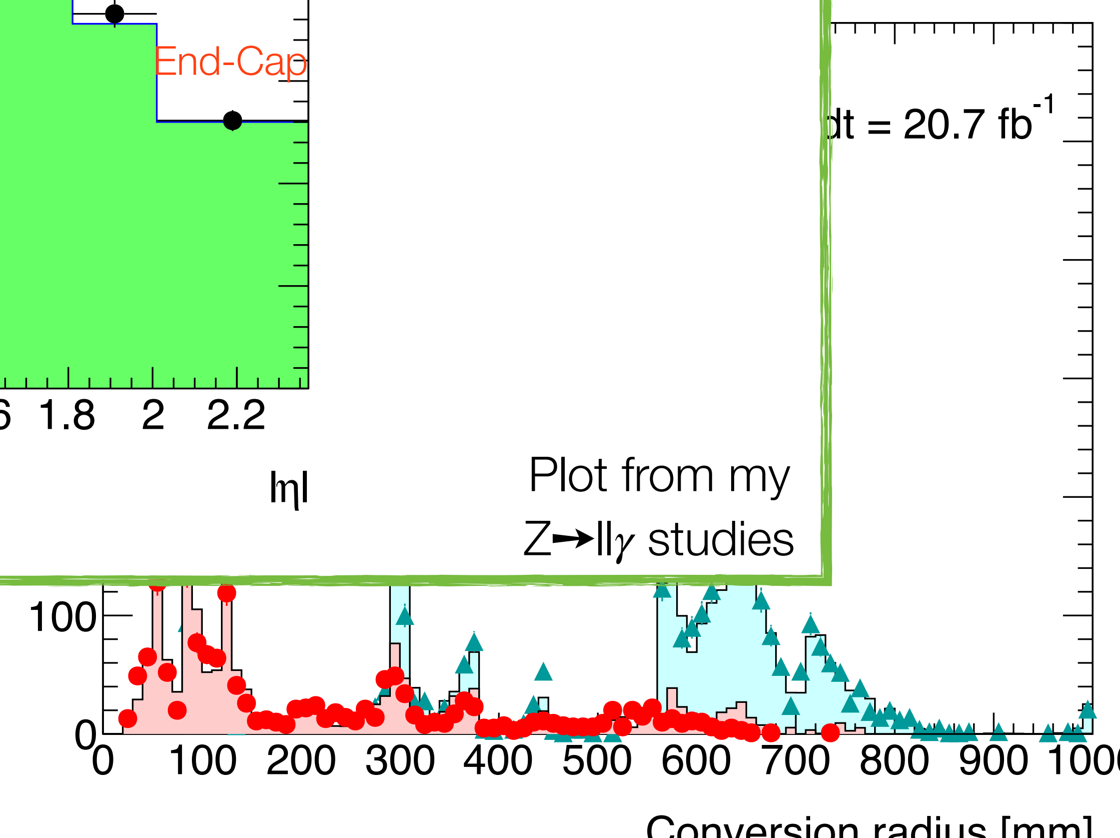

Energy reconstruction

- ✓ The cluster size is different between electrons and photons and calorimeter regions

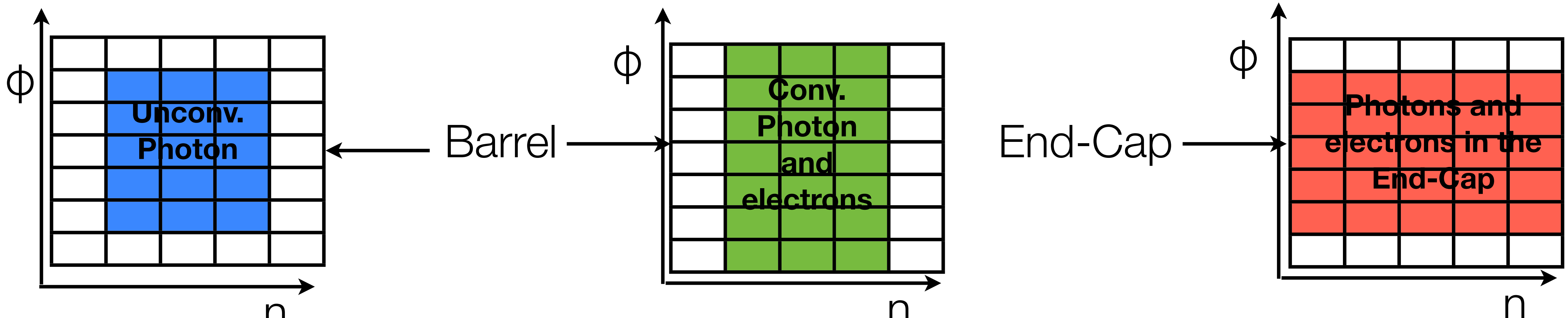

- ✓ A high voltage creates an electric field that allows the drifting of ionisation electrons in the LAr gap creating a signal current with is is collected in the electrodes.

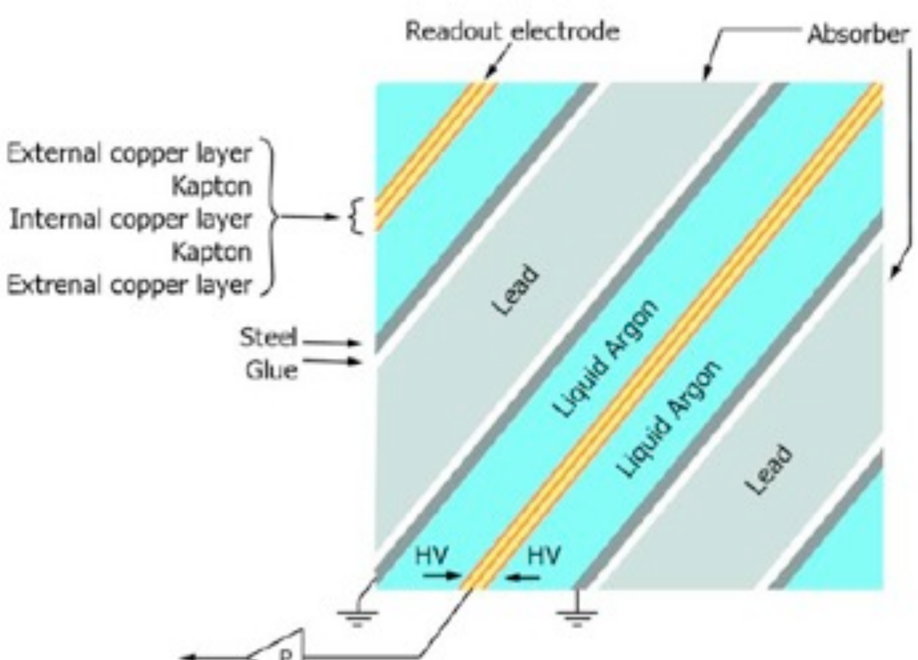

I investigated the effect of resistances from the electrodes in the energy measurement.

The effect is small in most regions of the detector, with the luminosities corresponding to LHC Run I.

ATL-LARG-INT-2013-003

- ✓ Total energy in the cluster is calculated from the energy in the individual layers. This inter-calibration is extracted from dedicated MC simulations.

Electron calibration

- Electrons from Z ➙ ee are used to EM scale on data (in-situ calibration)
  - Compares the Z peak in data and MC
  - Corrects the data energy scale (ES) for non-uniformities (within 1% in the barrel)
  - From differences in the peak resolution (data and MC) the constant term in data is extracted (~1% in the barrel, up to 3% in the end-caps)

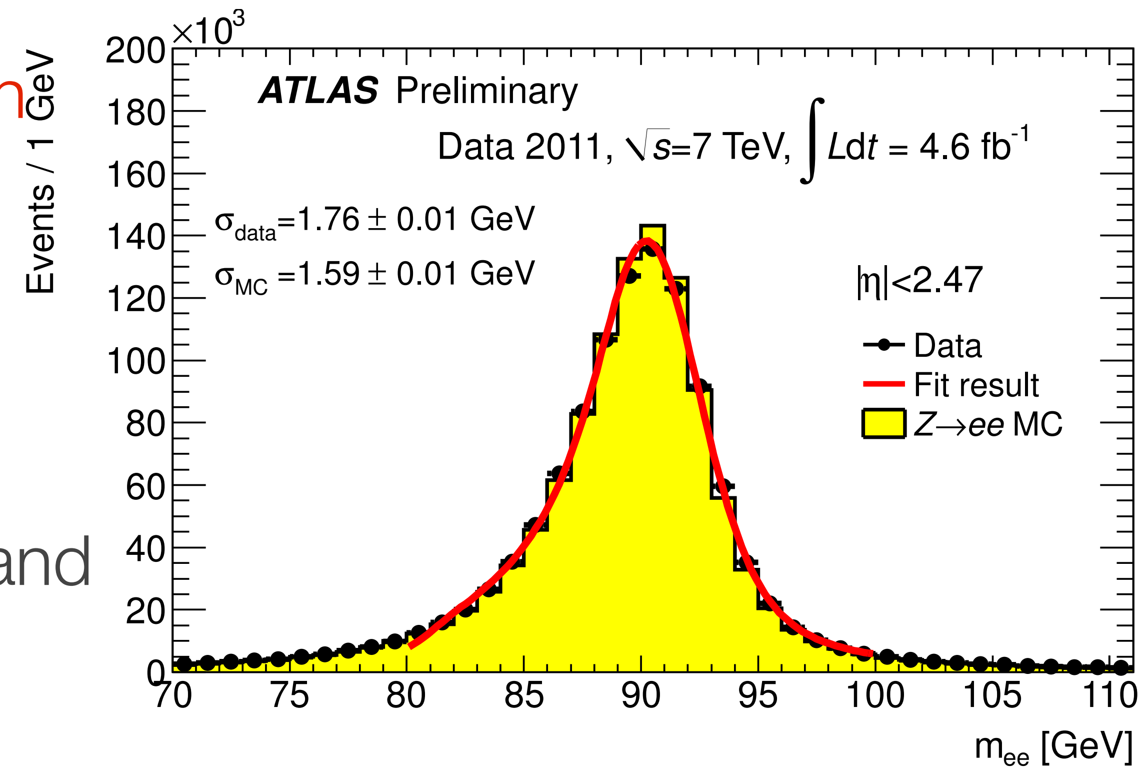

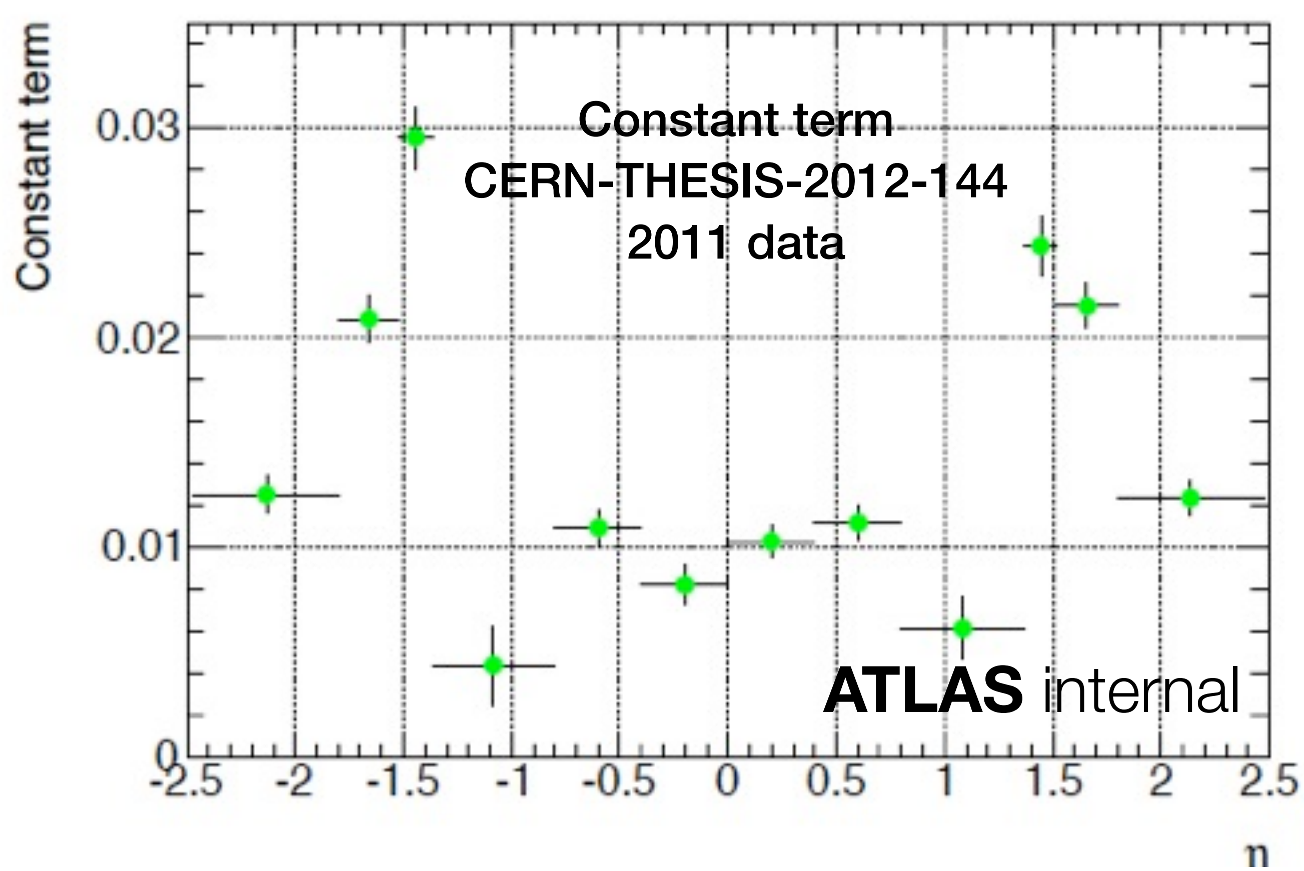

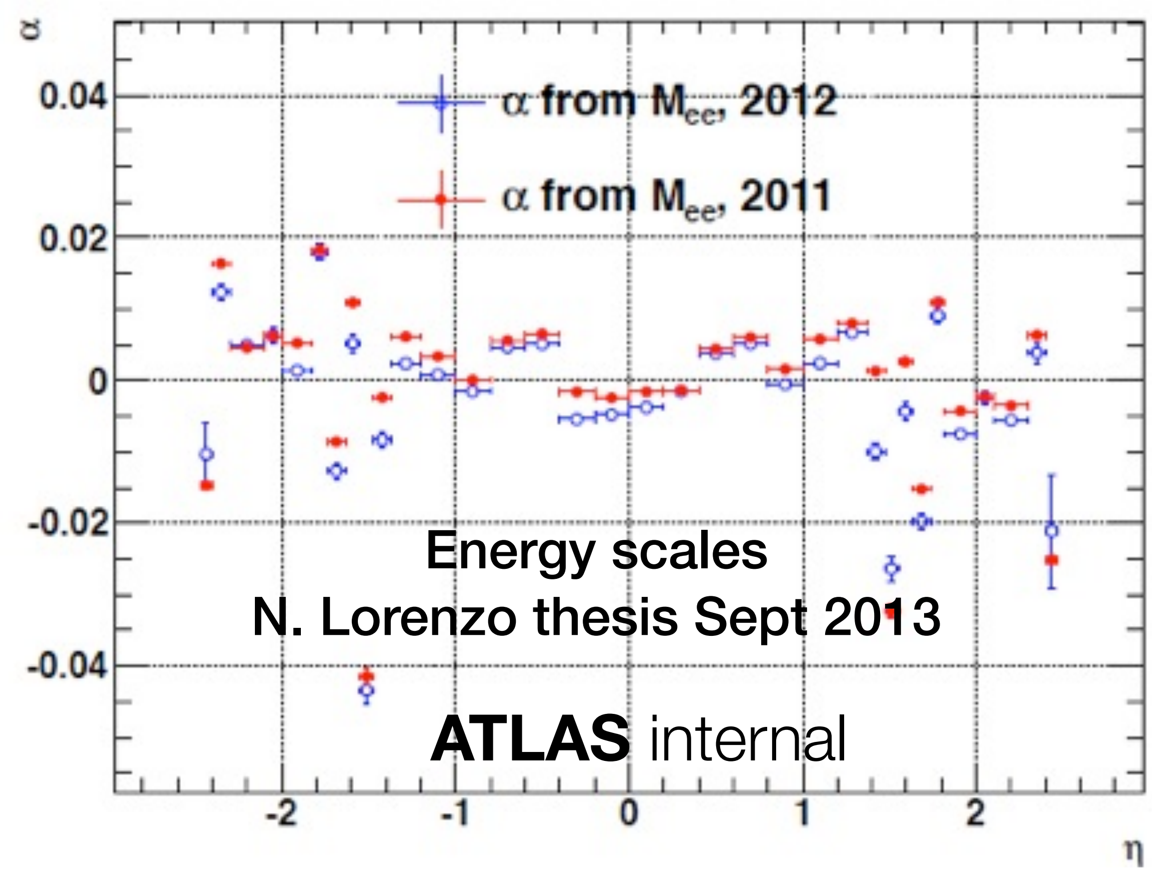

Photon calibration

- Electrons from Z ➞ ee are used to EM scale on data (in-situ calibration)
  - Compares the Z peak in data and MC
  - Corrects the data energy scale (ES) for non-uniformities (within 1% in the barrel)
  - From differences in the peak resolution (data and
MC) the
(~1% in

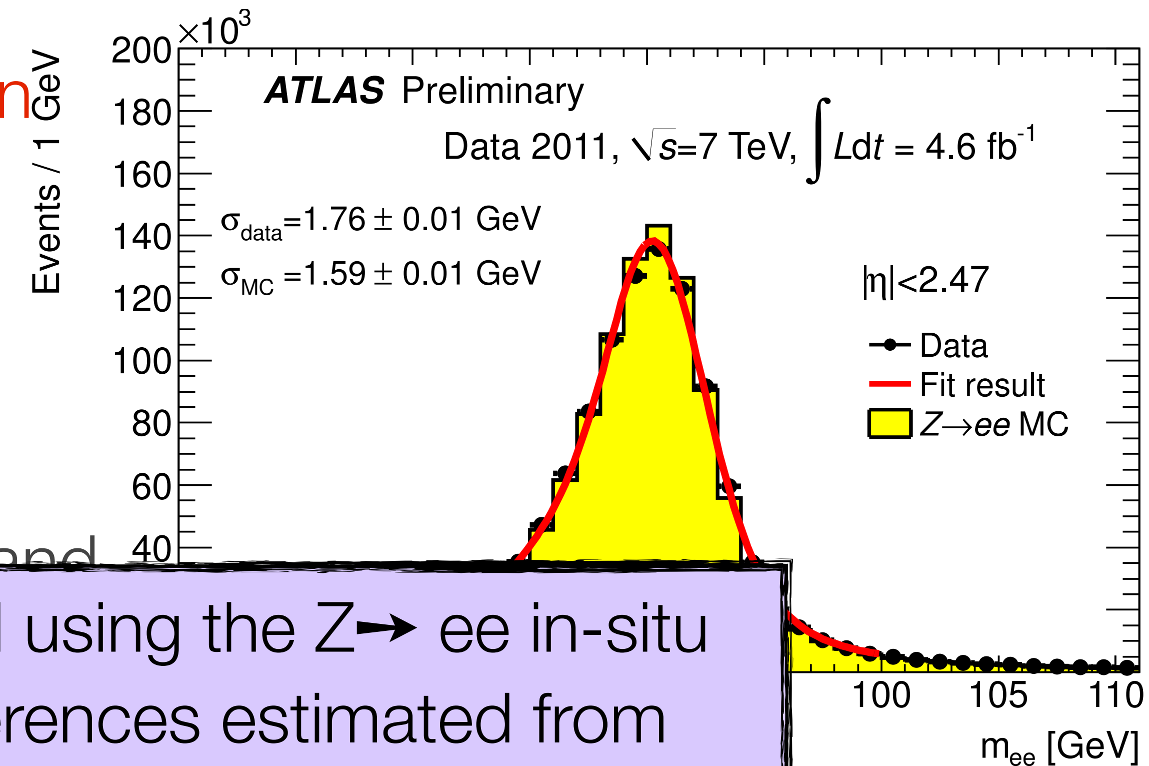

The photon energy scale is calibrated using the Z➞ ee in-situ scales, with systematics for e-γ differences estimated from dedicated MC simulations

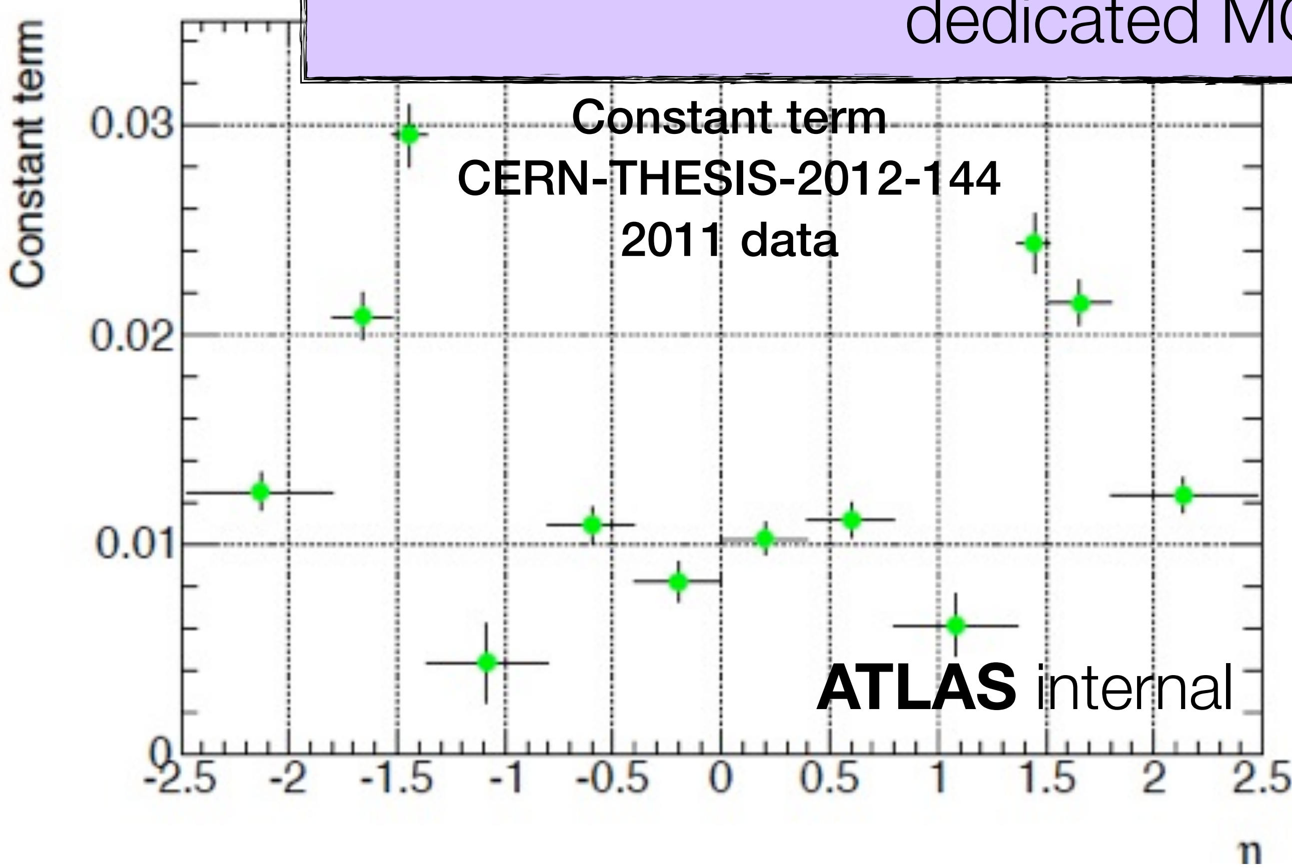

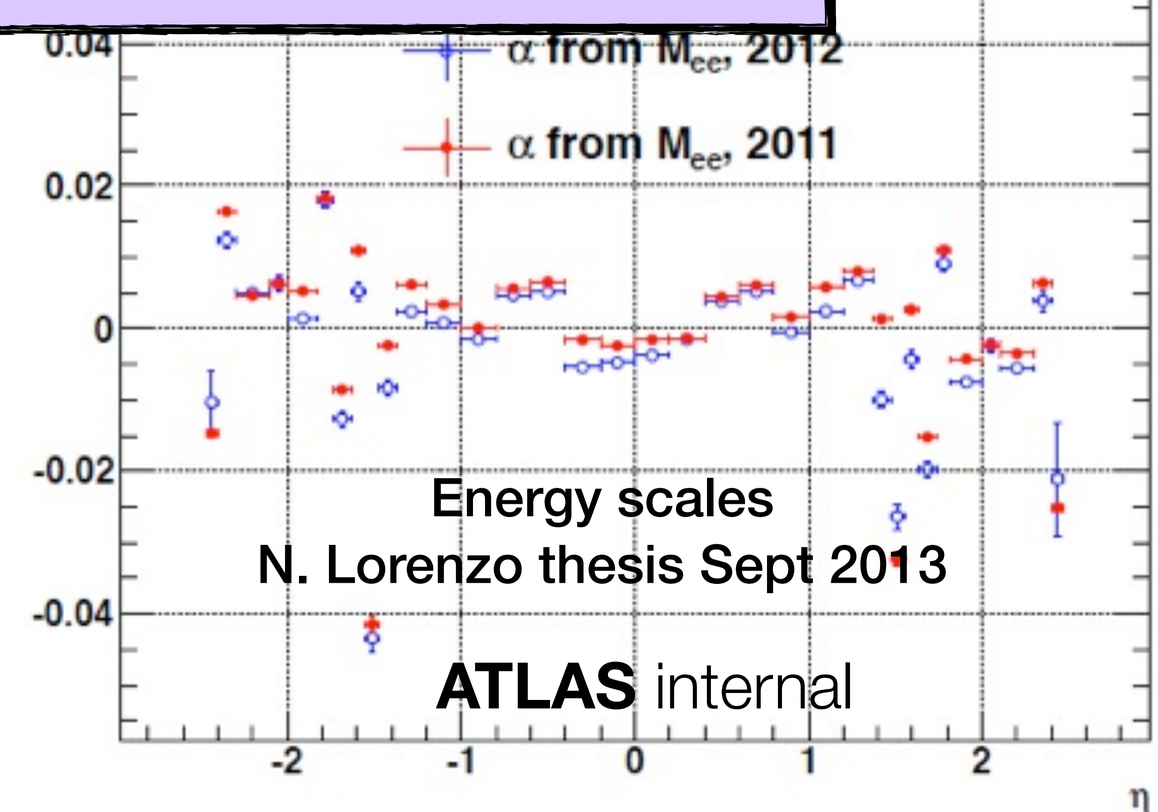

The H➞$\gamma\gamma$ analysis strategy

- Based on the diphoton invariant mass ($m\gamma\gamma$) as the main discriminating variable, which is built with a photon pair with well measured energies a directions.

- The $m\gamma\gamma$ spectrum is scanned from 110 to 150 GeV, looking for a narro resonance over a large smooth monotonically decreasing QCD background.

- The background is mainly composed by irreducible $\gamma\gamma$ (~75%), followed by the reducible γ-jet and di-jet (~25%).

Photon identification and isolation techniques suppress fake photons coming from jets.

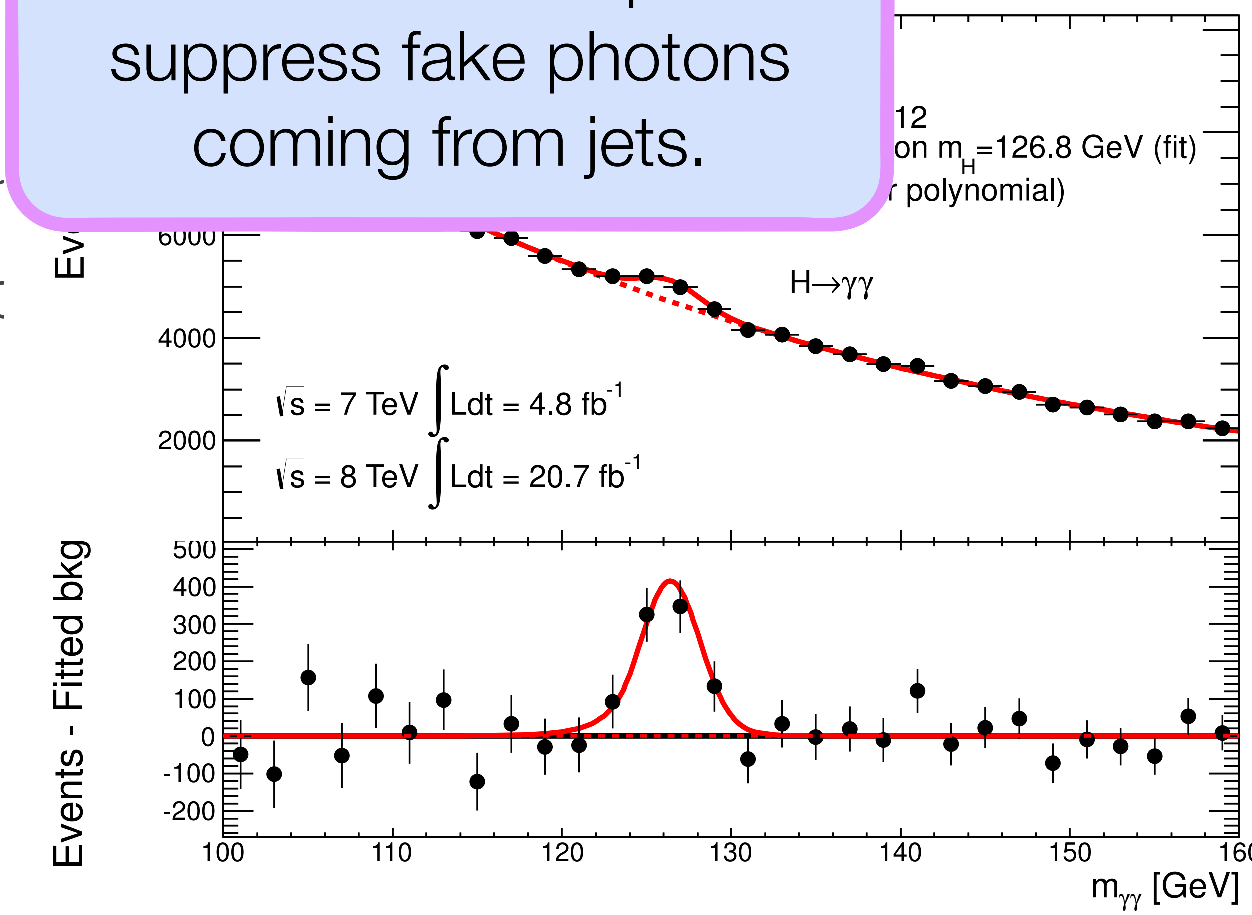

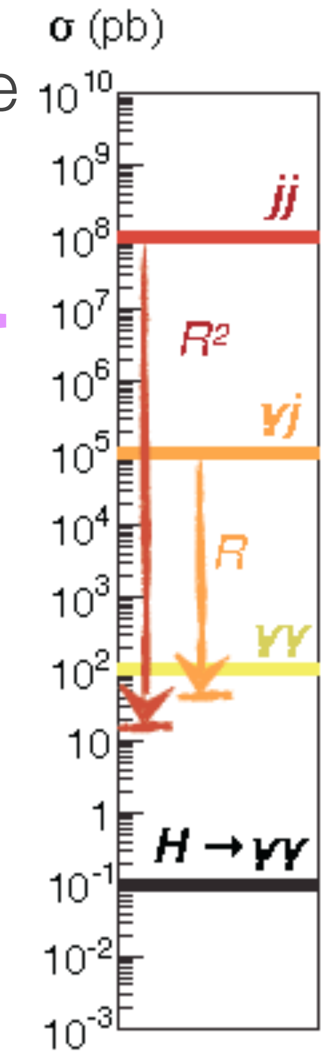

The H→$\gamma\gamma$ analysis strategy

- Based on the diphoton invariant mass ($m_{\gamma\gamma}$) as the main discriminating variable, which is built with a photon pair with well measured energies and directions.

- The $m_{\gamma\gamma}$ spectrum is scanned from 110 to 150 GeV, looking for a **narrow resonance** over a large smooth monotonically decreasing QCD background.

- The background is mainly composed by irreducible $\gamma\gamma$ (~75%), followed by the reducible (~25%).

how is it modelled?

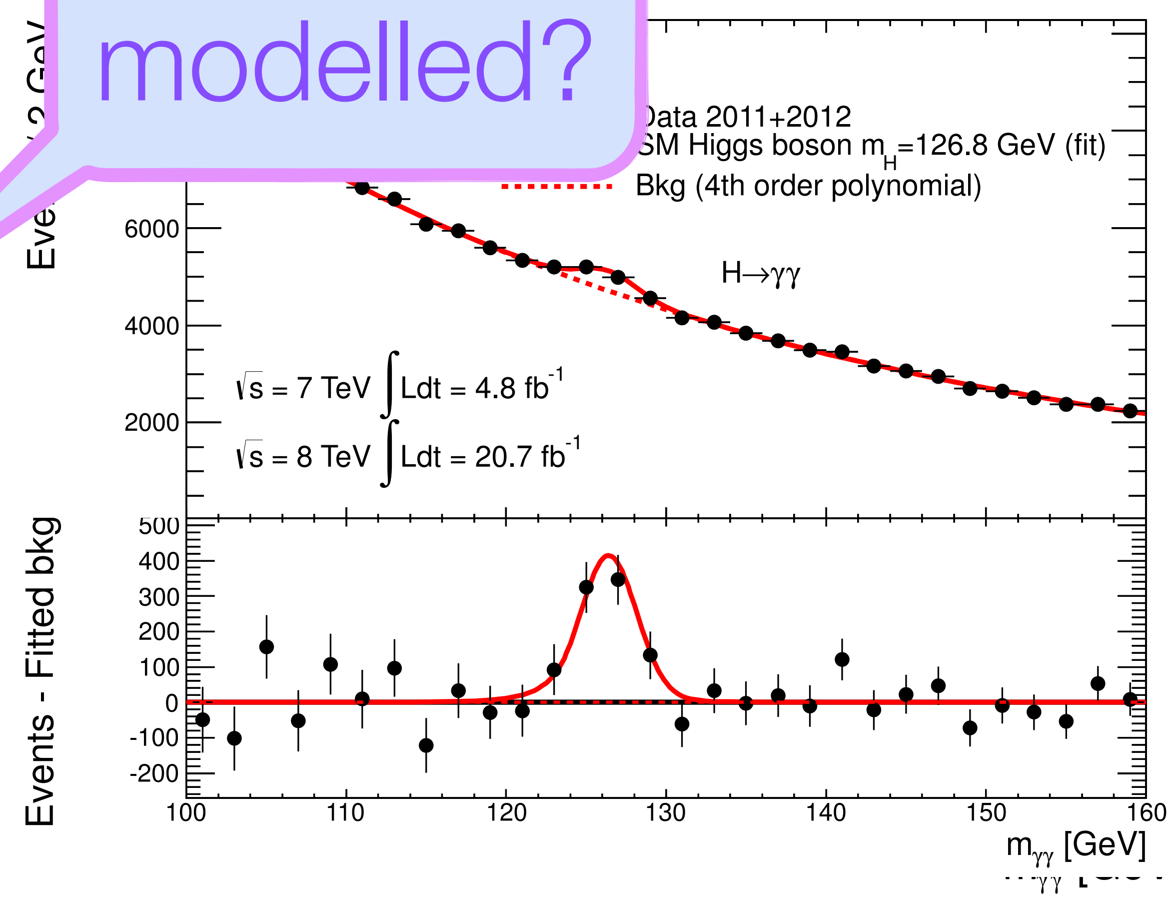

Signal mass, strength and significance

In a discovery logic the **Resolution** is fundamental to quantify the statistical significance of the signal!

Statistical significance

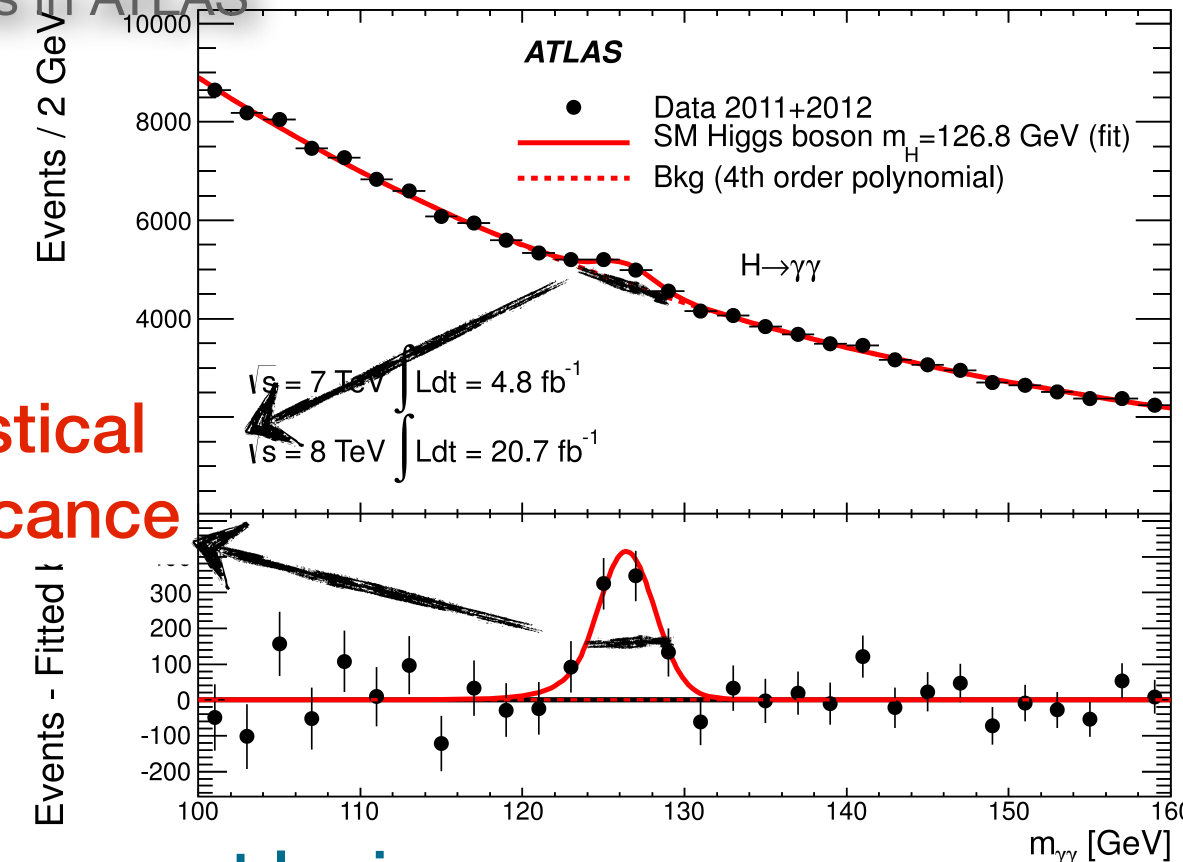

In a properties measurement logic:

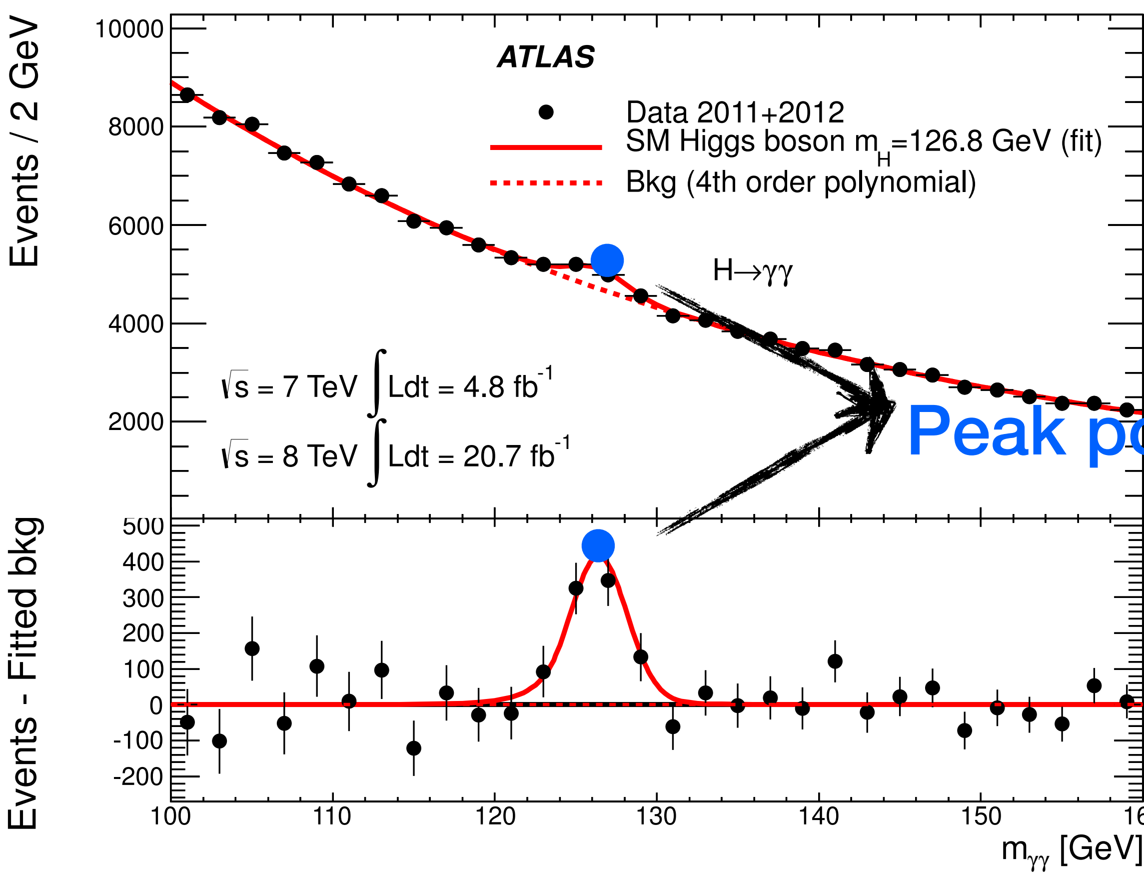

Peak position

Peak position is a fundamental input for the mass measurement!

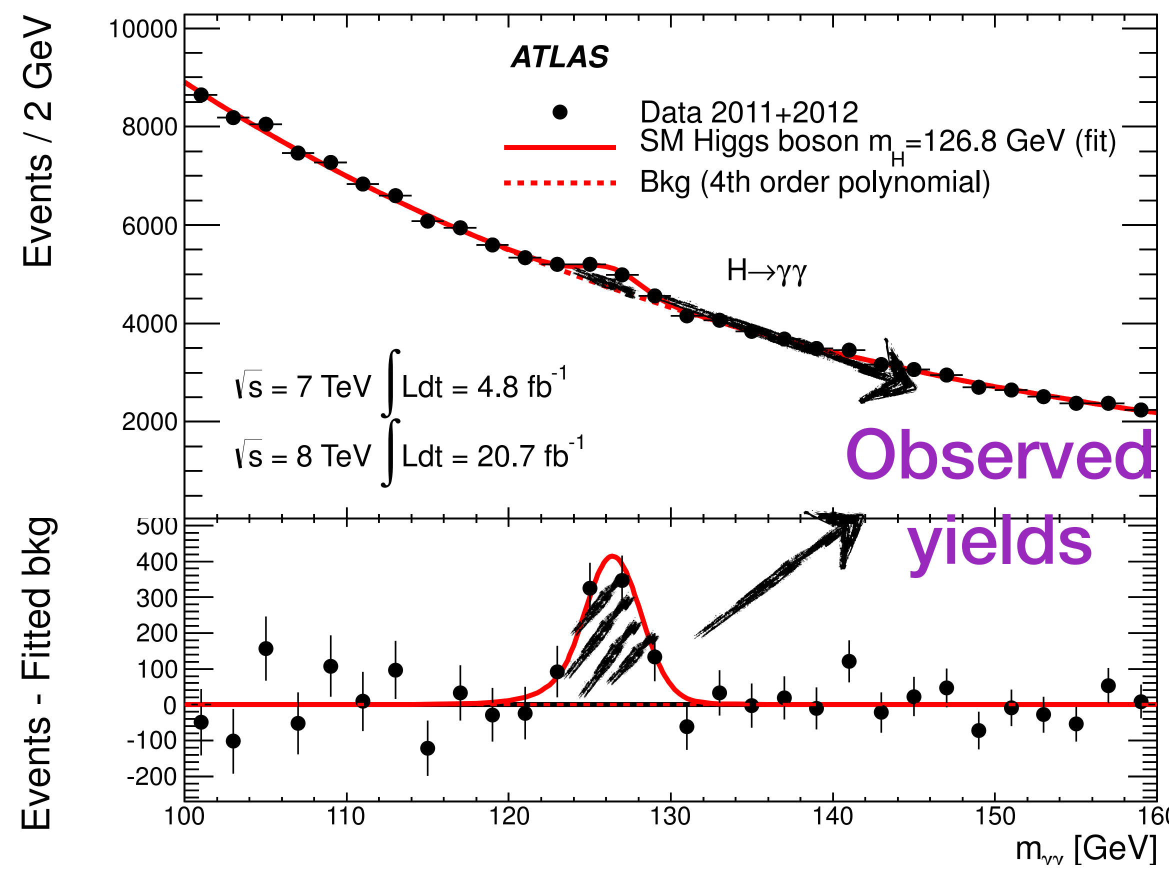

Observed yields

The **yields** are fundamental to the measurement of signal strength (μ) wrt the SM !

Signal invariant mass

$$M_{\gamma\gamma} = \sqrt{2E_{\mathrm{T}}^{1}E_{\mathrm{T}}^{2}\left[\cosh(\eta_1 - \eta_2) - \cos(\phi_1 - \phi_2)\right]},$$

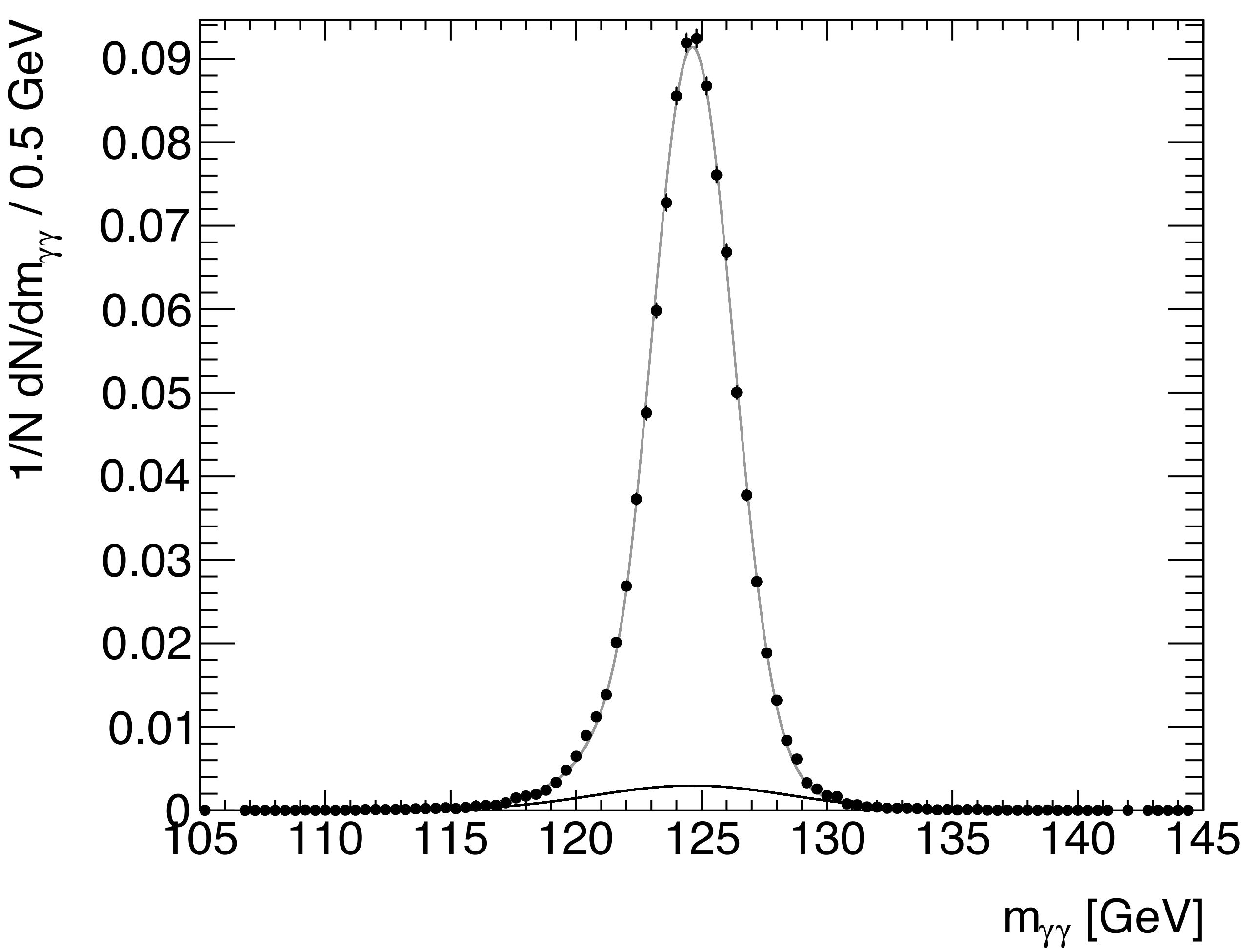

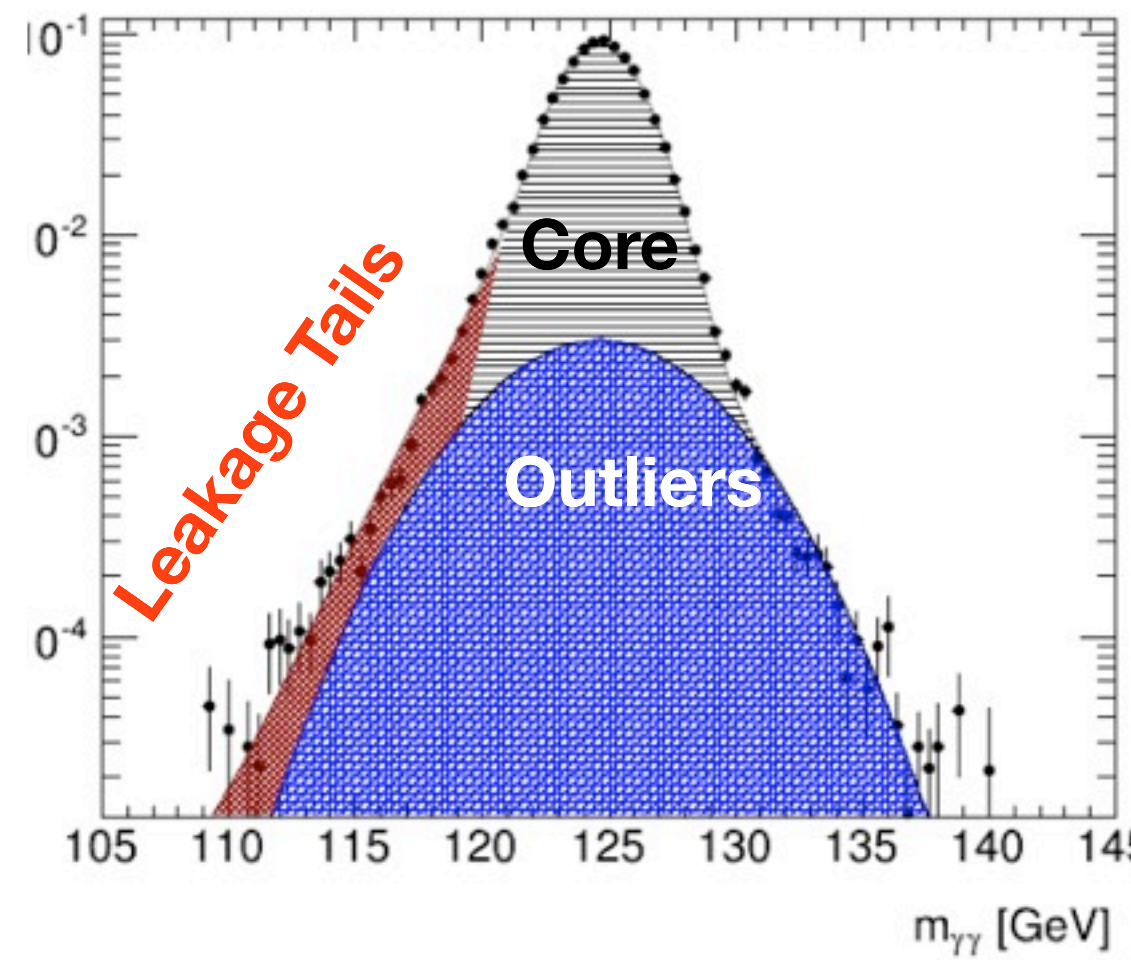

Signal invariant mass

The signal invariant mass at a fixed mH is modelled with a function of three components:

- Gaussian core
- Leakage tails → Crystal Ball function
- Outliers → Wide Gaussian

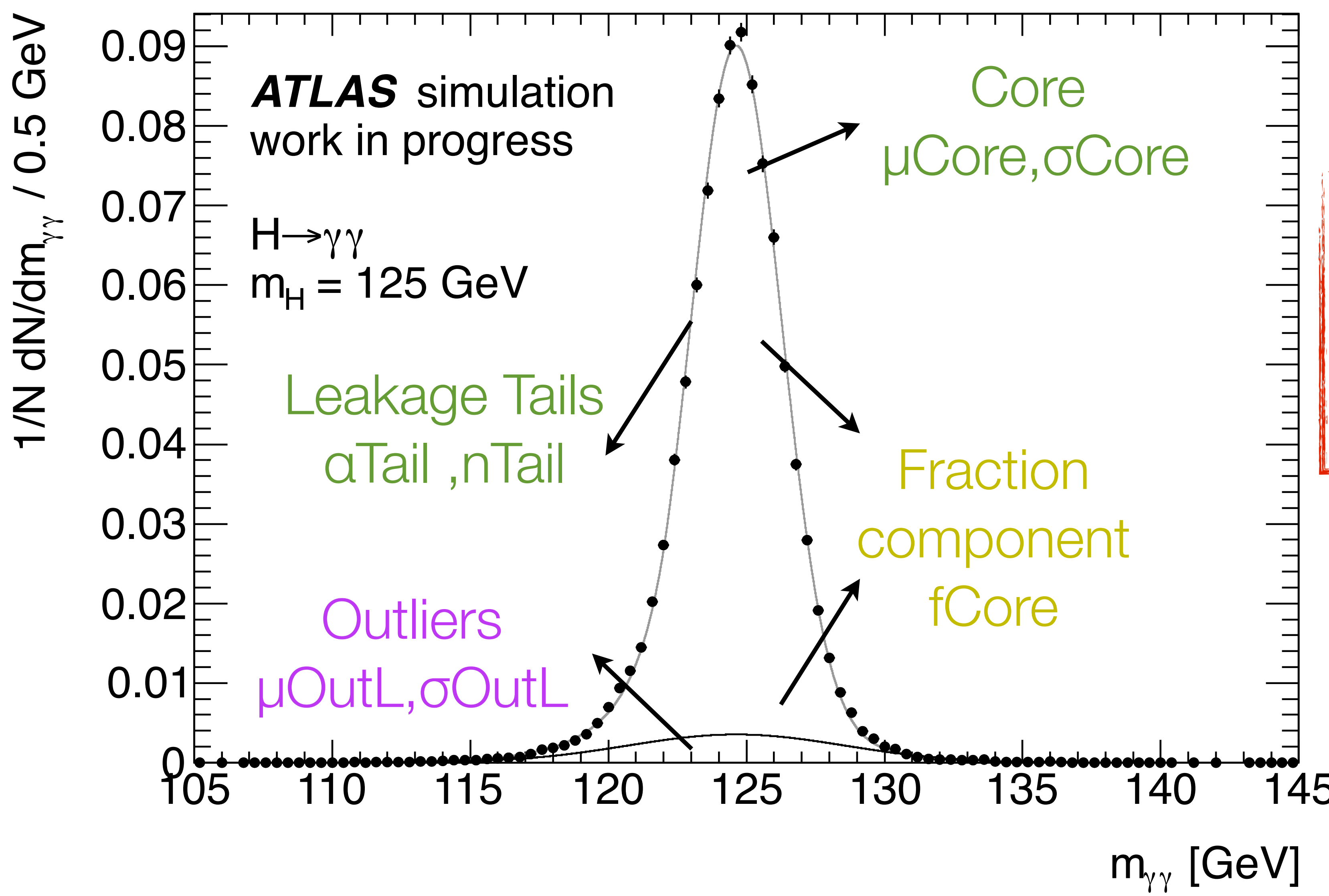

σCore = 1.7 GeV
Typical resolution in inclusive sample

The H➞$\gamma\gamma$ analysis strategy

- Based on the diphoton invariant mass ($m_{\gamma\gamma}$) as the main discriminating variable, which is built with a photon pair with well measured energies and directions.

- The background is mainly composed by irreducible $\gamma\gamma$ (~75%), followed by the reducible γ-jet and di-jet (~25%).

- The $m_{\gamma\gamma}$ spectrum is scanned from 110 to 150 GeV, looking for a narrow resonance over a large smooth monotonically decreasing QCD background.

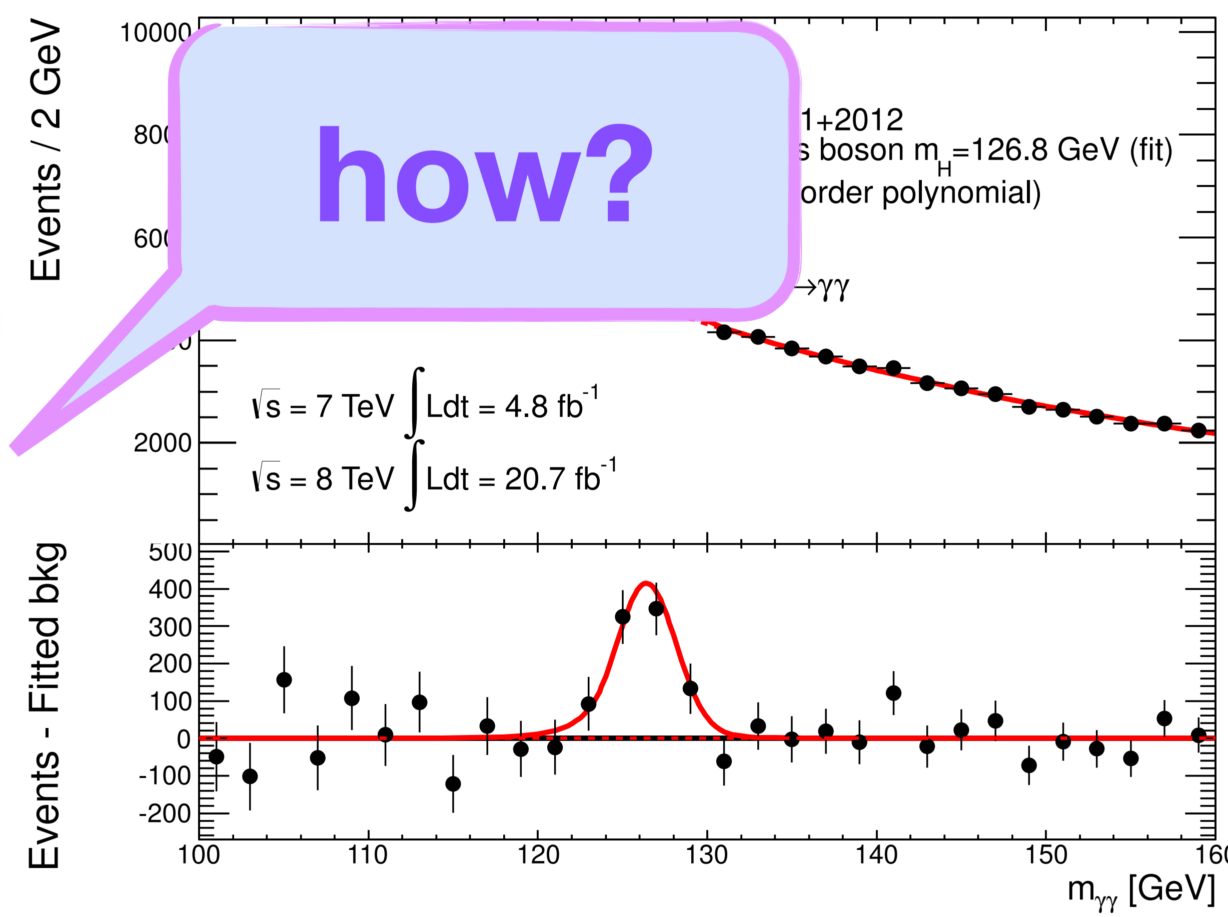

Likelihood function

- A likelihood function is built:

$$\mathcal{L}(\text{data}|\mu,\theta) = k^{-1}\prod_i^k (\mu S f_s(x) + B f_b(x)) \cdot e^{-(\mu S + B)}$$

m$\gamma\gamma$

Signal strength: a scale factor on the number of signal events wrt the SM

Signal and background PDFs as a function of the m$\gamma\gamma$

S and B are the total expected signal and observed background events.

The compatibility of the data with hypothetical values of μ, is evaluated through a test statistic, based on the profile likelihood ratio (CLs method).

Likelihood function

- A likelihood function is built:

$\mathcal{L}($ … $B)$

Numb … total
in the … and
… nts.

… f the

Background model $f_b(m_{\gamma\gamma})$:

One function for the whole mass range .

The models usually used are a single exponential,exponential of a polynomial or a high order polynomial (4th)... and is extracted from data.

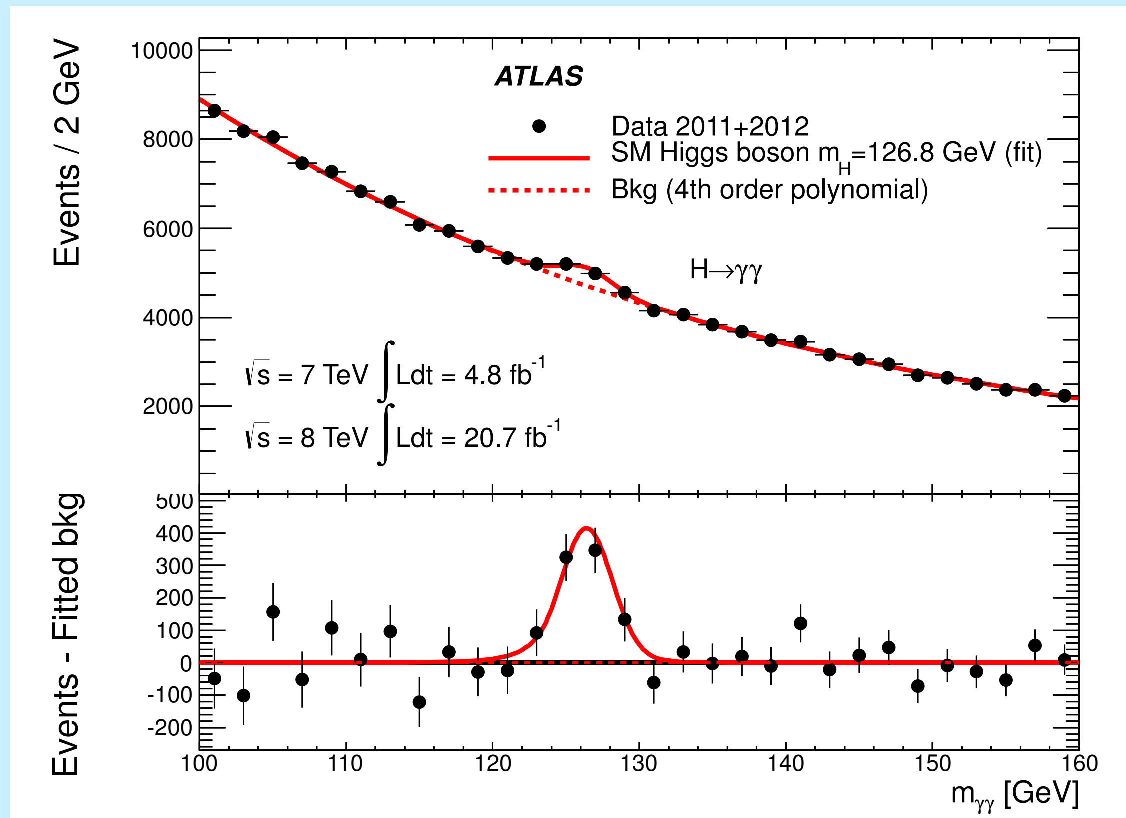

The compatibility of the data with hypothetical values of μ, is evaluated through a test statistic, based on the profile likelihood ratio (CLs method).

Likelihood function

- A likelihood function is built:

$\mathcal{L}($ … $B)$

Background model $f_b(m_{\gamma\gamma})$:

$f_b(m$
used
exp
poly
poly

Numb
in the

total
and
nts.

of the

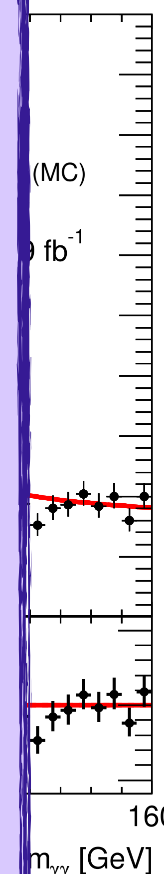

Signal model $f_S(m\gamma\gamma)$:

As for the background, we need a signal model valid in the 110-150 GeV range.

The signal MC samples are generated in 5 GeV mH steps, therefore an interpolation of the invariant mass PDF is needed.

My main contribution to the official H➝γγ analysis is the signal modelling, the so-called "Global Resolution Function".

The compatibility of the data with hypothetical values of μ, is evaluated through a test statistic, based on the profile likelihood ratio (CLs method).

Global resolution model

- The global resolution model is an analytical function of mH, with a full description of the signal in the whole mass range.

- Resolution follows a “self-similar" dependence with mass, i.e. its core peak is displaced with mass, its width scales monotonically with mass and tails are mass-independent.

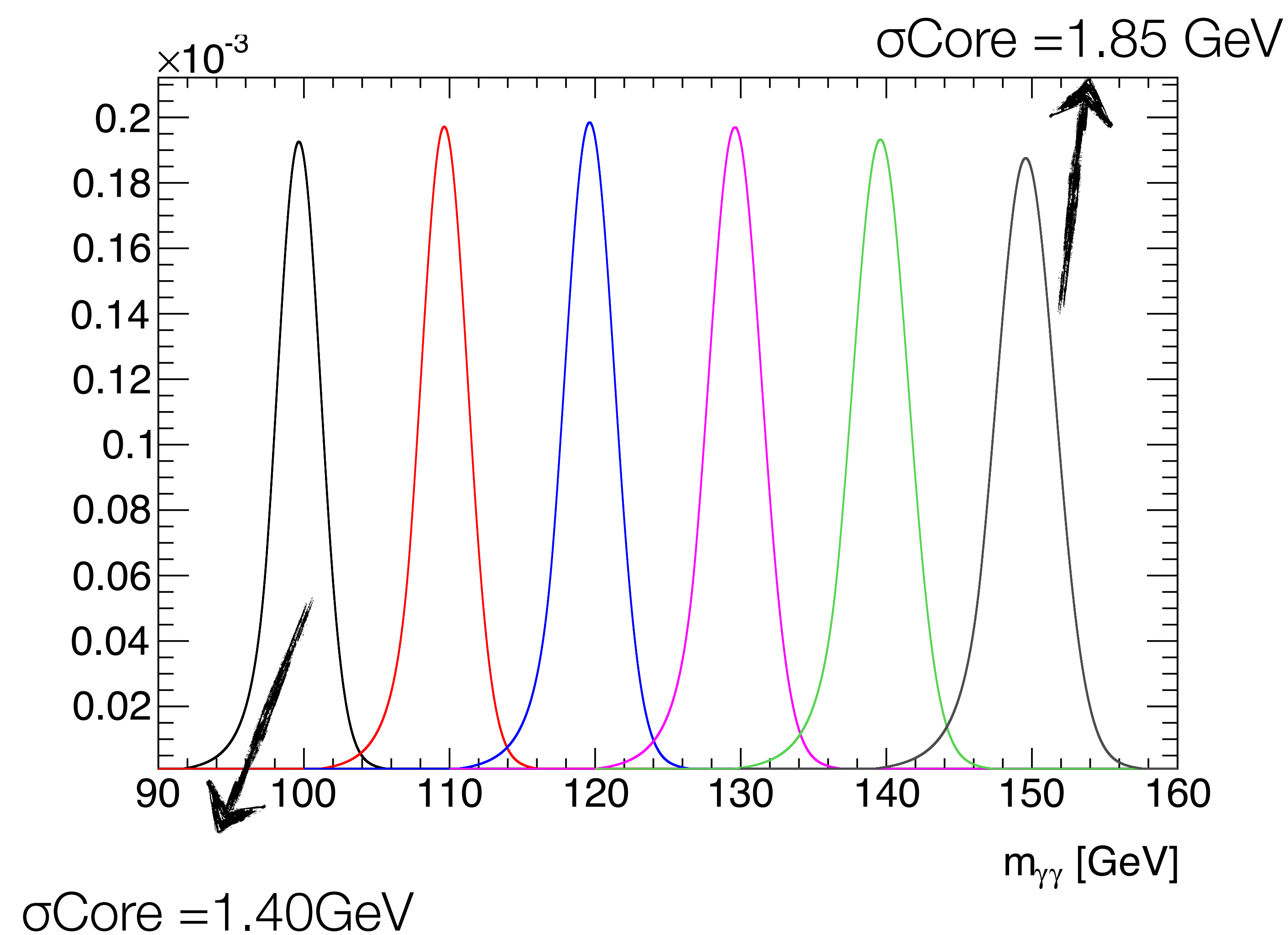

The parameters depending on mH are identified and both global and mass dependent parameters are extracted from a simultaneous two dimensional ($m_{\gamma\gamma}$ vs mH) fit to the MC samples.

Global resolution model

In summary: An analytical function of the mass with a reduced number of free parameters that describes the shape at all mass points.

Mass dependent parameters:

$\sigma Core\ (mH) = \sigma Core(125\ GeV) + \Delta_{\sigma Core} \times (mH - 125\ GeV)$

Typical value 10 MeV/GeV

$\Delta\mu Core\ (mH) = \Delta\mu Core(125\ GeV) + \Delta_{\mu Core} \times (mH - 125\ GeV)$

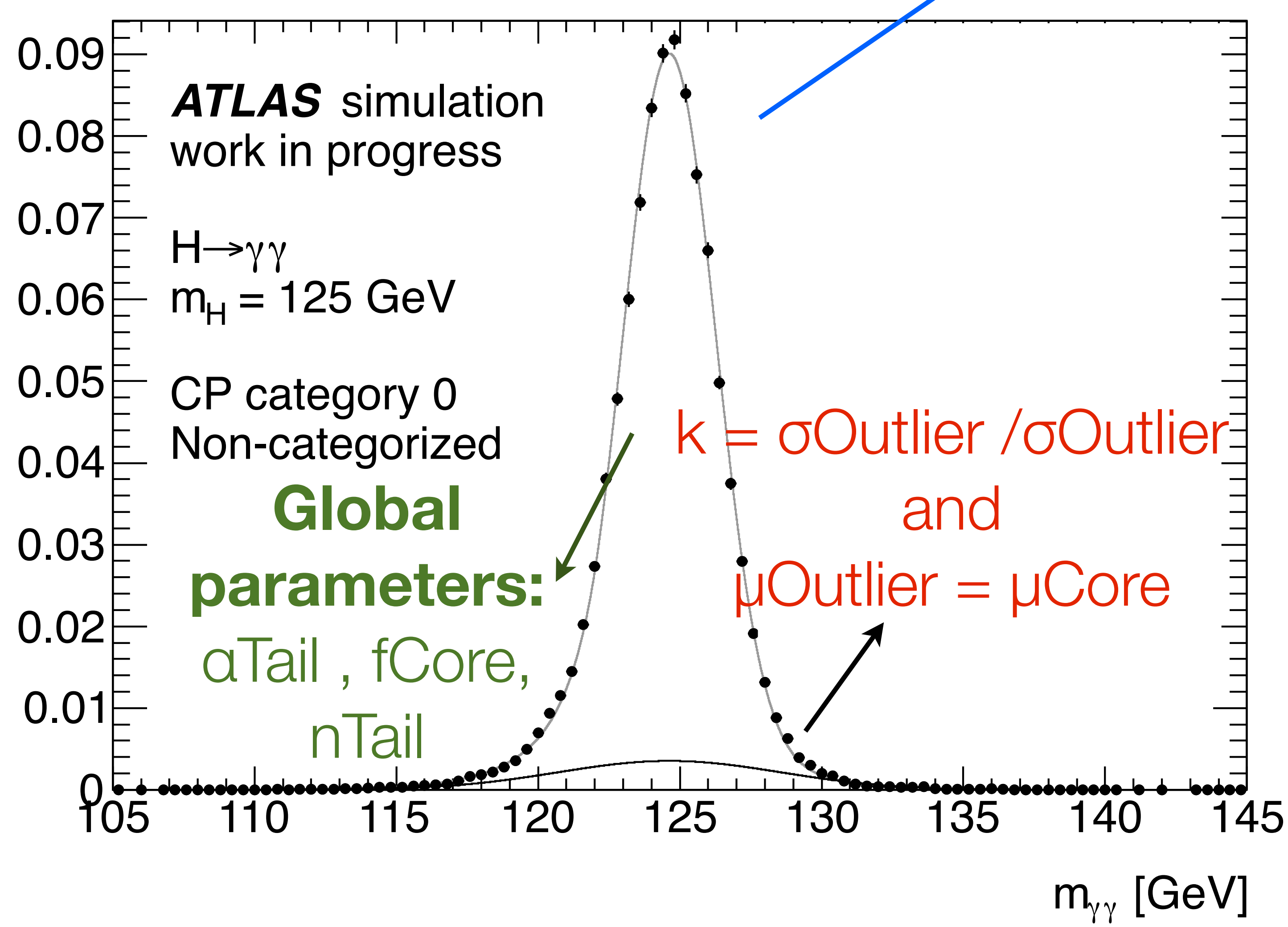

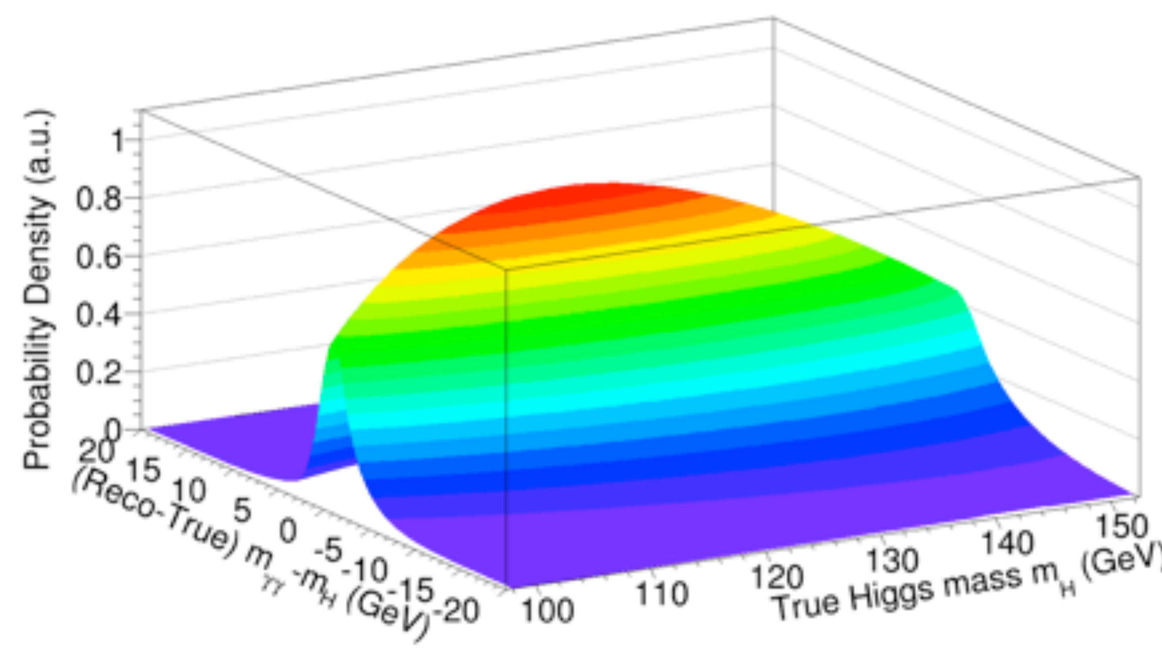

Global resolution model

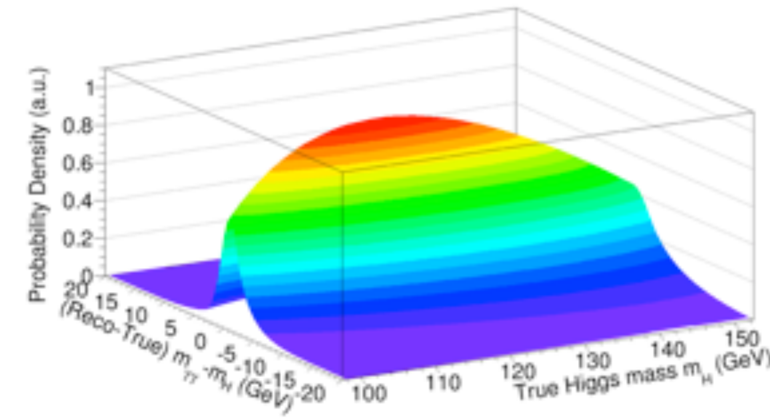

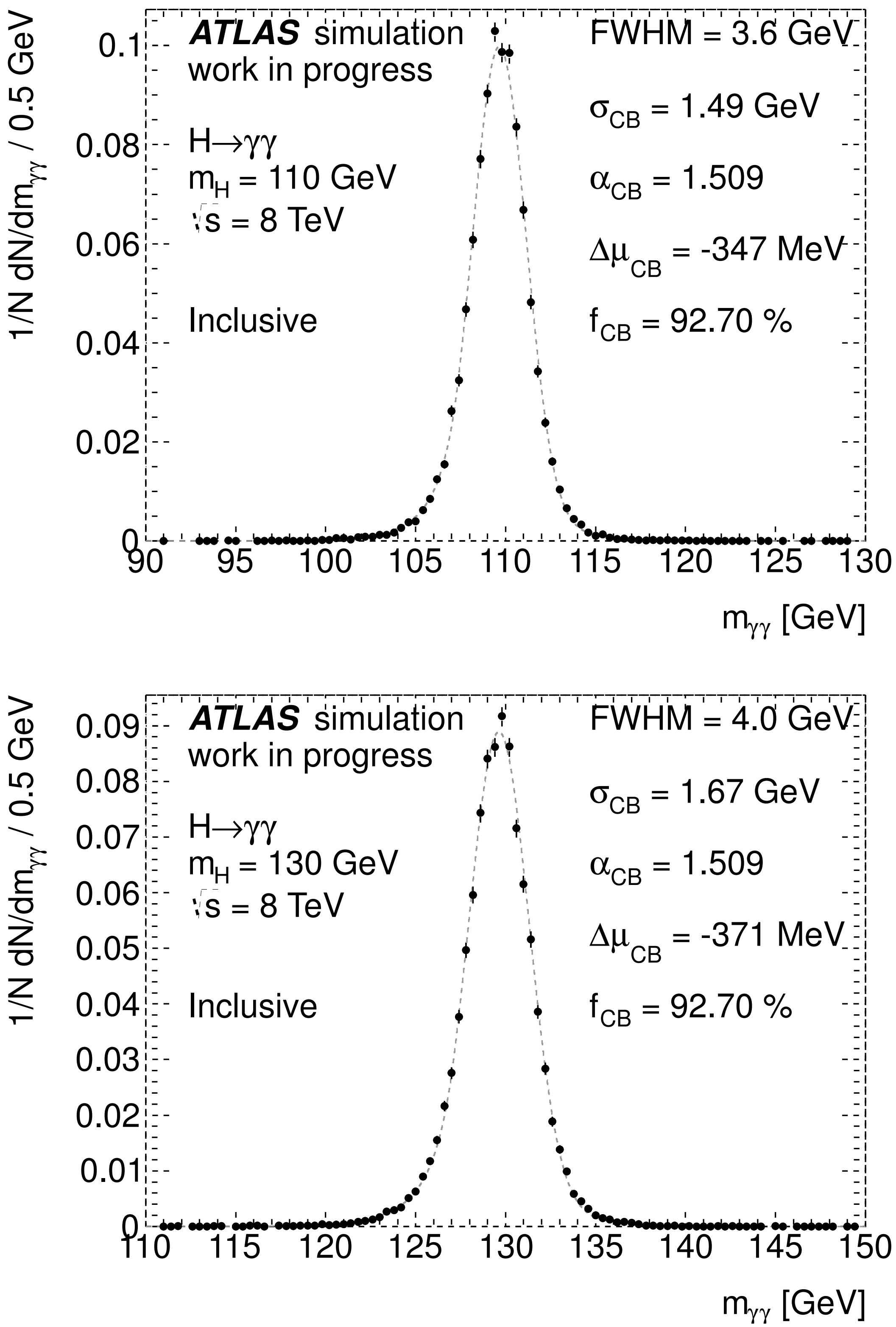

Validation of the global resolution model: PDF slice superimposed over the MC at different mass points.

Analytical function of the yields

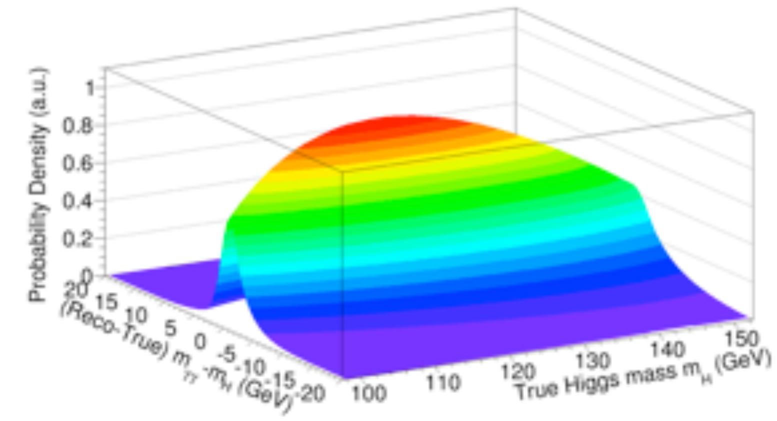

Reconstruction efficiency increases with mH, the XS and BR are functions of mH.
The expected yields are parameterised with a third order polynomial.

$$N(m_{\gamma\gamma}) = N_{125\mathrm{GeV}}\left[1 + \lambda_{\mathrm{lin}}\frac{(m_{\gamma\gamma}-125\mathrm{GeV})}{25\mathrm{GeV}} + \lambda_{\mathrm{sqrt}}\frac{(m_{\gamma\gamma}-125\mathrm{GeV})^2}{(25\mathrm{GeV})^2} + \lambda_{\mathrm{cubic}}\frac{(m_{\gamma\gamma}-125\mathrm{GeV})^3}{(25\mathrm{GeV})^3}\right]$$

	$gg \to H$		VBF		WH		ZH		ttH		Total
m_H [GeV]	$\varepsilon(\%)$	N_{evt}	$\varepsilon(\%)$	N_{evt}	$\varepsilon(\%)$	N_{evt}	$\varepsilon(\%)$	N_{evt}	$\varepsilon(\%)$	N_{evt}	N_{evt}
110	33.7	100.3	34.4	7.3	29.8	3.7	29.4	2.1	27.2	0.6	114.0
115	35.5	103.5	36.1	7.9	30.5	3.6	32.3	2.0	27.8	0.6	117.6
120	37.1	103.3	38	8.2	32.5	3.41	32.8	2.0	29.3	0.6	117.4
125	38.2	99.96	39.5	8.2	33.8	3.14	34.1	1.8	29.7	0.5	113.7
130	39	93.8	41.1	8	35.1	2.8	35.8	1.6	31	0.5	106.7
135	40.4	84.9	42.2	7.5	35.6	2.4	36.6	1.4	32.1	0.4	96.7
140	40.9	73.7	42.9	6.8	36.8	2.0	36.7	1.2	32.3	0.3	84.0
145	41.5	60.4	43.2	5.7	37.8	1.6	38.3	0.9	33.5	0.3	68.9
150	41.6	45.1	44.6	4.4	38.1	1.1	39.0	0.7	34.0	0.2	51.6

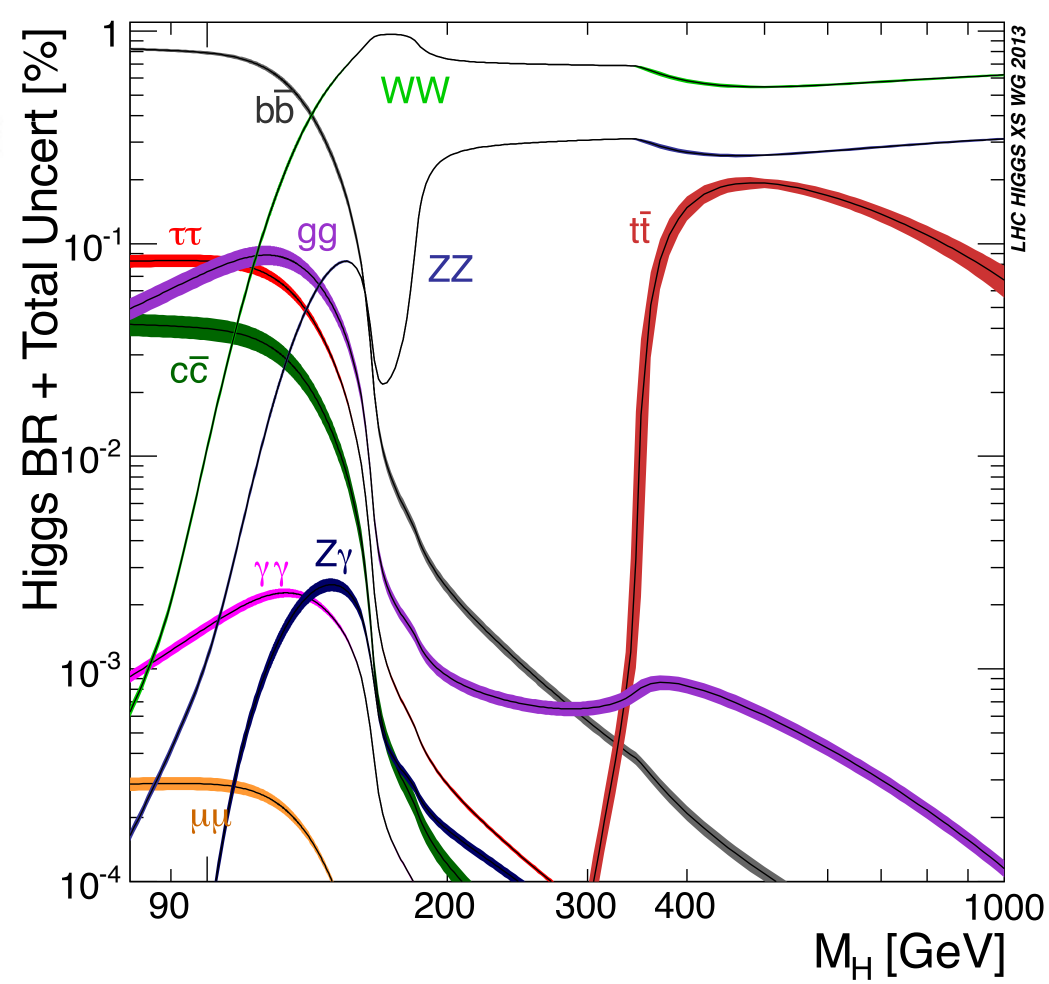

Categorisation

- Event categorisation increases the sensitivity of the search for a potential signal.
- Identify sub-samples with different discriminating power (i.e differences in resolutions and signal-to background ratios).

Good resolution,
less effective
background.
More sensitivity.

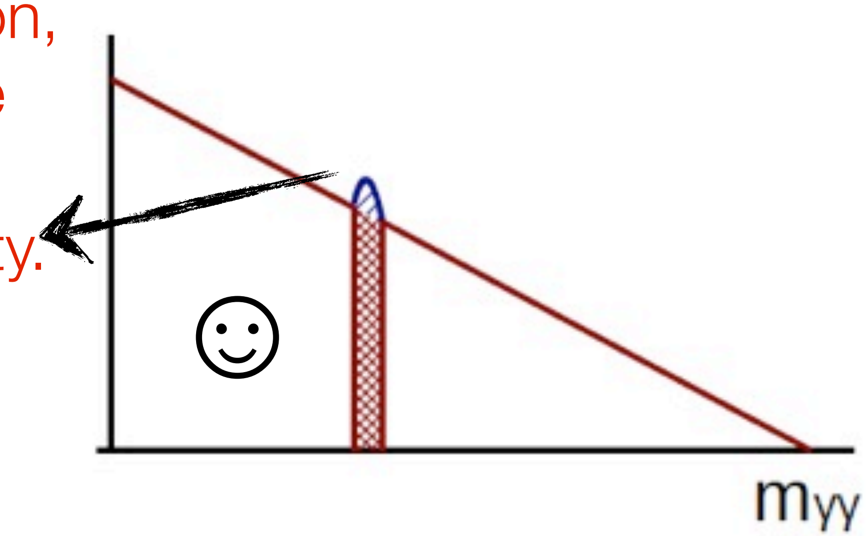

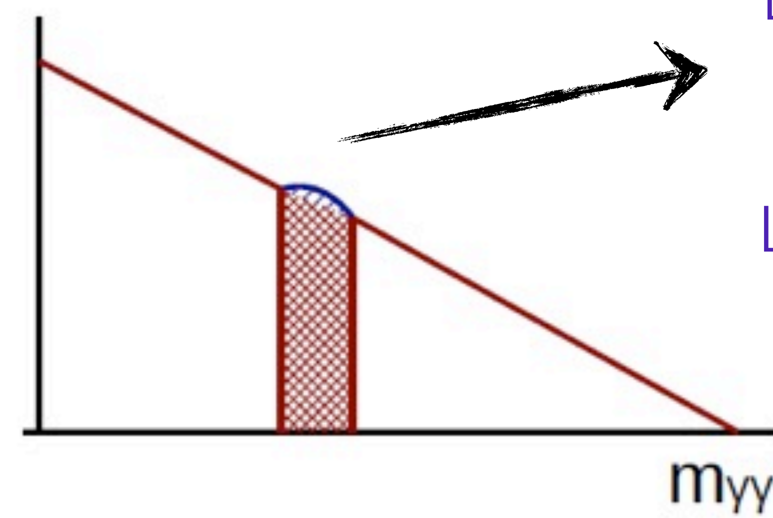

Bad resolution,
more effective
background.
Less sensitivity.

Good S/B.
More sensitivity.

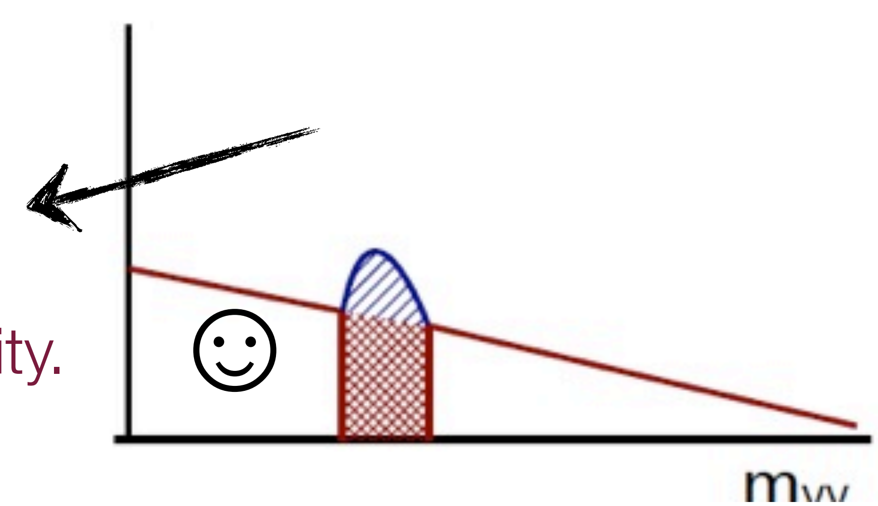

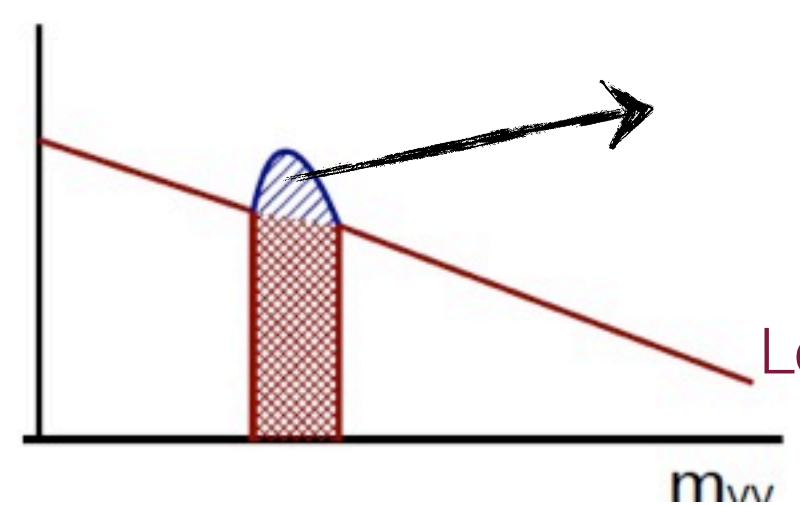

Bad S/B.
Less sensitivity.

Signal shape for conversion categories

- First ATLAS result (2010) was an inclusive analysis due to the low statistics (ATLAS-CONF-2011-004).
- With the increasing statistics in the 2011 dataset, categorisations were investigated.
- I investigated the resolution and calibration of the different types of photons (Unconverted, 1-track converted, 2-track converted), by studying the signal mass shape for different categories based in conversion status

Unconverted γ = 0

1-track conv γ = 1

2-track conv γ = 2

9 categories

γlead(2) γsubl (0)	γlead(2) γsubl (1)	γlead(2) γsubl (2)
γlead(1) γsubl (0)	γlead(1) γsubl (1)	γlead(1) γsubl (2)
γlead(0) γsubl (0)	γlead(0) γsubl (1)	γlead(0) γsubl (2)

Signal shape for conversion categories

γlead(2) γsubl (0)	γlead(2) γsubl (1)	γlead(2) γsubl (2)
γlead(1) γsubl (0)	γlead(1) γsubl (1)	γlead(1) γsubl (2)
γlead(0) γsubl (0)	γlead(0) γsubl (1)	γlead(0) γsubl (2)

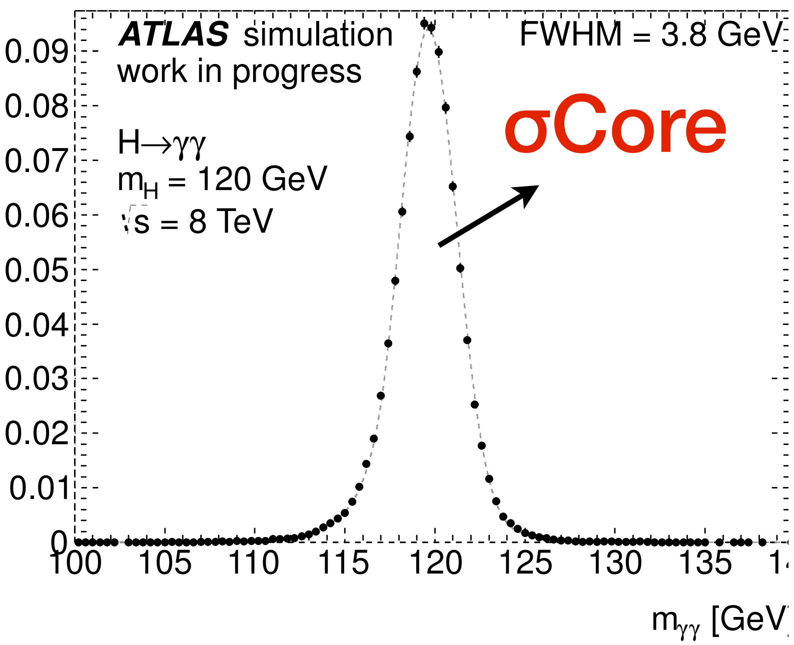

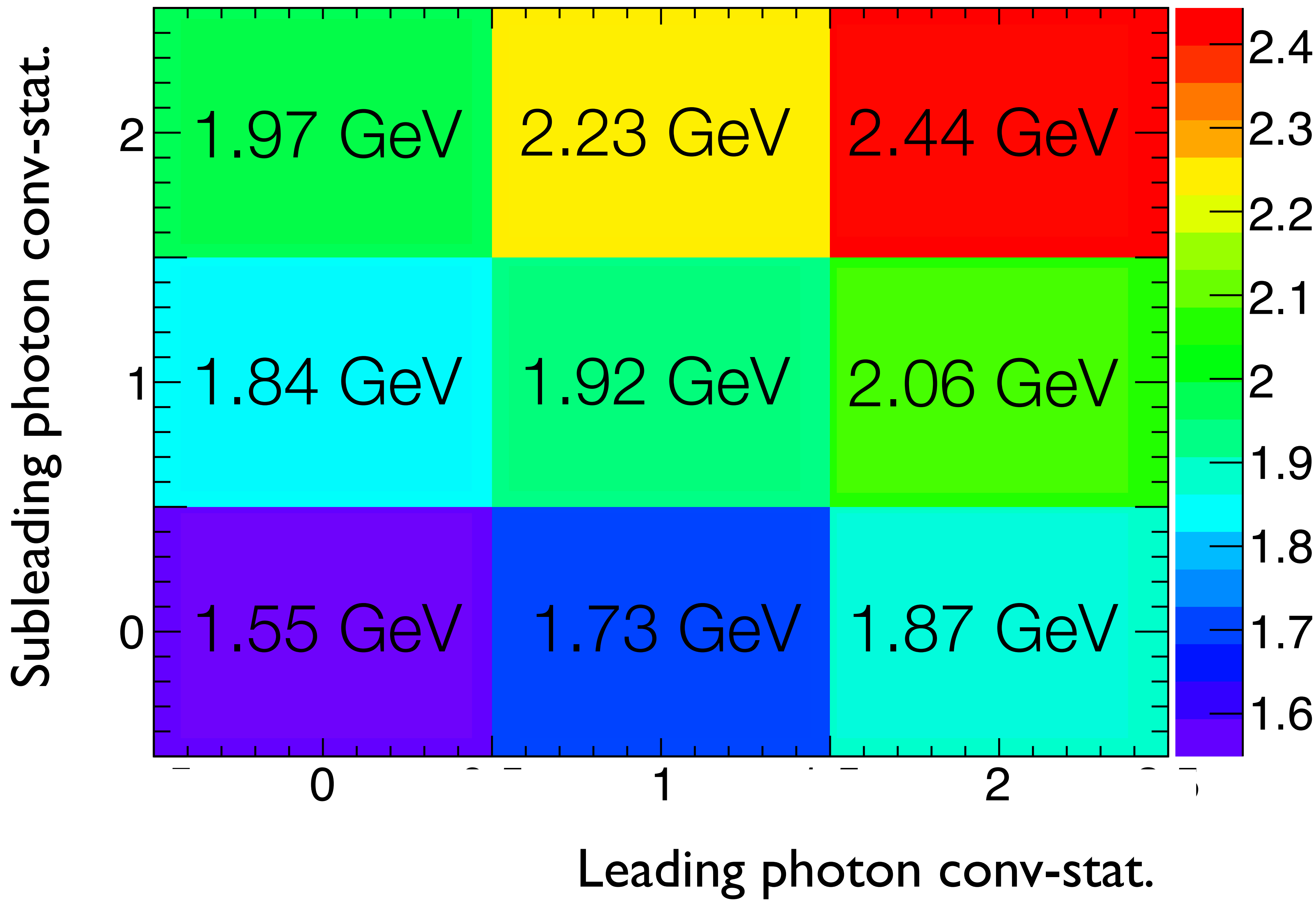

Small σCore= ☺

Large σCore= ☹

- Category with the best resolution is the 0-0 (about twice better than 2-2 which is the worst category).

Signal shape for conversion categories

γlead(2) γsubl (0)	γlead(2) γsubl (1)	γlead(2) γsubl (2)
γlead(1) γsubl (0)	γlead(1) γsubl (1)	γlead(1) γsubl (2)
γlead(0) γsubl (0)	γlead(0) γsubl (1)	γlead(0) γsubl (2)

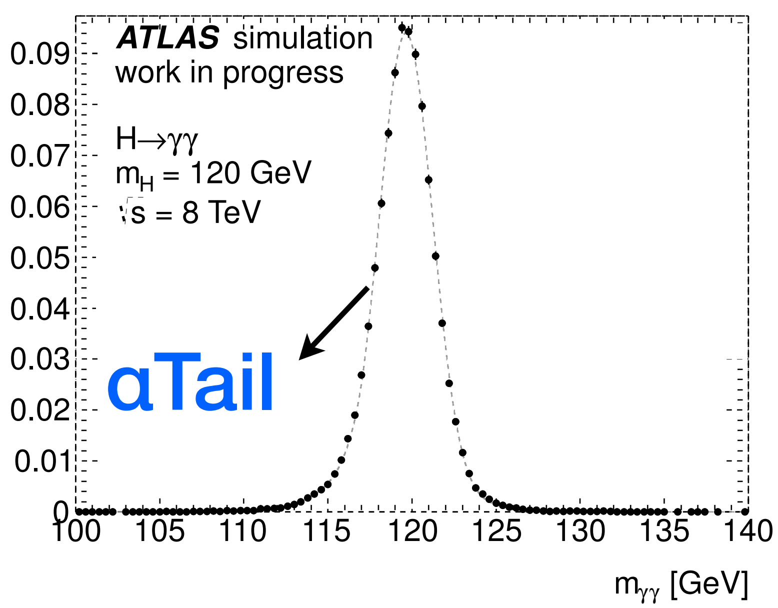

Large **αTail** = ☺

Small **αTail** = ☹

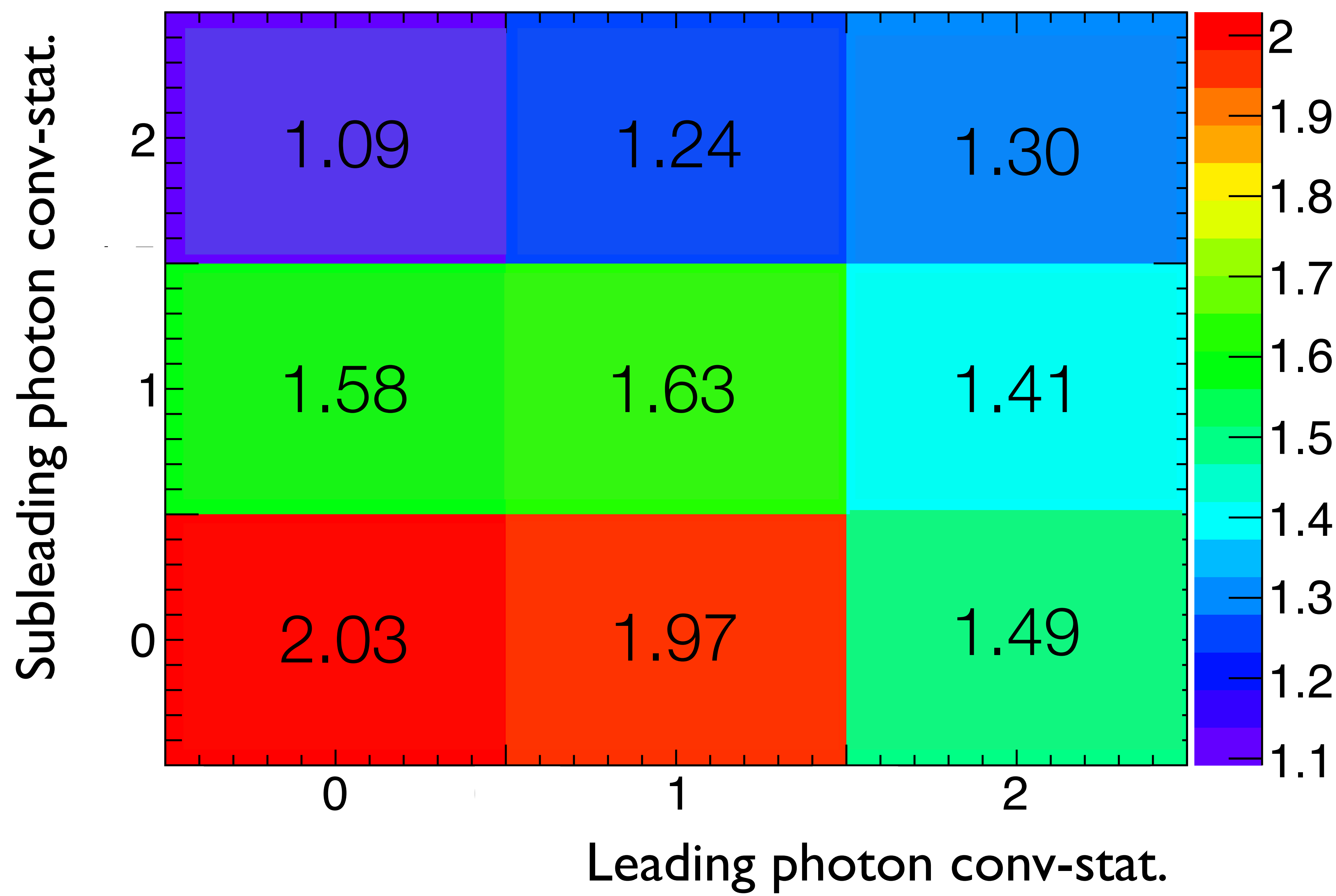

- The 0-0 category is almost gaussian.

Signal shape for conversion categories

γlead(2) γsubl (0)	γlead(2) γsubl (1)	γlead(2) γsubl (2)
γlead(1) γsubl (0)	γlead(1) γsubl (1)	γlead(1) γsubl (2)
γlead(0) γsubl (0)	γlead(0) γsubl (1)	γlead(0) γsubl (2)

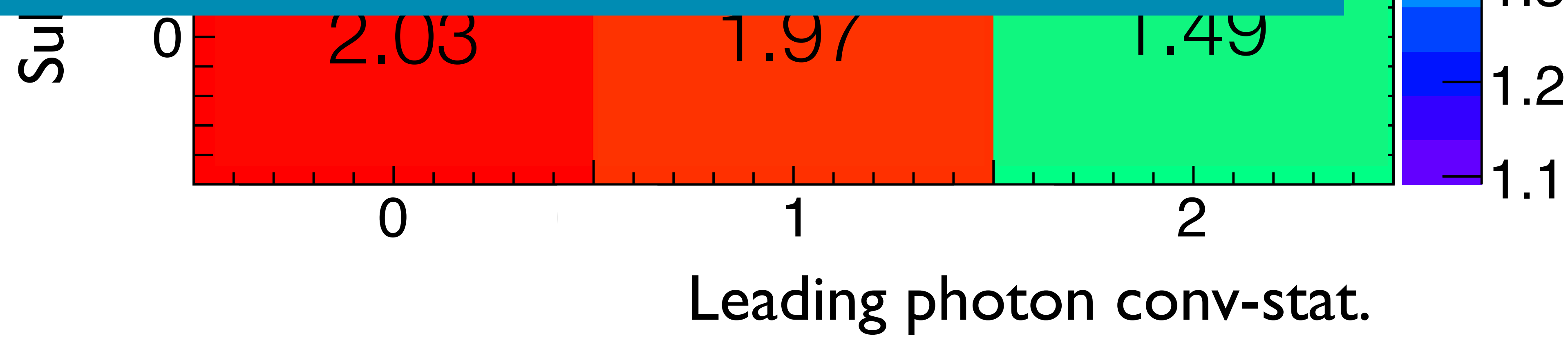

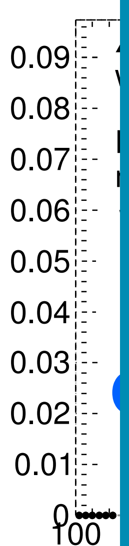

Conclusion 1: Resolution

- Following these results and considering that central photons have better resolution due to less upstream material. A category with two unconverted central photons is set.

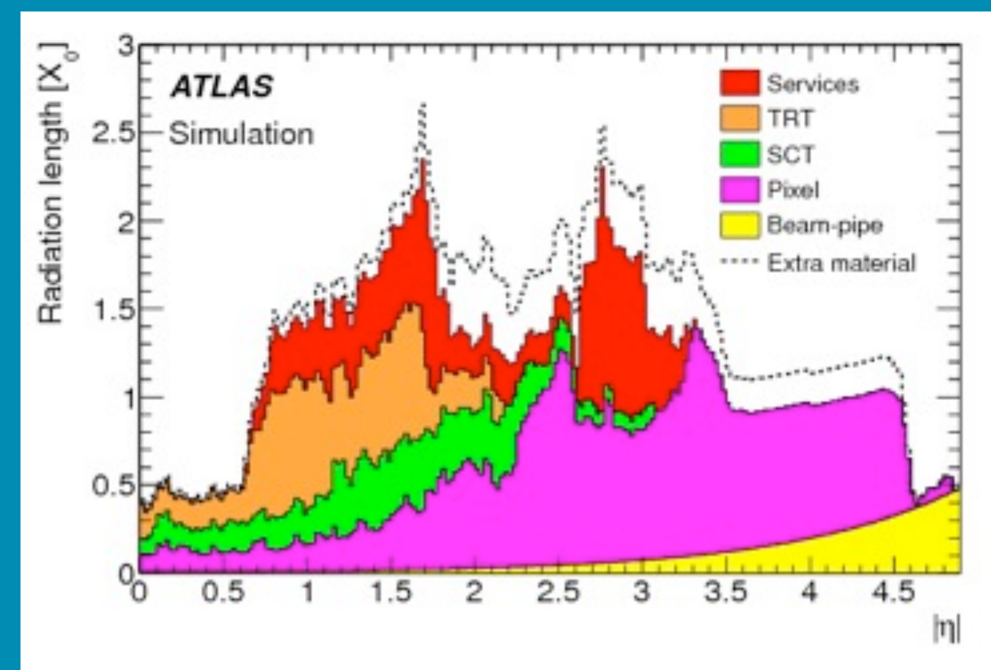

La

Small αTail =☹

- More gaussian category 0-0 against 2-2 with more pronounced tails.

MC converted photon energy scale (ES)

Sources of energy loss can affect the two types of converted photons (1 or 2-tracks):

Front energy loss due to the amount of upstream material before the calorimeter.

Out-of-cluster effect: caused by the magnetic field, makes the separation between the e^+e^- pair larger than the sliding window used for the cluster reconstruction (affects early conversions and mainly 2-track photons).

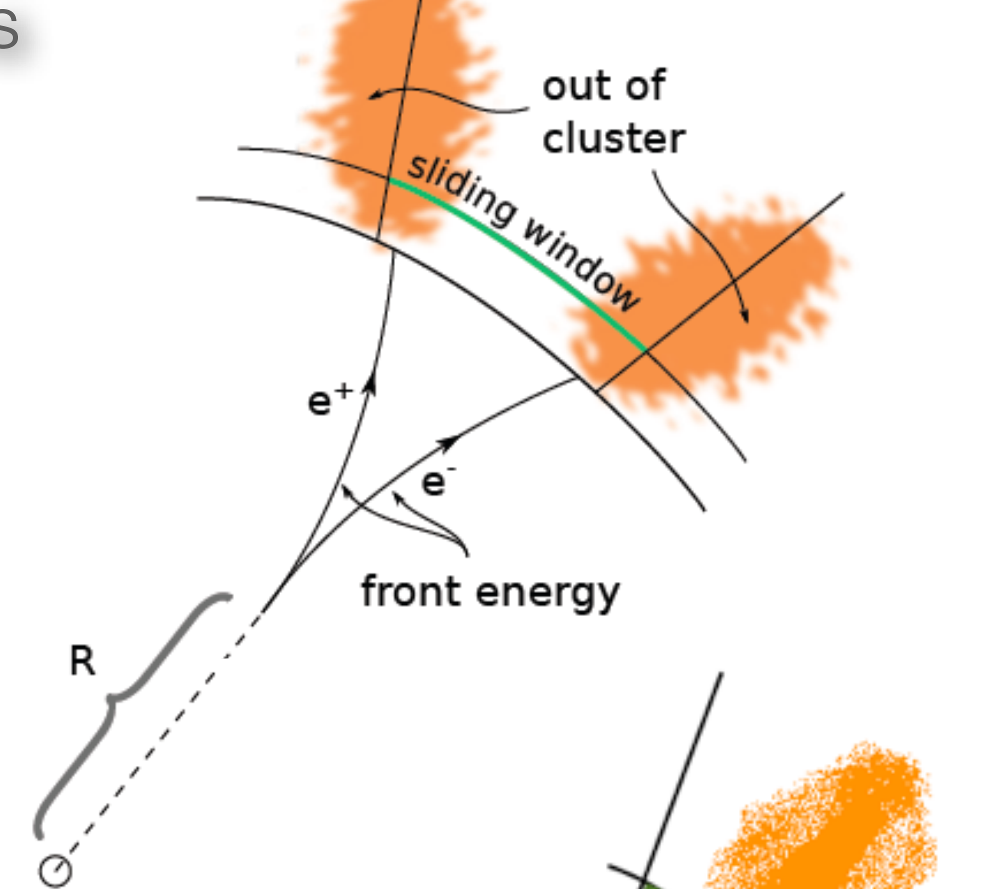

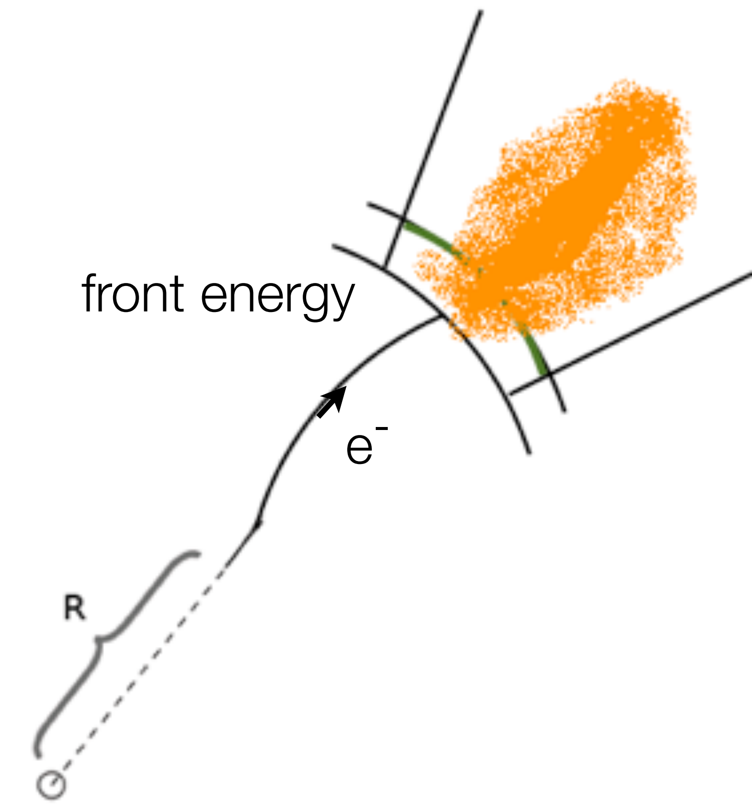

The EM cluster reconstruction and calibration treated both 1-track and 2-track converted photons in the same way.

A calibration algorithm was built to correct the energy of converted photons. The algorithm uses the photon pseudo-rapidity, the calibrated energy and the radius of conversion, and returns a factor to obtain an improved calibration.

MC converted photon ES: Calibration performance

$$\Delta = \frac{p_T^{reco} - p_T^{true}}{p_T^{true}}$$

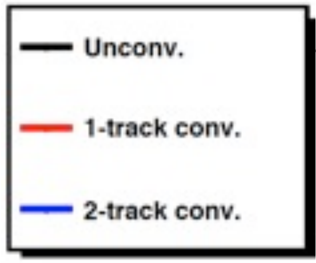

<Δ> vs Pt, in four representative regions of the calorimeter:

Before correction:

Barrel-Central **Barrel-Forward** **Transition** **End-Cap**

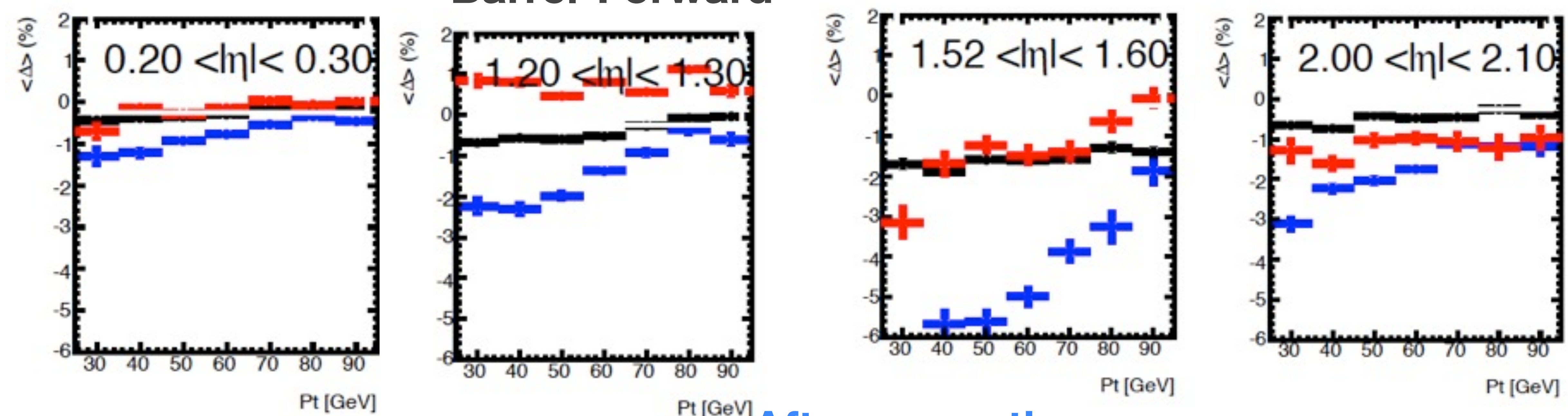

After correction:

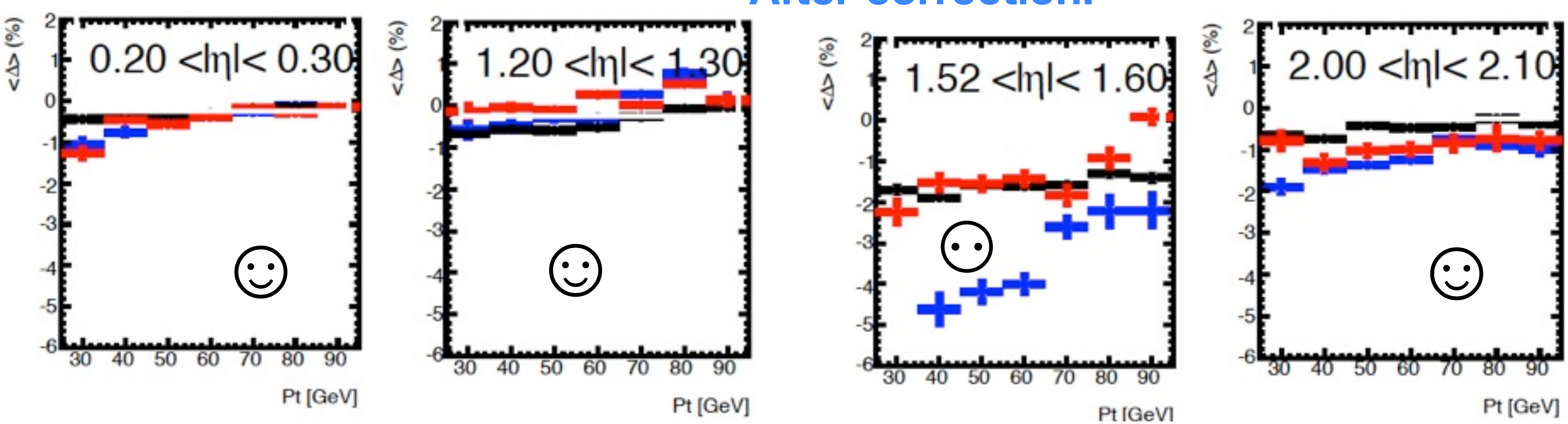

MC converted photon ES: Calibration performance

- Test the impact of the improved converted photon calibration on the H➞γγ invariant mass.
- The two extreme cases are tested, when the two photons are either with 1-track or 2-track conversions.
- 1-track case: the resolution improves by 4%. ☺
- 2-track case:the resolution improves in 2% and the leakage tails are reduced by 7%. ☺

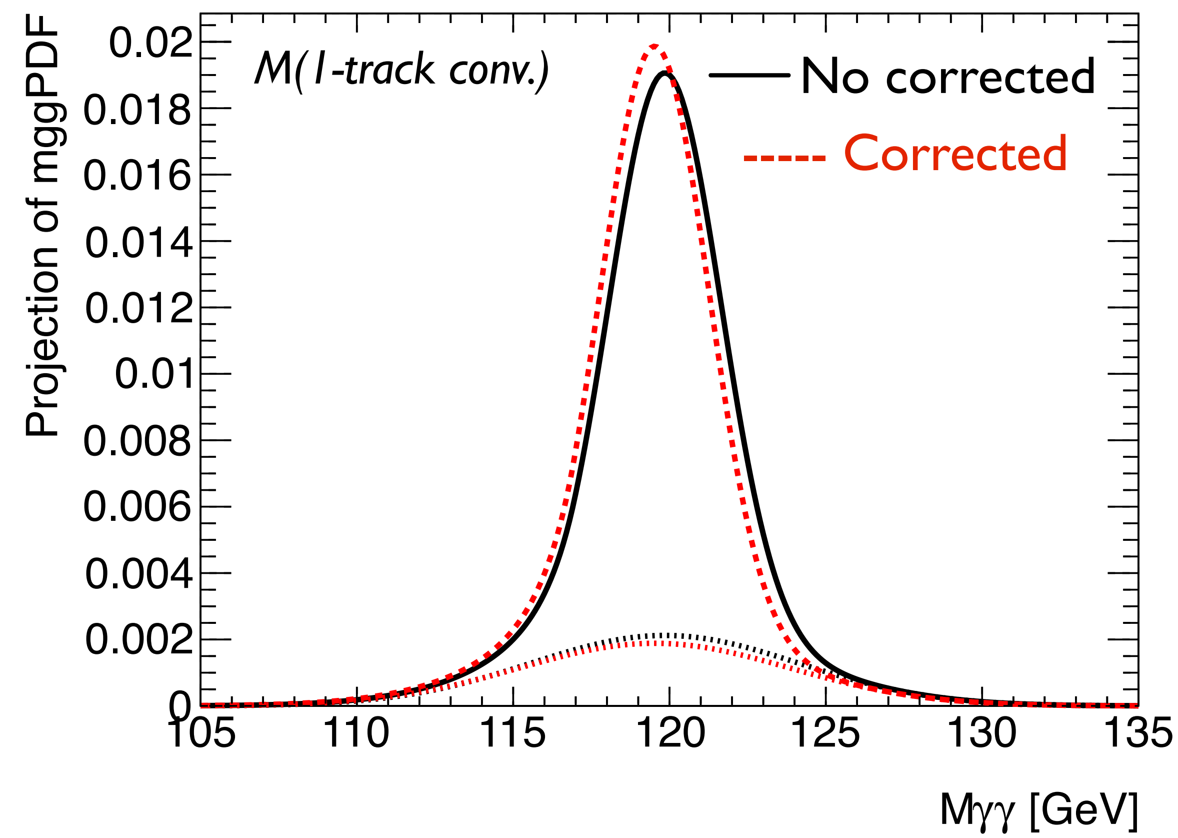

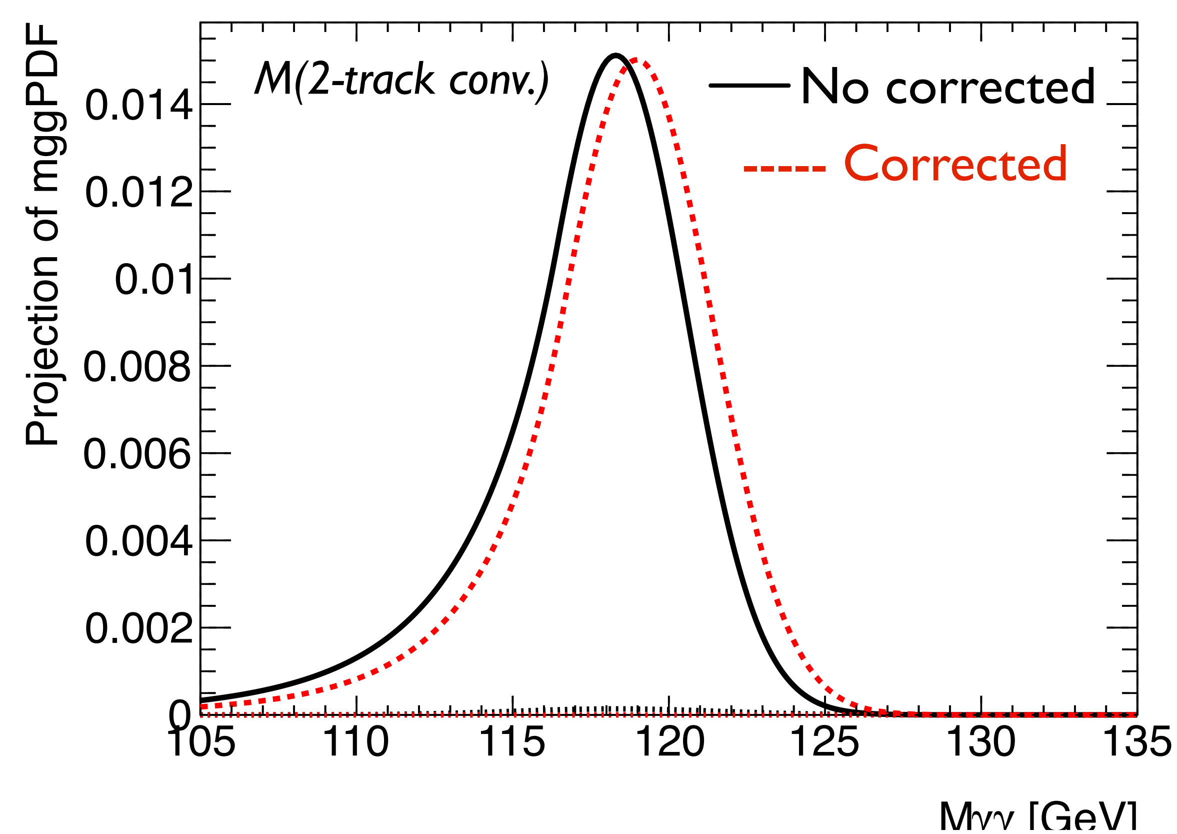

MC converted photon ES: Calibration performance

- Test the impact of the improved converted photon calibration on the H➙γγ invariant mass.
- The two extreme cases are tested, when the two photons are either with 1-track or 2-track conversions.
- 1-track case: the resolution improves by 4%. ☺
- 2-track case:the resolution improves in 2% and the leakage tails are reduced by 7%. ☺
- Difference in the mean value between 1-track and 2-track decreases **from 1.5 GeV to 500 MeV.** ☺

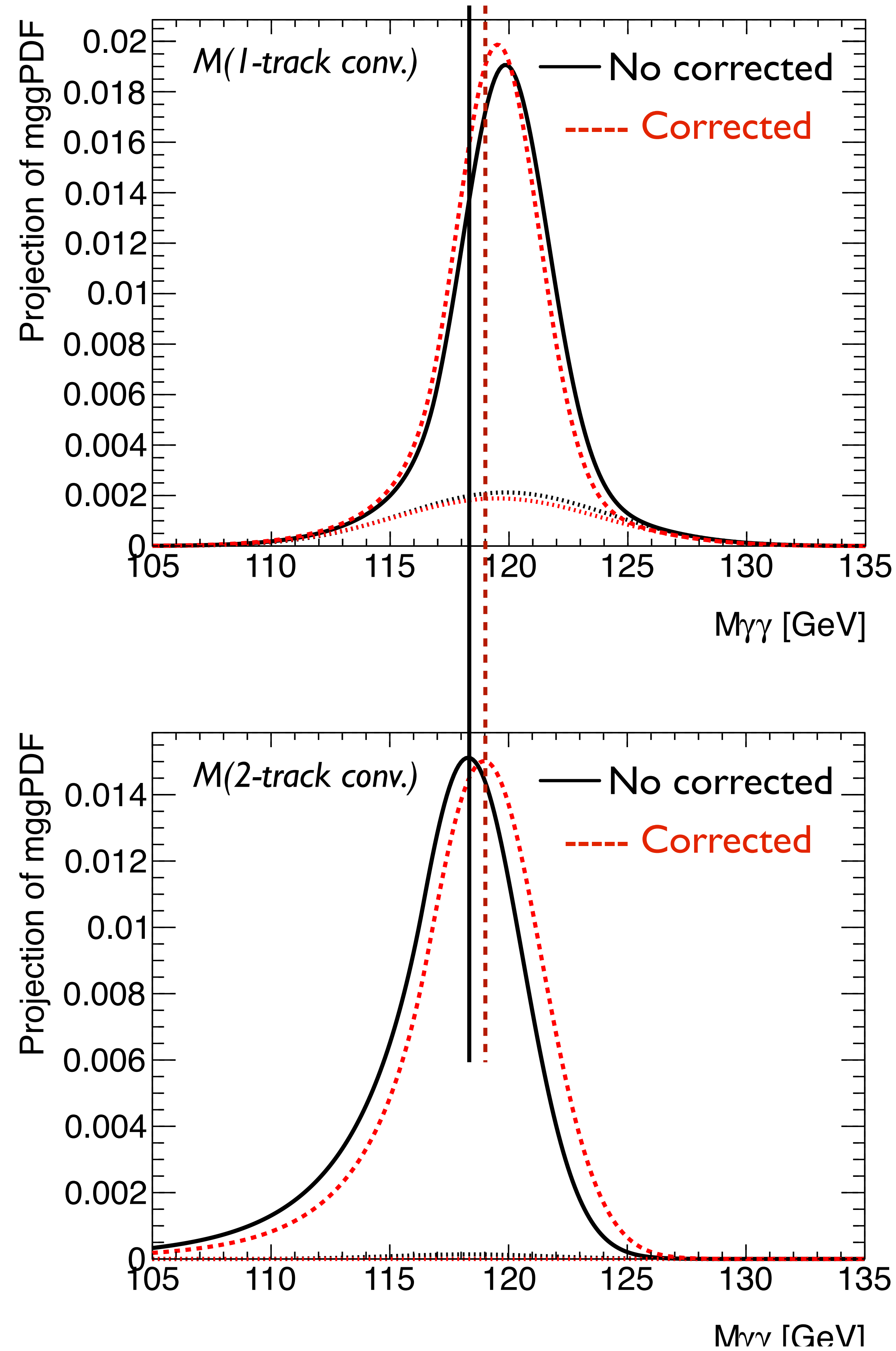

MC converted photon ES: Calibration performance

- Test the impact of this converted photon calibration on the H➞γγ invariant mass.
- The t… the tw… 2-trac…
- 1-trac… 4%.
- 2-trac… leaka…
- Differ… track and 2-track passes **from 1.5 GeV to 500 MeV.** ☺

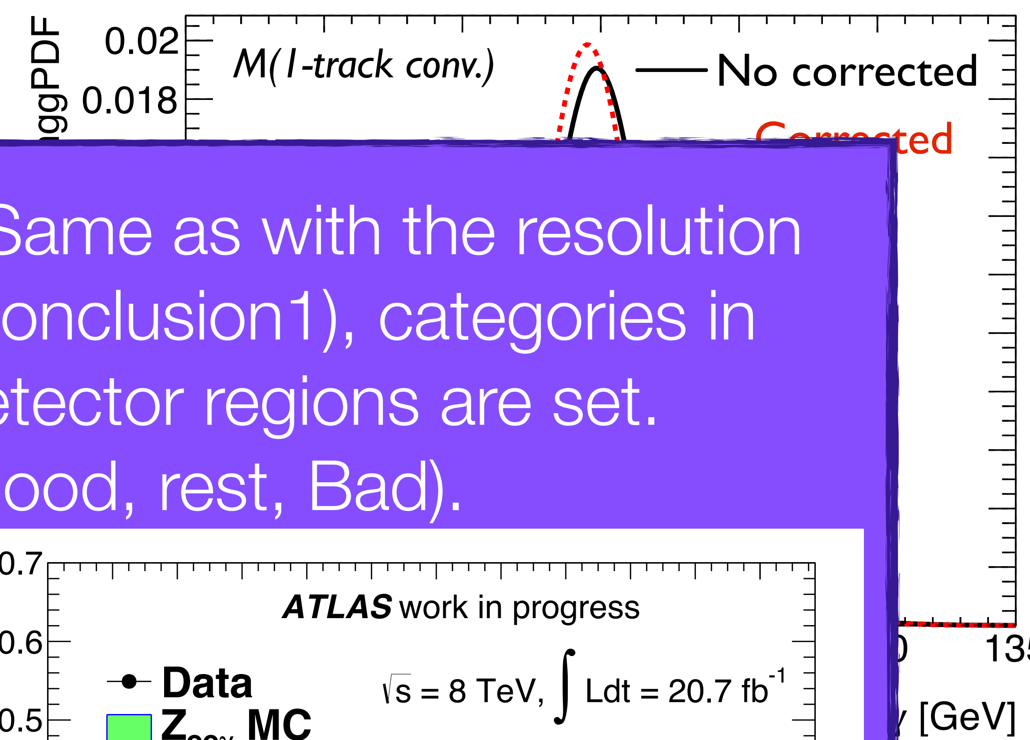

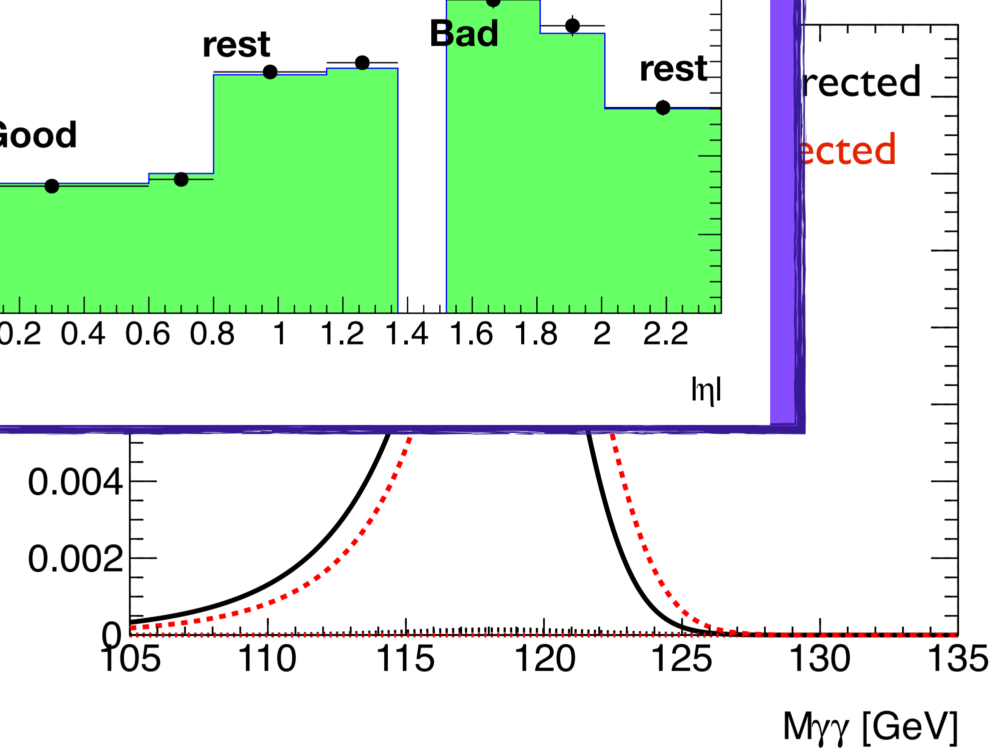

Conclusion 2: Calibration

- After these studies the calibration for converted photons is adopted in the H➞γγ analysis.

- Differences between 1-track and 2-track converted photons are reduced by the calibration. Therefore, they are merged into one category.

- Same as with the resolution (Conclusion1), categories in detector regions are set. (Good, rest, Bad).

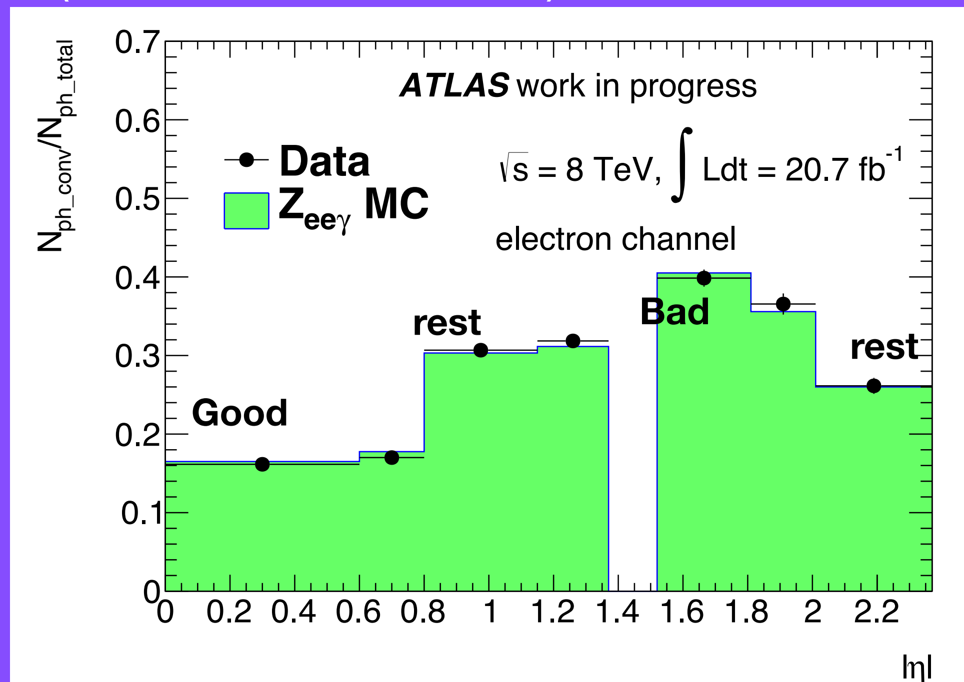

Observation of a new boson

Result from
Phys. Lett. B 716 (2012) 1-29
4th of July announcement

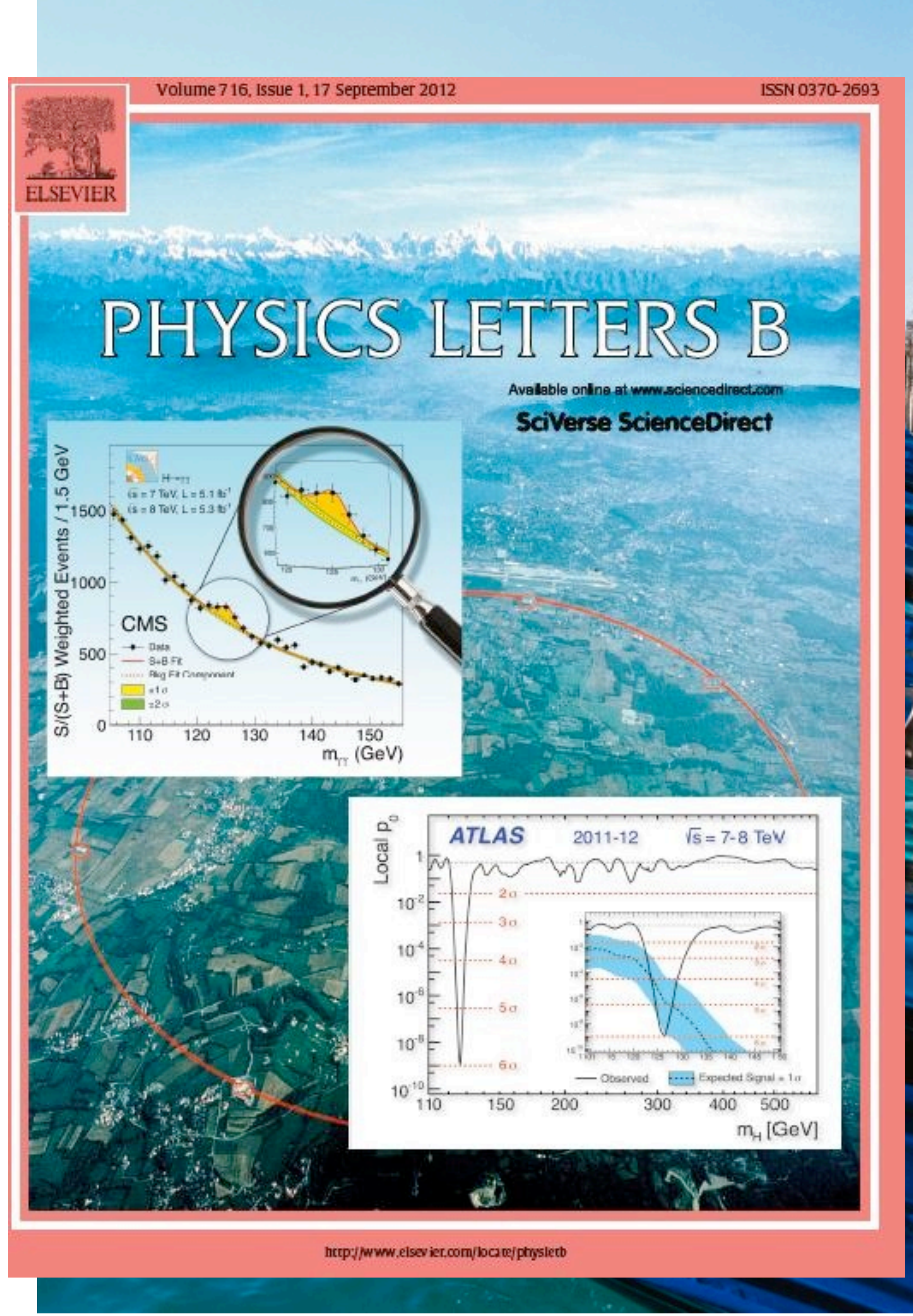

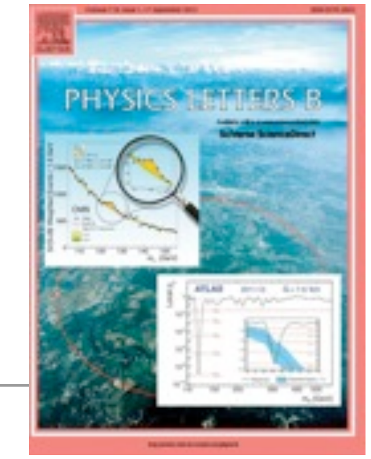

Observation of a new boson

- The discovery analysis uses 4.8+5.9 fb-1 of 7 and 8 TeV data.
- Selection:2 tightly identified photons, Pt > 40 / 30 GeV/c, |η| < 1.37 or 1.56 < |η| < 2.37
- Events separated into categories:
- The conversion status of the photon candidates
- The pseudo-rapidity of the photons.
- The component of diphoton Pt, transverse to thrust axis (pTt).
- A 2-jet selection with a VBF-like signature

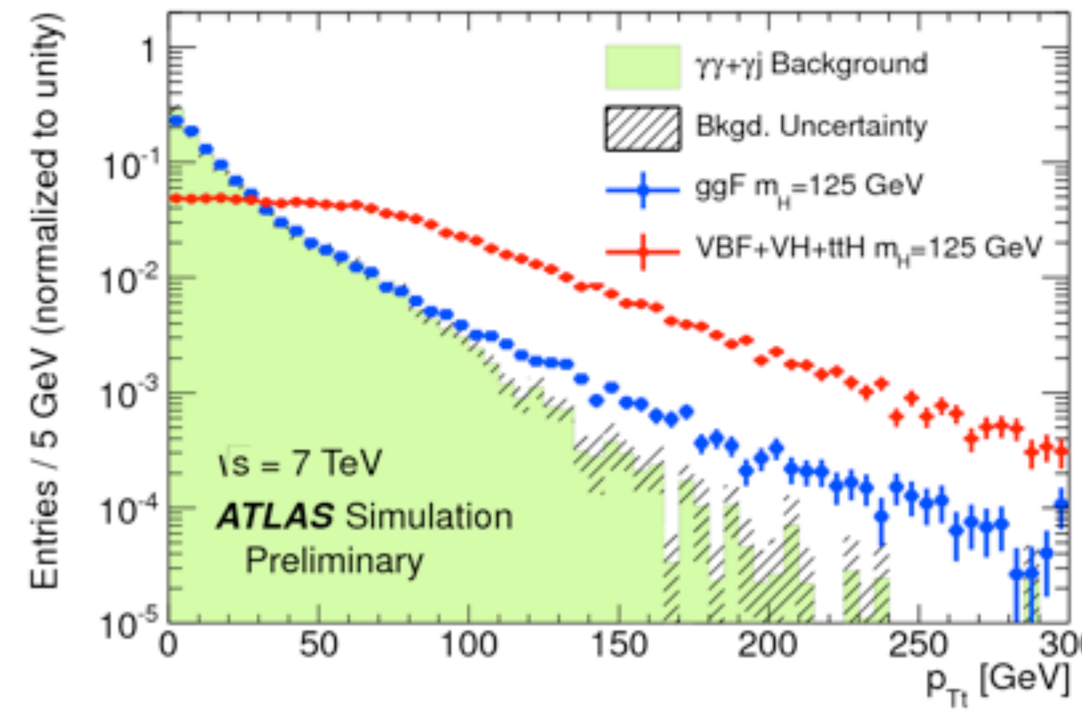

Conversion status ⊕

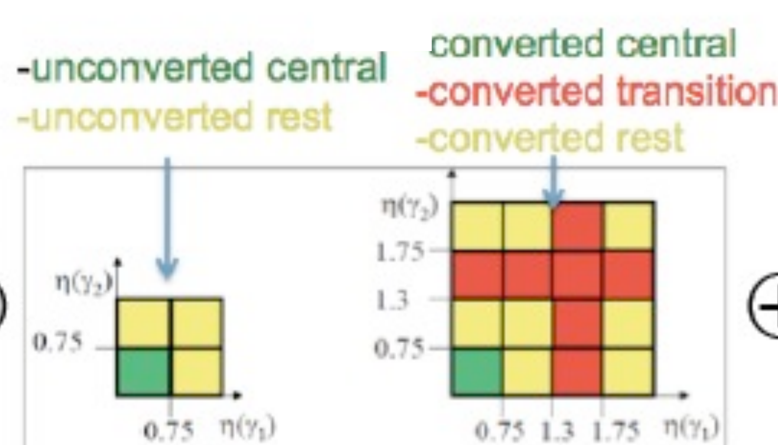

⊕

p_{Tt}< or > 60 GeV

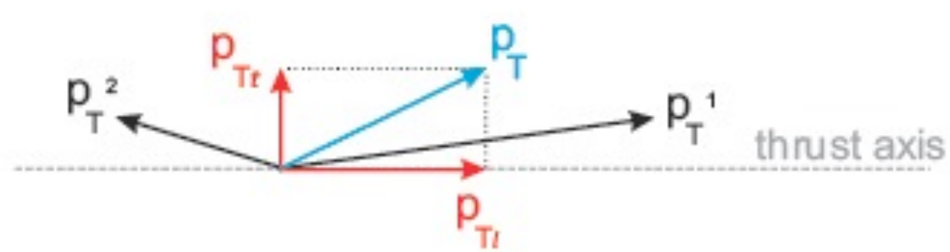

⊕ 2 jets (VBF)

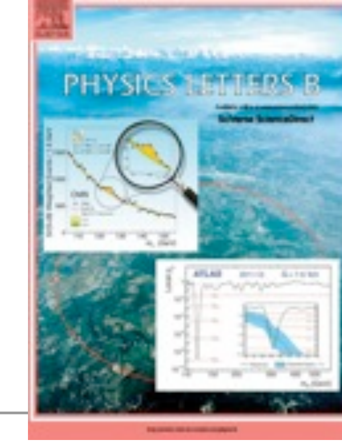

Observation of a new boson

Global resolution model is built for every category using the premises discussed before.

Categorisation exploits different resolution, different S/B (1% – 20%)

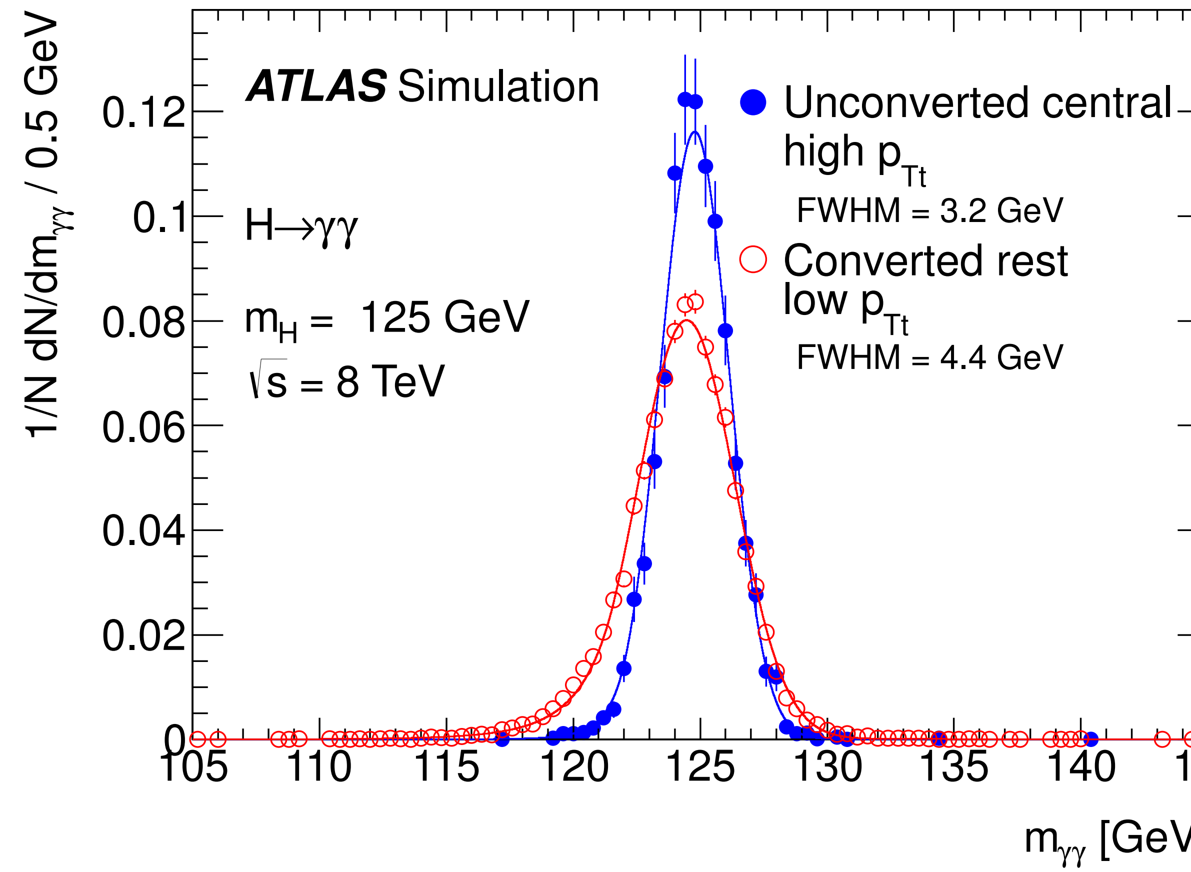

$\sqrt{s}$	Category	σ_{CB}	FWHM	Window [GeV]	Observed	S	B	S/B
8 TeV	Inclusive	1.64	3.88	123.14 - 129.12	3649	100.7	3584.8	0.028
	Unconv. central, low p_{Tt}	1.46	3.44	123.78 - 128.68	237	12.7	224.7	0.057
	Unconv. central, high p_{Tt}	1.37	3.24	123.98 - 128.59	16	2.3	13.6	0.169
	Unconv. rest, low p_{Tt}	1.58	3.73	123.42 - 128.8	1141	27.8	1122.5	0.025
	Unconv. rest, high p_{Tt}	1.52	3.57	123.66 - 128.76	75	4.7	68.3	0.069
	Conv. central, low p_{Tt}	1.64	3.86	123.16 - 128.95	207	8	186.6	0.043
	Conv. central, high p_{Tt}	1.5	3.53	123.61 - 128.74	13	1.5	9.7	0.155
	Conv. rest, low p_{Tt}	1.89	4.45	122.57 - 129.36	1311	24.2	1299.9	0.019
	Conv. rest, high p_{Tt}	1.65	3.9	123.18 - 129.09	71	4	71.3	0.056
	Conv. transition	2.59	6.1	121.36 - 130.88	849	11.5	821.2	0.014
	2-jet	1.59	3.74	123.38 - 129.01	19	2.7	13.3	0.203

23788 candidates at 7 TeV (**71.5** expected signal events) **35281** at 8 TeV (**100.7** expected signal events).

Observation of a new boson (4th July)

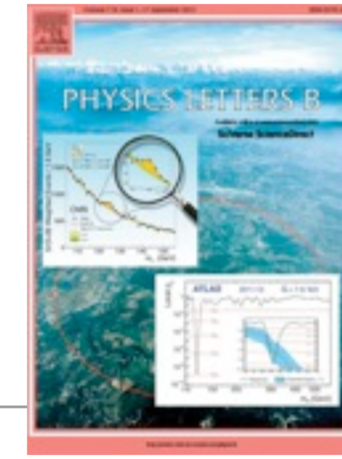

With the 4.7 +5.9 fb^{-1} of 7 and 8 TeV data, the excess observed at 126.5 GeV had a local significance of 4.5σ

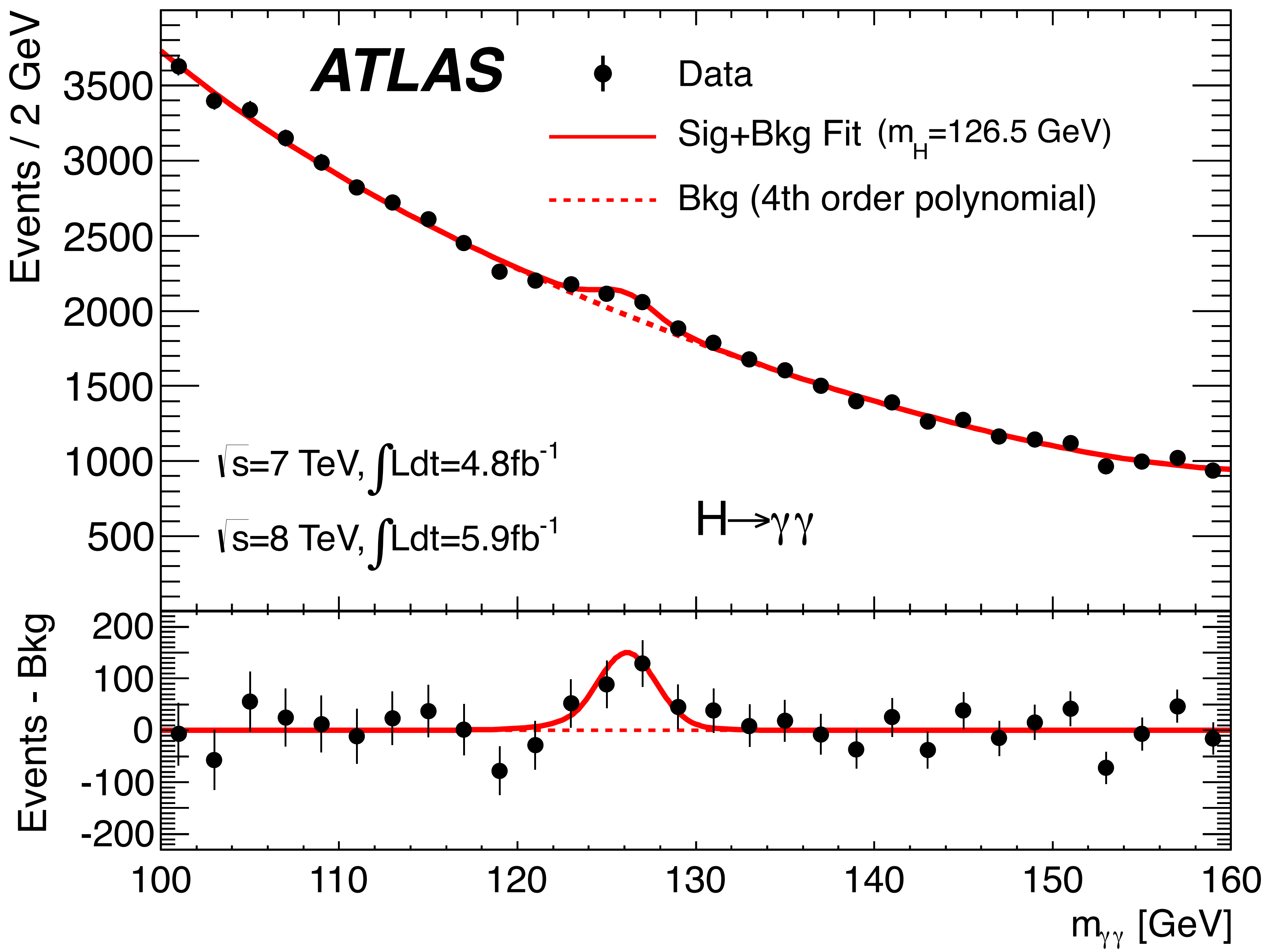

Update of the results: Complete Run I dataset

ATLAS-CONF-2013-029.

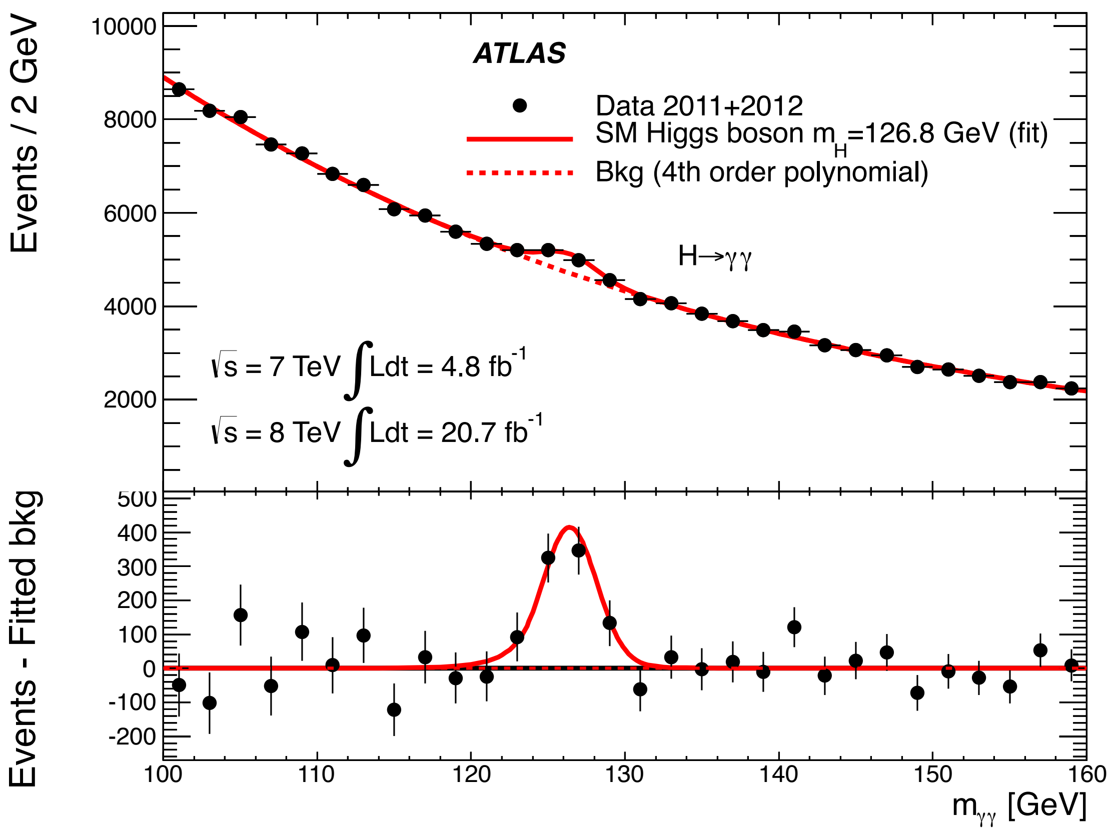

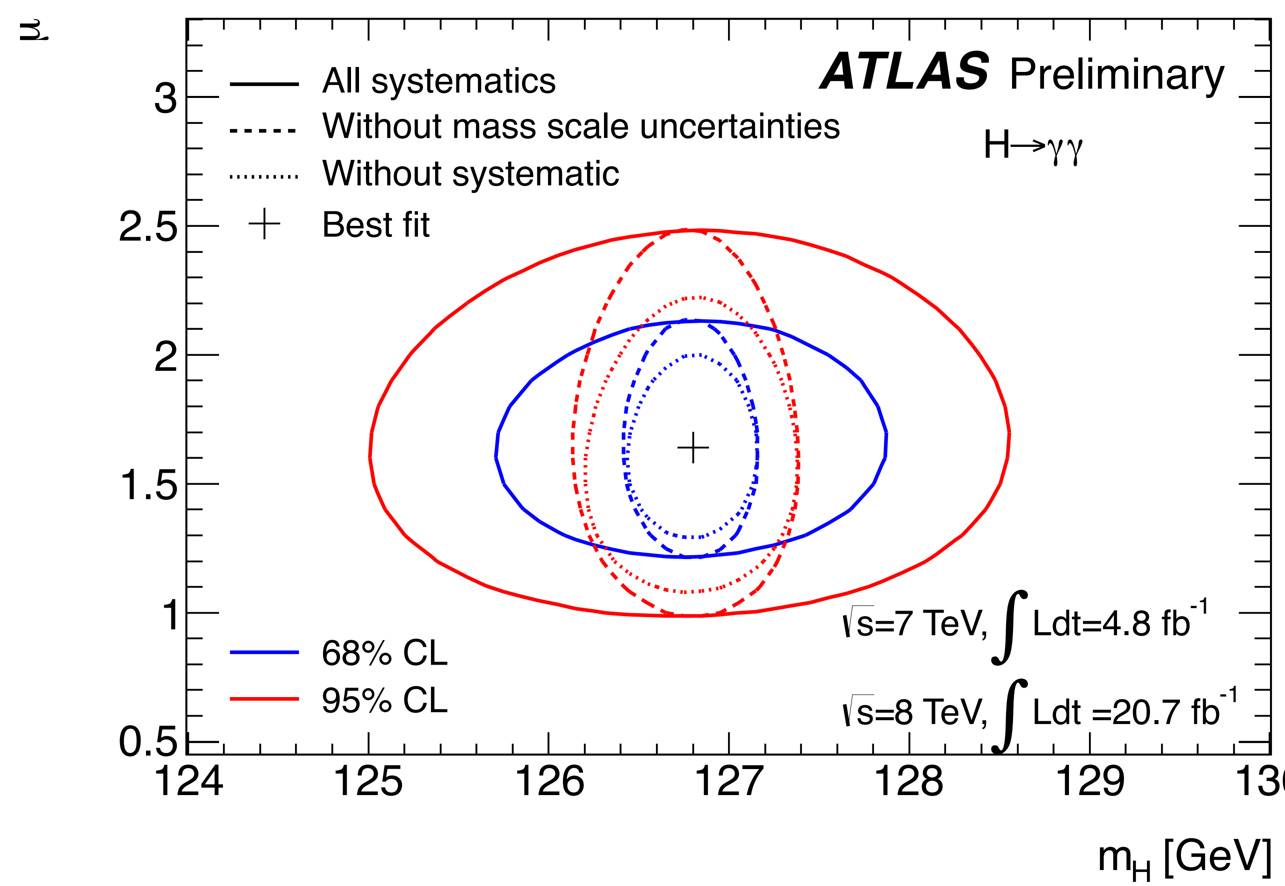

Dominated by statistical uncertainties. Contributions from theo. and exp. uncertainties are equivalent.
σ(sys): Systematics includes the signal yield, signal resolution and migration uncertainties.

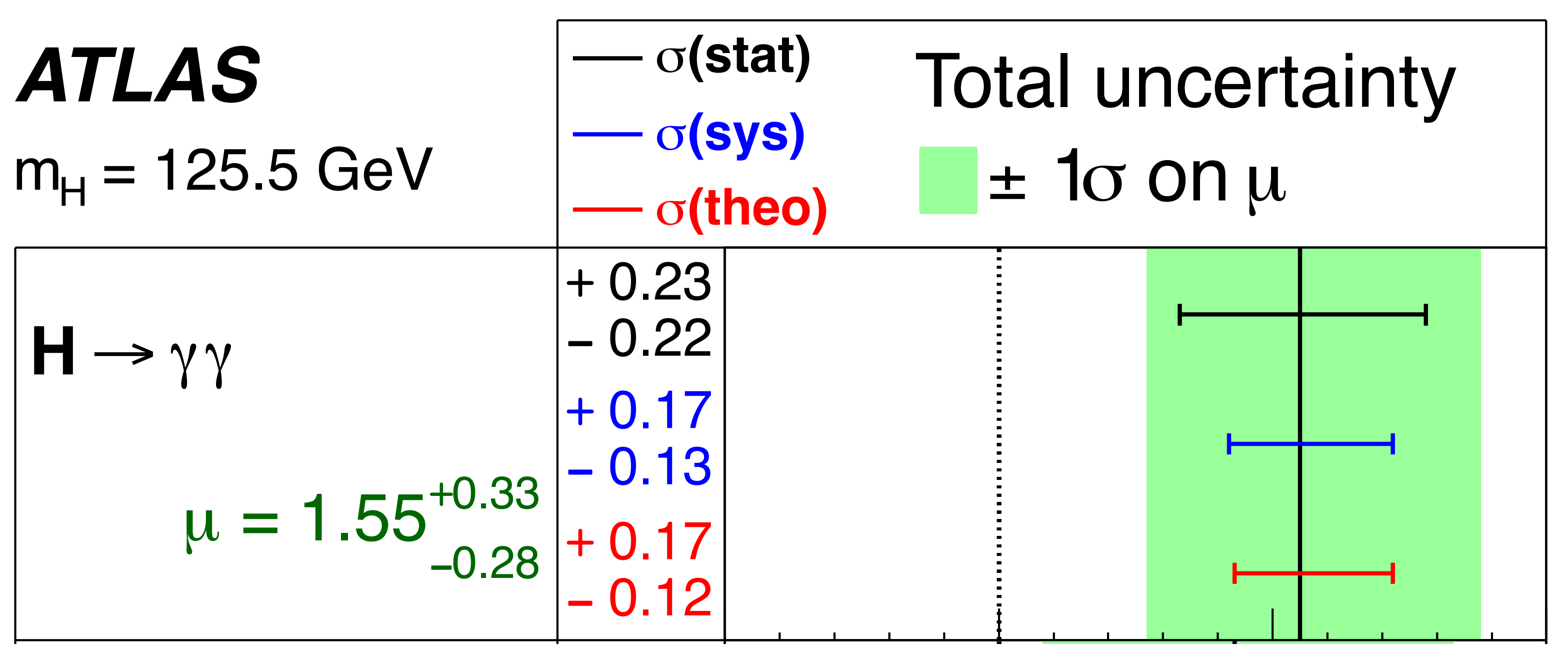

Update of the results

ATLAS-CONF-2013-029.

Measured mass in H➞$\gamma\gamma$:

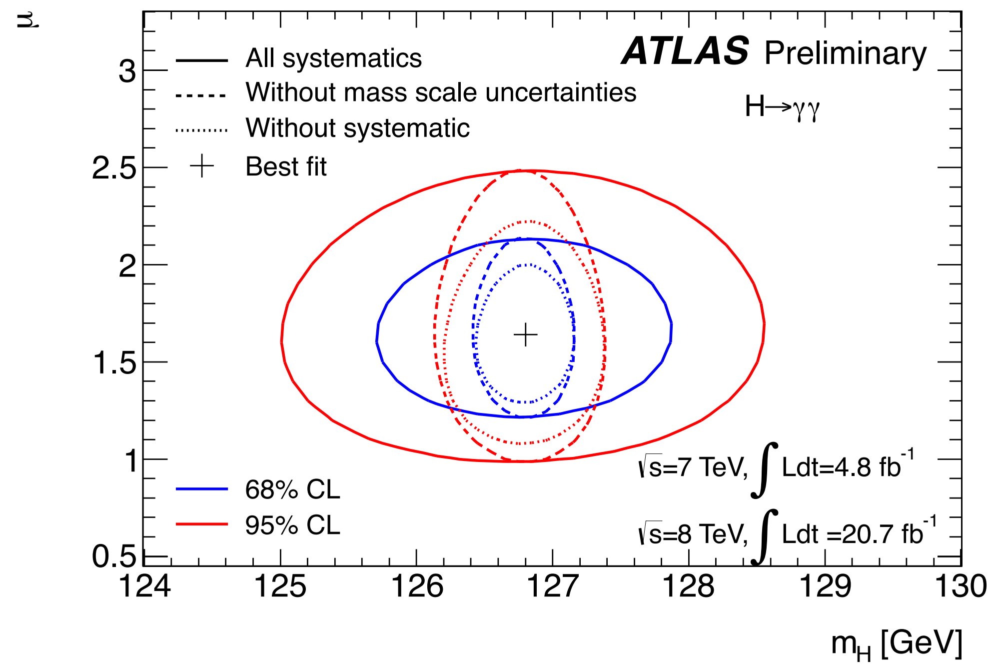

$$m_H = 126.8 \pm 0.2(stat.) \pm 0.7(sys.)\ \mathrm{GeV}$$

Mass measurement is dominated by the uncertainty on the photon ES.

The uncertainty on the ES from standard calibration is a function of Et and η.
In the H➞$\gamma\gamma$ Et range (Et>30 GeV), it has an average value of ±0.6%.

This uncertainty grows up to ±2% for lower Et photons (Et<15 GeV).

I performed an independent measurement of the photon ES using radiative Z decays.

H➙γγ and H➙Zγ channels

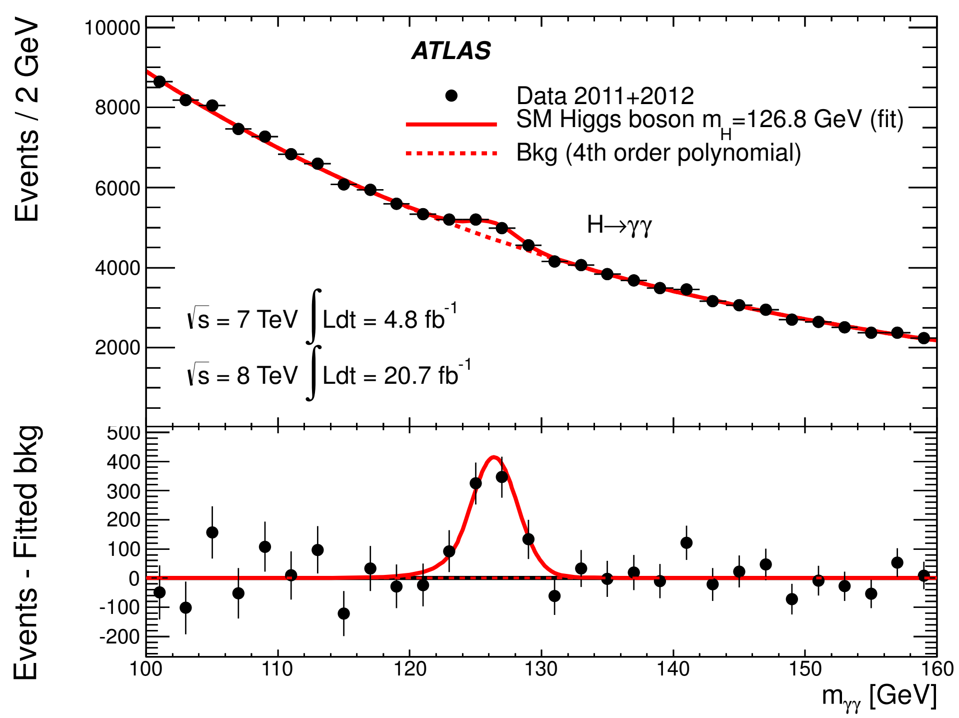

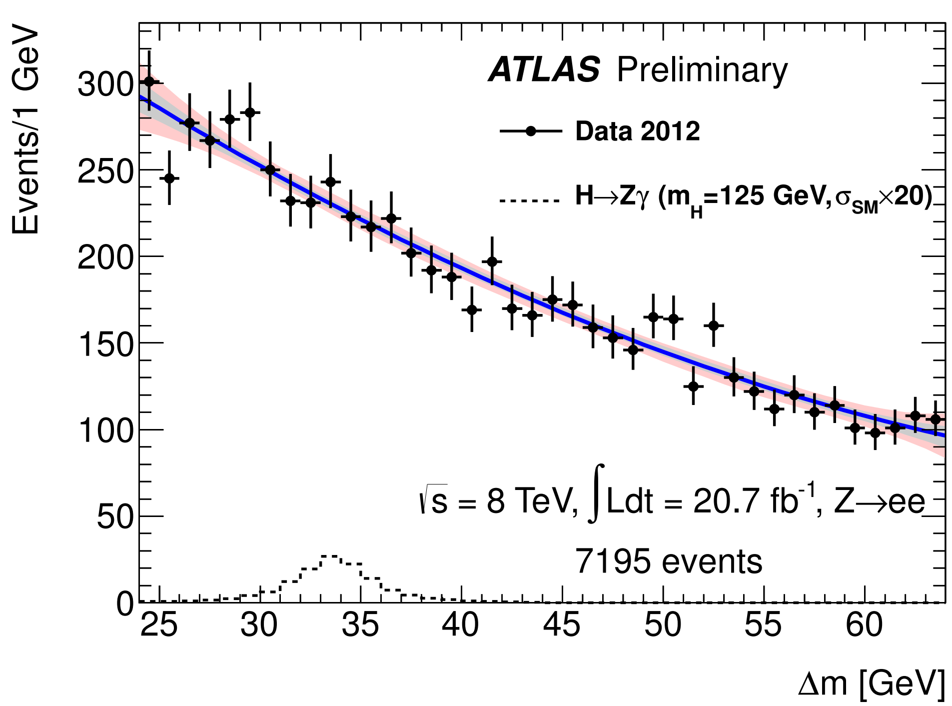

1. The SM and the Higgs boson
2. The LHC and the ATLAS experiment
3. The H➙γγ analysis in ATLAS (personal contributions)
4. Measurement of the photon energy scales using Radiative Z decays
5. The search for the Higgs boson in the H➙Zγ channel
6. Outlook

Radiative Z decays

Radiative Z FSR events provide a high-purity photon data sample.

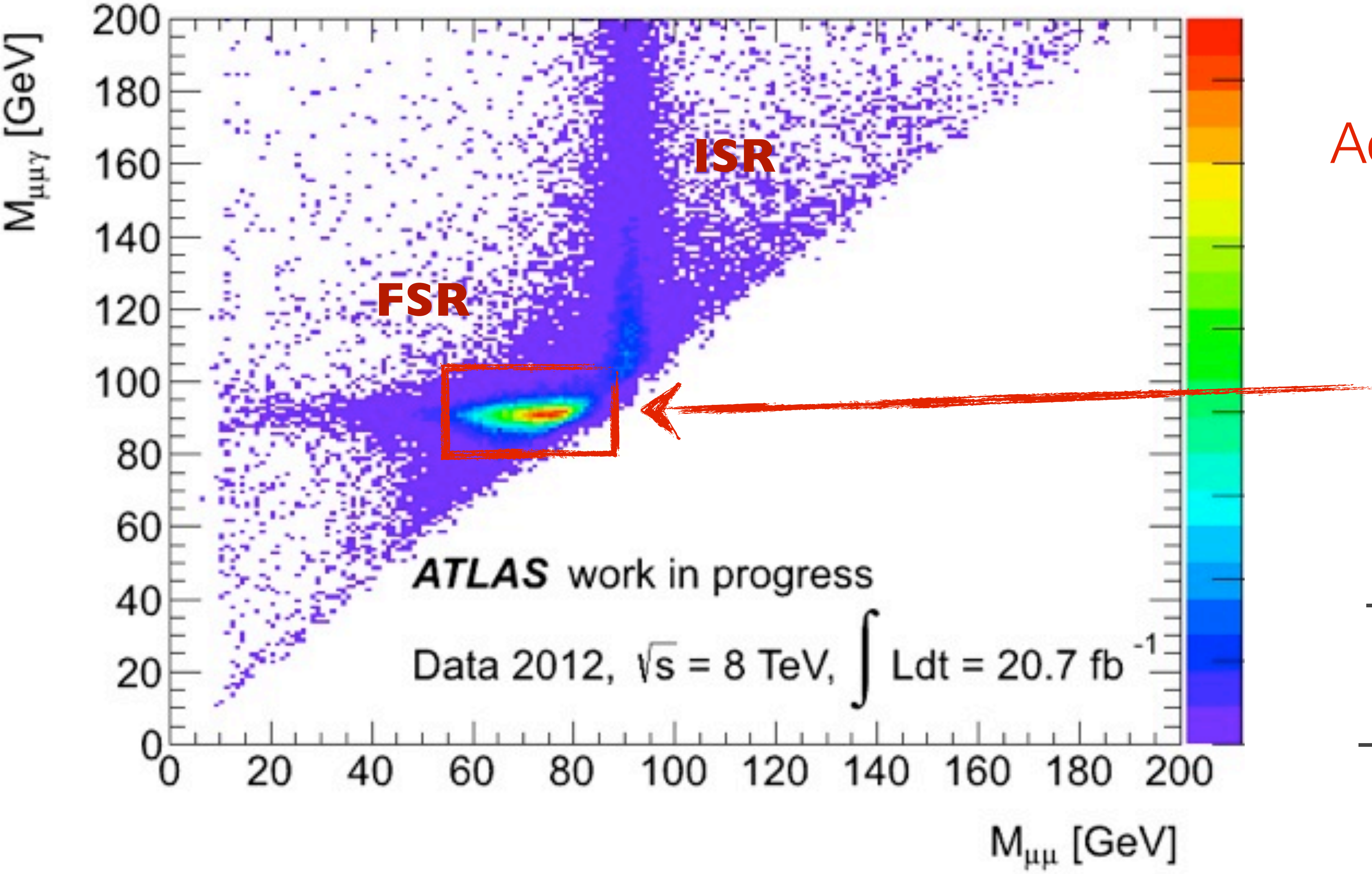

Advantage: For $Z \rightarrow ll\gamma$ the three body invariant mass follows the Z line shape.

- Simple selection:
- Two opposite-charged leptons and an isolated photon.
- A rectangular cut applied in the M_{ll}-$M_{ll\gamma}$ plane.

- The complete data 2012 is analysed in the $Z \rightarrow ee\gamma$ and $Z \rightarrow \mu\mu\gamma$ channels.

2011 analysis documented in ATL-COM-PHYS-2012-1473

Extraction of the photon energy scales

- For fully calibrated photons (MC+Z➞ee), any residual mis-calibration between data and MC can be parametrized as:

$$E_{MC} = E_{Data} / (1+\alpha)$$

α is extracted from the FSR sample

The double ratio method:

The photon energy in data is shifted by α and the three body invariant mass is recalculated. The mean value in the FSR Z peak is fitted in both data and MC, and R is evaluated:

$$R(\alpha) = \frac{M(ll\gamma(\alpha))_{Data} / M(ll)_{Data}}{M(ll\gamma)_{MC} / M(ll)_{MC}}$$

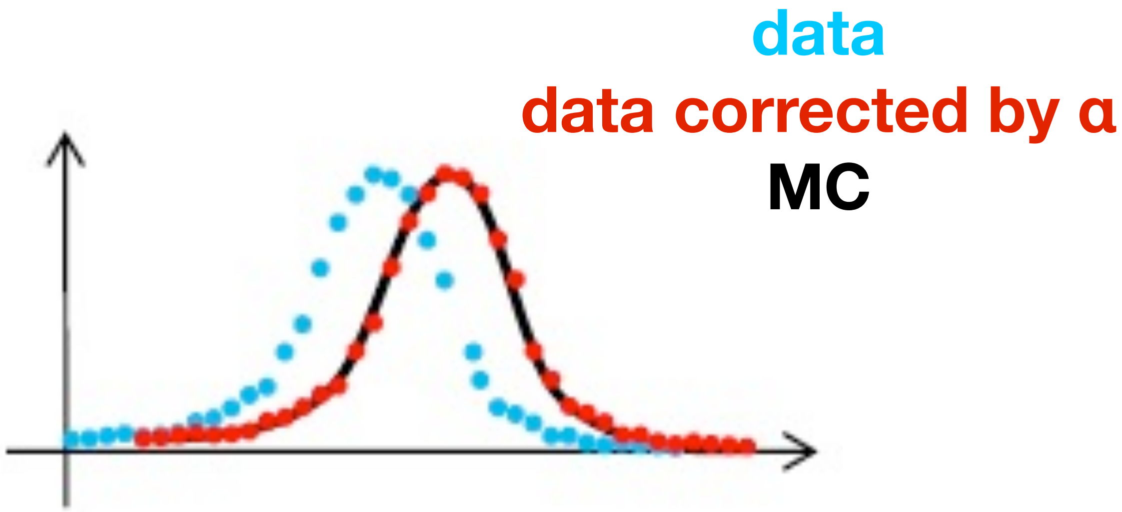

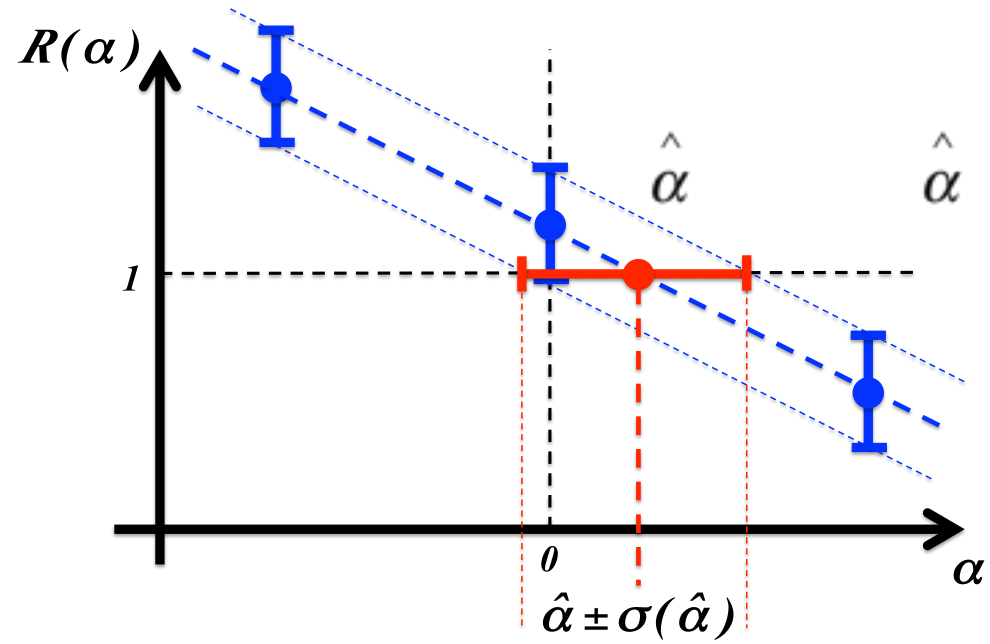

Extraction of the photon energy scales

- Sample of low pT photons.
- The $M_{ll\gamma}$ distributions are fitted with a:

Breit-Wigner ⊗ Crystal Ball → Z peak component

\+ *wide gaussian* → small background component

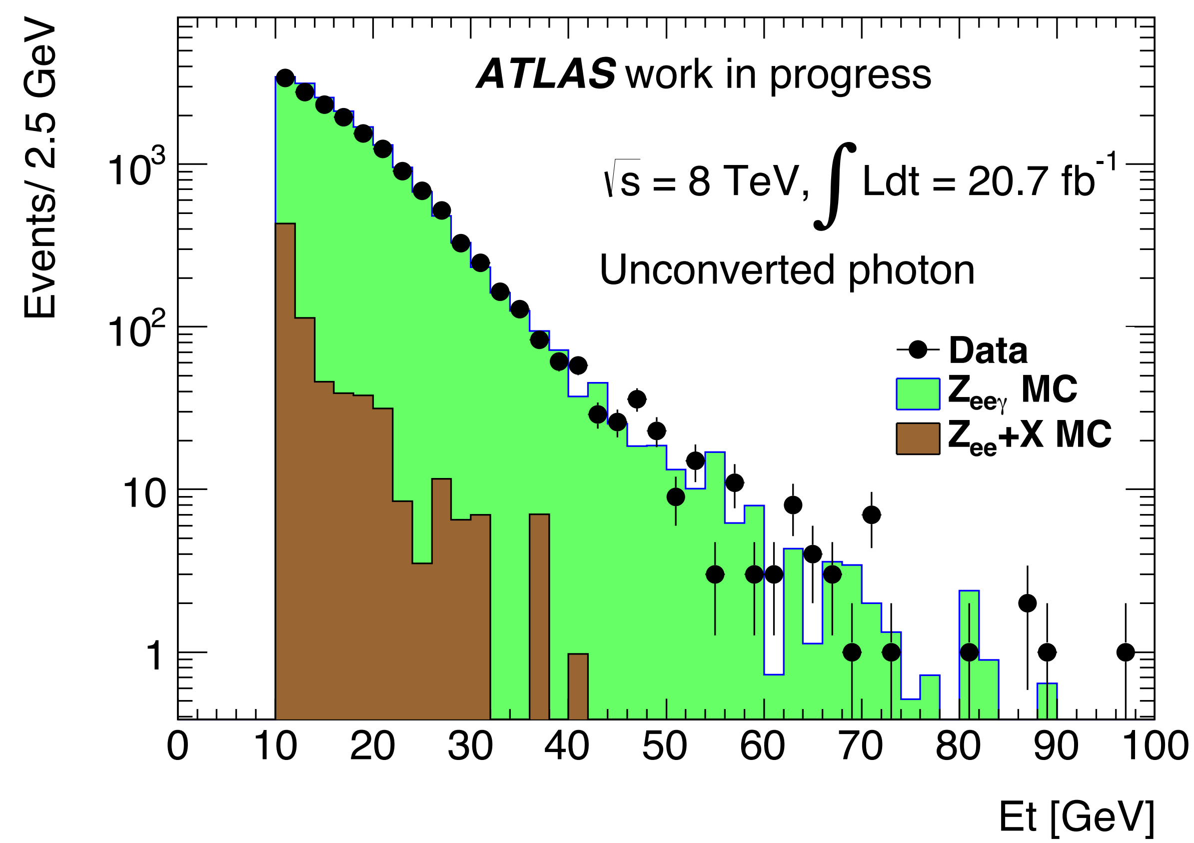

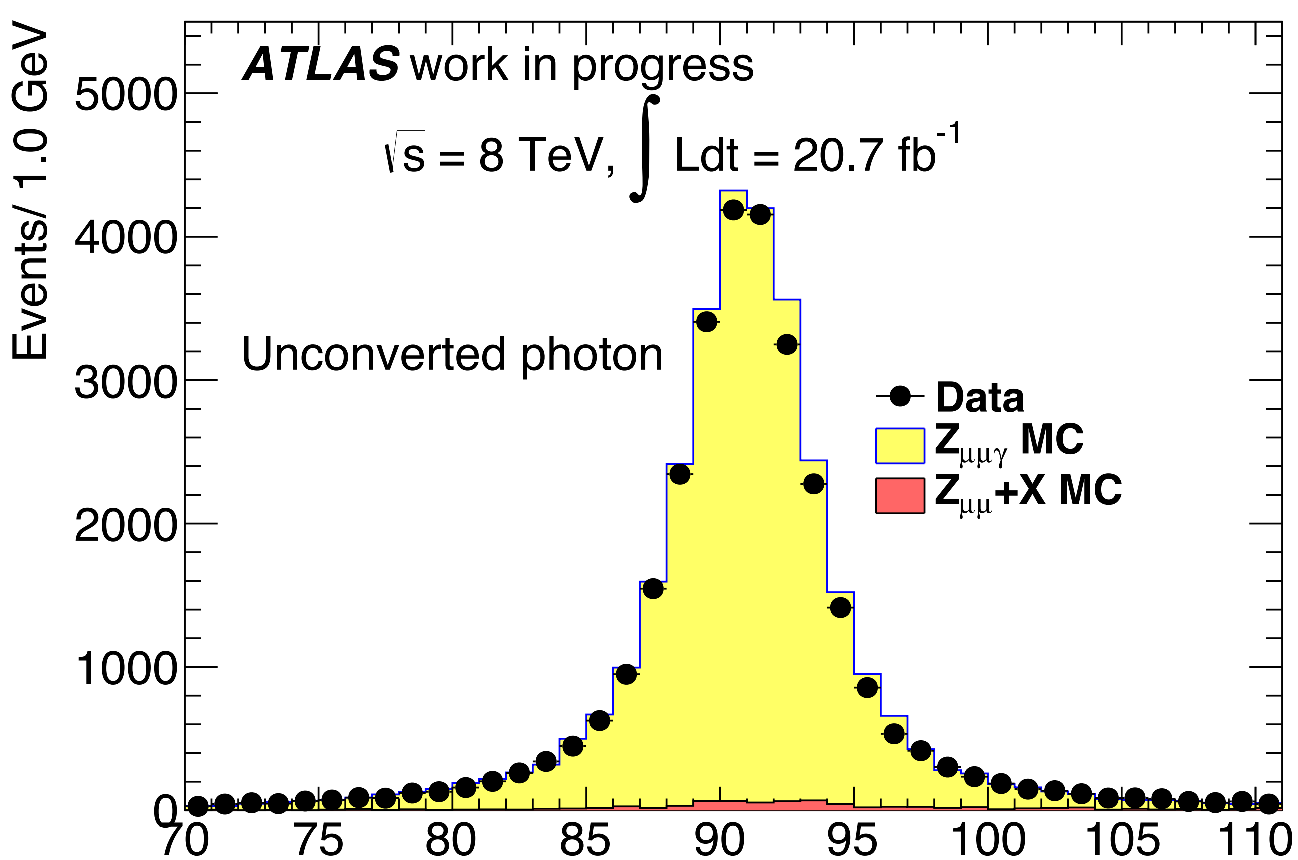

- The scales are extracted in different η and pT bins:

Pt bins [GeV] = [10,15], [15,20], [20-30],[30-60] GeV

|η| bins =[0.0,0.6],[0.6, 1.37], [1.52, 1.88] , [1.88,2.37]

Extraction of the photon energy scales

- Sample concerns low pT photons.
- The Mllg distributions are fitted with a:

Breit-Wigner ⊗ Crystal Ball → Z peak component

+ *wide gaussian* → small background component

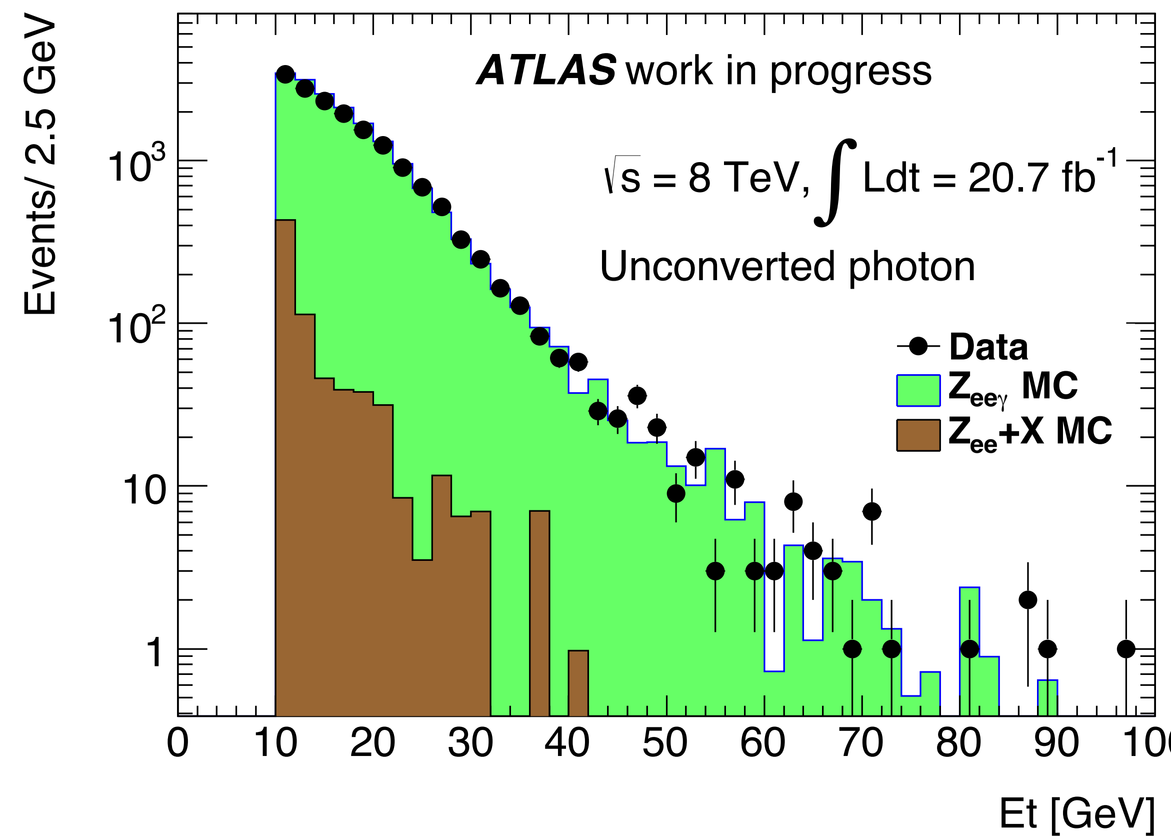

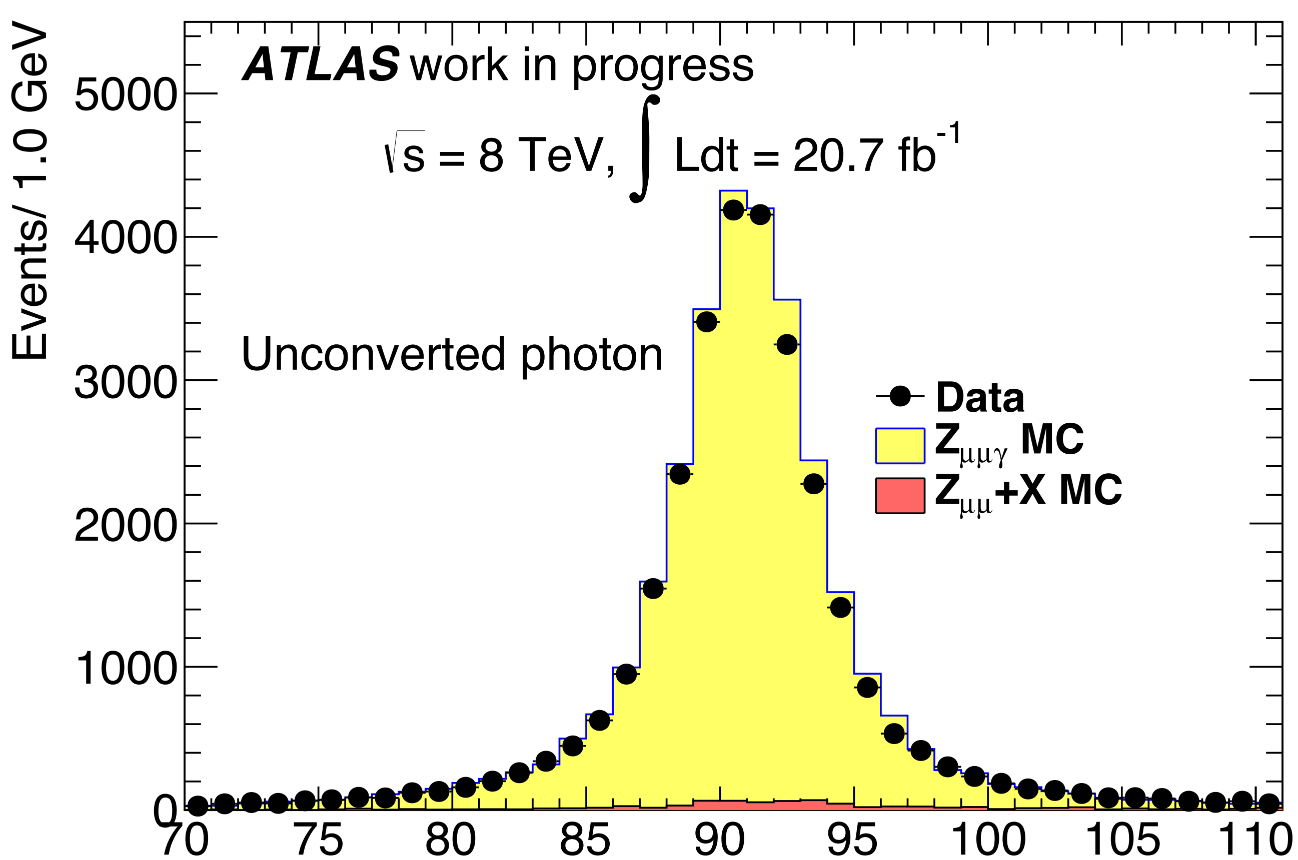

- The scales are extr… pT bins:

H→$\gamma\gamma$ photon pT range

Pt bins [GeV] = [10,15], [15,20], [20-30] [30-60] GeV

Barrel-Central Barrel-Forward

|η| bins =[0.0,0.6],[0.6, 1.37], [1.52, 1.88] , [1.88,2.37]

Transition End-Cap

Extraction of the photon energy scales

$Z \rightarrow \mu\mu\gamma$

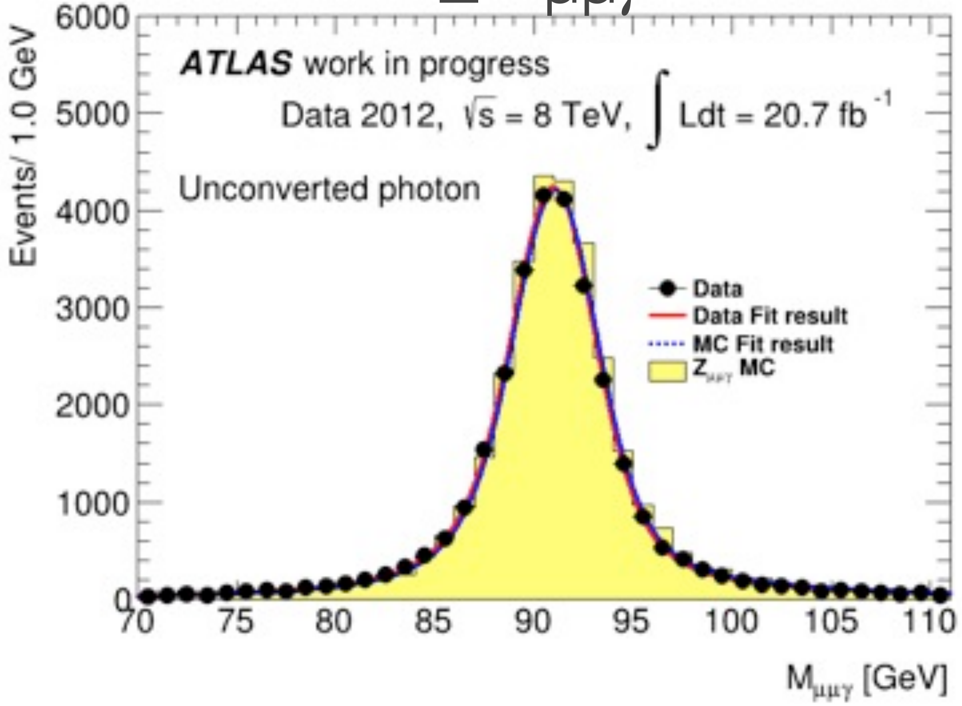

$Z \rightarrow ee\gamma$

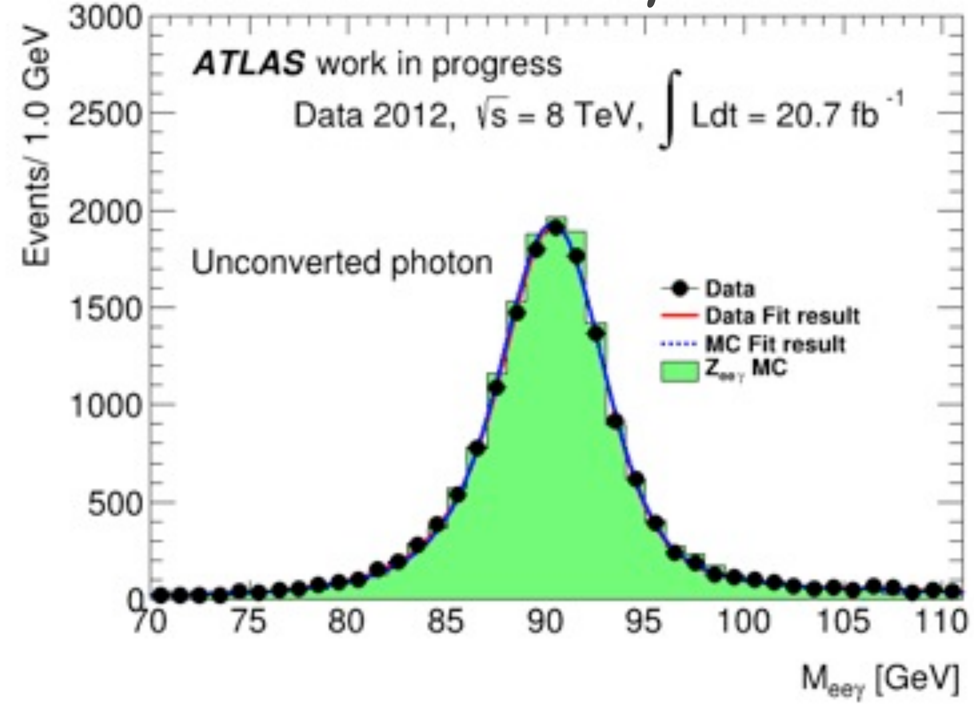

Fitted mean value of the $M_{ll\gamma}$ distributions, in η and pT bins:

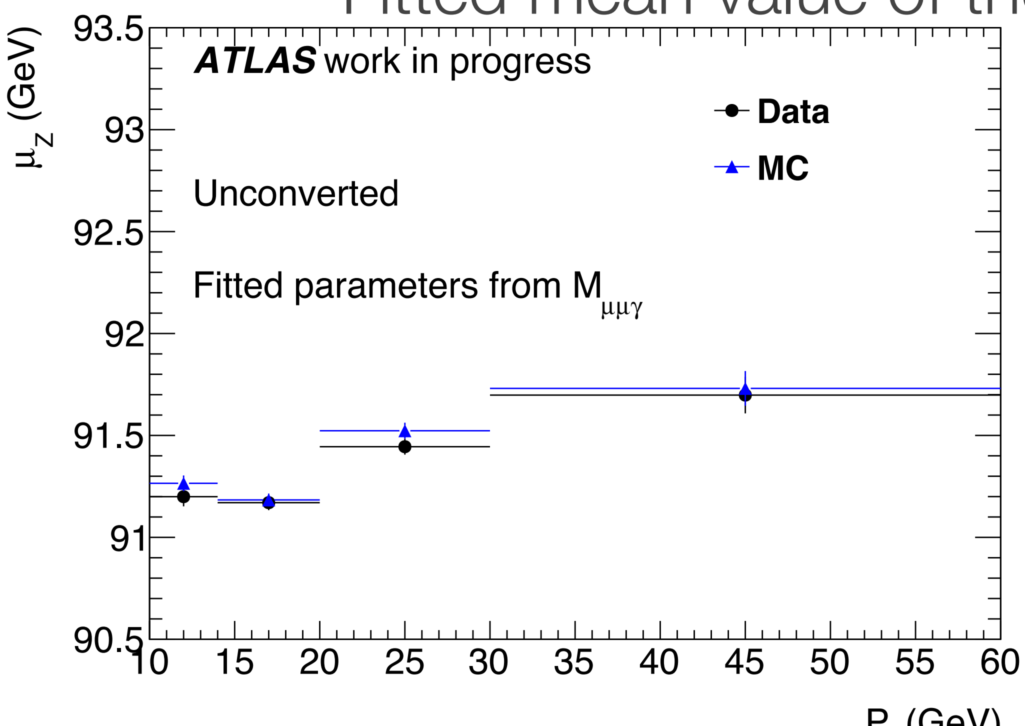

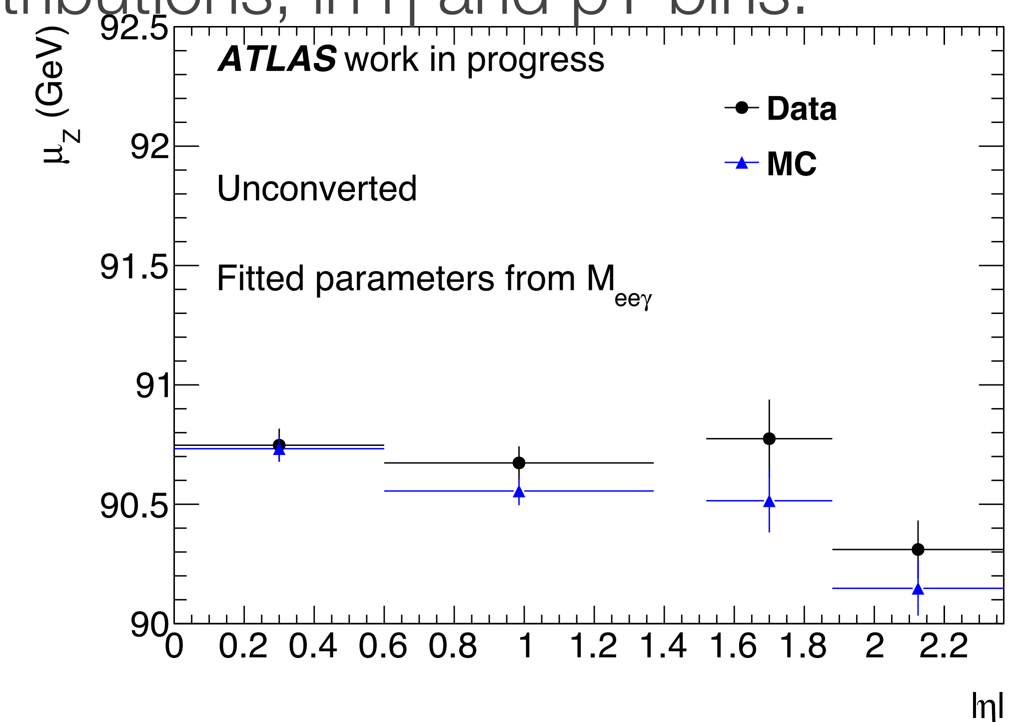

Same trends in data and MC are translated into stable scales.

Systematic uncertainties

The systematic uncertainties to the energy scale estimation:

- Lepton energy scale: Estimated by shifting the lepton momentum by its uncertainty and re-evaluating the scales.

Electron channel: ± 0.4 % **Muon Channel: <0.1%**

- Other uncertainties (fit model, background contamination): 0.1%.

Photon energy scales:

The error bars include both statistical and systematic components (most scales are dominated by statistical uncertainties).

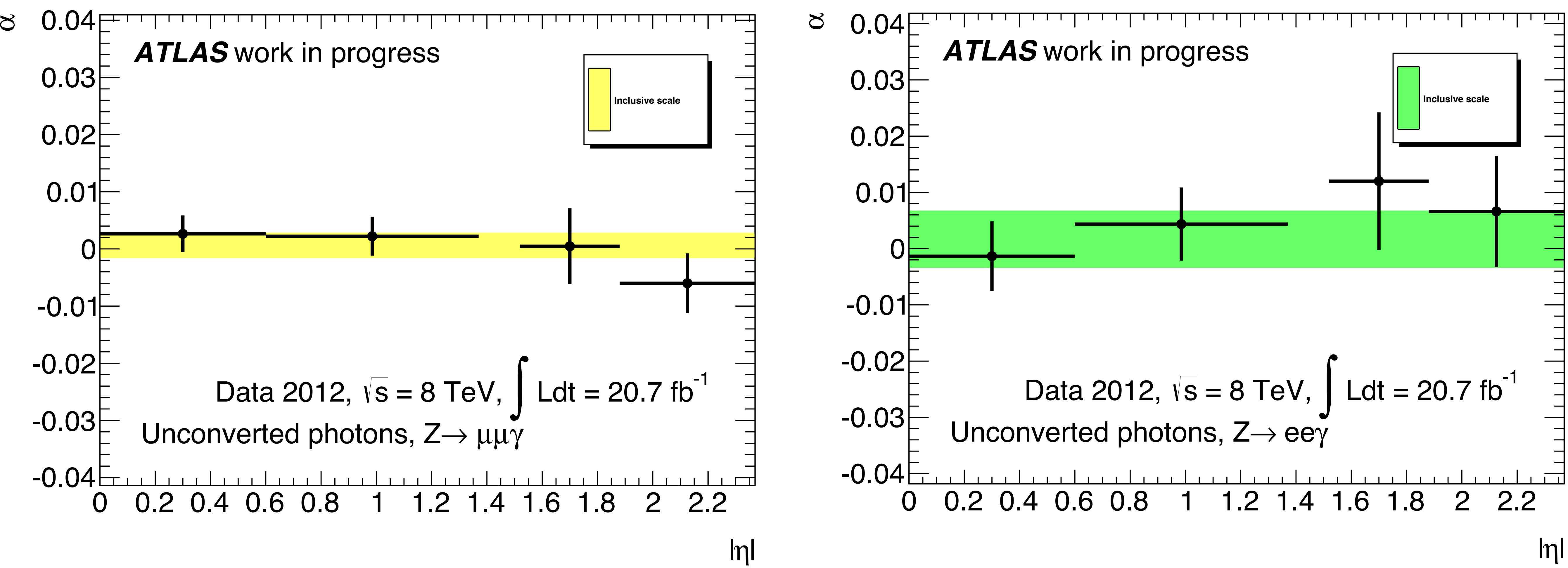

Colour band is inclusive scale (band width is 2σ)

Photon energy scales: Pt dependance

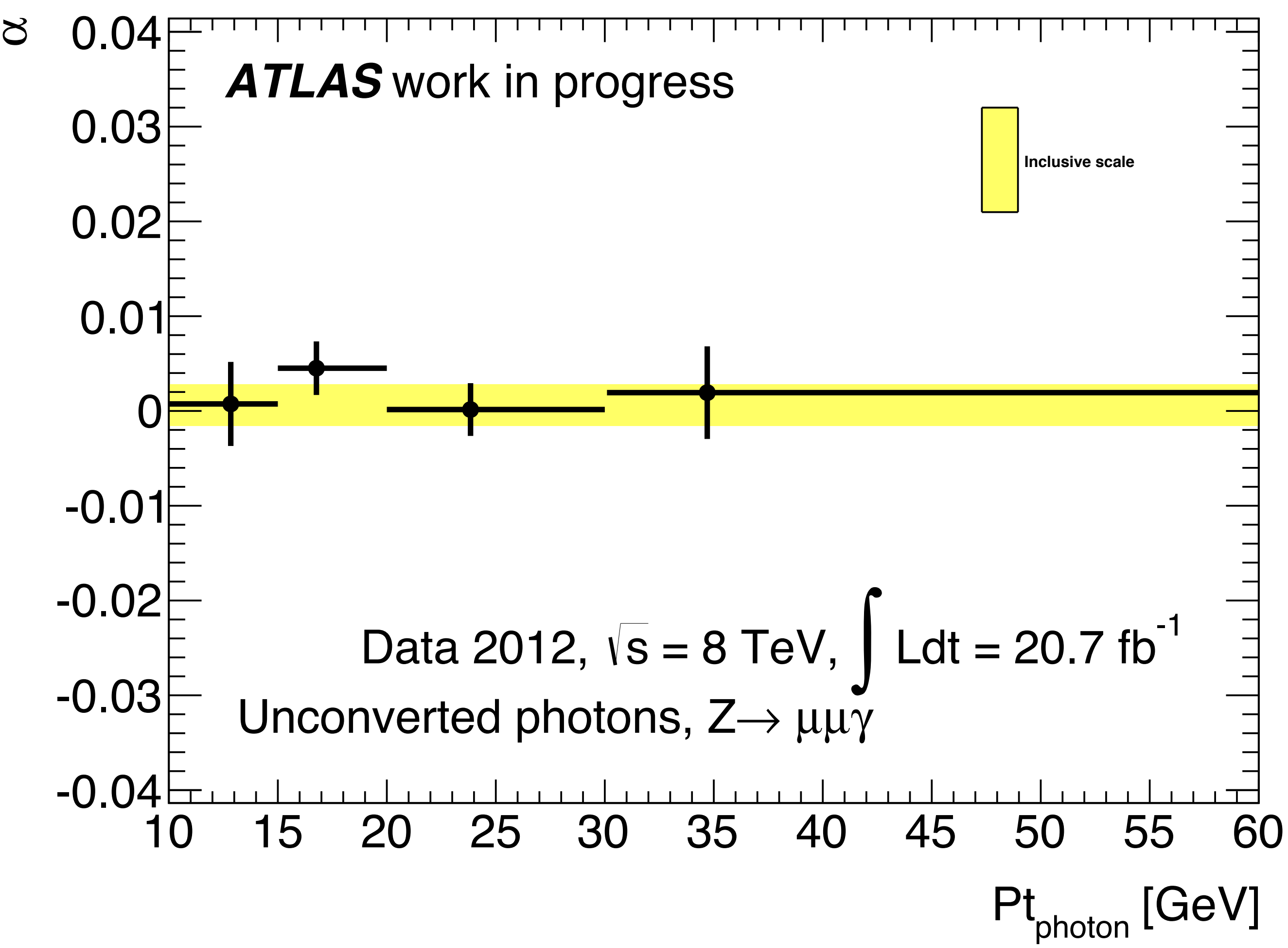

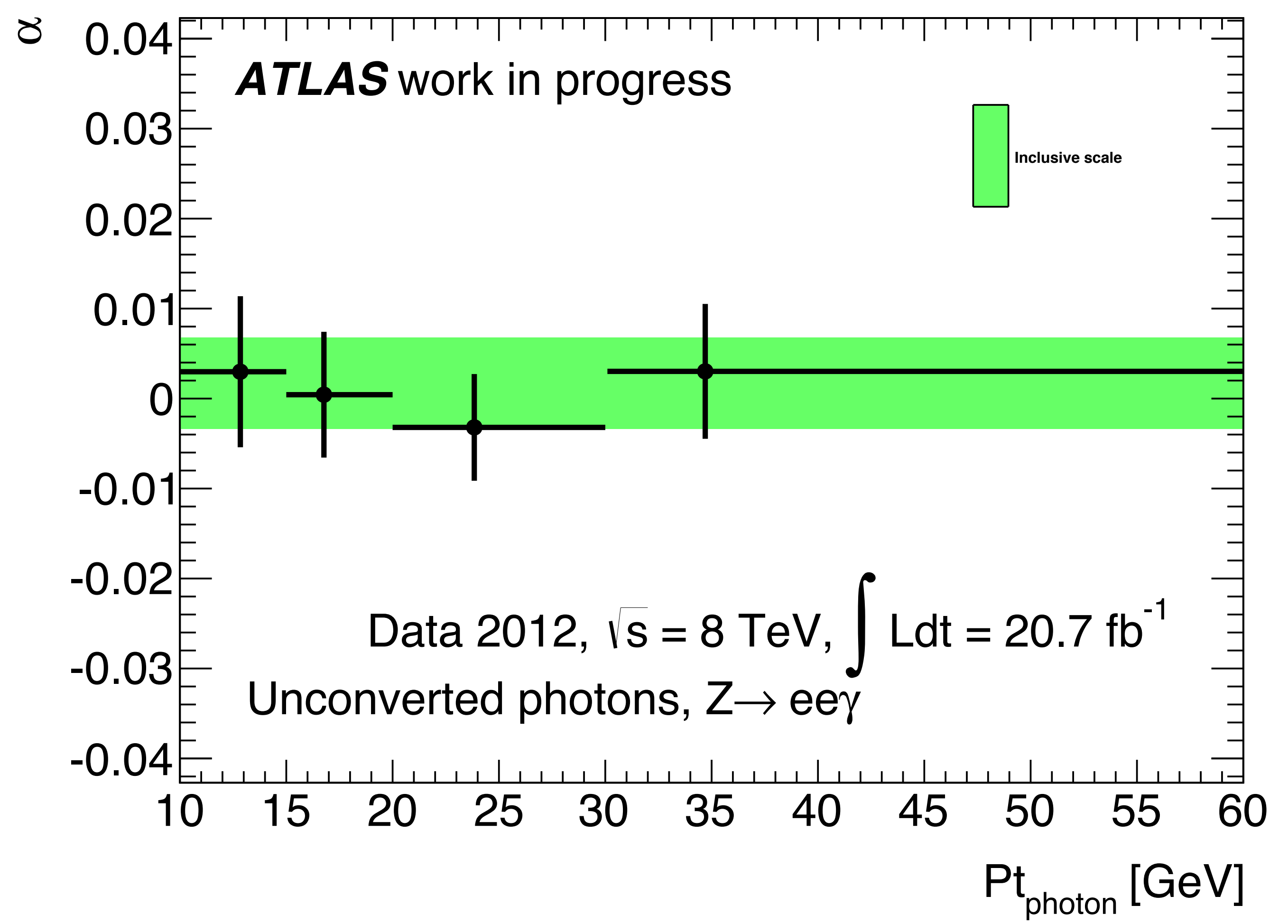

Most scales are compatible with 0 and within ±1%.

Combined photon energy scales

- The results in both channels are combined into one measurement:
  - Final scales extracted for fully-calibrated photons (MC calibration plus Z➞ee scales).
  - Photons without Z➞ee scales.

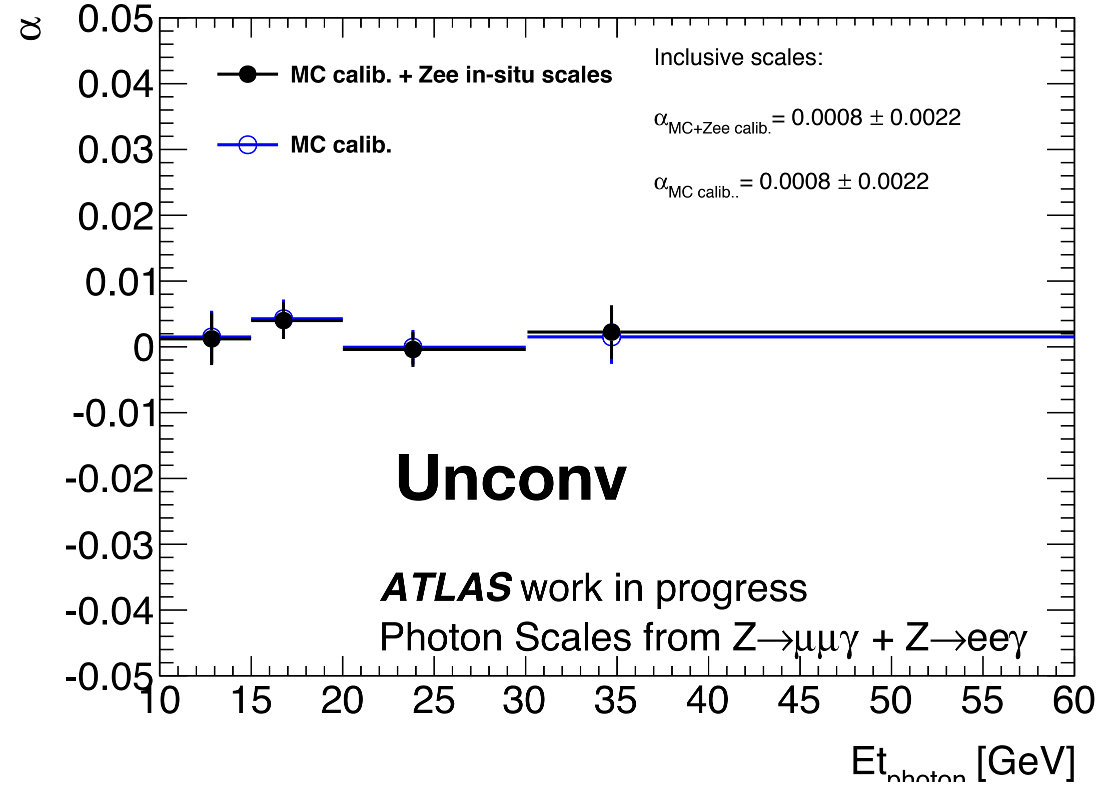

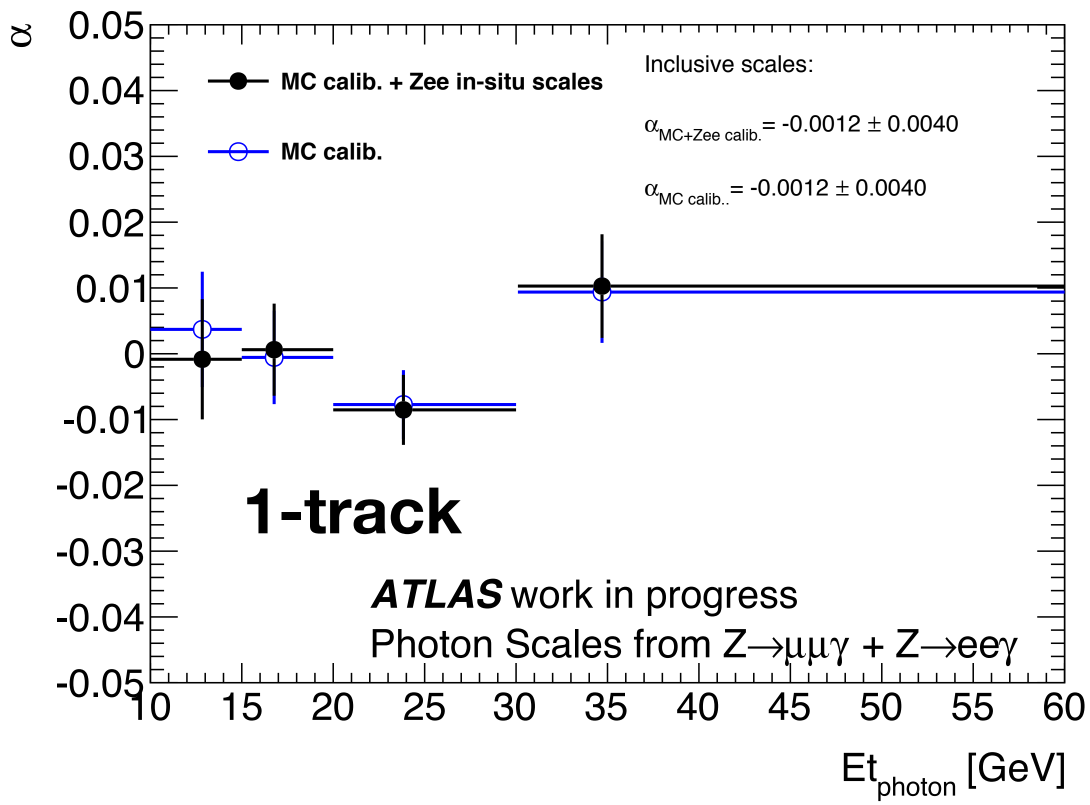

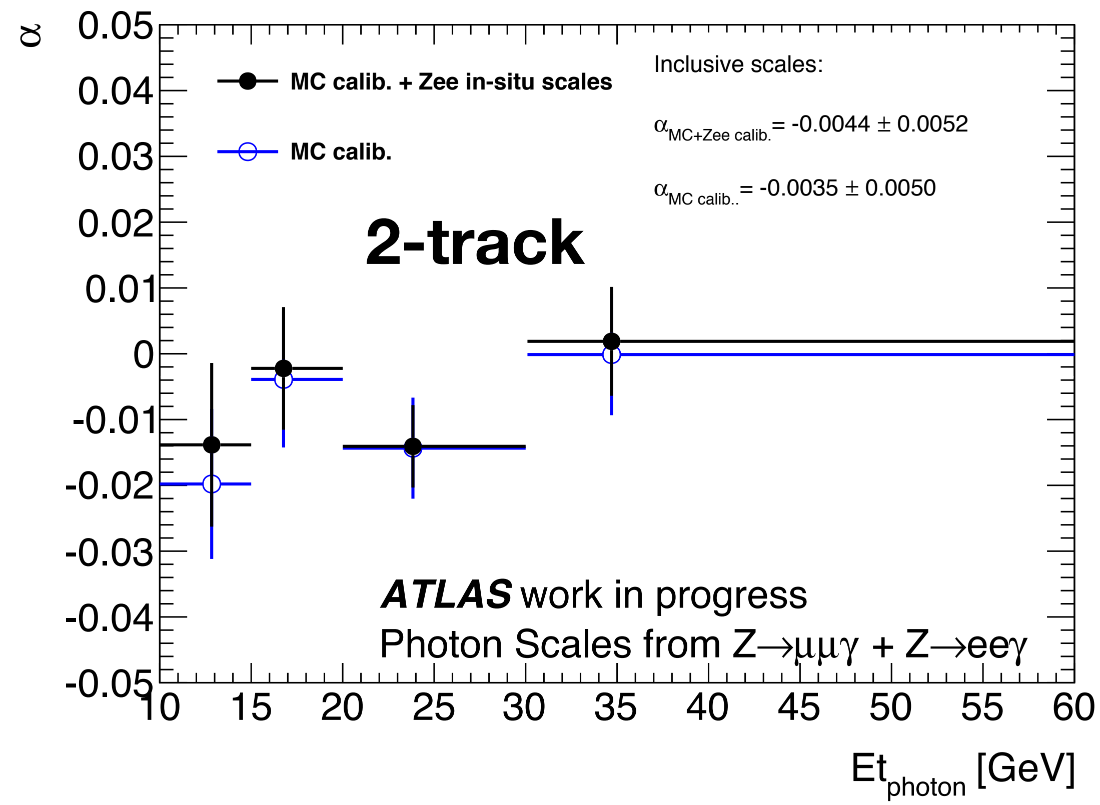

Combined photon energy scales

- The combine scales shows an overall good behaviour.
- Most of the scales are within 1.5σ from zero and within ±1%.
- Largest deviation is for 2-track conversions in the transition region of about (-3.0 ± 1.1)%.

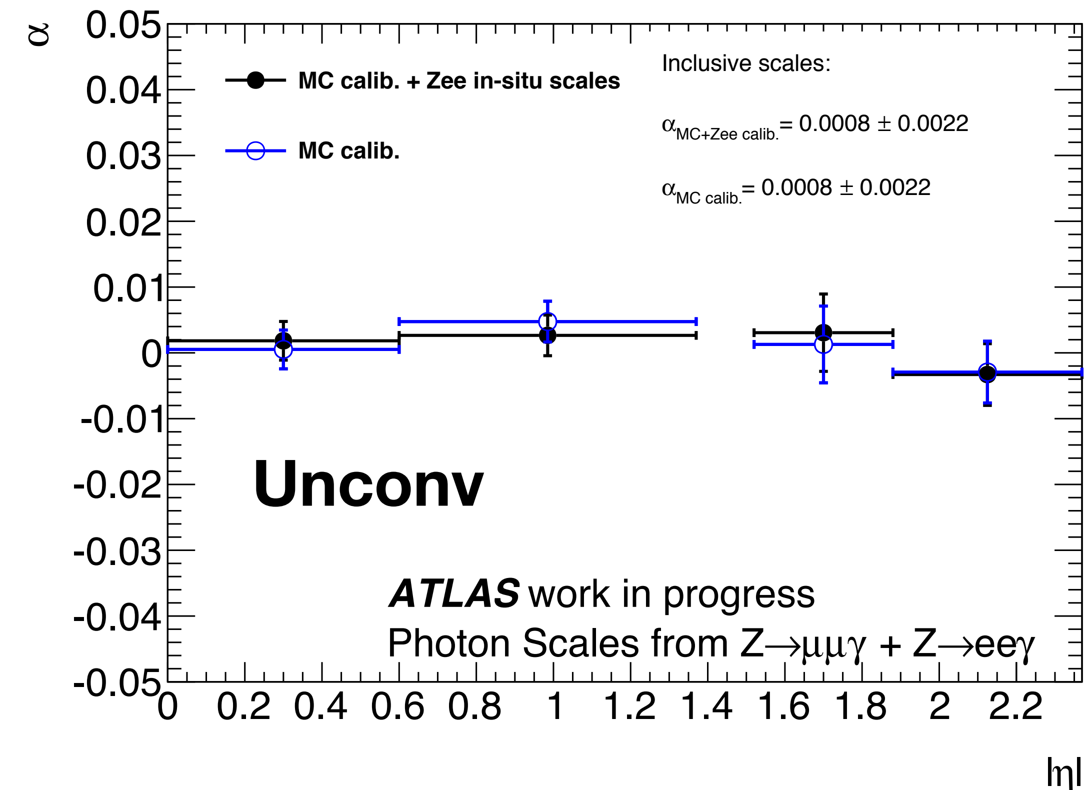

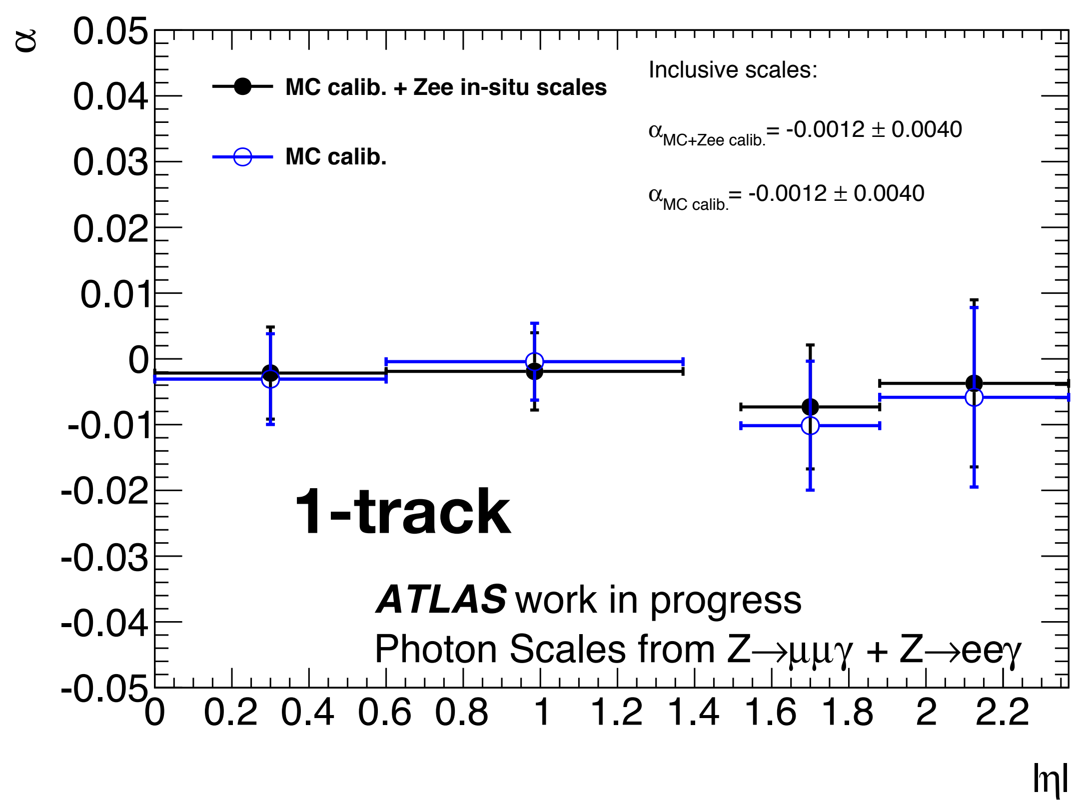

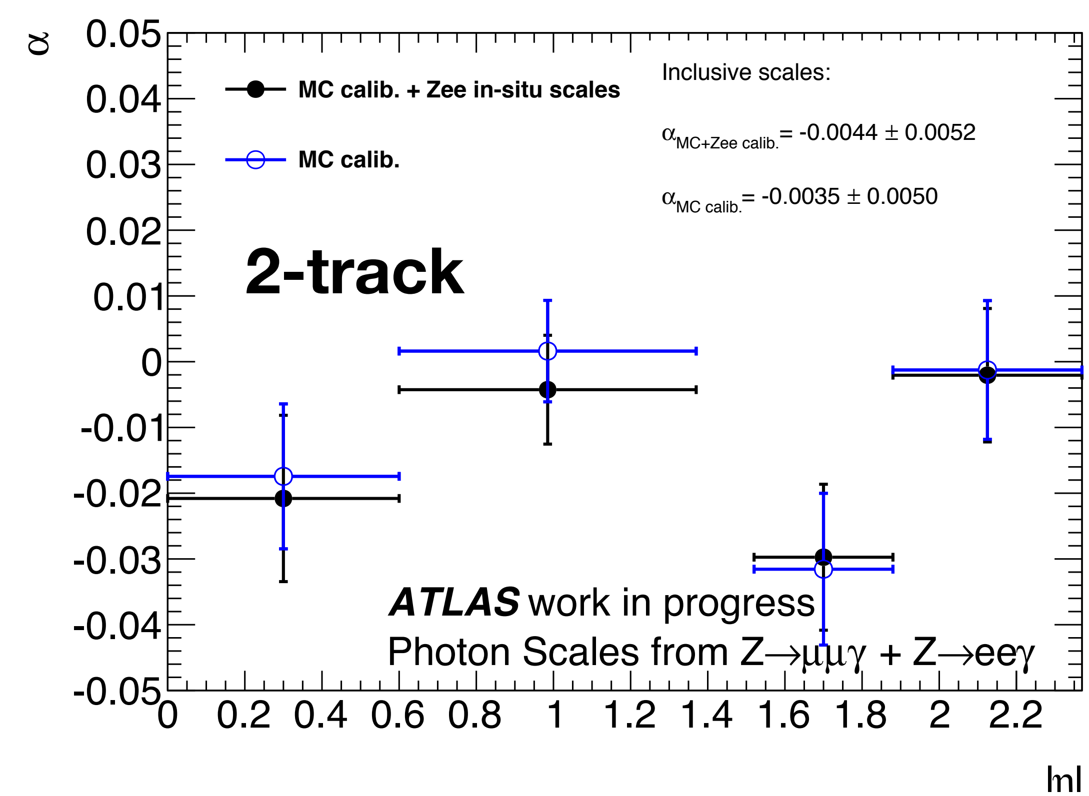

Photon energy scales: Conclusions

- For pT> 30 GeV, the precision in the ES measurement is competitive to the nominal systematic uncertainties associated to it in the H➞$\gamma\gamma$ mass measurement (±0.6%*).

- For low pT photons (pT<15 GeV), the precision is better than the one obtained with the standard calibration (up to 2% due to low energy extrapolation).

Photon scales (%)			
Pt. bin	Unconverted	Converted one-track	Converted two-track
10 GeV< p_T <15 GeV	+ 0.12± 0.40	- 0.08 ± 0.91	- 1.38 ± 1.24
15 GeV< p_T <20 GeV	+ 0.40 ± 0.28	+ 0.06 ± 0.70	- 0.22 ± 0.93
20 GeV< p_T <30 GeV	- 0.04 ± 0.26	- 0.85 ± 0.53	- 1.41 ± 0.63
p_T >30 GeV	+ 0.22 ± 0.41	+ 1.02 ± 0.79	- 0.19 ± 0.83

H➞$\gamma\gamma$ photon pT range*

Photon energy scales: Conclusions

- For pT> 30 GeV, the precision in the ES measurement is competitive to the nominal syste associated to measurement
- For low pT photons (pT<15 GeV), the precision is better than the one ard calibration ergy

These preliminary numbers are being updated using an improved geometry and aim at being released very soon.

Supporting note in process of documentation.
C. Rangel-Smith co-editor.

Photon scales (%)			
Pt. bin	Unconverted	Converted one-track	Converted two-track
10 GeV< p_T <15 GeV	+ 0.12± 0.40	- 0.08 ± 0.91	- 1.38 ± 1.24
15 GeV< p_T <20 GeV	+ 0.40 ± 0.28	+ 0.06 ± 0.70	- 0.22 ± 0.93
20 GeV< p_T <30 GeV	- 0.04 ± 0.26	- 0.85 ± 0.53	- 1.41 ± 0.63
p_T >30 GeV	+ 0.22 ± 0.41	+ 1.02 ± 0.79	- 0.19 ± 0.83

H→$\gamma\gamma$ photon pT range*

$H \rightarrow \gamma\gamma$ and $H \rightarrow Z\gamma$ channels

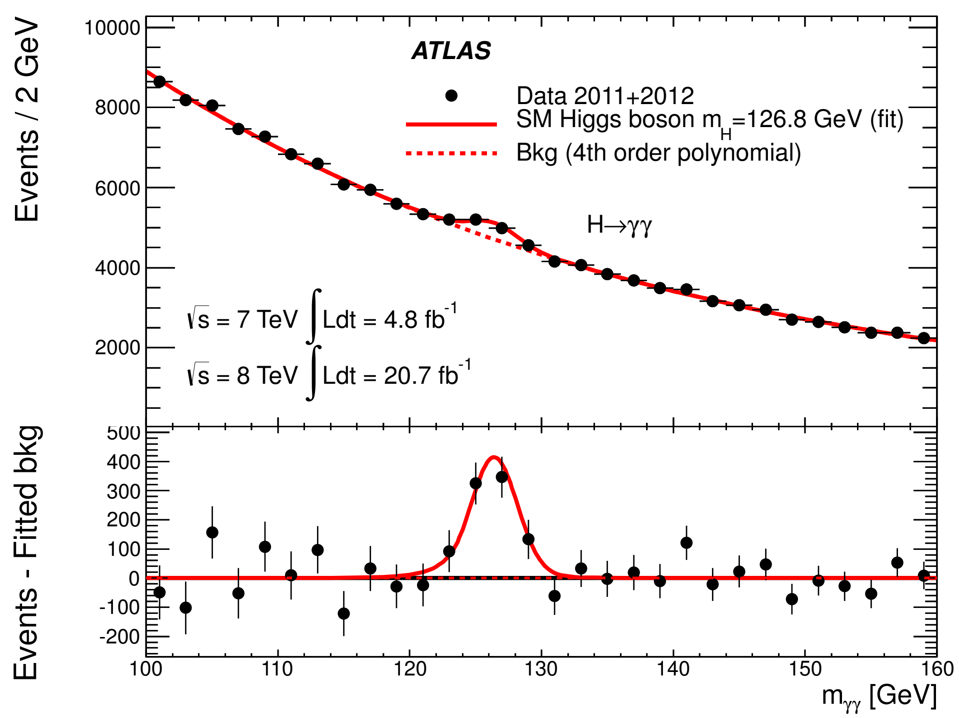

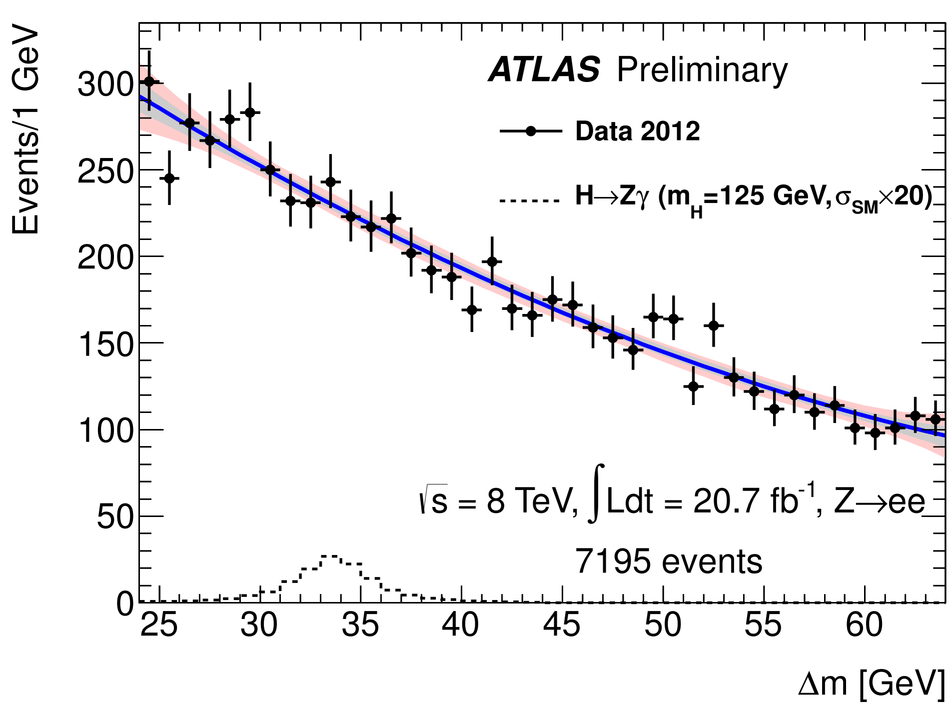

1. The SM and the Higgs boson
2. The LHC and the ATLAS experiment
3. The $H \rightarrow \gamma\gamma$ analysis in ATLAS (personal contributions)
4. Measurement of the photon energy scales using Radiative Z decays
5. The search for the Higgs boson in the $H \rightarrow Z\gamma$ channel
6. Outlook

Why H➙Zγ ?

ATLAS-CONF-2013-009

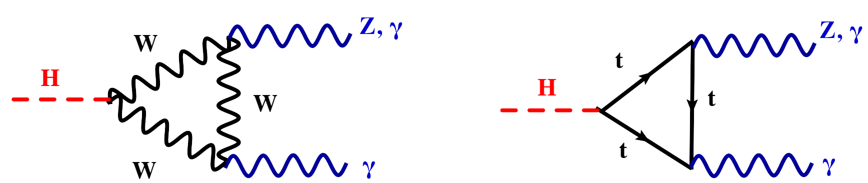

Pro: Sensitivity to new physics!

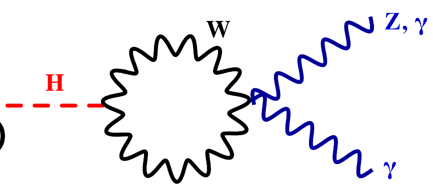

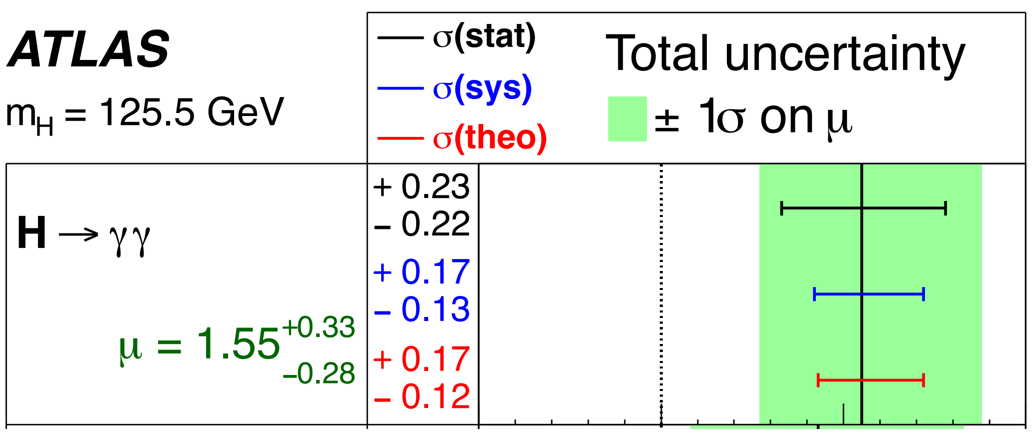

Pro: Analysis strategy can be very similar to H→γγ.

Pro: H→Zγ→γll channel kinematics of the decay can be cleanly reconstructed. We can use many of the tools developed in Higgs to γγ.

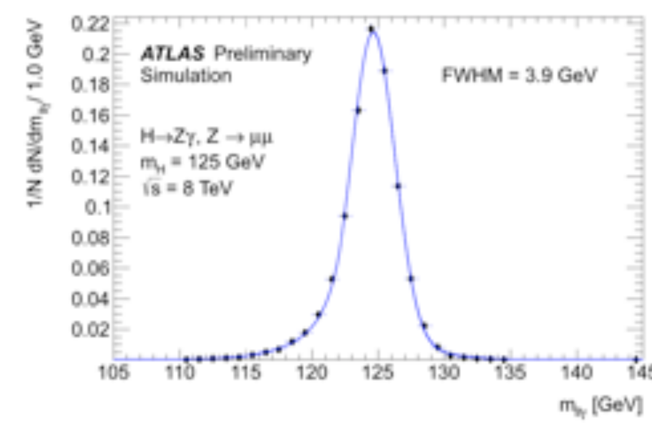

Pro: Similar selection to the Radiative Z samples (two leptons and an isolated photon). The ISR sample is the main background (82%) followed by Z+jets (17%), and smaller contributions from tt and WZ.

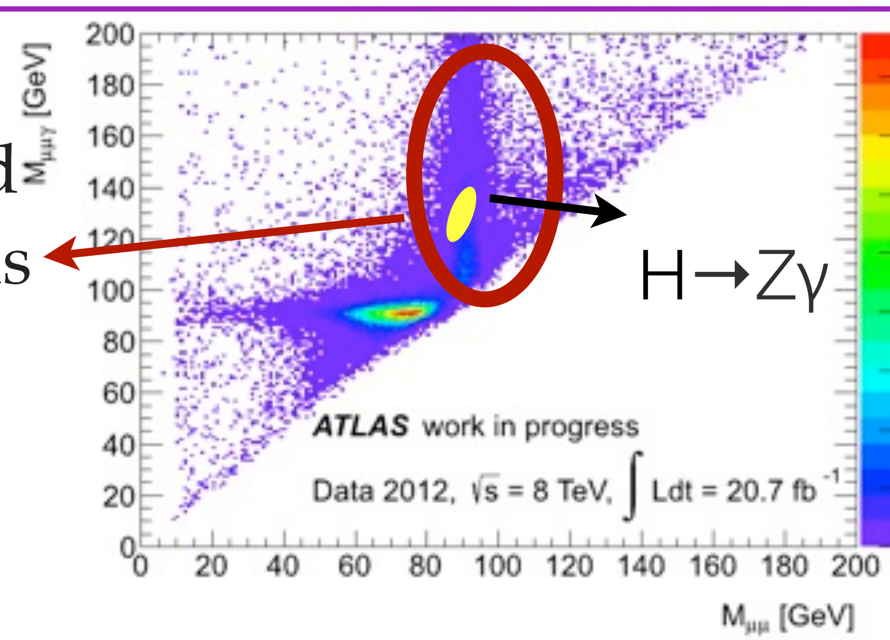

Why H➙Zγ ?

ATLAS-CONF-2013-009

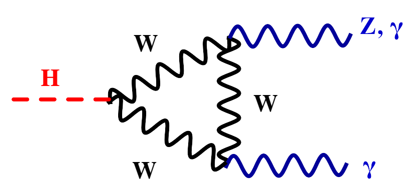

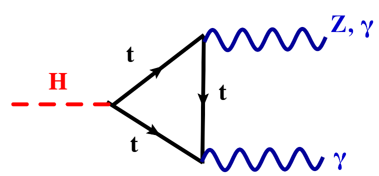

- Pro: Sensitivity to new physics!

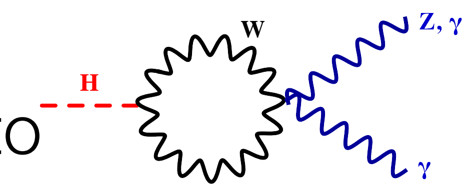

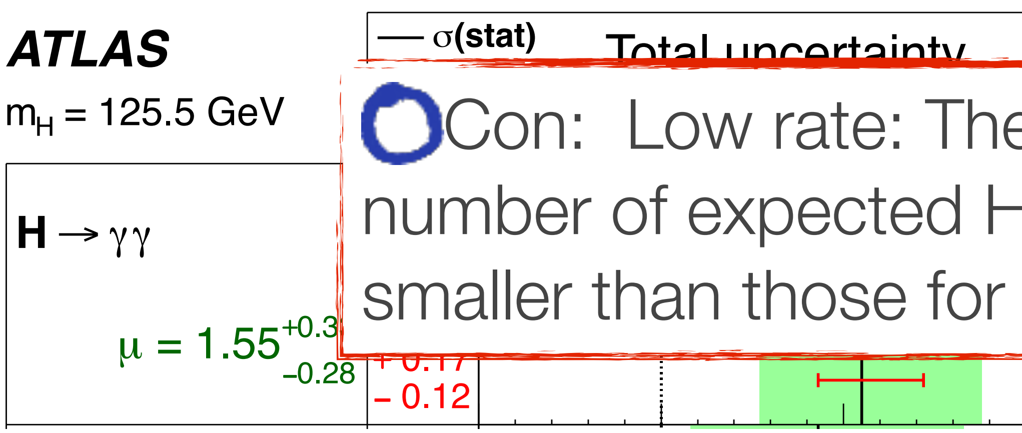

- Pro: Analysis strategy very similar to H→γγ.
- Pro: H→Zγ→γll channel kinematics of the decay can be cleanly reconstructed. We can use many of the tools developed in Higgs to γγ.

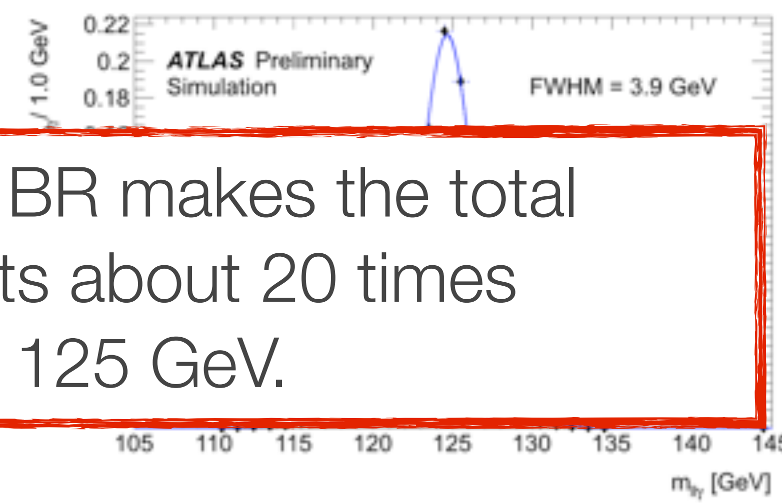

- Con: Low rate: The low Z➙ll BR makes the total number of expected Higgs events about 20 times smaller than those for H➙ γγ at 125 GeV.

- Pro: Similar selection to the Radiative Z samples (two leptons and an isolated photon). The ISR sample is the main background (82%) followed by Z+jets (17%)

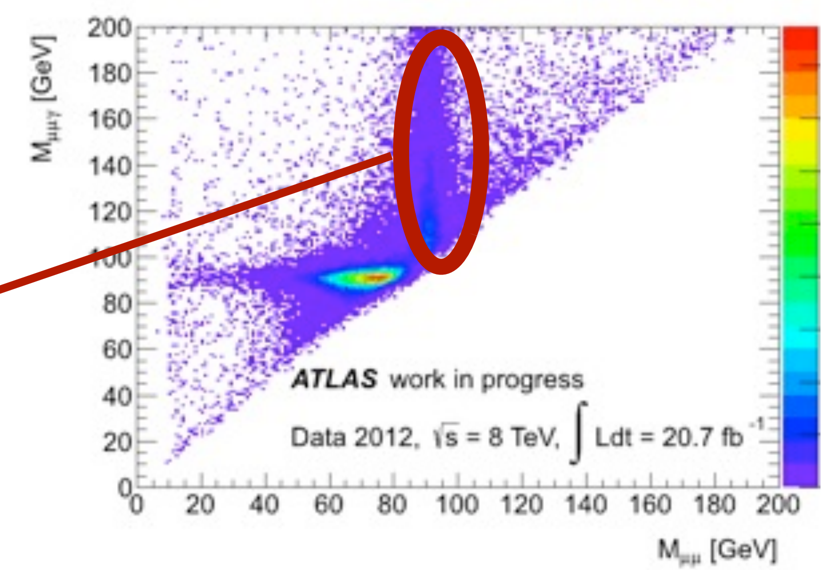

Why H→Zγ ?

ATLAS-CONF-2013-009

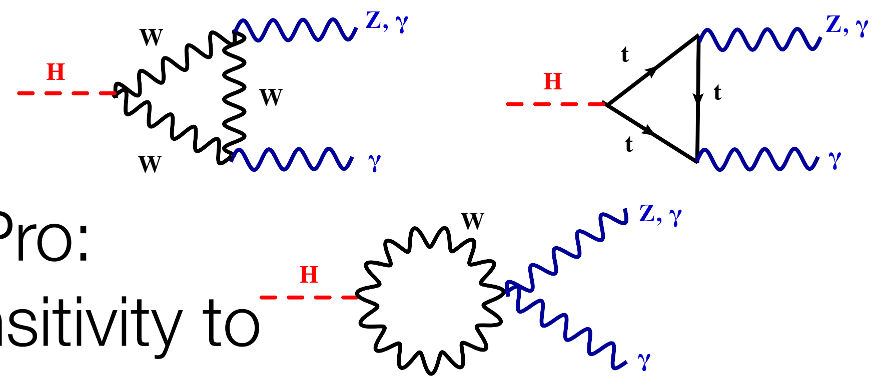

Pro: Sensitivity to new physics!

Pro: Analysis strategy very similar to H→γγ.

Pro: H→Zγ→γll channel kinematics of the decay can be cleanly reconstructed. We can use many of the tools developed in Higgs to γγ.

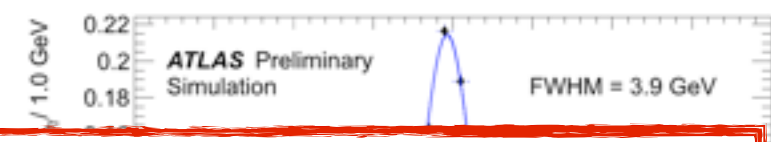

Con: Low rate: The low Z→ll BR makes the total

I'll review my contributions to the first ATLAS result of this search

Pro: Similar selection to the Radiative Z samples (two leptons and an isolated photon). The ISR sample is the main background (82%) followed by Z+jets (17%)

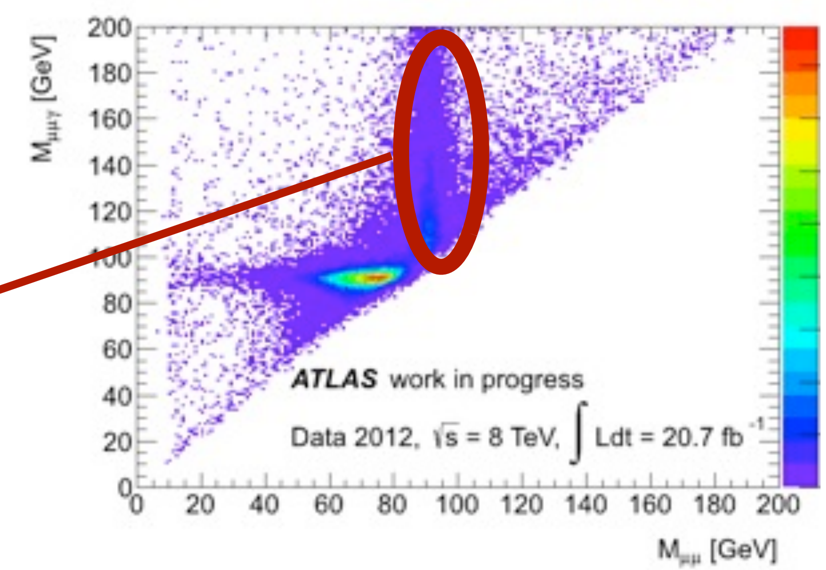

H➞Zγ background model

The signal photons are harder than the ISR Zγ background photons.

Using the pT of the photon as discriminant variable is inviable because the region where the S/B is improved, has a peaking background at around the most interesting region ($m_{ll\gamma}$ = 125 GeV).

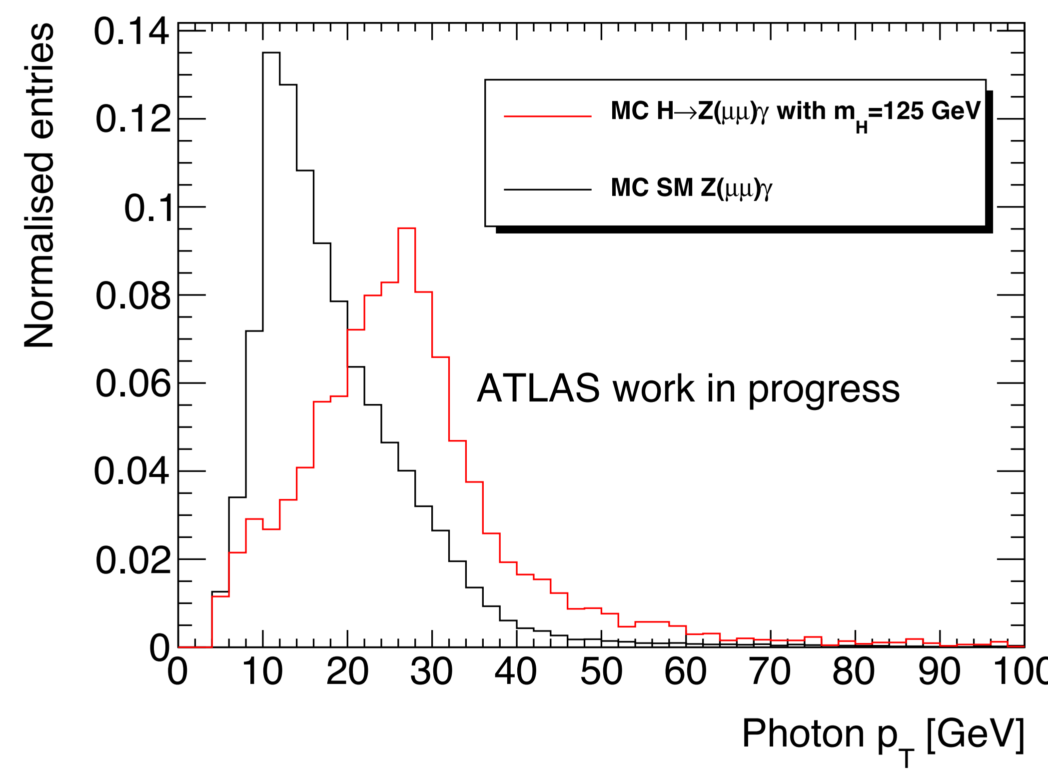

The pT cut on the photon is fixed at pT > 15 GeV.
And the search range is 120 GeV to 150 GeV.

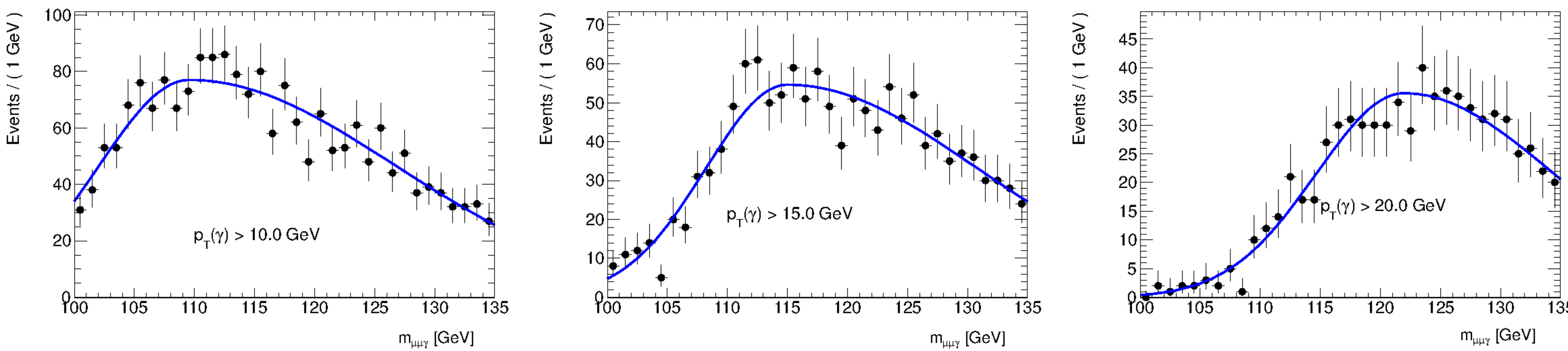

H➞Zγ signal model

- Using $M_{ll\gamma}$, is the easiest extension from H➞γγ
- It does not contain all the information.

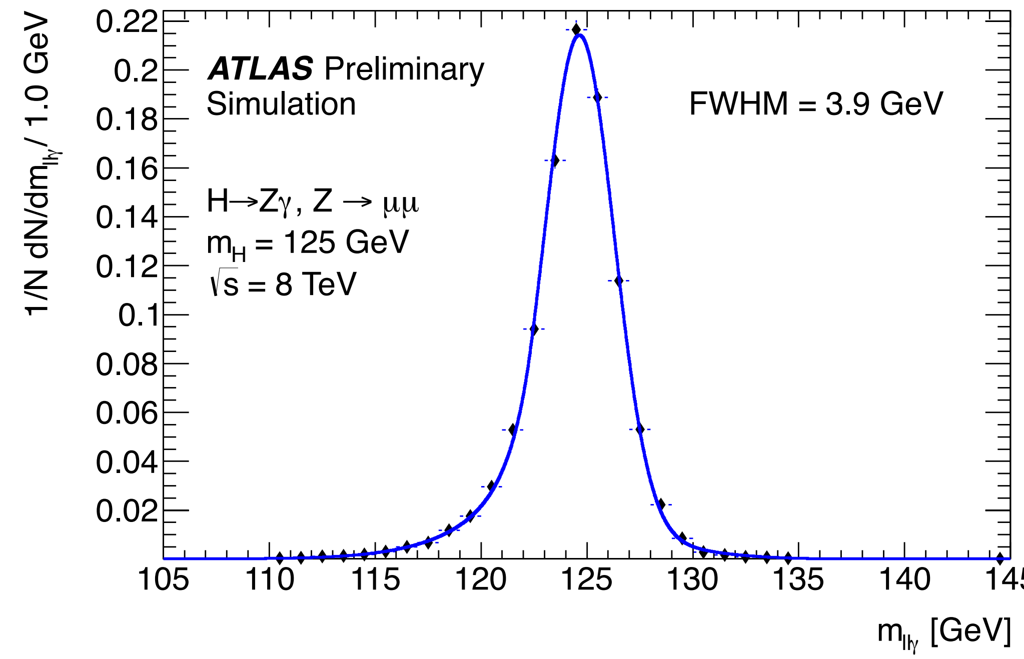

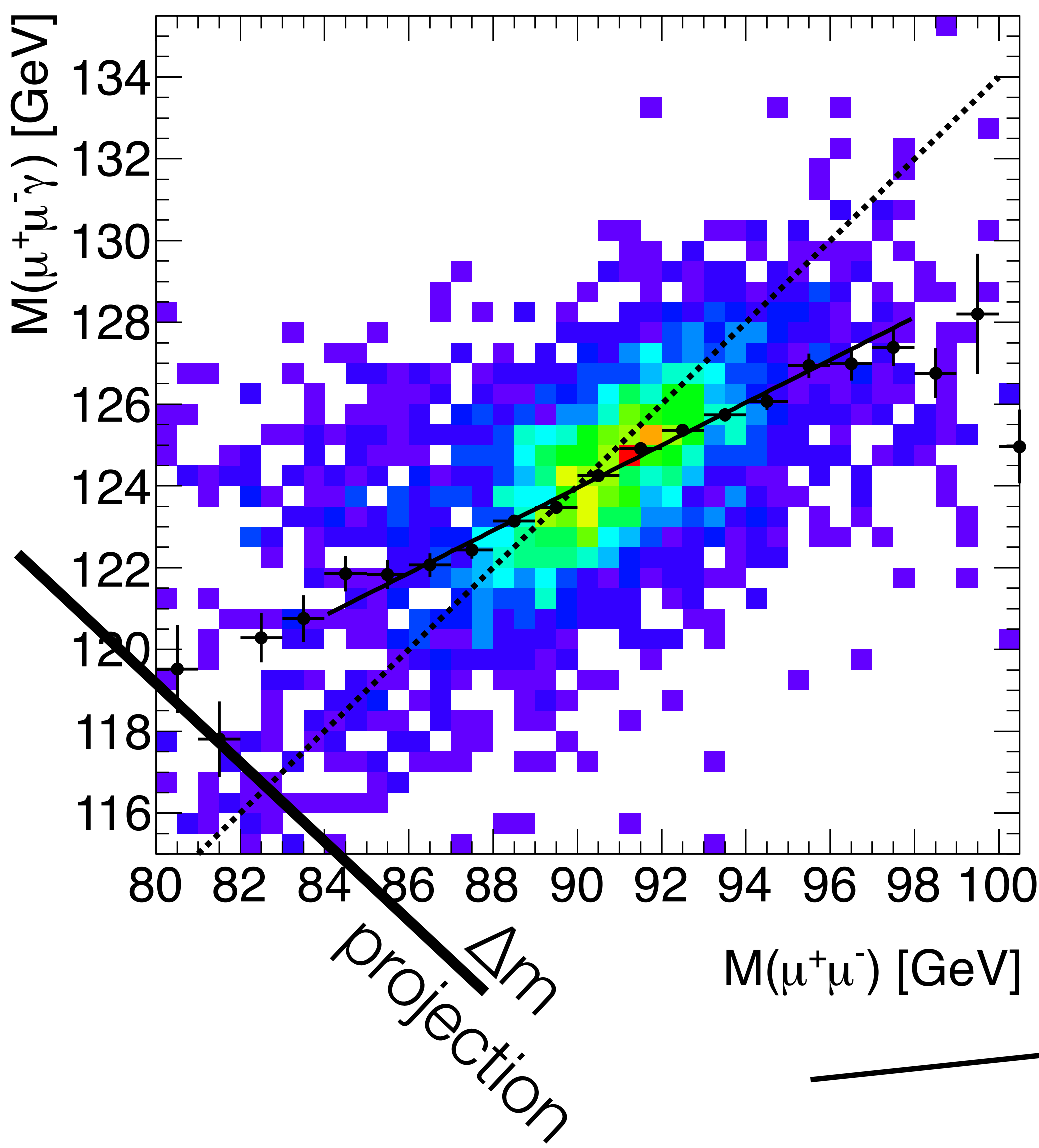

- Correlation pattern observed between the three and two-body invariant masses:

The correlation follows 0.5 GeV/GeV slope.

The resolution in $\Delta m = M_{ll\gamma} - M_{l}$ is narrower than in $M_{ll\gamma}$.

H➙Zγ signal model

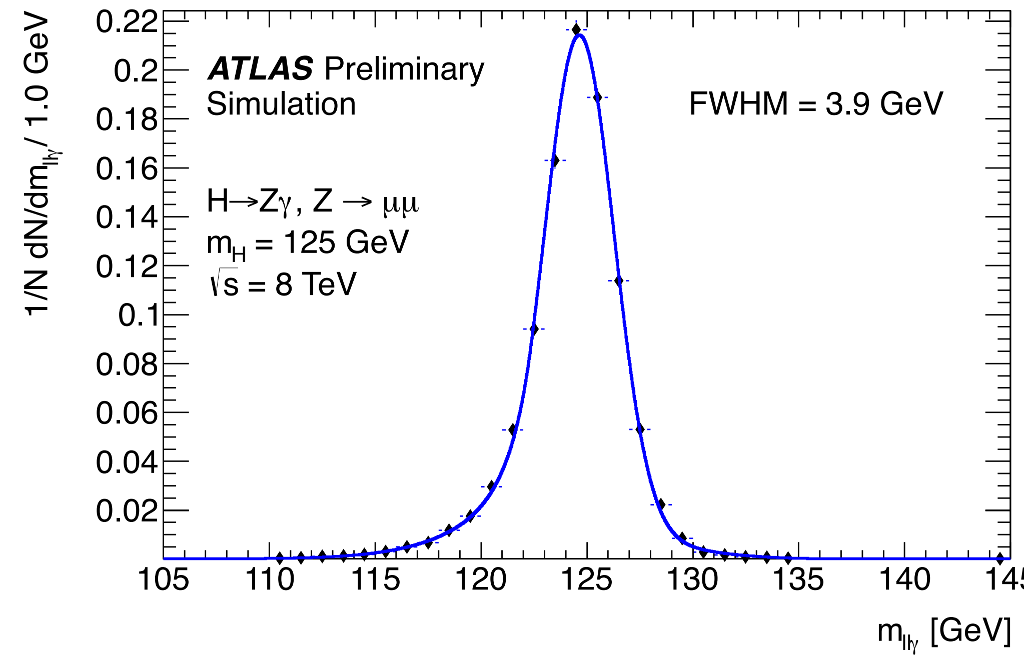

- Using $M_{ll\gamma}$, is the easiest extension from H➙γγ
- It does not contain all the information.

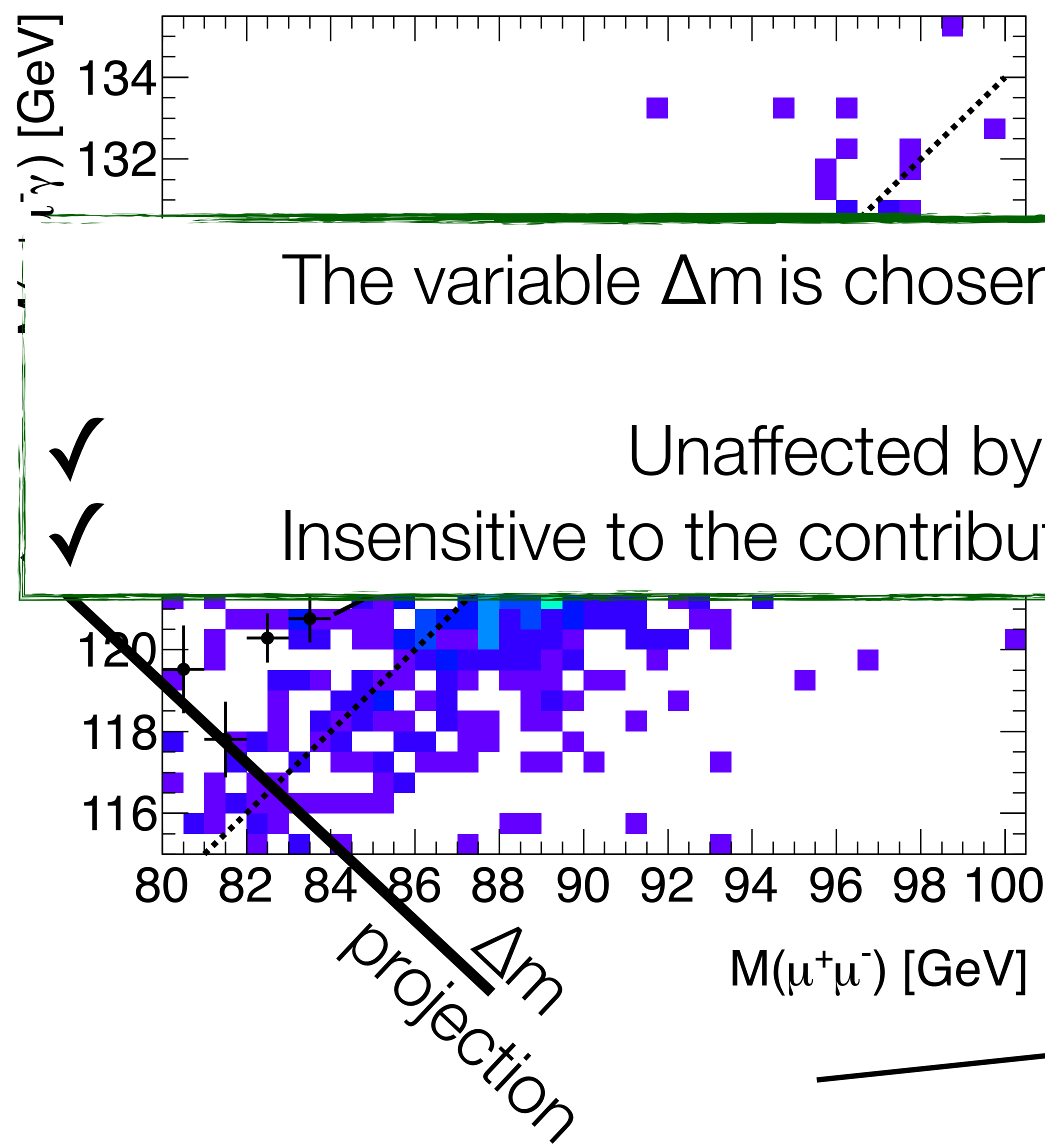

- Correlation pattern observed between the

The variable Δm is chosen as the discriminant variable for the search.

✓ Unaffected by lepton energy scale uncertainties.

✓ Insensitive to the contribution to the signal from FSR in H ➙ μμ decays.

The resolution in $\Delta m = M_{ll\gamma} - M_{l}$ is narrower than in $M_{ll\gamma}$.

H→Zγ signal properties

ATL-COM-PHYS-2013-081
Signal internal note.
C. Rangel-Smith co-editor.

15 SM Higgs events expected in 7 TeV + 8 TeV data sample at 125 GeV

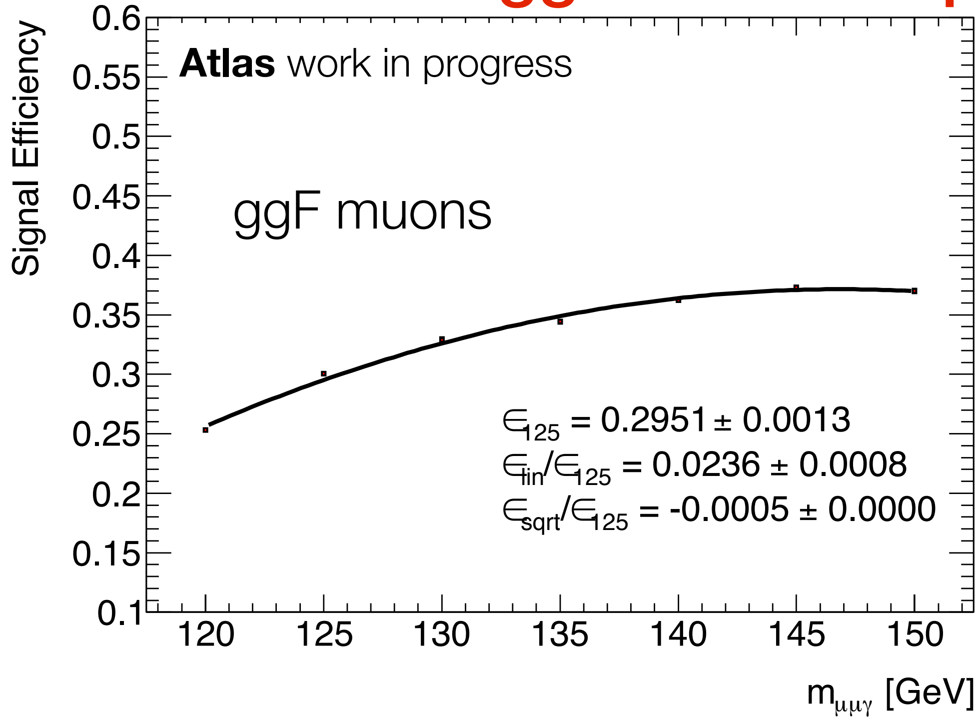

m_H [GeV]	$Z \to ee$, 8 TeV ε [%]	S	$Z \to \mu\mu$, 8 TeV ε [%]	S
120	21.3	4.0	25.8	4.9
125	24.6	5.9	29.7	7.2
130	27.3	7.7	32.8	9.3
135	29.4	9.0	35.1	10.7
140	30.9	9.5	36.6	11.3
145	31.7	9.2	37.3	10.8
150	32.0	8.1	37.2	9.4

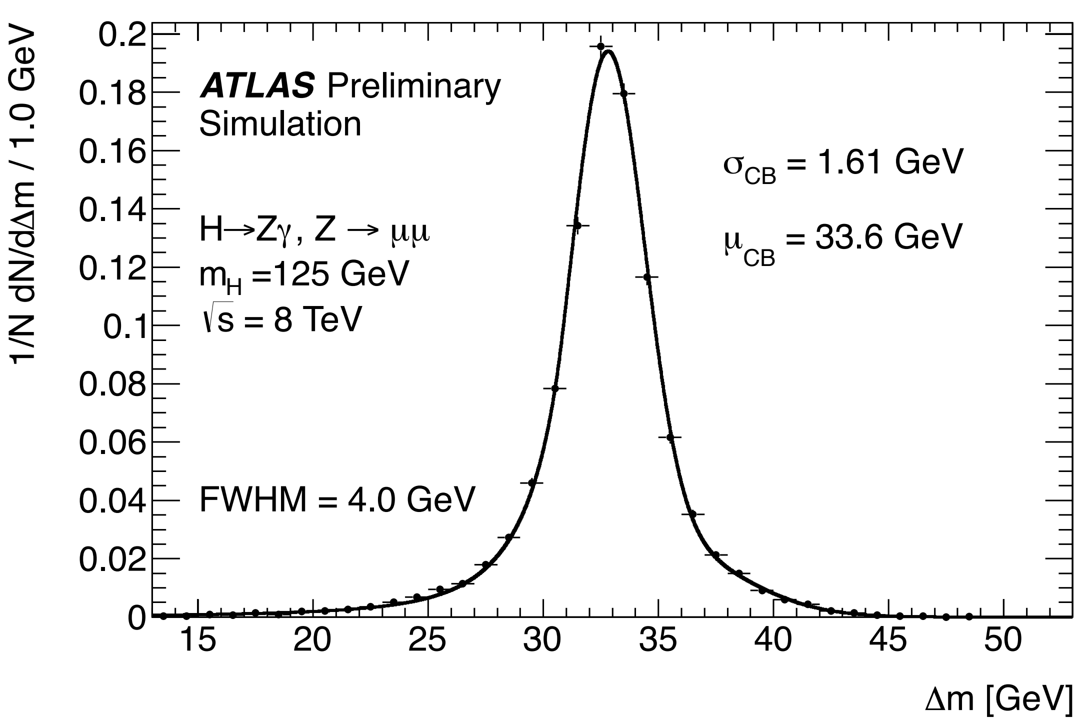

- Δm signal distribution is modelled with a Crystal Ball + wide gaussian for the tails.
- The global resolution model is built under the same premises of the one in H→γγ:
- An analytical function of Δm with a set of Δm dependent (σCB, μCB, μGA) and global parameters (k,fCB,aCB,nCB).

H→Zγ first ATLAS result

ATLAS-CONF-2013-009

- Performed over 4.6+20.7 of 7 and 8 TeV data.
- **Final Background model:**
- The model with best sensitivity to the signal and smaller bias is a third-order Chebychev polynomial in the fit range 24 < Δm <64 GeV.
- **Systematic uncertainties (analysis dominated statistical uncertainties).**

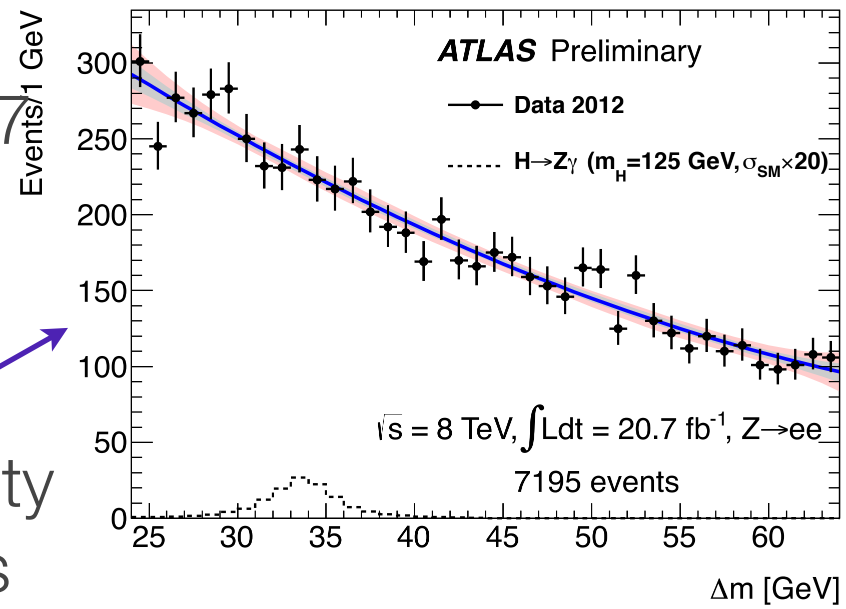

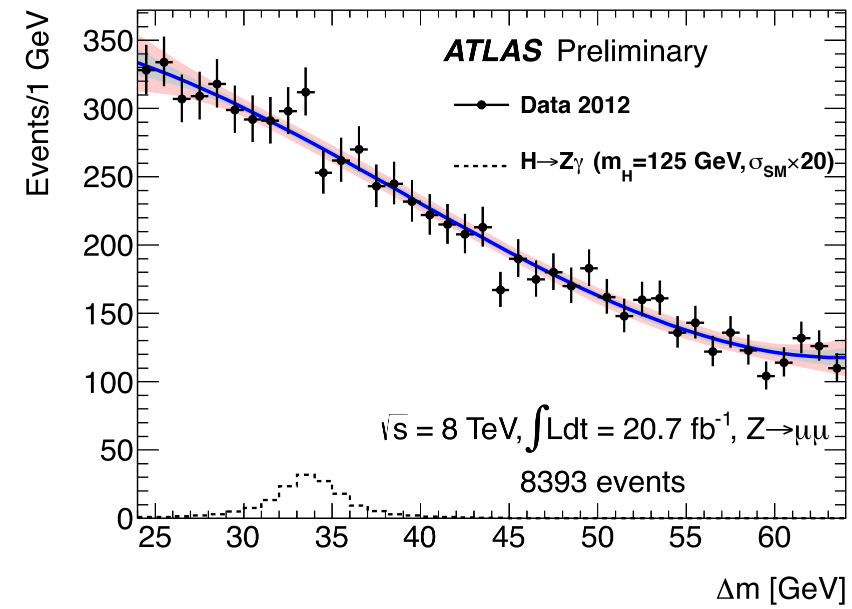

Systematic Uncertainty	$H \to Z(ee)\gamma(\%)$	$H \to Z(\mu\mu)\gamma(\%)$
Signal Yield		
Luminosity	3.6 (1.8)	3.6 (1.8)
Trigger efficiency	0.4 (0.2)	0.8 (0.7)
Acceptance of kinematic selection	4.0 (4.0)	4.0 (4.0)
γ identification efficiency	2.9 (2.9)	2.9 (2.9)
electron reconstruction and identification efficiency	2.7 (3.0)	
μ reconstruction and identification efficiency		0.6 (0.7)
e/γ energy scale	1.4 (0.3)	0.3 (0.2)
e/γ isolation	0.4 (0.3)	0.4 (0.2)
e/γ energy resolution	0.2 (0.2)	0.0 (0.0)
μ momentum scale		0.1 (0.1)
μ momentum resolution		0.0 (0.1)
Signal Δm resolution		
e/γ energy resolution	5.0 (5.0)	2.4 (2.4)
μ momentum resolution		0.0 (1.5)
Signal Δm peak position		
e/γ energy scale	0.2 (0.2) GeV	0.2 (0.2) GeV
μ momentum scale		negligible

H➞Zγ first ATLAS result

ATLAS-CONF-2013-009

The H➞Zγ is largest around 140 GeV,the expected exclusion is ~ 7 x SM in that mass region. At 125 GeV the expected and observed limits are 13.5 and 18.2 x SM, respectively.

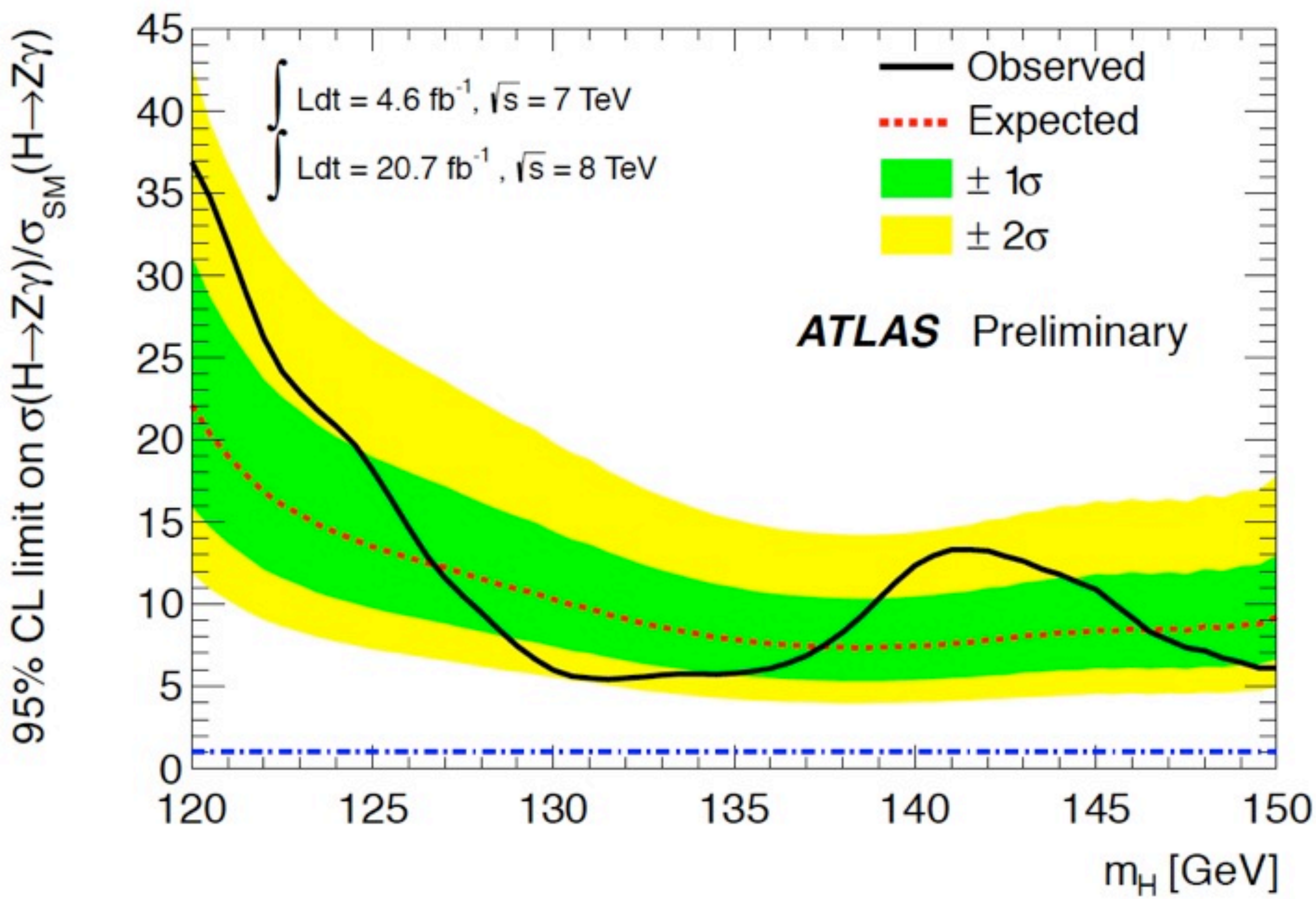

H➙Zγ first ATLAS result

ATLAS-CONF-2013-009

The H➙Zγ is largest around 140 GeV,the expected exclusion is ~ 7 x SM in that mass region. At 125 GeV the expected and observed limits are 13.5 and 18.2 x SM, respectively.

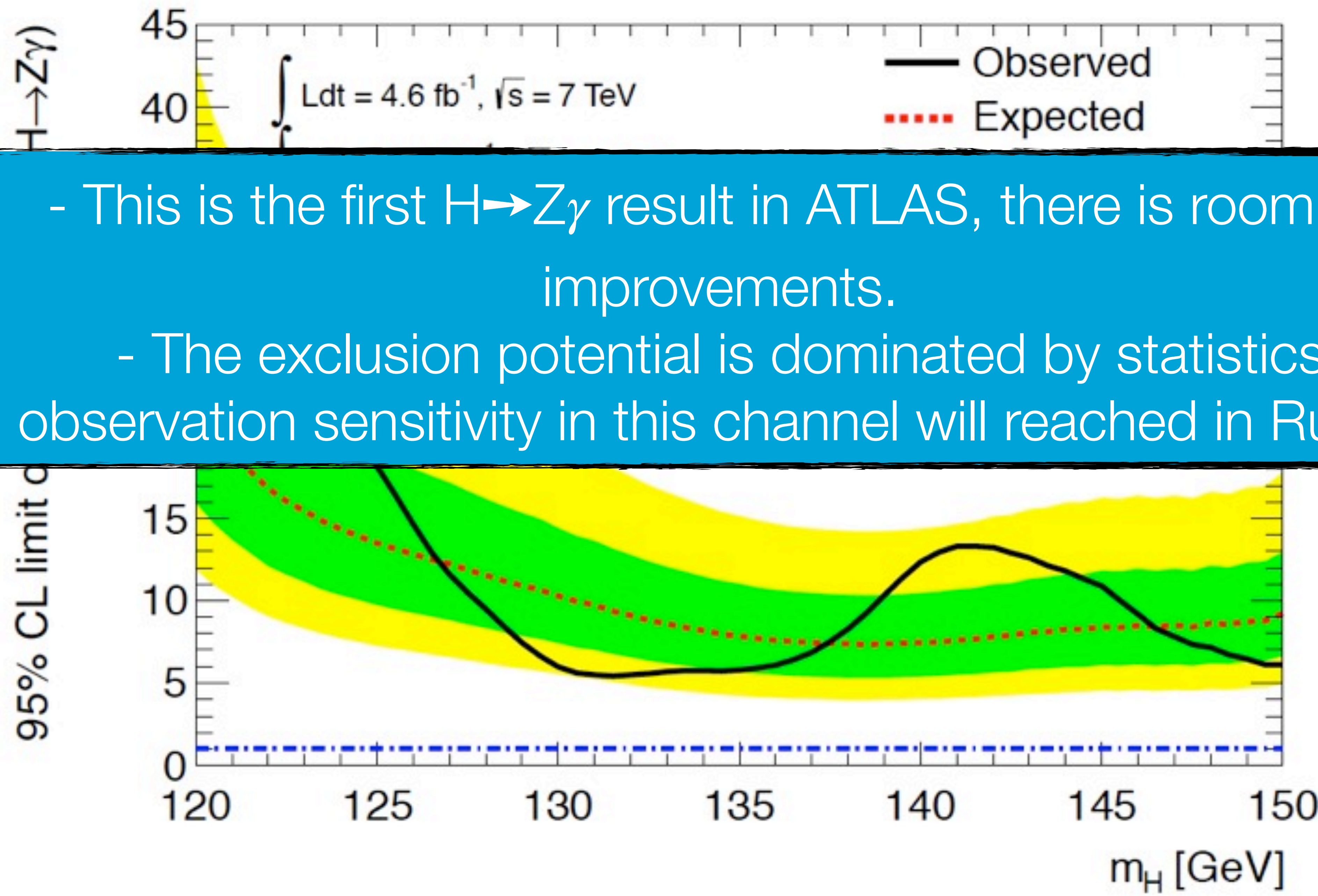

- This is the first H➙Zγ result in ATLAS, there is room for improvements.
- The exclusion potential is dominated by statistics, observation sensitivity in this channel will reached in Run II.

H➛γγ and H➛Zγ channels

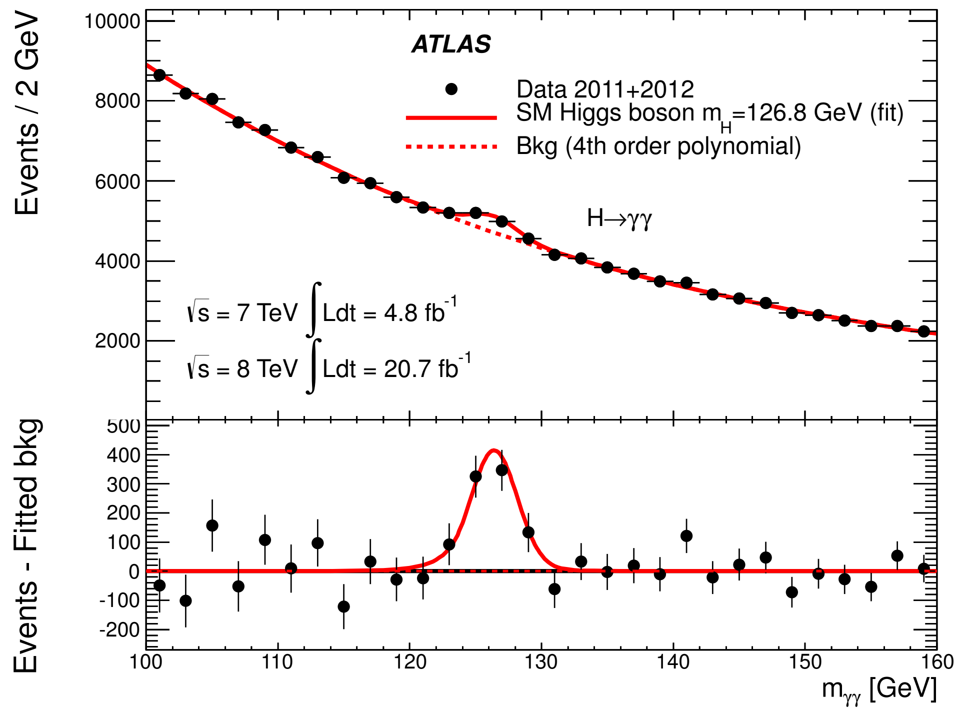

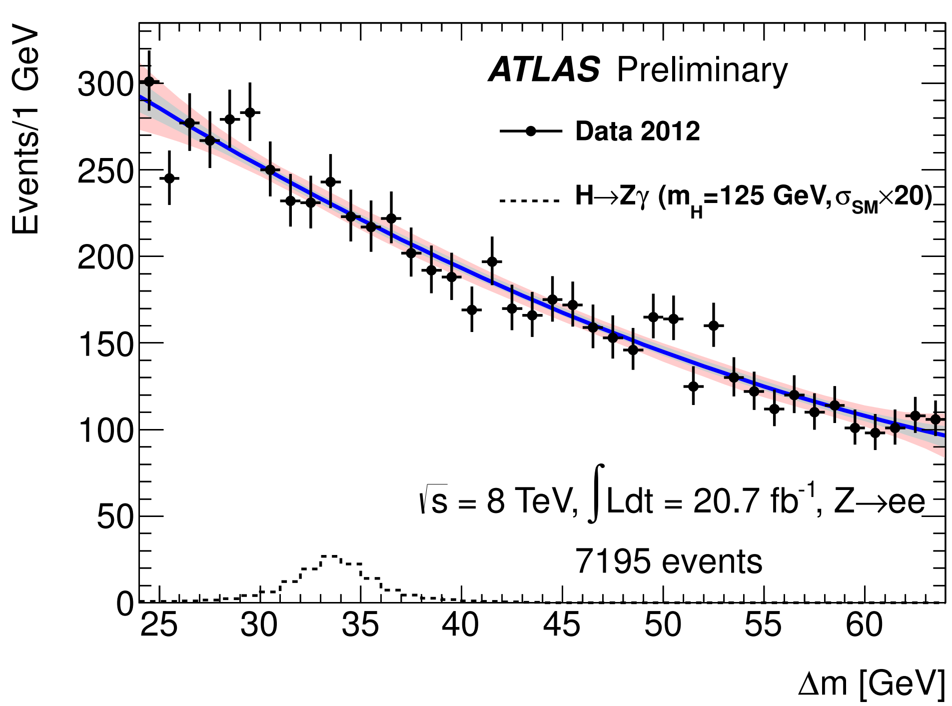

1. The SM and the Higgs boson
2. The LHC and the ATLAS experiment
3. The H➛γγ analysis in ATLAS (personal contributions)
4. Measurement of the photon energy scales using Radiative Z decays
5. The search for the Higgs boson in the H➛Zγ channel
6. **Outlook**

Outlook

We observed a Higgs boson was in this time period

- Contributions to the H→$\gamma\gamma$ analysis in ATLAS
  - MC photon performance studies
  - Validation of a calibration for converted photons
  - Provided a global resolution model for the signal parametrisation (yields and resolution). This model has been adopted by other analysis in ATLAS.

Outlook

We observed a Higgs boson was in this time period

- Contributions to the H➞$\gamma\gamma$ analysis in ATLAS
  - MC photon performance studies
  - Validation of a calibration for converted photons
  - Provided a global resolution model for the signal parametrisation (yields and resolution). This model has been adopted by other analysis in ATLAS.
- Independent measurement of the photon energy scale,
  - As a validation to the standard Z➞ee photon calibration
  - For photons in the H➞$\gamma\gamma$ energy range, the precision in the ES measurement is in the same order as their associated nominal systematic uncertainties.
  - For low pT photons (pT<15 GeV), the precision in the ES is better than the one obtained with the standard calibration.

Outlook

We observed a Higgs boson was in this time period

- Contributions to the $H \to \gamma\gamma$ analysis in ATLAS
  - MC photon performance studies
  - Validation of a calibration for converted photons
  - Provided a global resolution model for the signal parametrisation (yields and resolution). This model has been adopted by other analysis in ATLAS.
- Independent measurement of the photon energy scale,
  - As a validation to the standard $Z \to ee$ photon calibration
  - For photons in the $H \to \gamma\gamma$ energy range, the precision in the ES measurement is in the same order as their associated nominal systematic uncertainties.
  - For low pT photons (pT<15 GeV), the precision in the ES is better than the one obtained with the standard calibration.
- Contributions to the first search of the Higgs boson in the $H \to Z\gamma$ channel
  - Background model, choice of the discriminating variable and signal modelling
  - Observation sensitivity should be reached in the LHC Run II.

Outlook (2)

We observed a Higgs boson in this time period

- The Higgs discovery
  - Measurements of the spin, couplings, decay rates and (differential) cross-sections are being performed in all accessible Higgs channels in ATLAS and CMS.
  - Results show that this new particle is in general consistent with the SM Higgs boson.

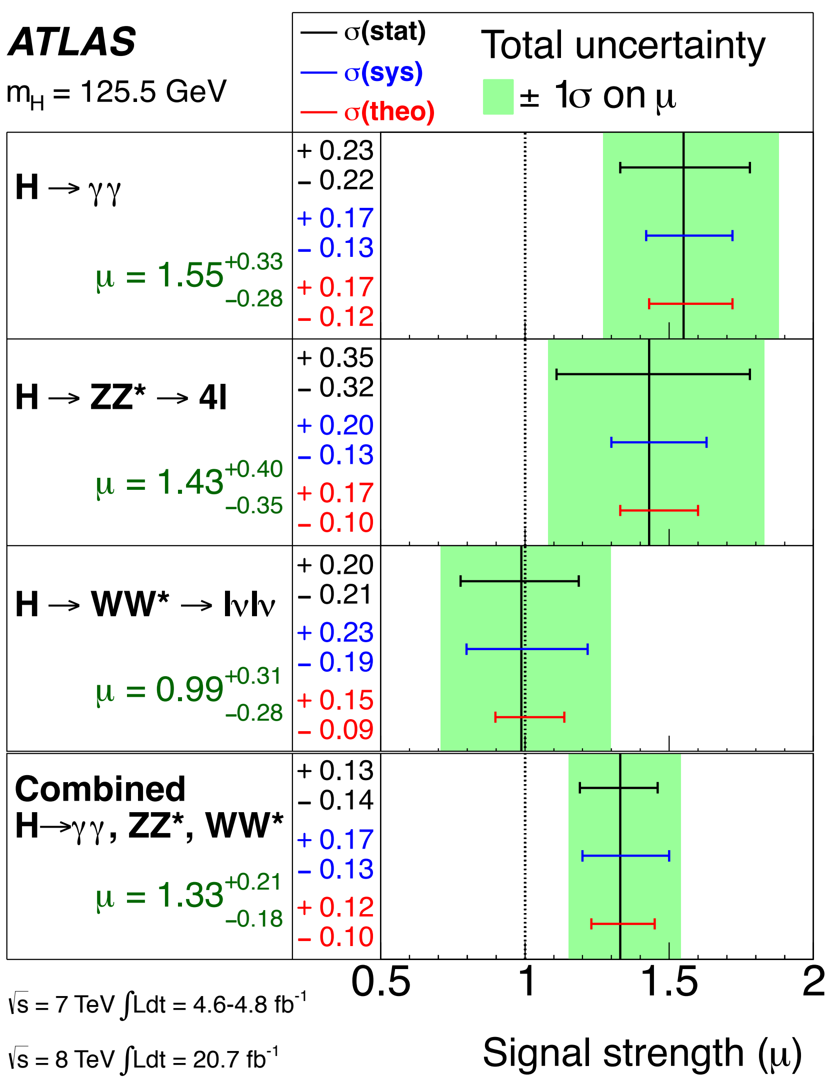

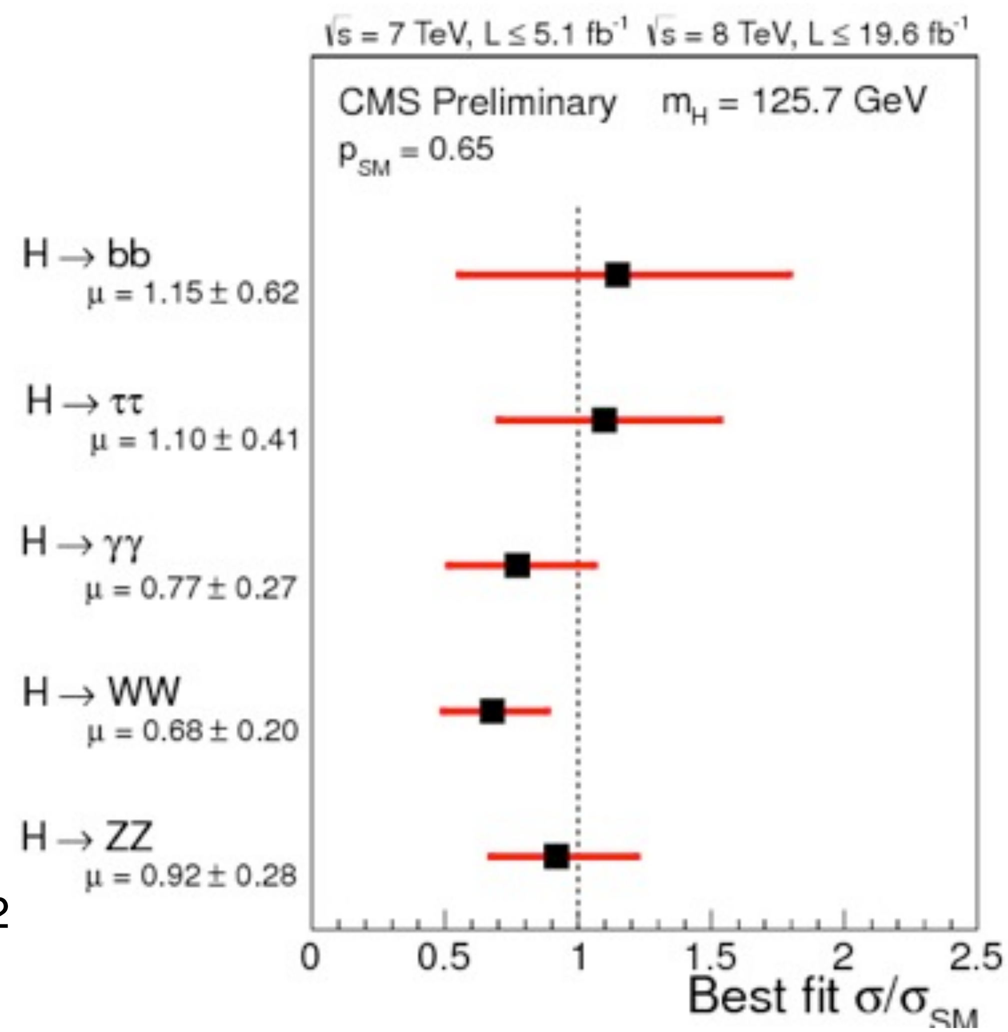

More analyses and data are needed to confirm whether this new particle is the SM Higgs boson.

"I think I've found the Higgs boson!"

Back-up

Electroweak fit

Parameter	Input value	Free in fit	Fit Result	Fit without M_H measurements	Fit without exp. input in line
M_H [GeV]$^{\circ}$	$125.7^{+0.4}_{-0.4}$	yes	$125.7^{+0.4}_{-0.4}$	94.7^{+25}_{-22}	94.7^{+25}_{-22}
M_W [GeV]	80.385 ± 0.015	–	$80.367^{+0.006}_{-0.007}$	$80.367^{+0.006}_{-0.007}$	80.360 ± 0.011
Γ_W [GeV]	2.085 ± 0.042	–	2.091 ± 0.001	2.091 ± 0.001	2.091 ± 0.001
M_Z [GeV]	91.1875 ± 0.0021	yes	91.1878 ± 0.0021	91.1878 ± 0.0021	91.1978 ± 0.0114
Γ_Z [GeV]	2.4952 ± 0.0023	–	2.4954 ± 0.0014	2.4954 ± 0.0014	2.4950 ± 0.0017
$\sigma^0_{\rm had}$ [nb]	41.540 ± 0.037	–	41.479 ± 0.014	41.479 ± 0.014	41.471 ± 0.015
R^0_ℓ	20.767 ± 0.025	–	20.740 ± 0.017	20.740 ± 0.017	20.715 ± 0.026
$A^{0,\ell}_{\rm FB}$	0.0171 ± 0.0010	–	$0.01626^{+0.0001}_{-0.0002}$	$0.01626^{+0.0001}_{-0.0002}$	0.01624 ± 0.0002
A_ℓ $^{(\star)}$	0.1499 ± 0.0018	–	0.1472 ± 0.0007	0.1472 ± 0.0007	–
$\sin^2\theta^\ell_{\rm eff}(Q_{\rm FB})$	0.2324 ± 0.0012	–	$0.23149^{+0.00010}_{-0.00008}$	$0.23149^{+0.00010}_{-0.00008}$	0.23150 ± 0.00009
A_c	0.670 ± 0.027	–	$0.6679^{+0.00034}_{-0.00028}$	$0.6679^{+0.00034}_{-0.00028}$	0.6680 ± 0.00031
A_b	0.923 ± 0.020	–	$0.93464^{+0.00005}_{-0.00007}$	$0.93464^{+0.00005}_{-0.00007}$	0.93463 ± 0.00006
$A^{0,c}_{\rm FB}$	0.0707 ± 0.0035	–	0.0738 ± 0.0004	0.0738 ± 0.0004	0.0737 ± 0.0004
$A^{0,b}_{\rm FB}$	0.0992 ± 0.0016	–	0.1032 ± 0.0005	0.1032 ± 0.0005	0.1034 ± 0.0003
R^0_c	0.1721 ± 0.0030	–	0.17223 ± 0.00006	0.17223 ± 0.00006	0.17223 ± 0.00006
R^0_b	0.21629 ± 0.00066	–	0.21548 ± 0.00005	0.21548 ± 0.00005	0.21547 ± 0.00005
$\overline{m}_c$ [GeV]	$1.27^{+0.07}_{-0.11}$	yes	$1.27^{+0.07}_{-0.11}$	$1.27^{+0.07}_{-0.11}$	–
$\overline{m}_b$ [GeV]	$4.20^{+0.17}_{-0.07}$	yes	$4.20^{+0.17}_{-0.07}$	$4.20^{+0.17}_{-0.07}$	–
m_t [GeV]	173.20 ± 0.87	yes	173.53 ± 0.82	173.53 ± 0.82	$176.11^{+2.88}_{-2.35}$
$\Delta\alpha^{(5)}_{\rm had}(M^2_Z)$ $^{(\dagger\triangle)}$	2757 ± 10	yes	2755 ± 11	2755 ± 11	2718^{+49}_{-43}
$\alpha_s(M^2_Z)$	–	yes	$0.1190^{+0.0028}_{-0.0027}$	$0.1190^{+0.0028}_{-0.0027}$	0.1190 ± 0.0027
$\delta_{\rm th} M_W$ [MeV]	$[-4, 4]_{\rm theo}$	yes	4	4	–
$\delta_{\rm th} \sin^2\theta^\ell_{\rm eff}$ $^{(\dagger)}$	$[-4.7, 4.7]_{\rm theo}$	yes	-0.6	-0.5	–

$^{(\circ)}$Average of ATLAS ($M_H = 126.0 \pm 0.4\,(\text{stat}) \pm 0.4\,(\text{sys})$) and CMS ($M_H = 125.3 \pm 0.4\,(\text{stat}) \pm 0.5\,(\text{sys})$) measurements assuming no correlation of the systematic uncertainties. $^{(\star)}$Average of LEP ($A_\ell = 0.1465 \pm 0.0033$) and SLD ($A_\ell = 0.1513 \pm 0.0021$) measurements, used as two measurements in the fit. The fit w/o the LEP (SLD) measurement gives $A_\ell = 0.1474^{+0.0008}_{-0.0009}$ ($A_\ell = 0.1467^{+0.0006}_{-0.0004}$). $^{(\dagger)}$In units of 10^{-5}. $^{(\triangle)}$Rescaled due to α_s dependency.

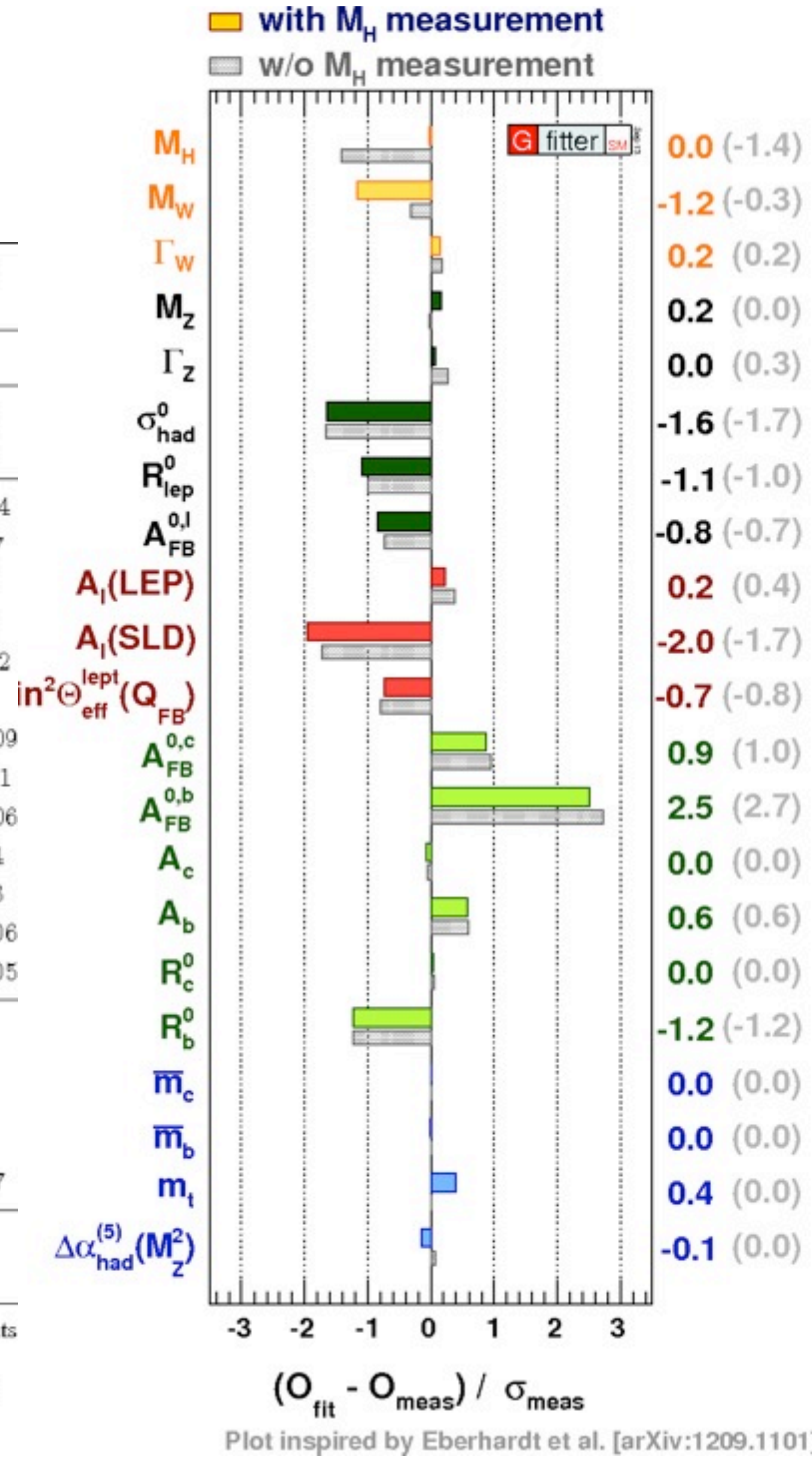

Mw vs mt

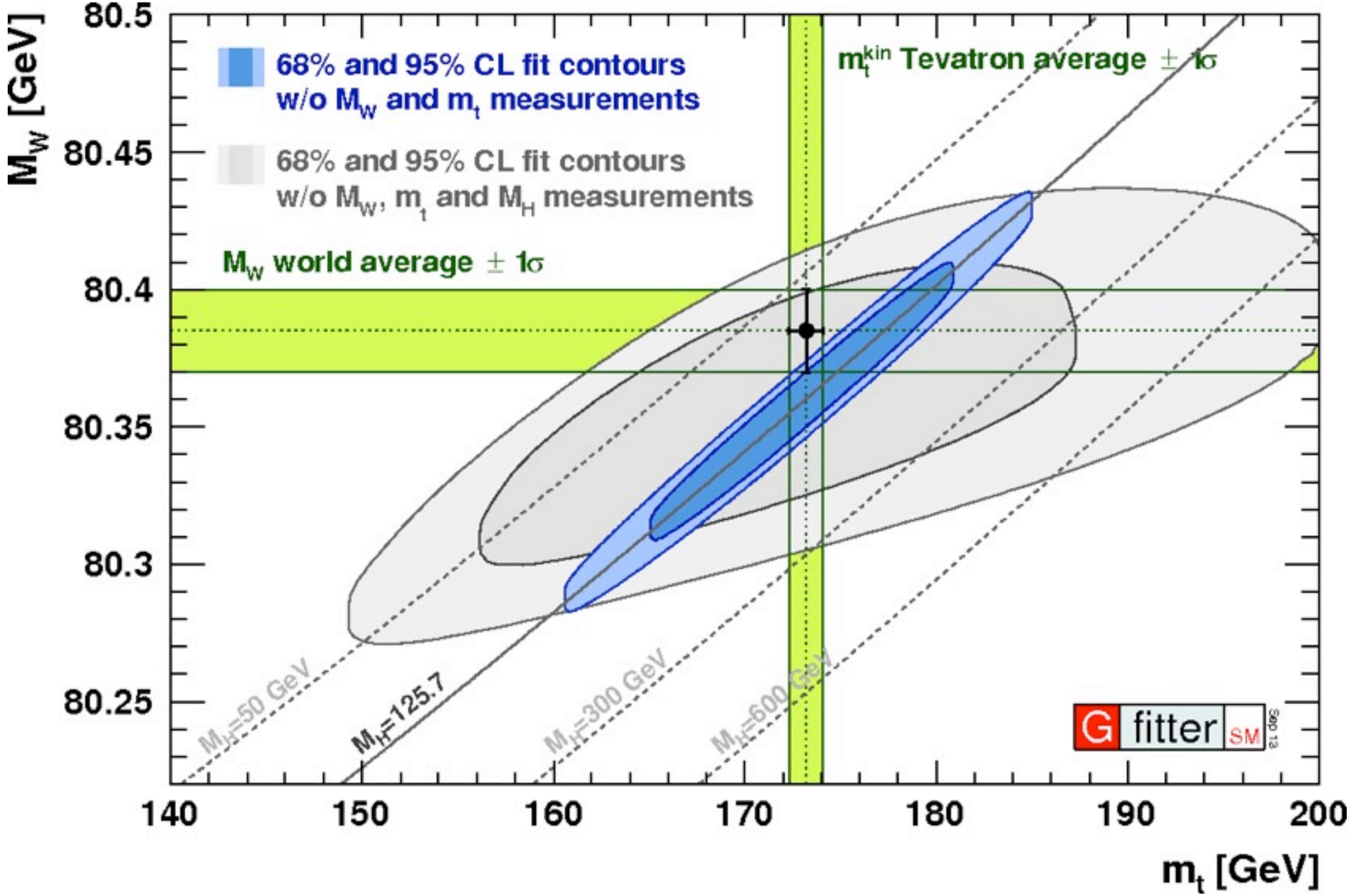

Contours of 68% and 95% confidence level obtained from scans of fits with fixed variable pairs M_W vs. m_t. The narrower blue and larger grey allowed regions are the results of the fit including and excluding the M_H measurements, respectively.

Femiophobic model

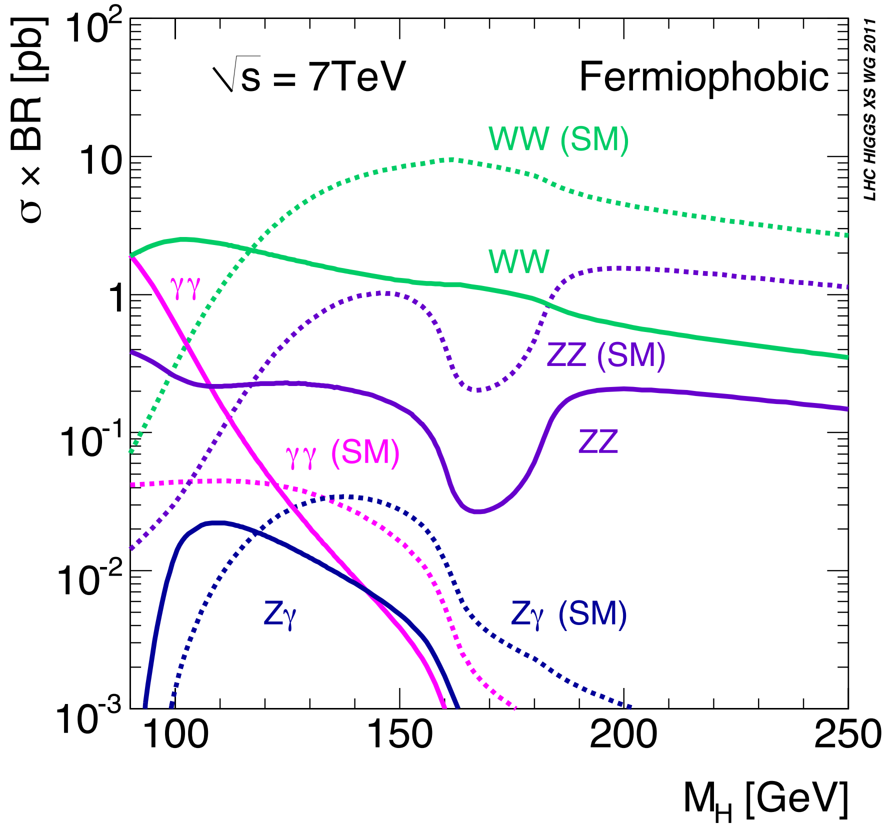

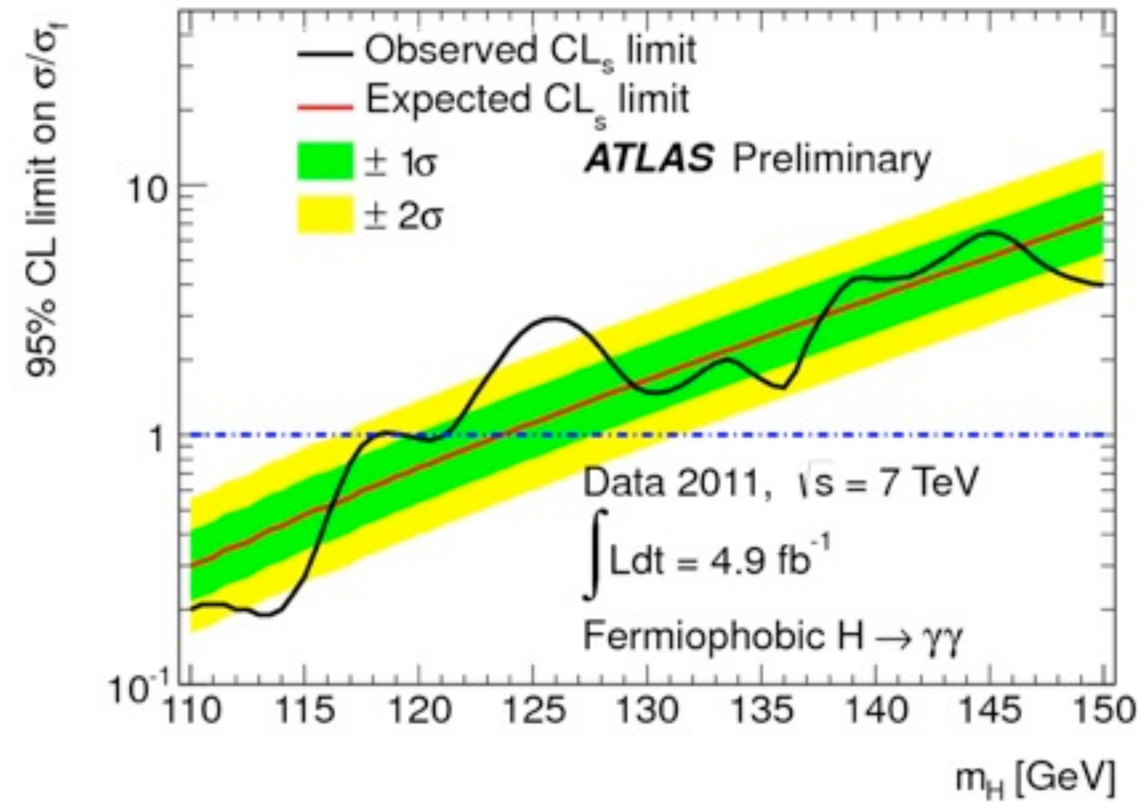

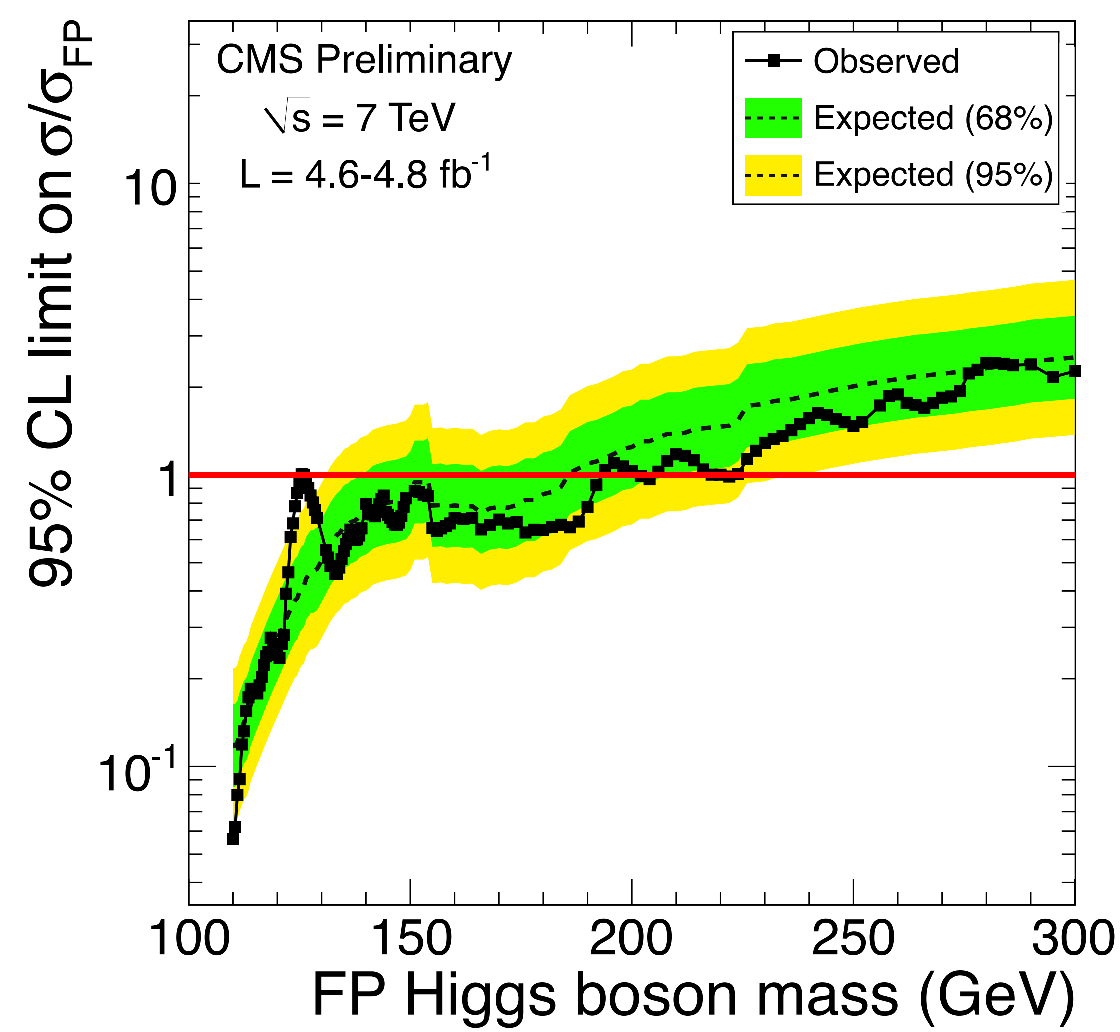

Benchmark model with no Higgs couplings to fermions, bosonic couplings at SM values:

- Higgs production through VBF, WH, ZH
- H → γγ enhanced compared to SM for mH <125GeV

4th generation

The fourth generation interferes destructively with the W boson loop, resulting in a net decrease of the partial decay width into gamma gamma.
A slight increase the Zgamma branching fraction.

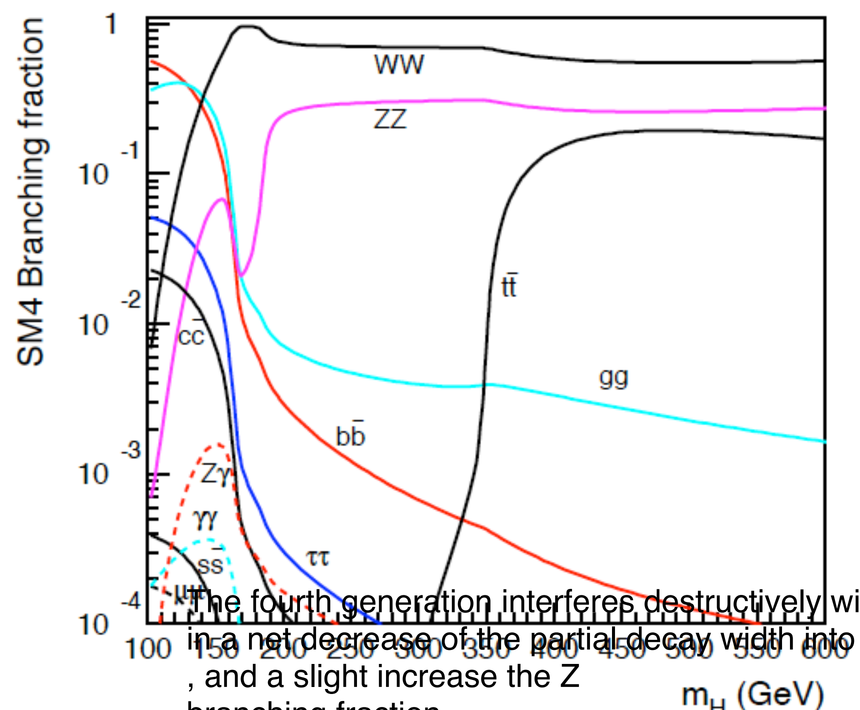

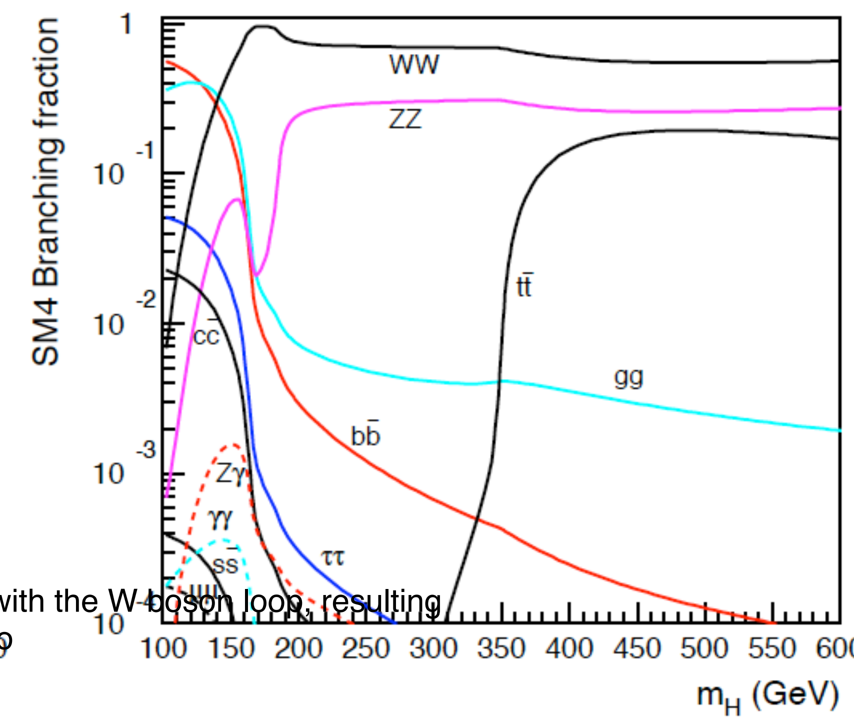

The fourth generation interferes destructively with the W-boson loop, resulting in a net decrease of the partial decay width into , and a slight increase the Z branching fraction.

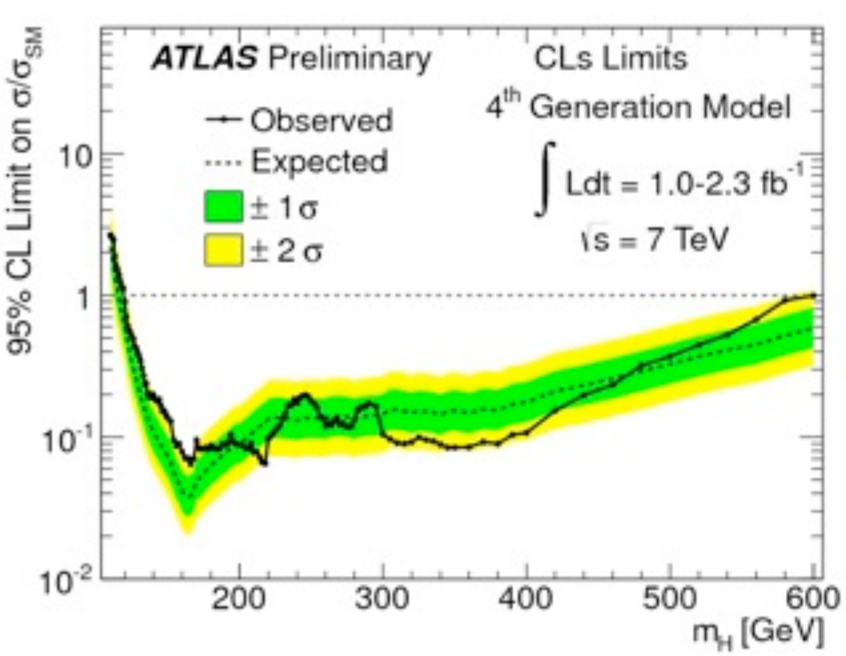

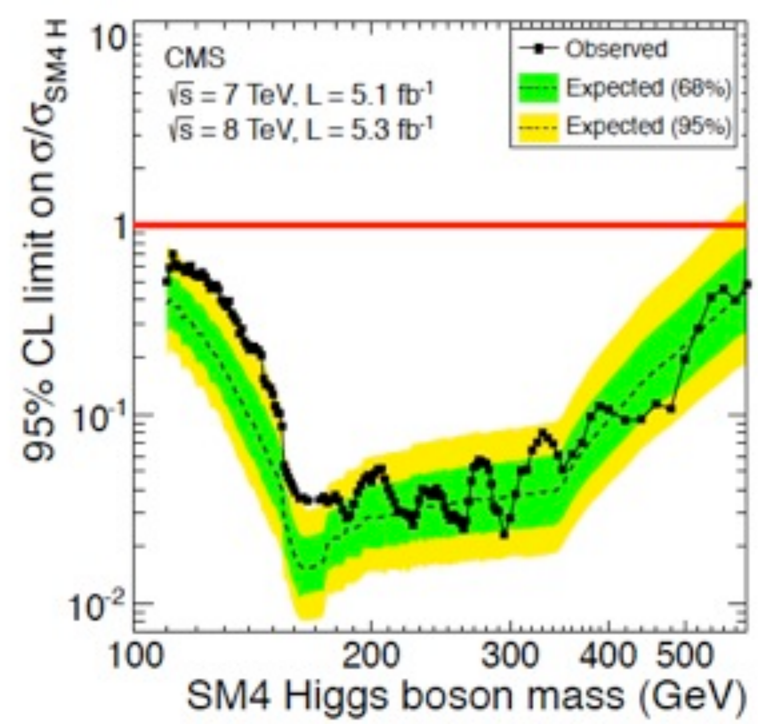

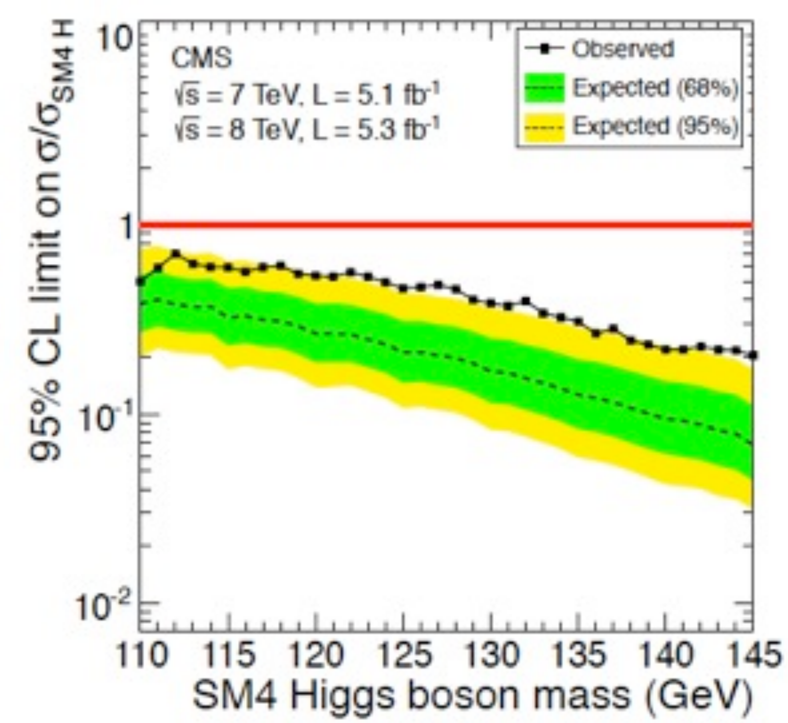

ATLAS VS CMS CALORIMETERS

ATLAS: Liquid argon + Pb absorbers

- high granularity and longitudinally

segmentation (better e/ ID)
- electrical signals, high stability in

calibration & radiation resistant

-σ/E = 10%/E + 0.007

– ATLAS solenoid is located just in front of the barrel ECAL, resulting in significant energy loss by electrons and photons in the material in front of the active ECAL

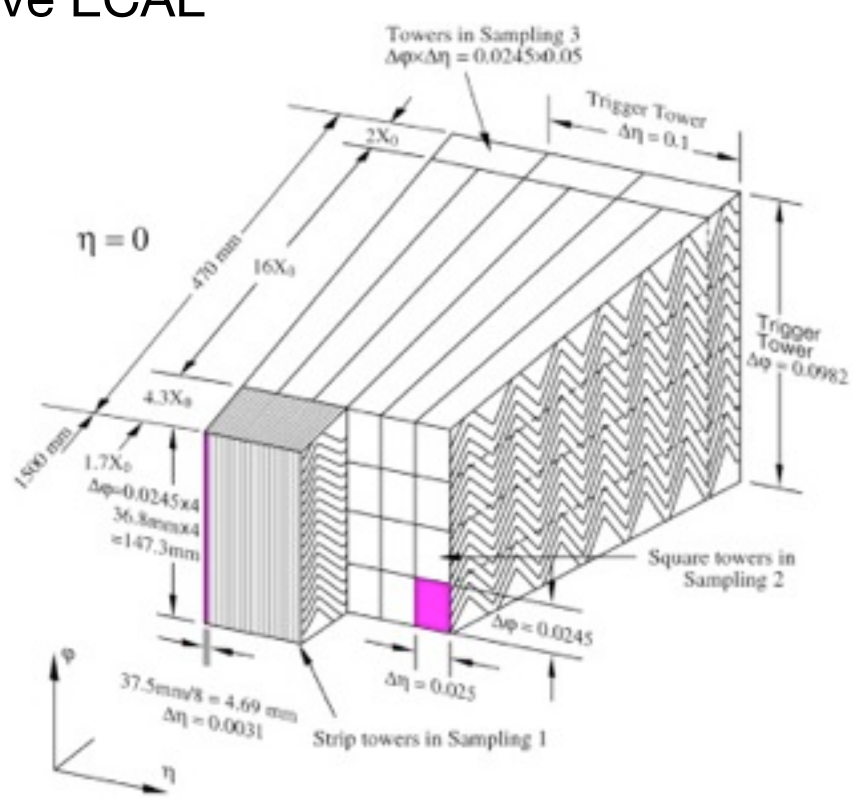

CMS: $PbWO_4$ crystal calorimeter

- higher intrinsic resolution

- Correction factors, to account for response changes, are calculated online.

- σ/E = 3%/E + 0.003

- The full EM calorimetry and most of its hadronic calorimetry are situated inside the solenoid coil and therefore bathed in the strong 4 T magnetic field

•

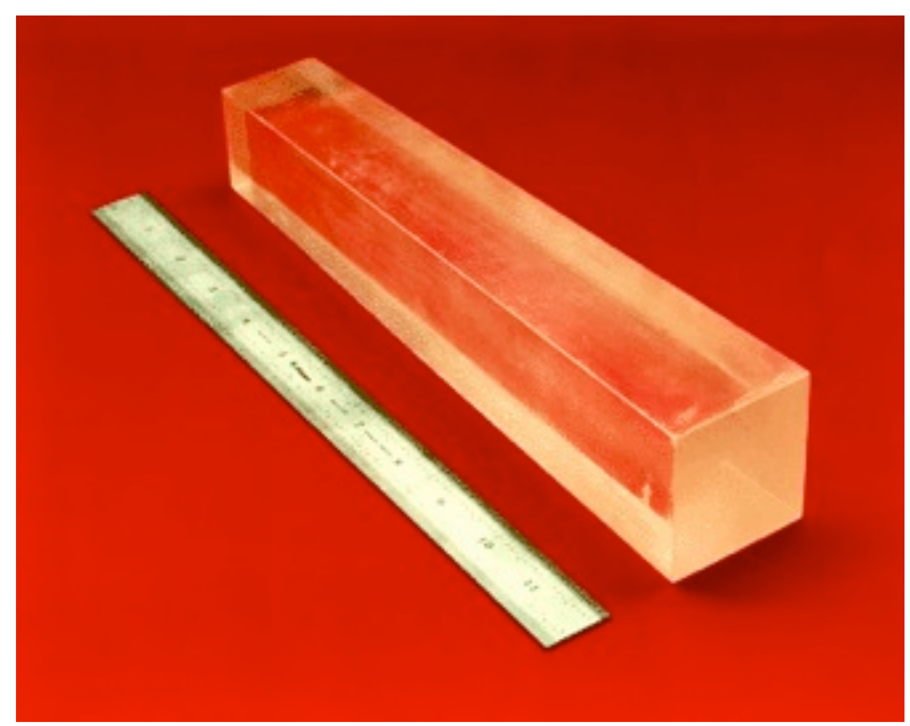

MC calibration

$$E_{e/\gamma} = [a\,(E_{cal},\eta) + b\,(E_{cal},\eta)\,E_{ps} + c\,(E_{cal},\eta)\,E_{ps}^2$$

$$+\frac{s_{cl}(X,\eta)}{f_{out}(X,\eta)}\sum_{i=1}^{3} E_i \times (1 + f_{leak}\,(X,\eta))] \times (F\,(\eta,\phi))\,.$$

Ee in the electron/photon energy.

Eps is the energy deposited in the active material of the pre-sampler.

η is the cluster barycentre, corrected for the “S-shape" effect.

a, b, c are coefficients parametrized in terms of the energy deposited by a particle in the calorimeter (**E**cal) and **η**.

X is the longitudinal barycentre or shower depth.

scl (X; **η**) is the Accordion sampling factor in the cluster.

fout (**X; η**) is the correction for the energy deposited in the calorimeter outside the cluster.

fleak (**X; η**) is the correction for the energy deposited behind the calorimeter.

F (η,ϕ) is the energy correction depending from the impact point inside a cell (energy modulation).

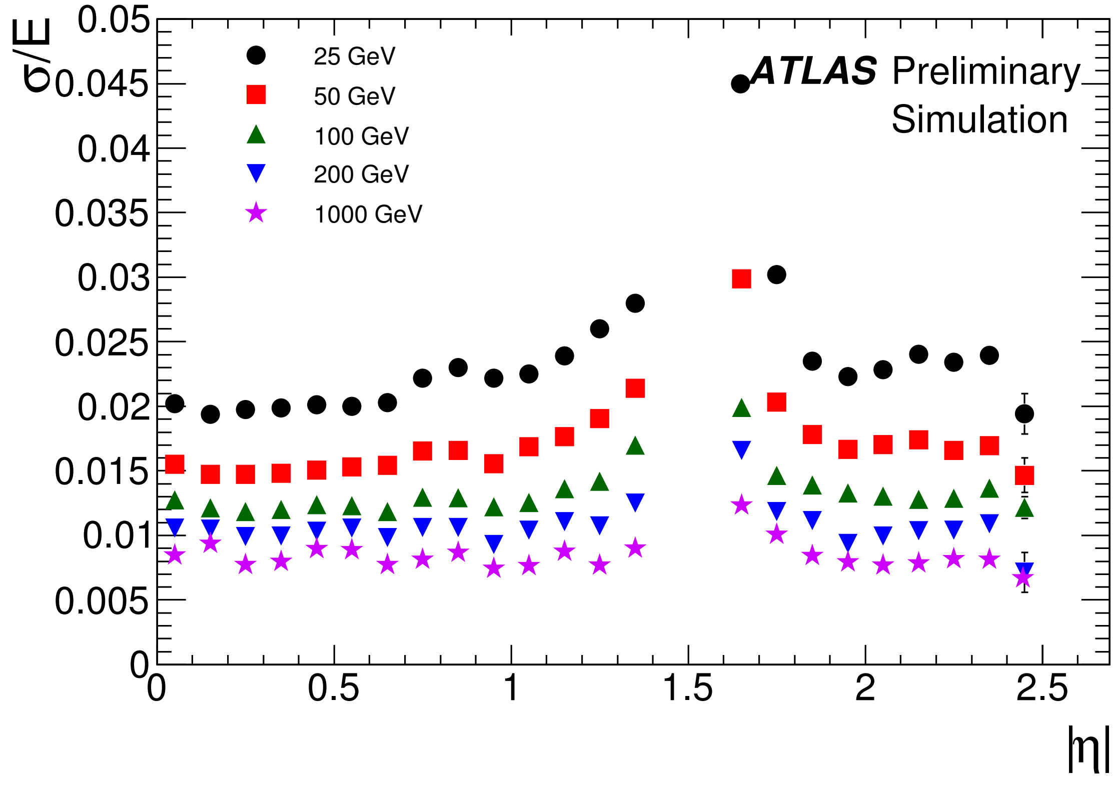

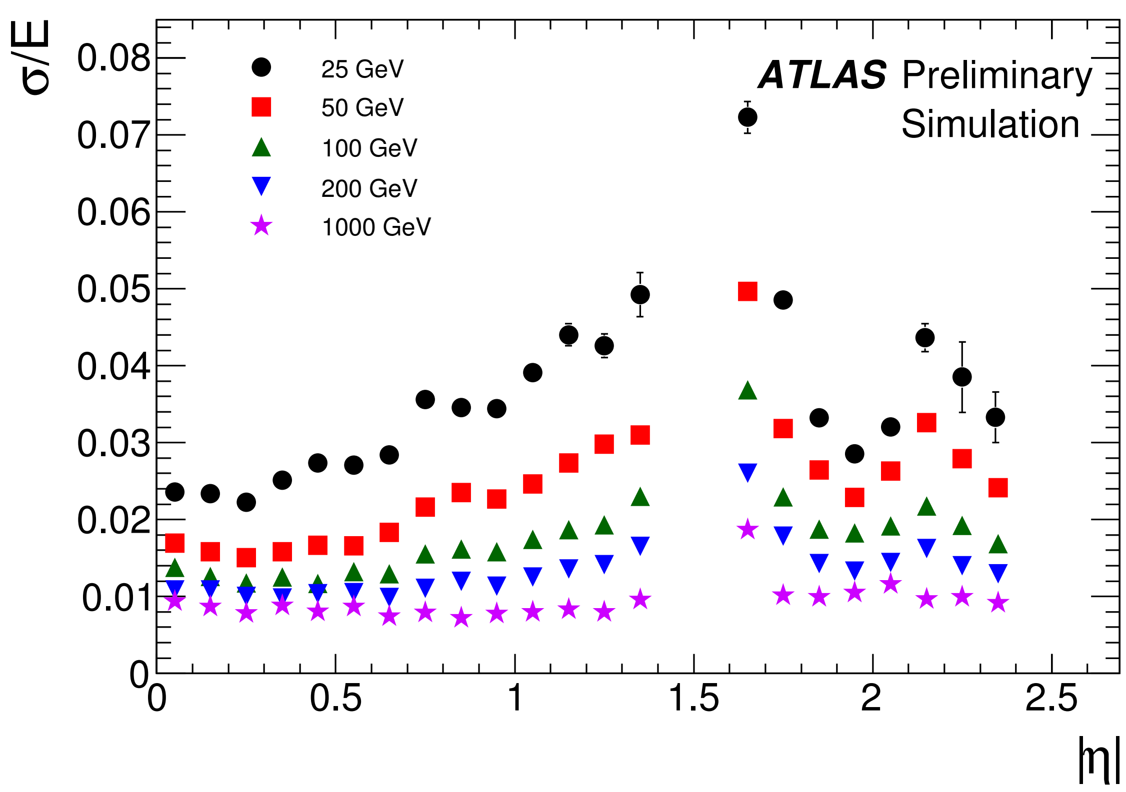

Stability of the energy response

Very good stability w.r.t. number of interactions / bunch crossing

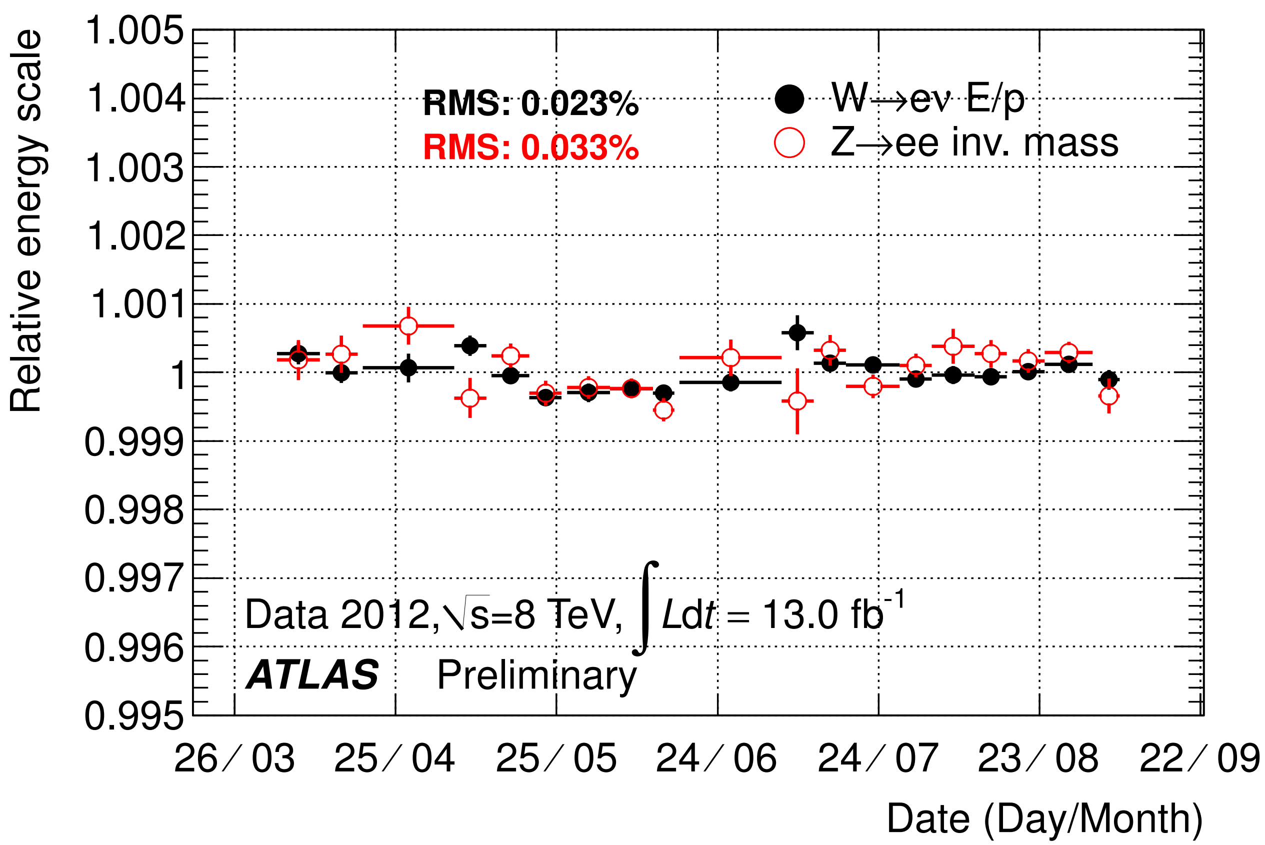

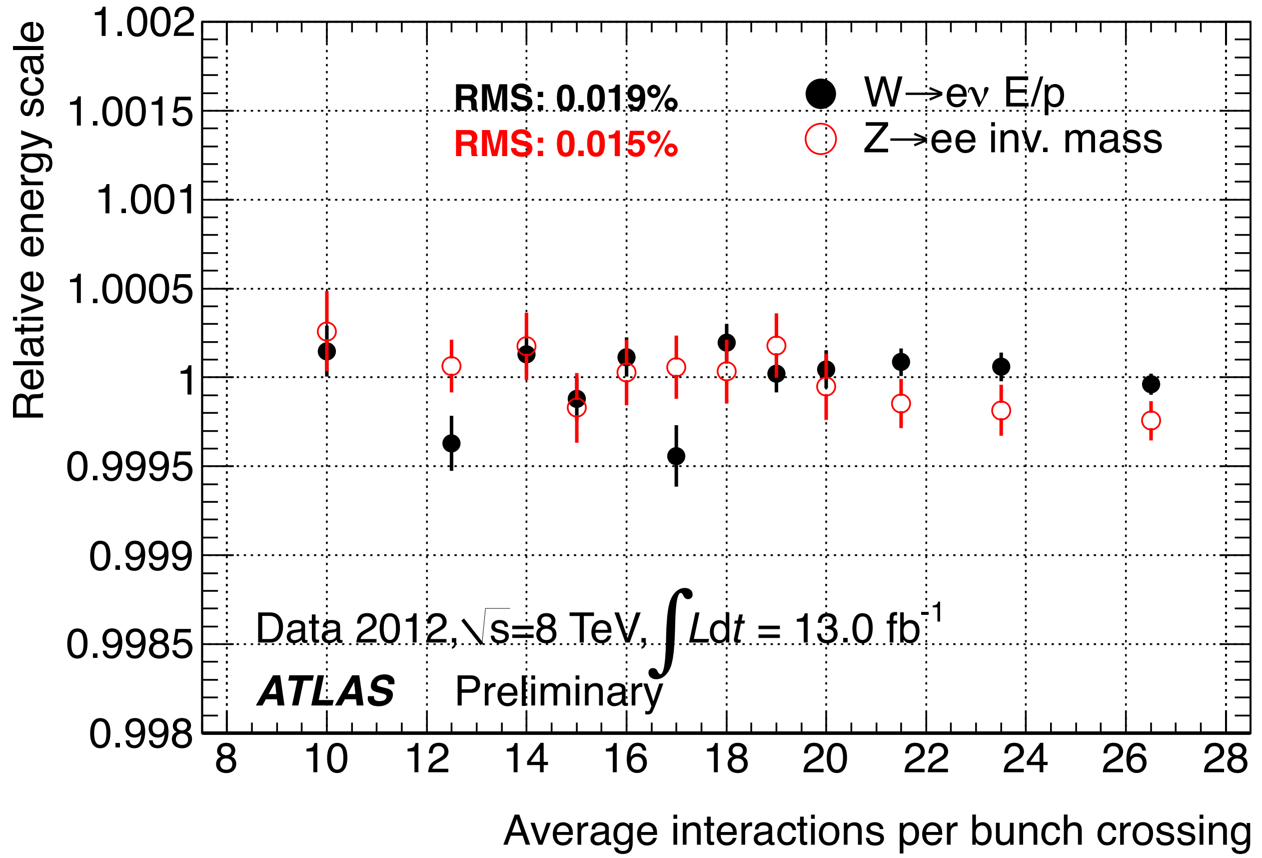

Uncertainty in the photon energy scale

- Main sources of the uncertainty in the photon ES
  - **Method uncertainties**: ES obtained from a comparison of Z → ee line-shape between data ar MC
    - Background contamination
    - Fit Range
  - **Material systematic**: Energy scales of photons u: MC extrapolation electron → photon
    - If the upstream material mapping is different from actual geometry, there is a mis-calibration for photons
  - **Pre-sampler ES**: The MC calibration uses the measured pre-sampler energy to correct for energy lost upstream of the active EM calorimeter, making the calibration sensitive to the pre-sampler ES.

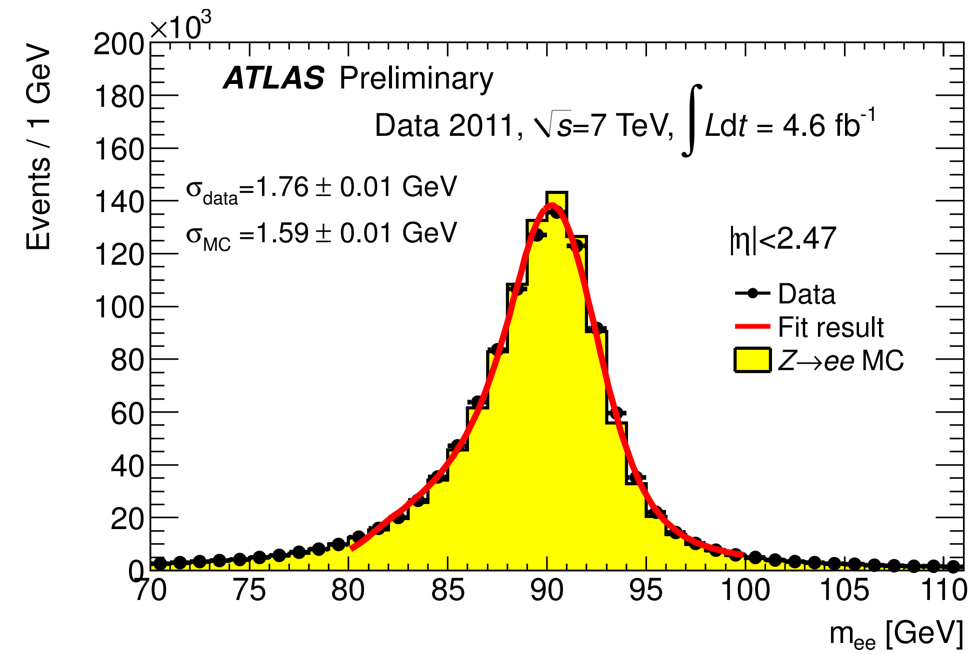

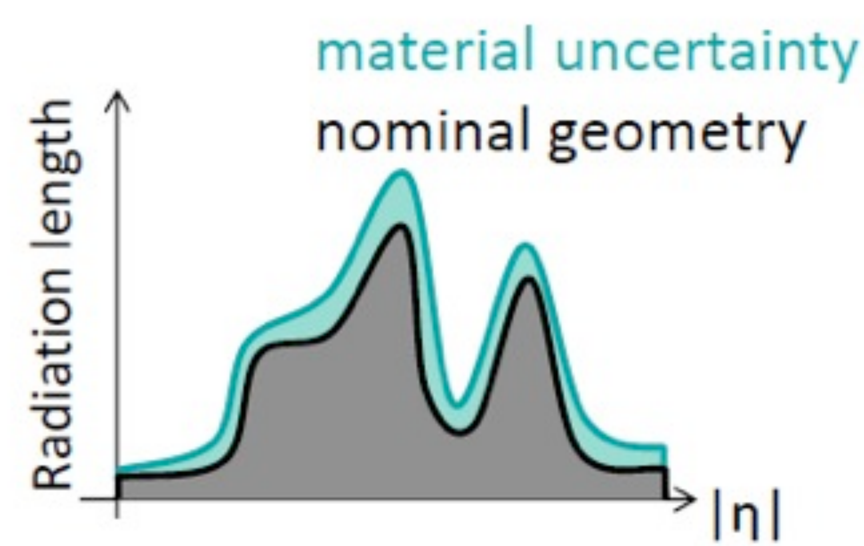

Energy resolution constant term:

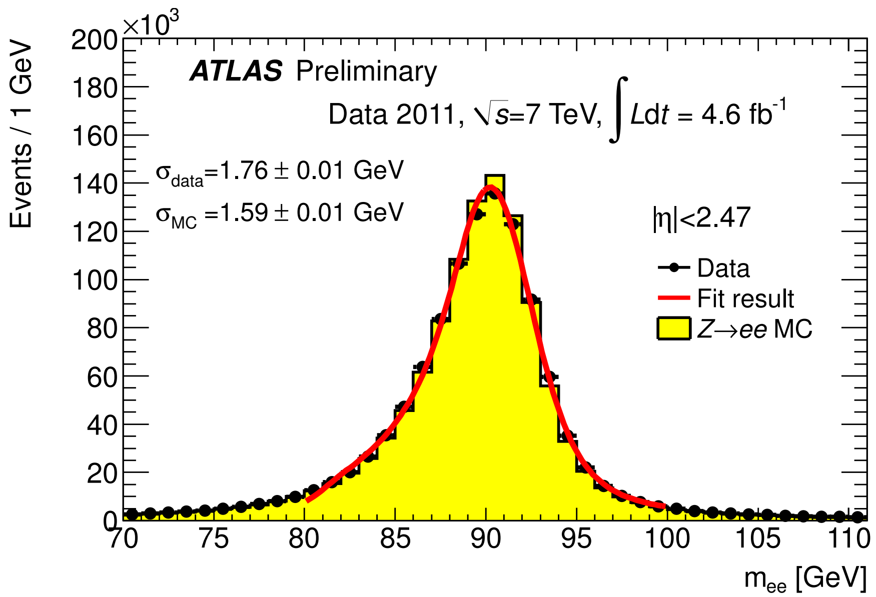

$$c_{\mathrm{data}} = \sqrt{2 \cdot \left(\left(\frac{\sigma}{m_Z} \right)^2_{\mathrm{data}} - \left(\frac{\sigma}{m_Z} \right)^2_{\mathrm{MC}} \right) + c^2_{\mathrm{MC}}}$$

SubSystem	$\lvert eta \rvert$-range	effective constant term (c_{data})
EMB	$\lvert\eta\rvert < 1.37$	$1.2\% \pm 0.1\%(stat)^{+0.5\%}_{-0.6\%}(syst)$
EMEC (OW)	$1.52 < \lvert\eta\rvert < 2.47$	$1.8\% \pm 0.4\%(stat) \pm 0.4\%(syst)$
EMEC (IW)	$2.5 < \lvert\eta\rvert < 3.2$	$3.3\% \pm 0.2\%(stat) \pm 1.1\%(syst)$
FCal	$3.2 < \lvert\eta\rvert < 4.9$	$2.5\% \pm 0.4\%(stat)^{+1.0\%}_{-1.5\%}(syst)$

The dominant uncertainty is due to the uncertainty on the sampling term (constant term is extracted assuming that the sampling term is correctly reproduced by the simulation).

To assign a systematic uncertainty due to this assumption, the simulation was modified by increasing the sampling term by 10%.

The uncertainty due to the fit procedure was estimated by varying the fit range. The uncertainty due to pile-up was investigated by comparing simulated MC samples with and without pile-up and was found to be negligible.

Photon identification

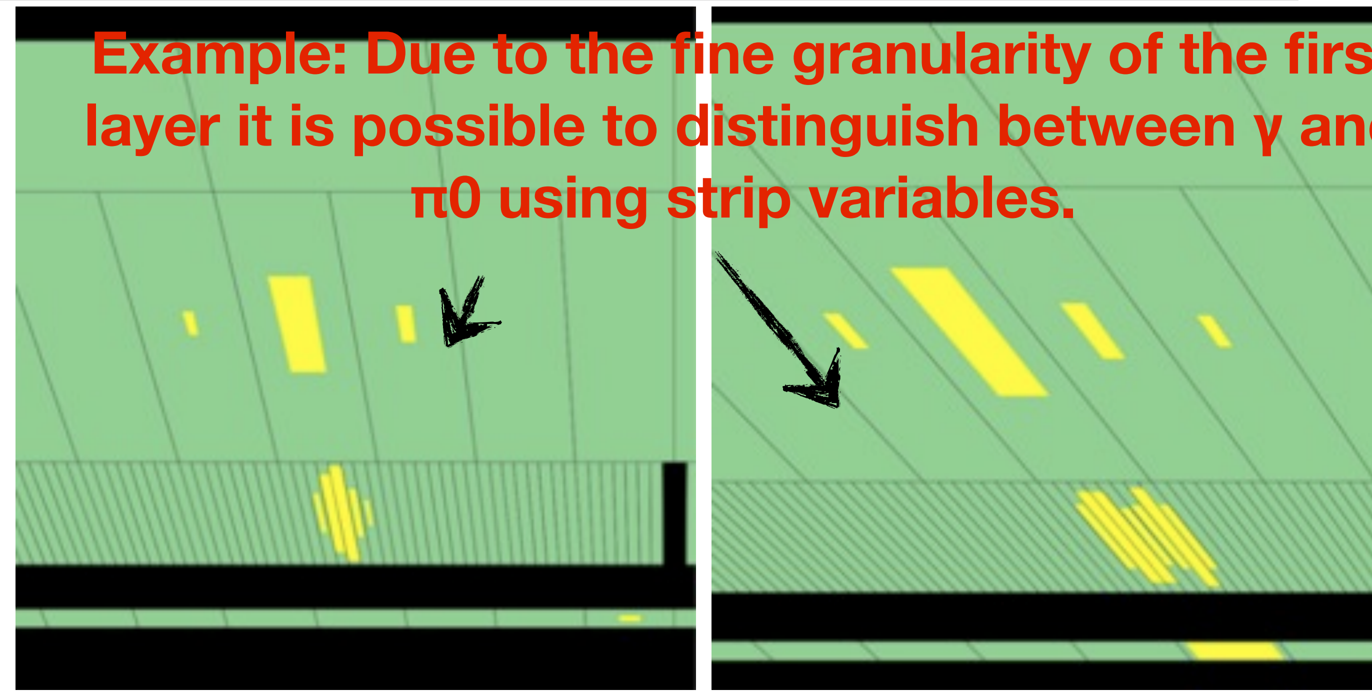

- Cuts on shower shape variables to discriminate isolated photons from QCD jets.

- R_η variable: ratio of energies of middle cells in $\Delta\eta \times \Delta\phi$ =3x7 over 7x7. In photons it peaks close to 1

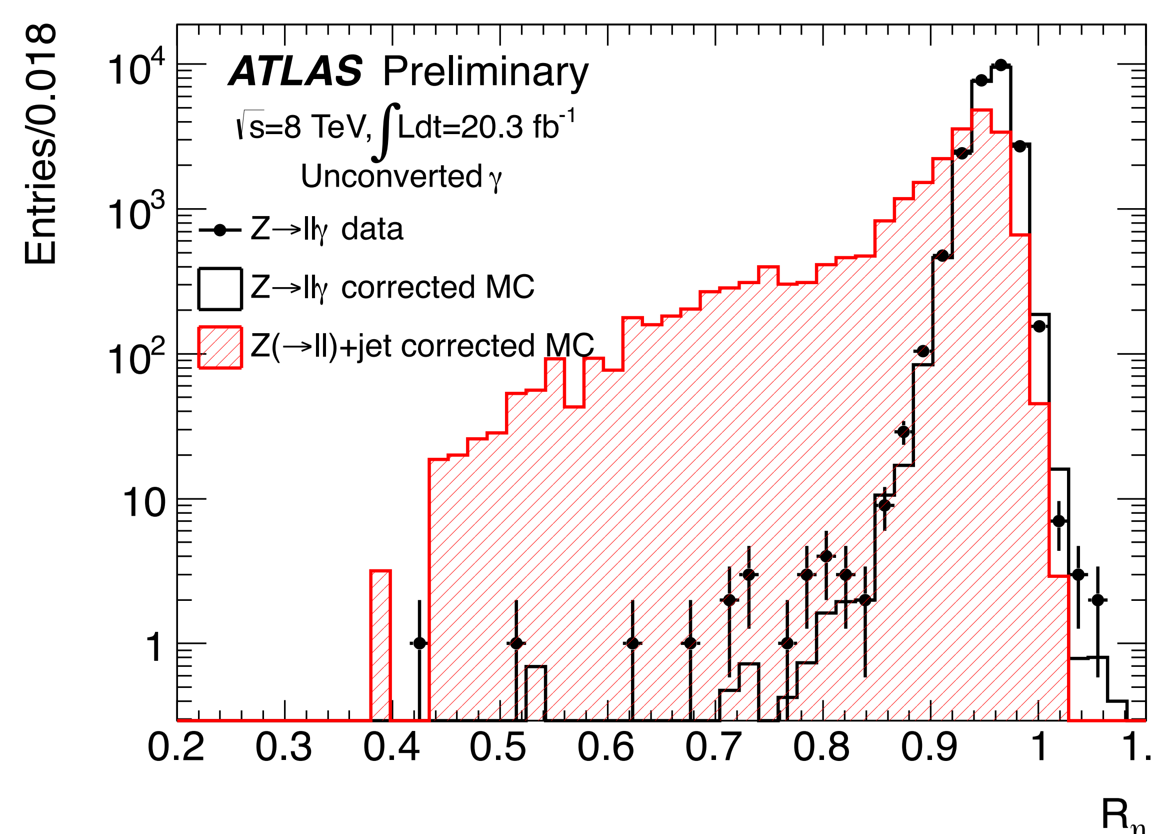

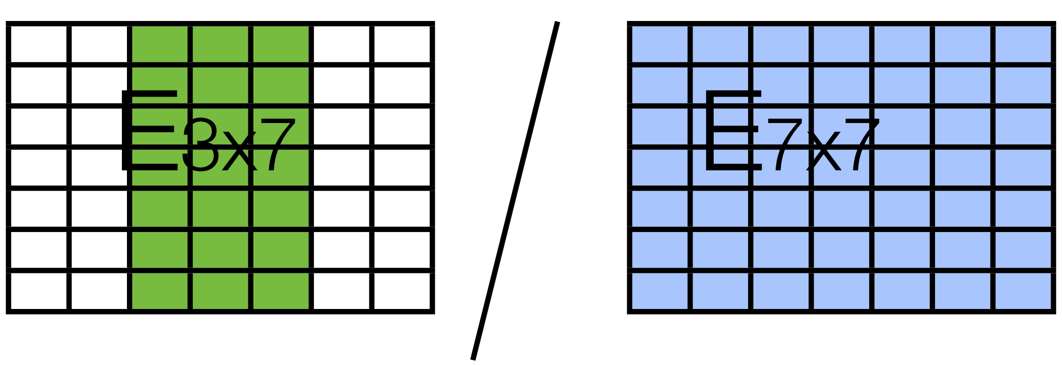

Identification variables

	variable	Definition	description
Loose	R_{had1}	$R_{\mathrm{had}_1} = \frac{E_T^{\mathrm{had}_1}}{E_T}$	Hadronic leakage
Loose	R_η	$R_\eta = \frac{E^{S2}_{3\times7}}{E^{S2}_{7\times7}}$	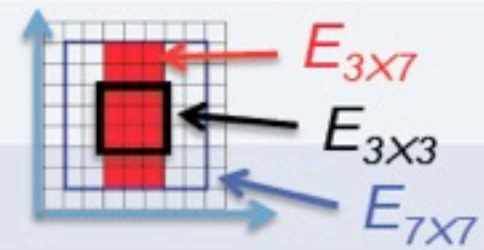
Loose	R_Φ	$R_\phi = \frac{E^{S2}_{3\times3}}{E^{S2}_{3\times7}}$	
Loose	ω_2	$\omega_2 = \sqrt{\frac{\sum E_i \eta_i^2}{\sum E_i} - \left(\frac{\sum E_i \eta_i}{\sum E_i}\right)^2}$	Shower width in middle layer
Tight	ω_{s3}	$\omega_{s\,3} = \sqrt{\frac{\sum E_i (i - i_{\max})^2}{\sum E_i}}$	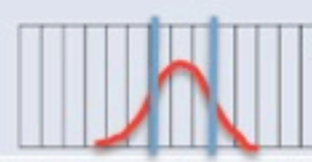 Shower width in 3 strips around the hottest strip
Tight	$\omega_{s\ tot}$	$\omega_{s\,\mathrm{tot}} = \sqrt{\frac{\sum E_i (i - i_{\max})^2}{\sum E_i}}$	Shower width in all strips
Tight	F_{side}	$F_{\mathrm{side}} = \frac{E(\pm3) - E(\pm1)}{E(\pm1)}$	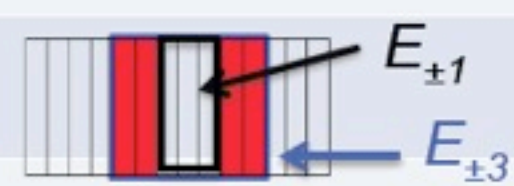
Tight	ΔE	$\Delta E = E^{S1}_{2^{\mathrm{nd}}\max} - E^{S1}_{\min}$	
Tight	E_{ratio}	$E_{\mathrm{ratio}} = \frac{E^{S1}_{1^{\mathrm{st}}\max} - E^{S1}_{2^{\mathrm{nd}}\max}}{E^{S1}_{1^{\mathrm{st}}\max} + E^{S1}_{2^{\mathrm{nd}}\max}}$	

Photon Identification efficiency

The identification efficiency is measured in function of Et for η regions.

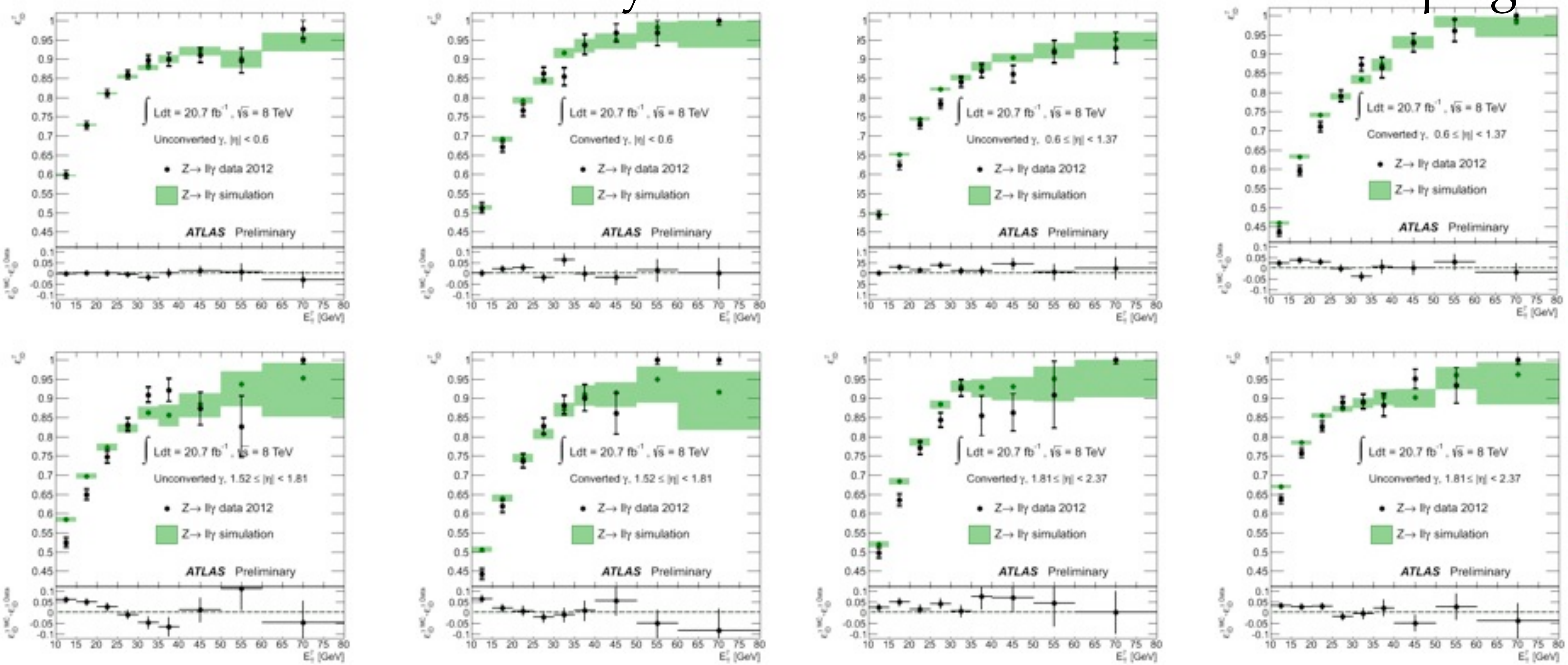

Systematic uncertainties comes from the non-100% purity of the sample, and the method to estimate it. As purity increases with Et, the systematics decreases.

Other 2 methods used in ATLAS for photonID, these results agrees in the overlap region, and they essentially dominate at low Et.

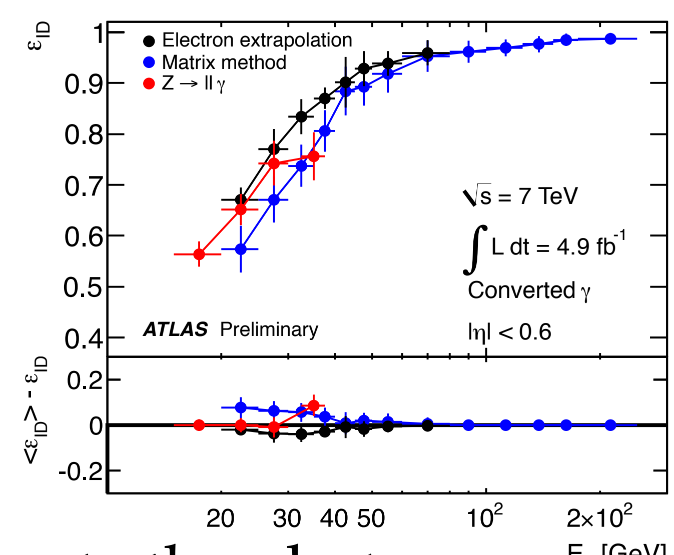

The FSR sample is also used to estimate the photon trigger efficiency, in addition to the bootstrap method.

CMS Photon Identification MVA

Photon ID is crucial for $H \rightarrow \gamma\gamma$.
MVA Photon ID is validated with the $Z \rightarrow \mu\mu\gamma$ sample.

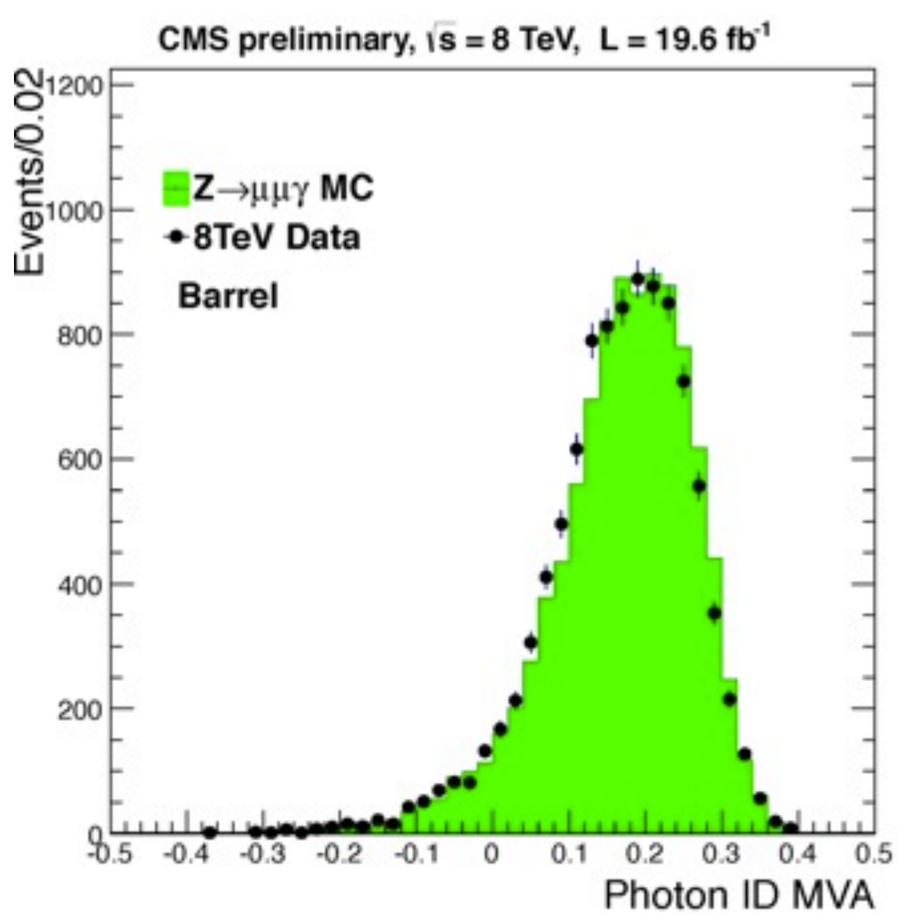

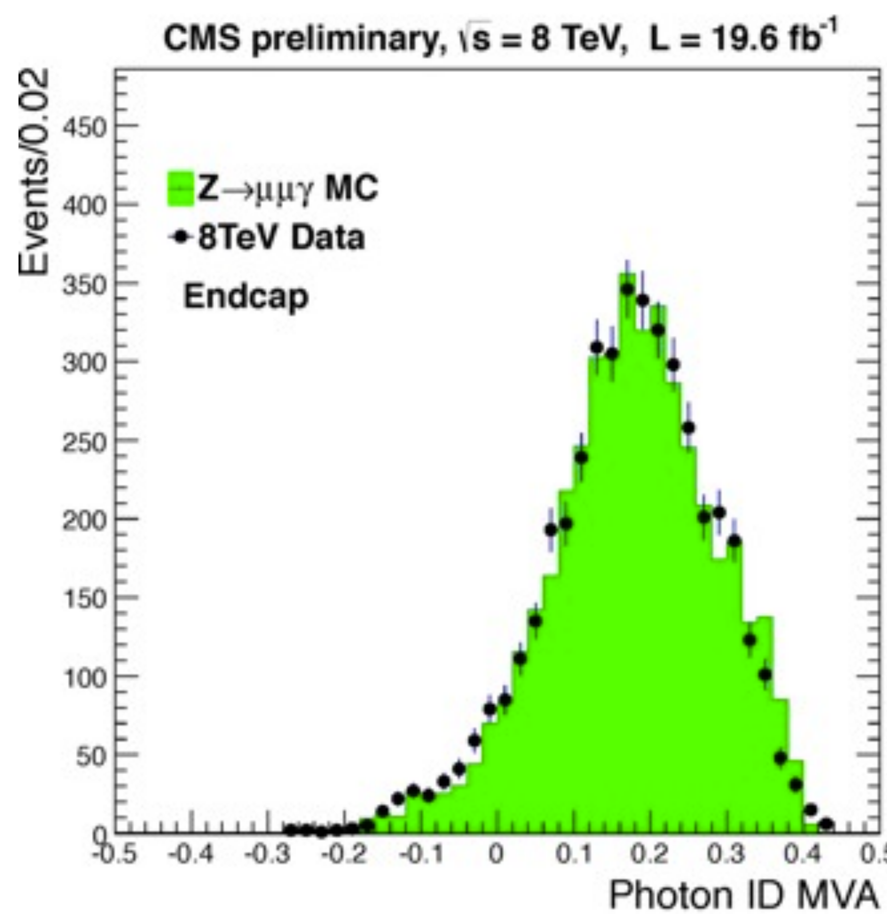

A comparison of the photon ID MVA score obtained with barrel and End-Cap in data and MC simulation.

Reference: https://twiki.cern.ch/twiki/bin/view/CMSPublic/Hig13001TWiki#Photon_identification_MVA

Photon Isolation

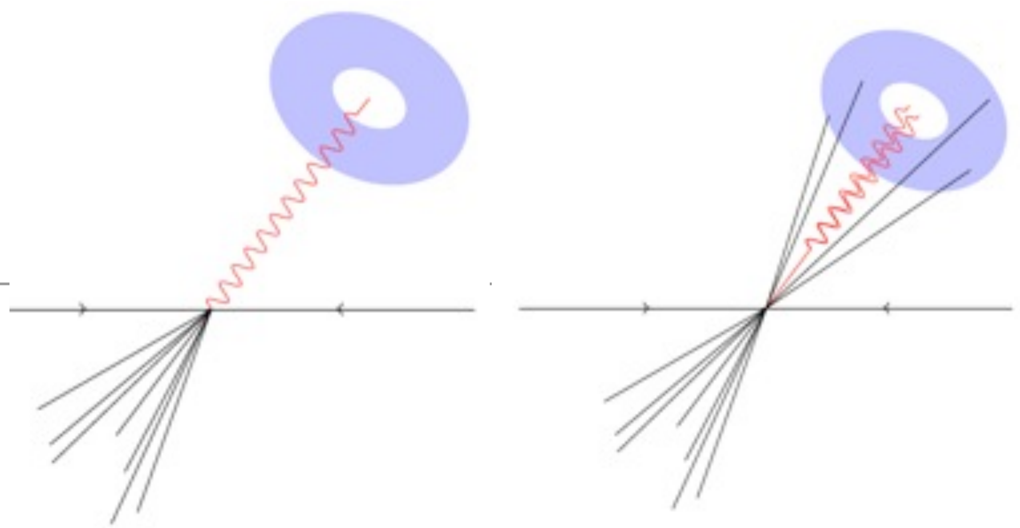

•Photon Isolation: sum of the transverse energy of positive-energy topological clusters. Used to reject single photons against π^0 from jets.

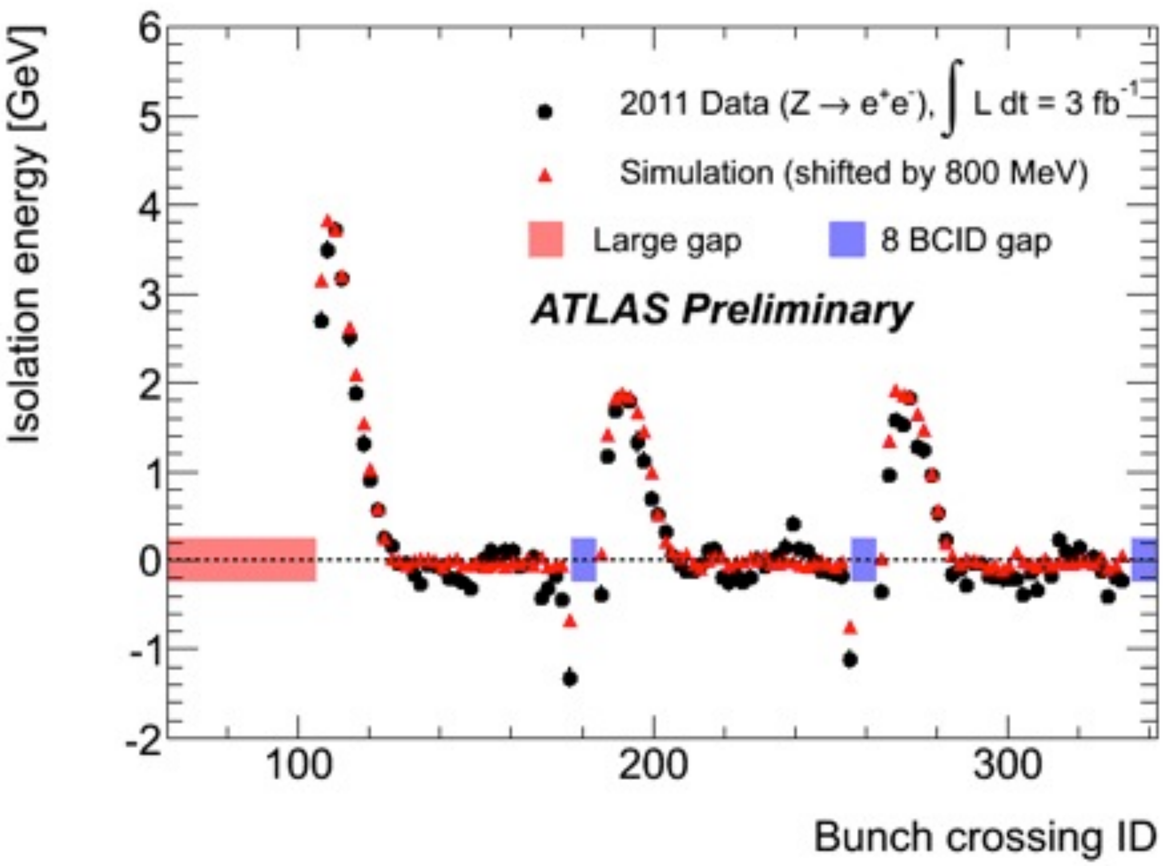

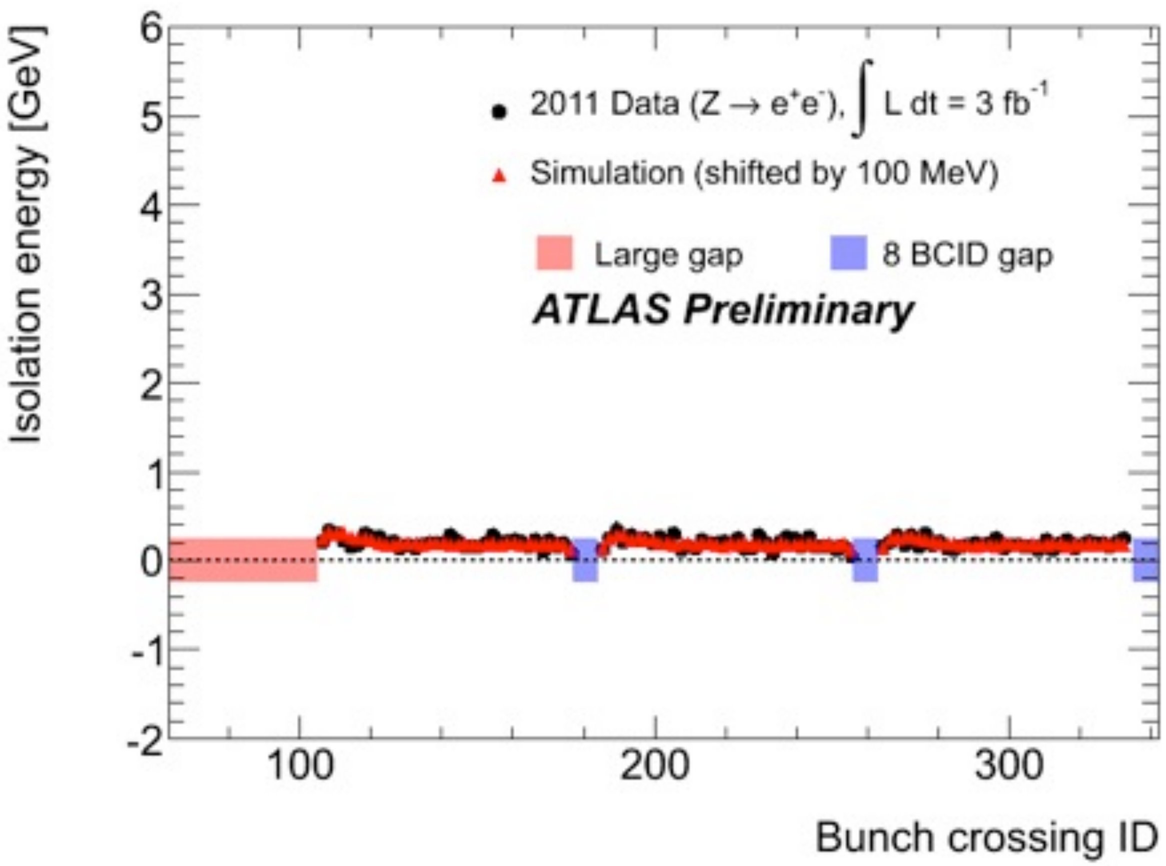

The isolation can be based on the electromagnetic and hadronic calorimeter cells or on topological clustering. The calorimeter isolation based on topological cluster is less-sensitive to pile-up a. This is achieved by consistently using topological cluster energies for both the raw isolation and the ambient energy density corrections.

Background decomposition

- Several methods based on varying photon identification and isolation criteria are used to determine the composition of the diphoton candidate events:

- **Template fit:** A template of the two-dimensional isolation energy distribution of the diphoton candidates. Each dimension corresponds to the isolation energy for one of the photon candidates.

- **2×2D sidebands**: Extract 4 yields from candidates' counts in signal region(TI) and background control region (non-Tight, non-isolated)
  - MC inputs: signal fractions leaking to the non-Tight region, fraction: $\alpha = N_{j\gamma}/(N_{\gamma j} + N_{j\gamma})$ → Main technique used in $H \rightarrow \gamma\gamma$ and $H \rightarrow Z\gamma$

- **4×4 matrix**: All tight di-photon candidates are tested for calorimetric isolation, defining 4 possible pass/fail outcomes: through the matrix, these are translated into 4 event weights, describing how much the event is likely to be γγ, γj, jγ, jj
  - No MC inputs.

Di-photon invariant mass reconstruction

- The di-photon invariant mass is evaluated from the following expression:

$$M_{\gamma\gamma} = \sqrt{2E_{\mathrm{T}}^{1}E_{\mathrm{T}}^{2}\left[\cosh(\eta_1 - \eta_2) - \cos(\phi_1 - \phi_2)\right]},$$

Photon η has to be corrected by the PV.

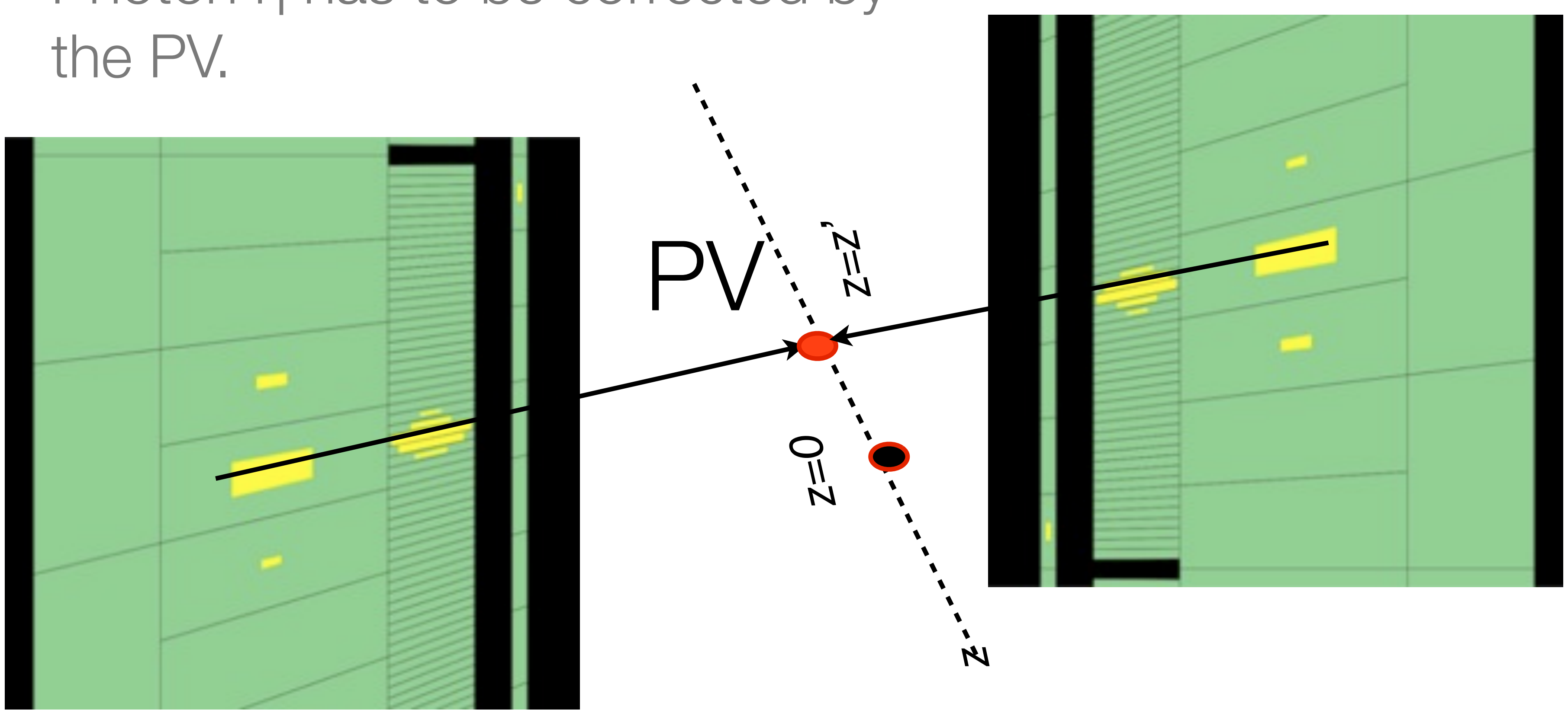

The PV is identify by building a likelihood:

- Flight direction of the photons (using the calo pointing tecnique)
- The average beam spot position
- The sum of $|pT|^2$ of the tracks associated to the PV

PV selection

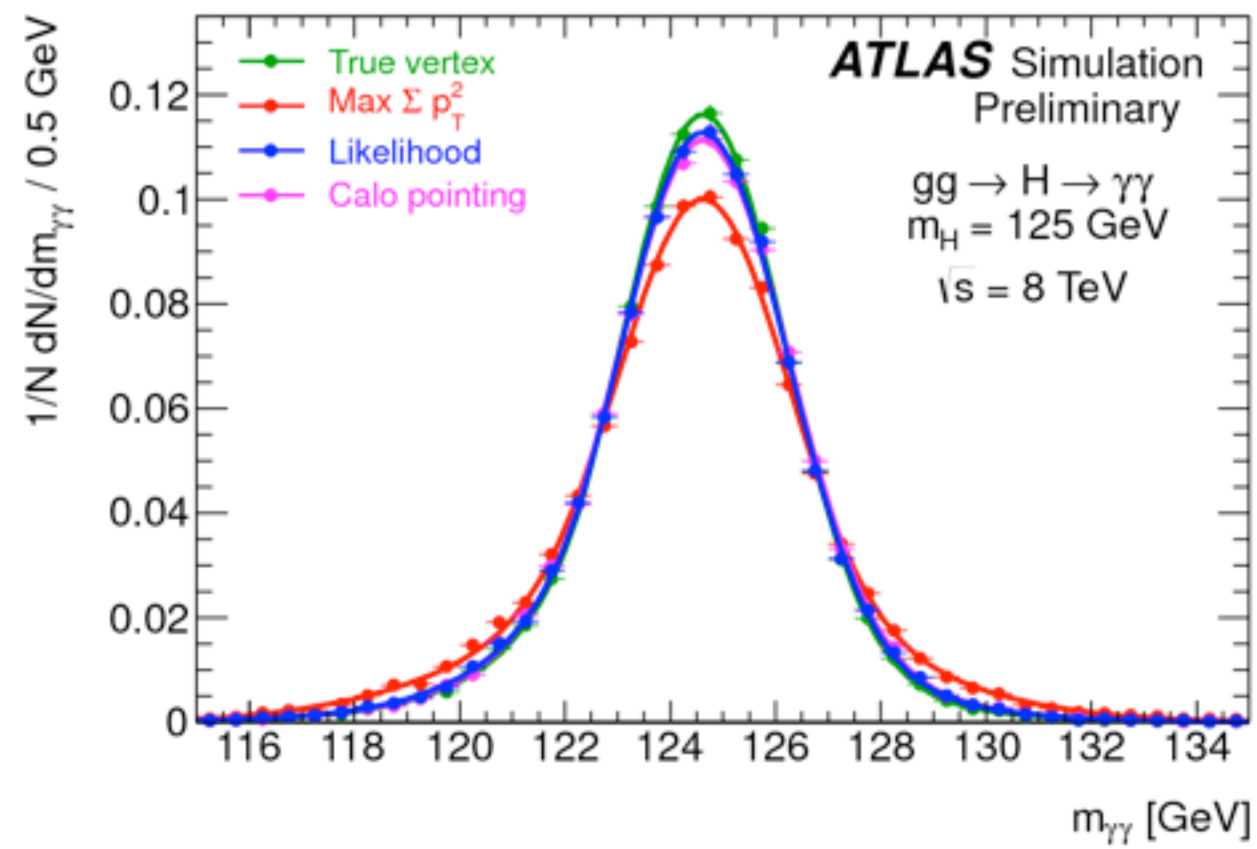

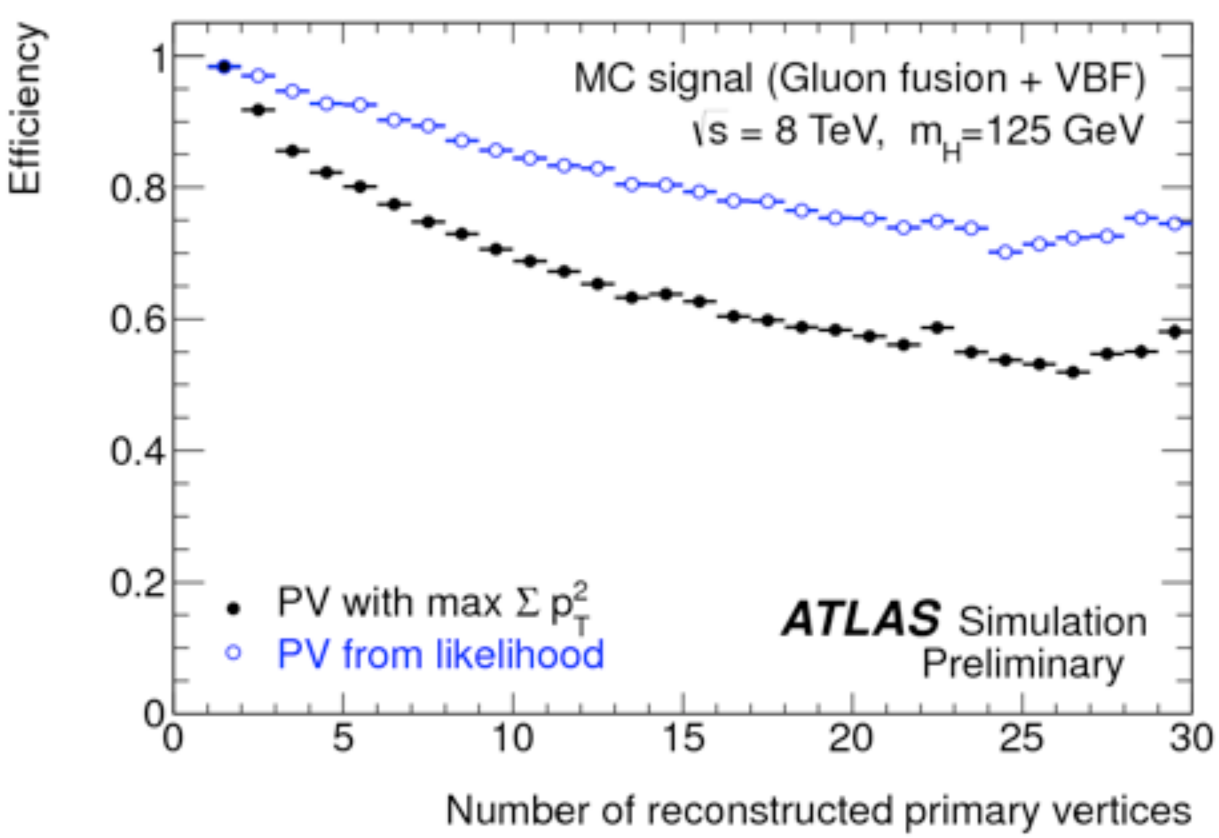

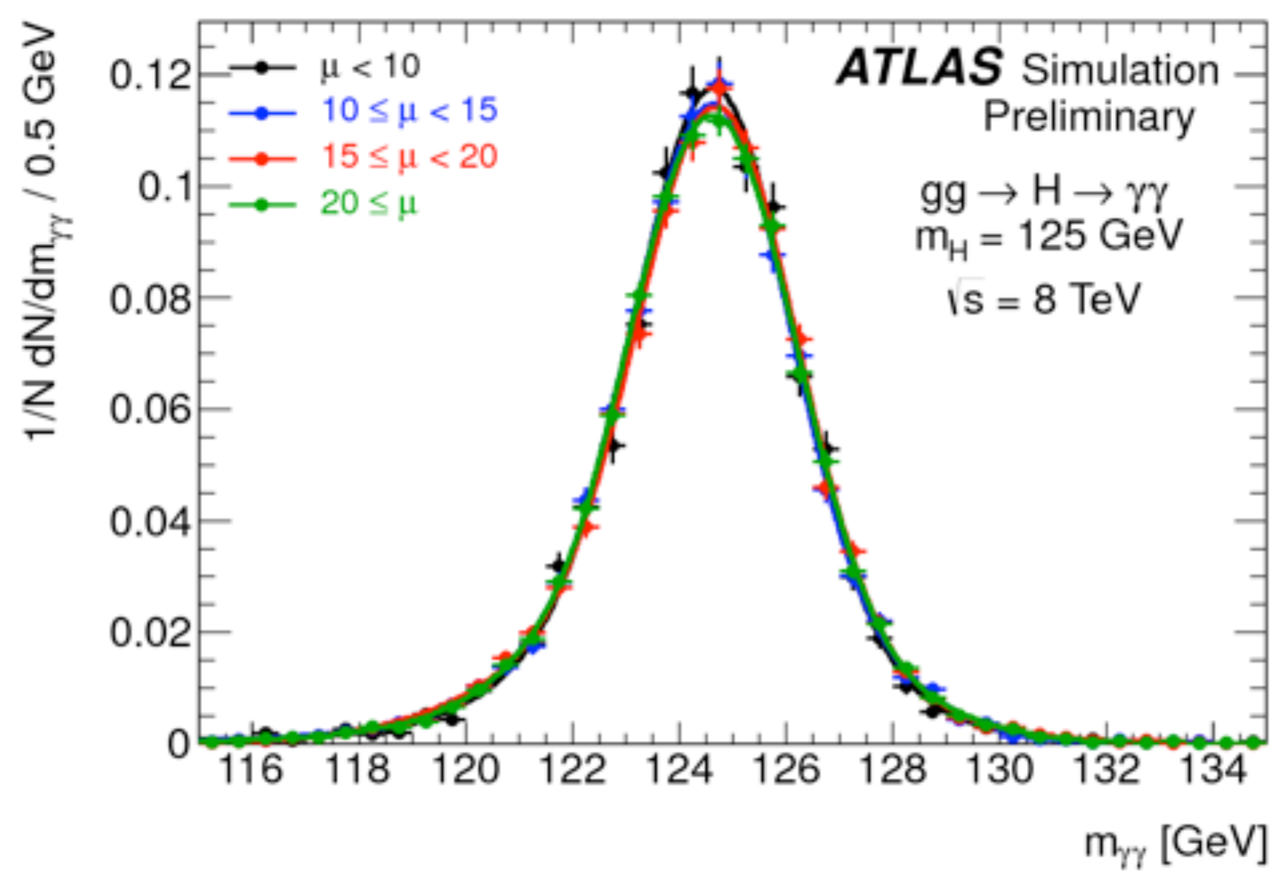

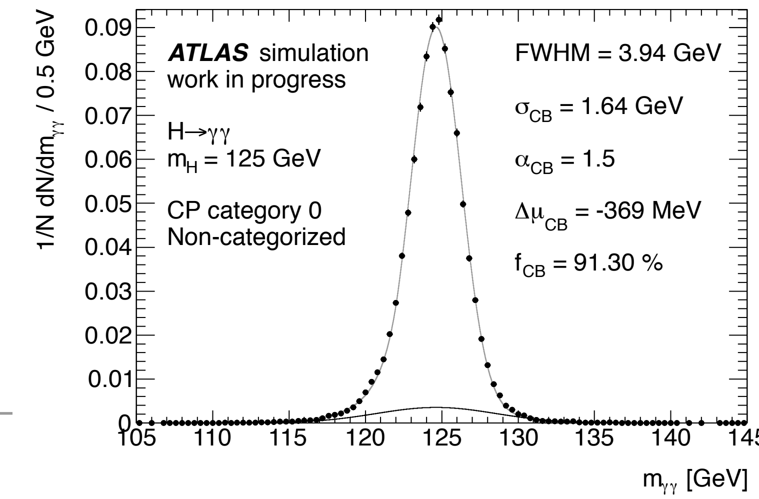

Global resolution model

- The signal resolution at a fixed mH mass is a function of 7 free parameters with large correlations:

$$R(m_{\gamma\gamma}) = f_{CB} CB\left[m_{\gamma\gamma}; \mu_{CB}, \alpha_{CB}, \sigma_{CB}, n_{CB}\right] + (1 - f_{CB})\, GA\left[m_{\gamma\gamma}; \mu_{GA}, \sigma_{GA}\right].$$

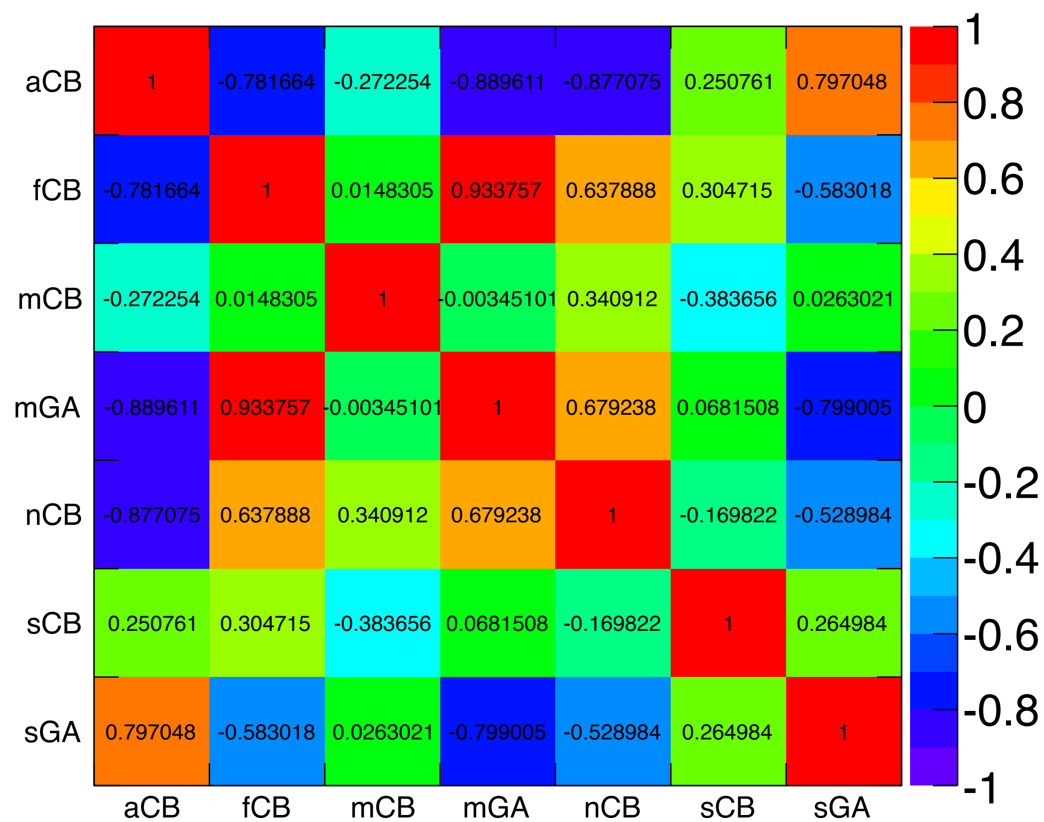

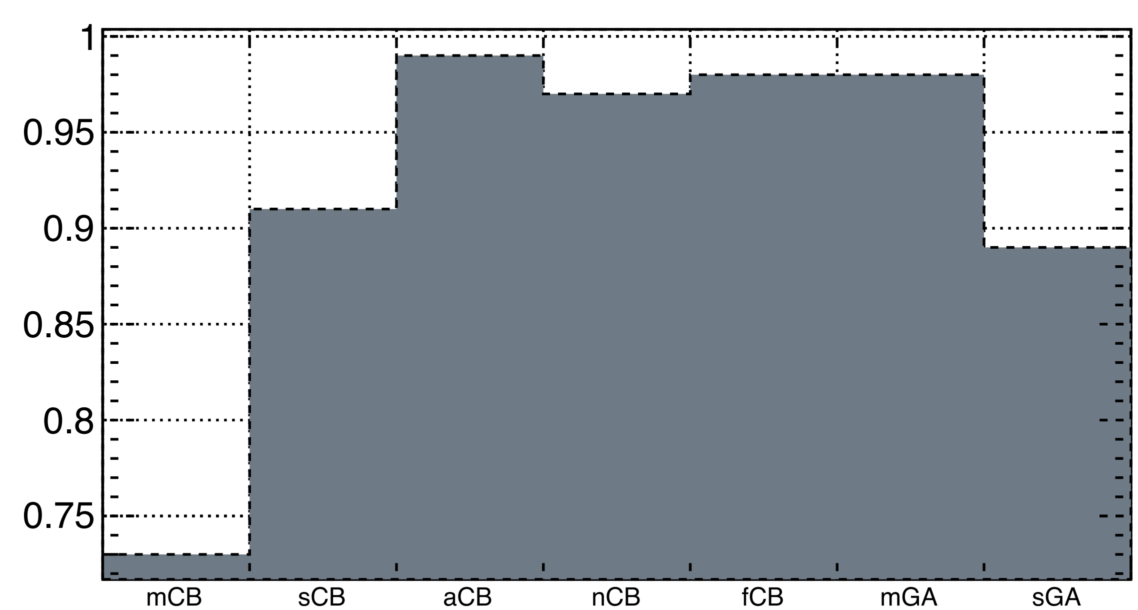

Each parameter is highly correlated all others (up to 99%).

Calibration of conversion categories

γlead(2) γsubl (0)	γlead(2) γsubl (1)	γlead(2) γsubl (2)
γlead(1) γsubl (0)	γlead(1) γsubl (1)	γlead(1) γsubl (2)
γlead(0) γsubl (0)	γlead(0) γsubl (1)	γlead(0) γsubl (2)

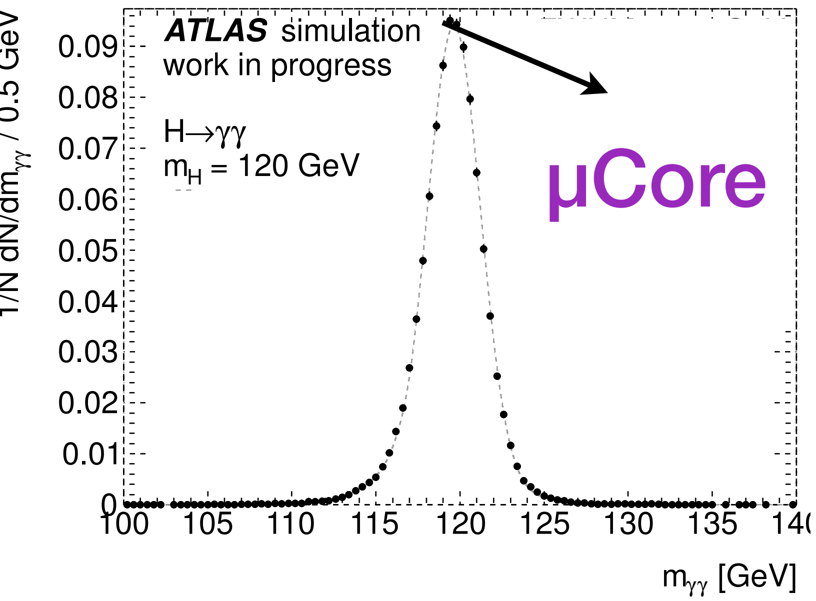

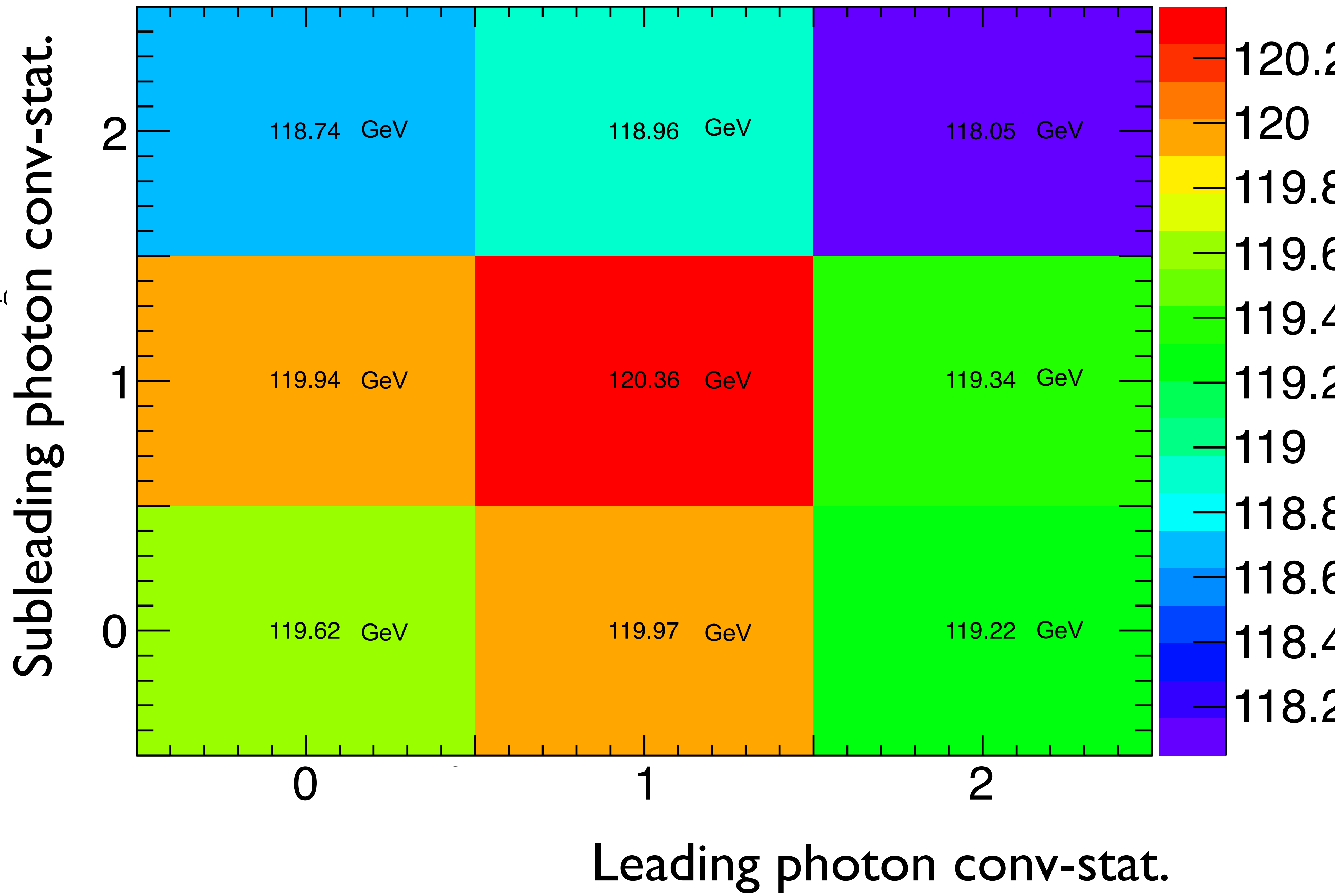

- Opposite sing shift between categories 1-1 and 2-2.
- About 2% difference which is not negligible compared with average resolution of 1.7 GeV).

MC photon energy scale

- In order to test the photon energy scale and resolution in MC, a variable Δ is used for each of the 3 conversion categories for pT and η bins.

$$\Delta = \frac{p_{\mathrm{T}}^{reco} - p_{\mathrm{T}}^{true}}{p_{\mathrm{T}}^{true}}$$

- The mean value of the Δ distribution is fitted with a gaussian in a asymmetric restricted range between -1.5 and +2.0, set to avoid bias from potential asymmetries in the distribution due to energy leakage.

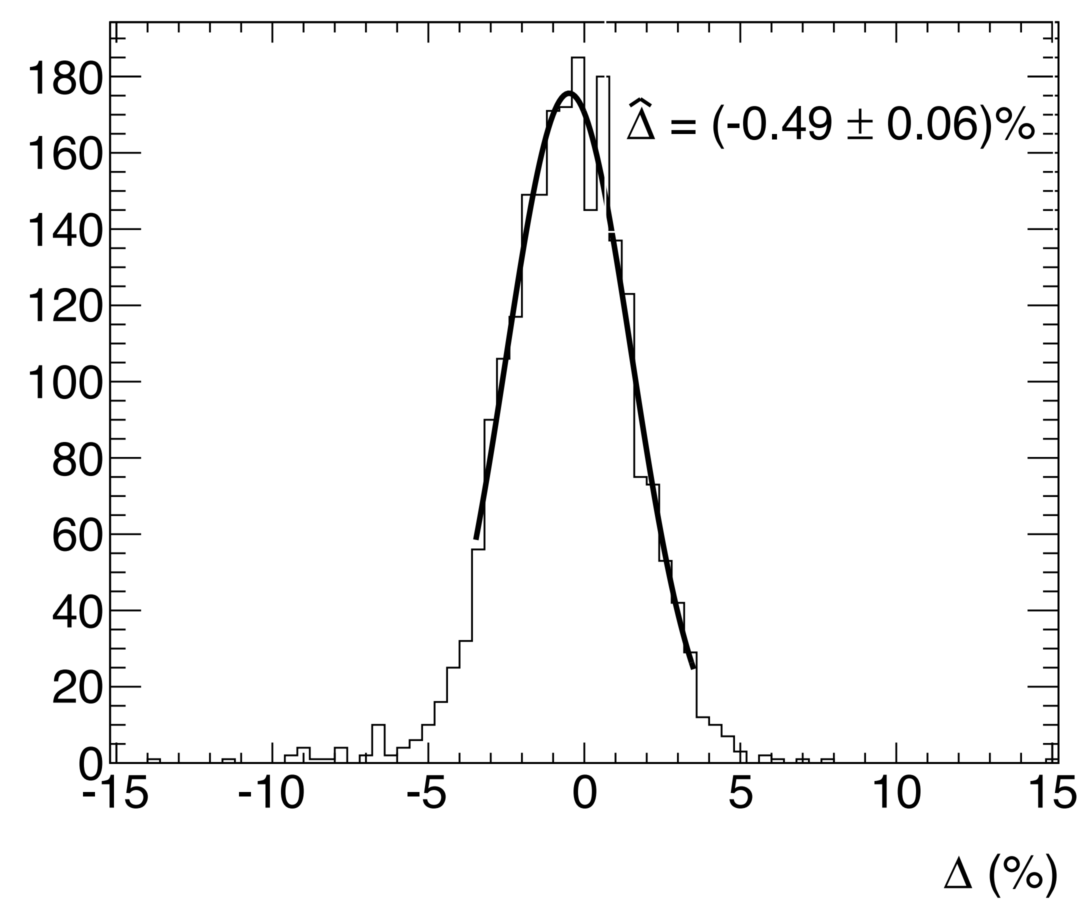

MC photon scale

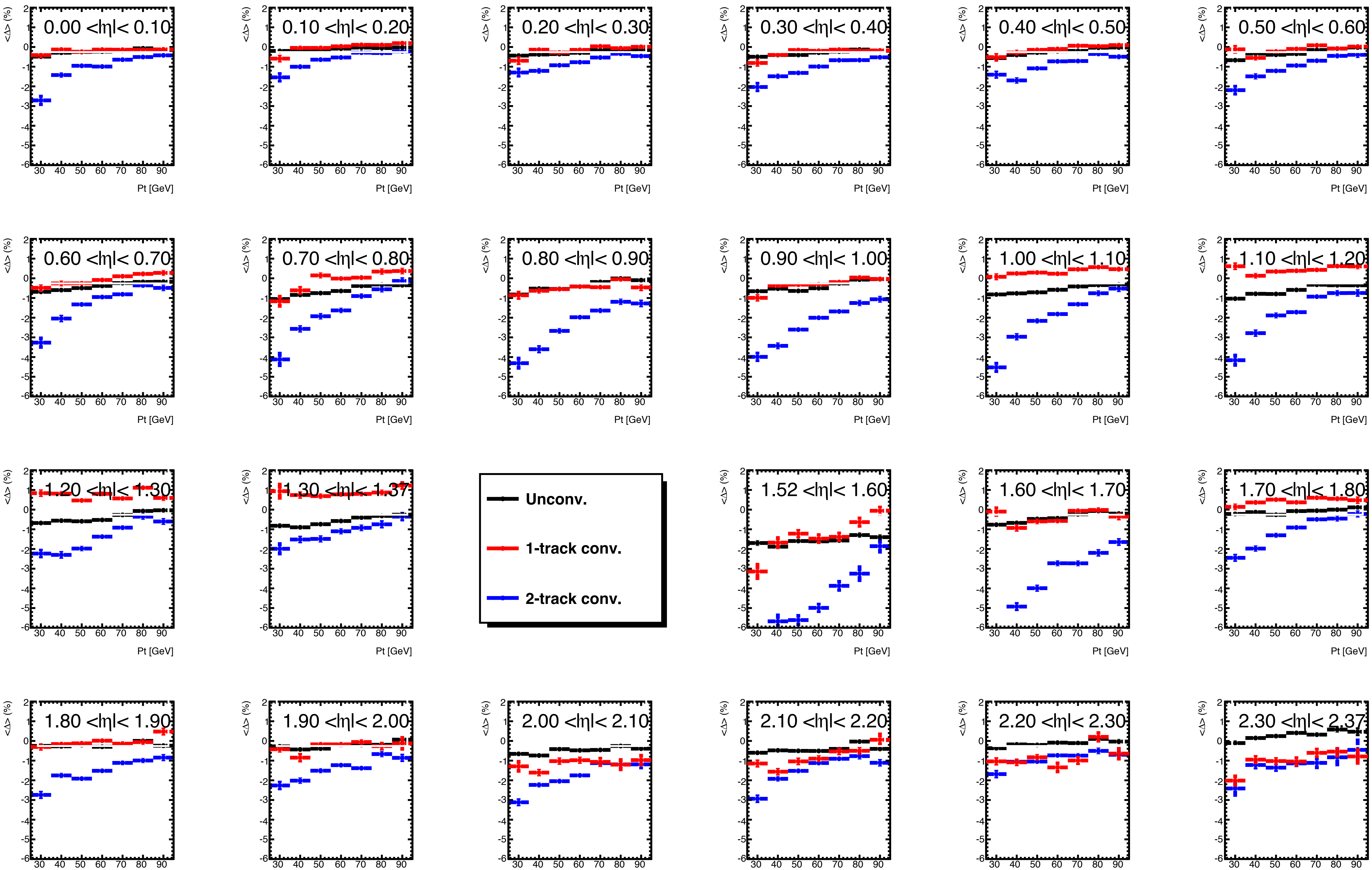

MC photon scale: Corrected

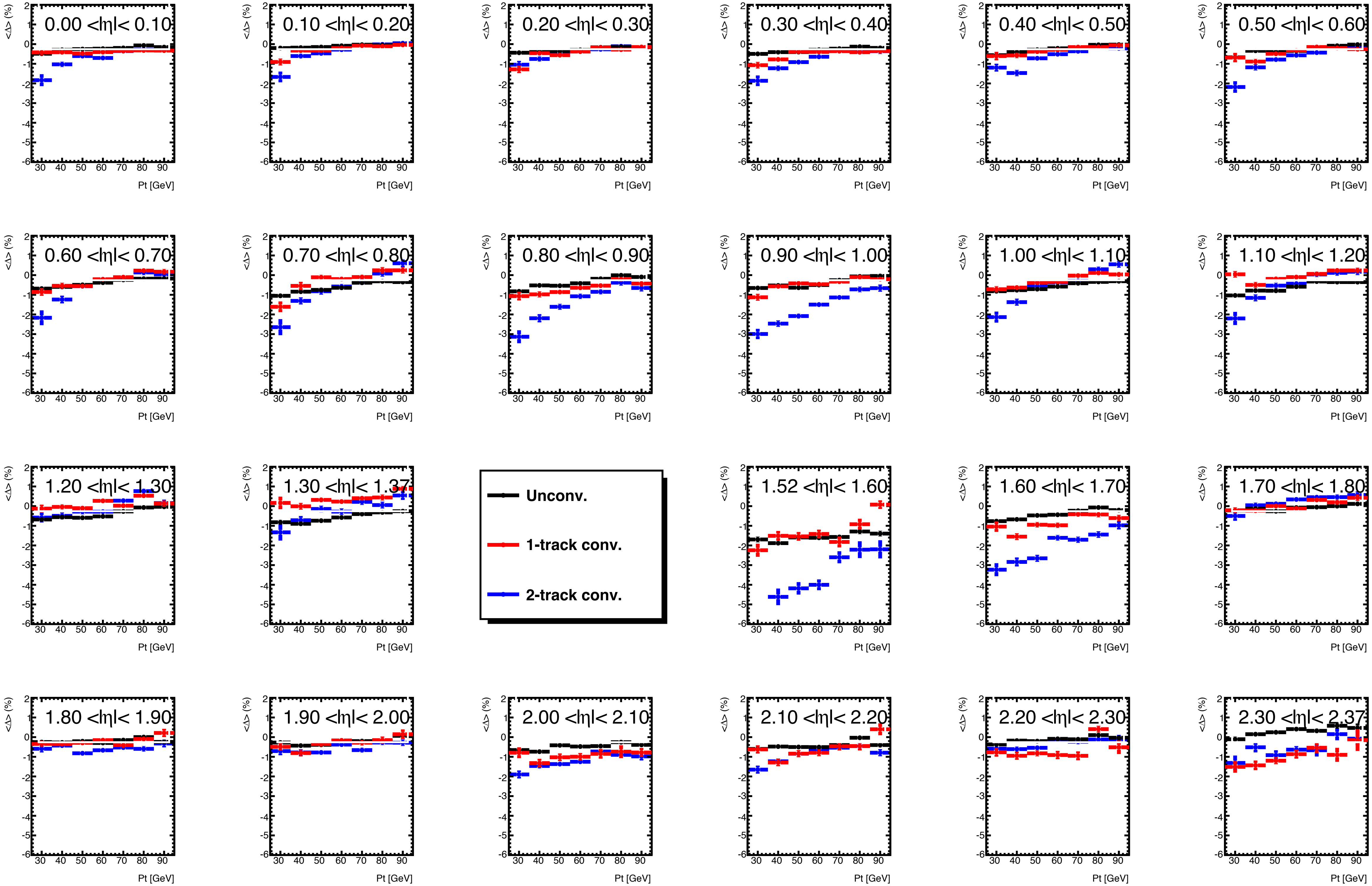

Why pTt?

- The categorization based on the pTt variable leads to a better sensitivity for the Higgs boson signal than one based on pTgg due to the resolution of pTt being better than that of pTgg.
- Moreover, the shape of the mgg distribution based on the pTt categorization can be better described with an exponential shape, which is not the case for the pTgg categorization.
- By introducing these pTt categories, the expected sensitivity of the analysis is improved by 5 – 10% depending on the hypothesized Higgs boson mass.

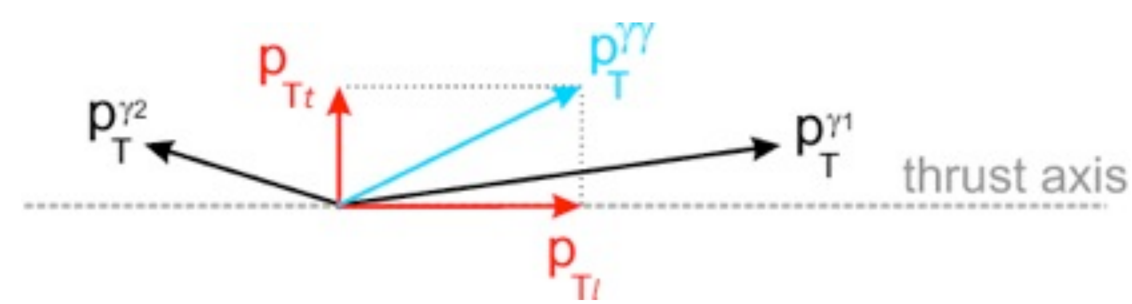

Signal Yields brake down by processes

$\sqrt{s}$	Category	Events [N_{evt}]	$gg \to H$ [%]	VBF [%]	WH [%]	ZH [%]	ttH [%]
7 TeV	Inclusive	79.4	87.8	7.3	2.9	1.6	0.4
	Unconv. central, low p_{Tt}	10.5	92.9	4.0	1.8	1.0	0.2
	Unconv. central, high p_{Tt}	1.5	66.5	15.7	9.9	5.7	2.4
	Unconv. rest, low p_{Tt}	21.6	92.8	3.9	2.0	1.1	0.2
	Unconv. rest, high p_{Tt}	2.8	65.4	16.1	10.8	6	1.8
	Conv. central, low p_{Tt}	6.7	92.8	4.0	1.9	1.0	0.2
	Conv. central, high p_{Tt}	1.0	66.6	15.3	10.0	5.7	2.5
	Conv. rest, low p_{Tt}	21.1	92.8	3.8	2.0	1.1	0.2
	Conv. rest, high p_{Tt}	2.7	65.3	15.9	11.0	5.9	1.8
	Conv. transition	9.5	89.4	5.2	3.3	1.7	0.3
	2-jet	2.2	22.5	76.7	0.4	0.2	0.1
8 TeV	Inclusive	111.9	87.9	7.3	2.7	1.6	0.5
	Unconv. central, low p_{Tt}	14.2	94.0	4.3	1.7	1.0	0.3
	Unconv. central, high p_{Tt}	2.5	73.5	14.3	7.0	4.3	2.4
	Unconv. rest, low p_{Tt}	30.9	93.7	4.2	2.0	1.1	0.2
	Unconv. rest, high p_{Tt}	5.2	72.9	14.0	7.9	4.7	1.7
	Conv. central, low p_{Tt}	8.9	94	4.3	1.7	1.0	0.3
	Conv. central, high p_{Tt}	1.6	73.8	13.6	7.2	4.2	2.3
	Conv. rest, low p_{Tt}	26.9	93.8	4.2	2.0	1.1	0.2
	Conv. rest, high p_{Tt}	4.5	72.1	14.1	8.5	4.8	1.8
	Conv. transition	12.8	90.1	5.9	3.1	1.8	0.4
	2-jet	3.0	30.8	69.3	0.4	0.2	0.2

Categories

Both unconverted:

- Central
- Rest

At least one converted:

- Central
- Transition
- Rest

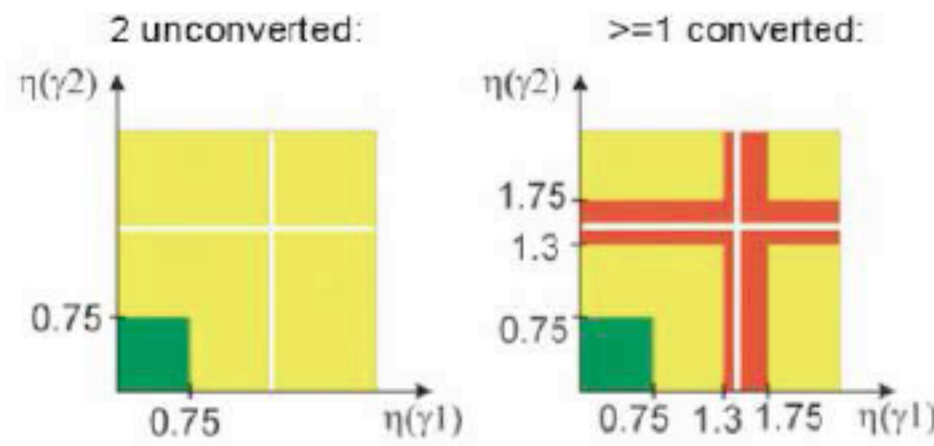

Resolution:

Good
Medium
Poor

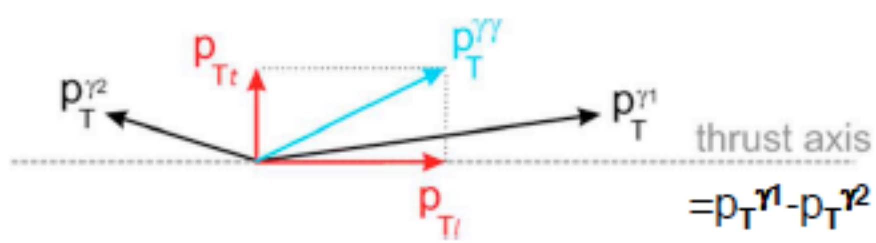

Variable p_{Tt} is strongly correlated with diphoton p_T but has better detector resolution and retains a monotically falling invariant mass for background

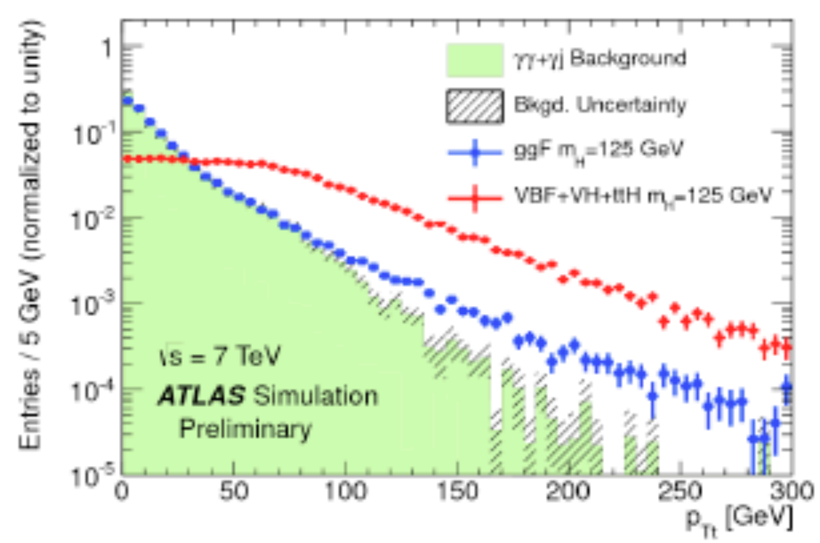

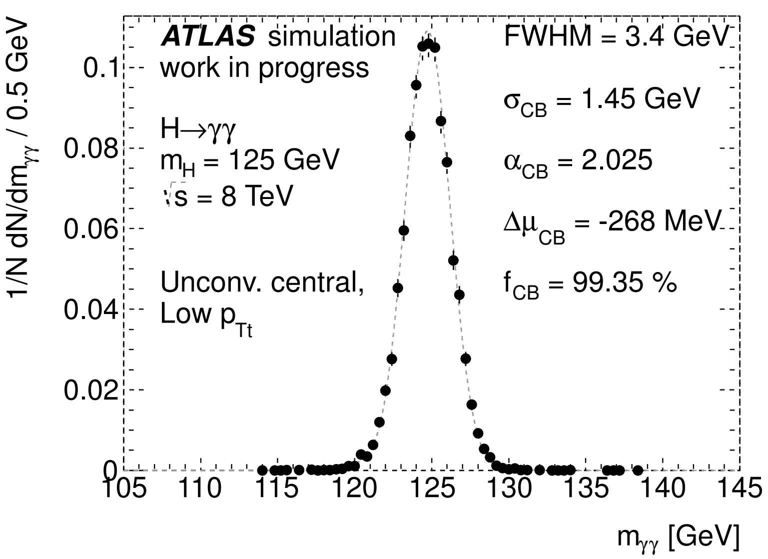
ATLAS simulation
work in progress
FWHM = 3.4 GeV
σ_{CB} = 1.45 GeV
α_{CB} = 2.025
$\Delta\mu_{CB}$ = -268 MeV
f_{CB} = 99.35 %
$H\rightarrow\gamma\gamma$
m_H = 125 GeV
$\sqrt{s}$ = 8 TeV
Unconv. central,
Low p_{Tt}
$1/N\ dN/dm_{\gamma\gamma}$ / 0.5 GeV
$m_{\gamma\gamma}$ [GeV]

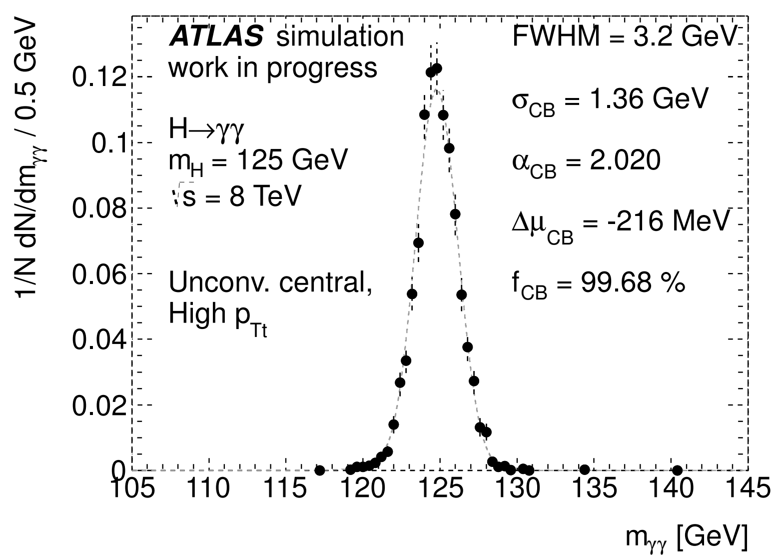
ATLAS simulation
work in progress
FWHM = 3.2 GeV
σ_{CB} = 1.36 GeV
α_{CB} = 2.020
$\Delta\mu_{CB}$ = -216 MeV
f_{CB} = 99.68 %
$H\rightarrow\gamma\gamma$
m_H = 125 GeV
$\sqrt{s}$ = 8 TeV
Unconv. central,
High p_{Tt}
$1/N\ dN/dm_{\gamma\gamma}$ / 0.5 GeV
$m_{\gamma\gamma}$ [GeV]

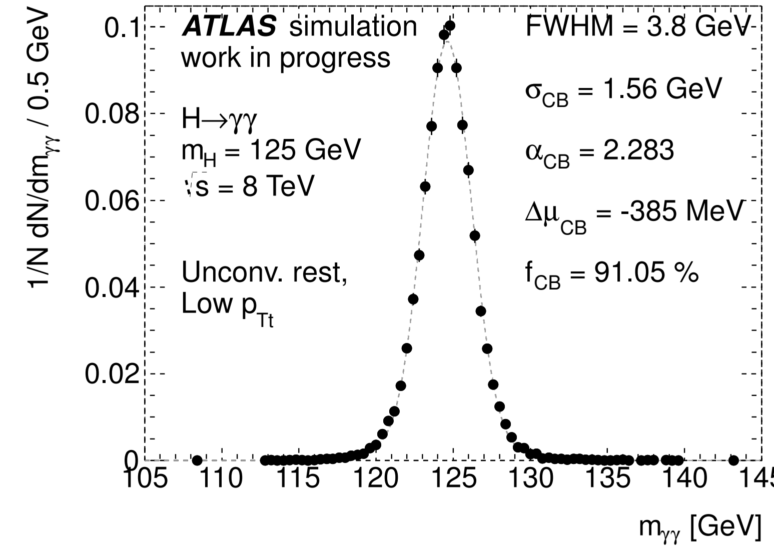
ATLAS simulation
work in progress
FWHM = 3.8 GeV
σ_{CB} = 1.56 GeV
α_{CB} = 2.283
$\Delta\mu_{CB}$ = -385 MeV
f_{CB} = 91.05 %
$H\rightarrow\gamma\gamma$
m_H = 125 GeV
$\sqrt{s}$ = 8 TeV
Unconv. rest,
Low p_{Tt}
$1/N\ dN/dm_{\gamma\gamma}$ / 0.5 GeV
$m_{\gamma\gamma}$ [GeV]

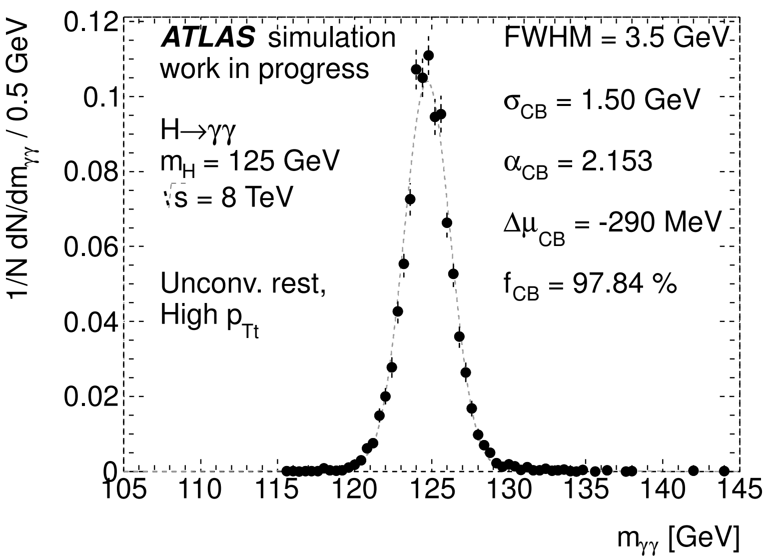
ATLAS simulation
work in progress
FWHM = 3.5 GeV
σ_{CB} = 1.50 GeV
α_{CB} = 2.153
$\Delta\mu_{CB}$ = -290 MeV
f_{CB} = 97.84 %
$H\rightarrow\gamma\gamma$
m_H = 125 GeV
$\sqrt{s}$ = 8 TeV
Unconv. rest,
High p_{Tt}
$1/N\ dN/dm_{\gamma\gamma}$ / 0.5 GeV
$m_{\gamma\gamma}$ [GeV]

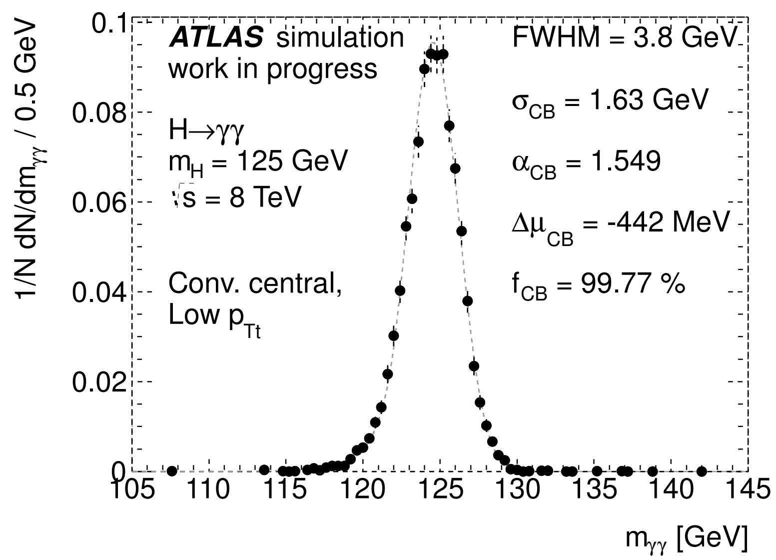
ATLAS simulation
work in progress
FWHM = 3.8 GeV
σ_{CB} = 1.63 GeV
α_{CB} = 1.549
$\Delta\mu_{CB}$ = -442 MeV
f_{CB} = 99.77 %
$H\rightarrow\gamma\gamma$
m_H = 125 GeV
$\sqrt{s}$ = 8 TeV
Conv. central,
Low p_{Tt}
$1/N\ dN/dm_{\gamma\gamma}$ / 0.5 GeV
$m_{\gamma\gamma}$ [GeV]

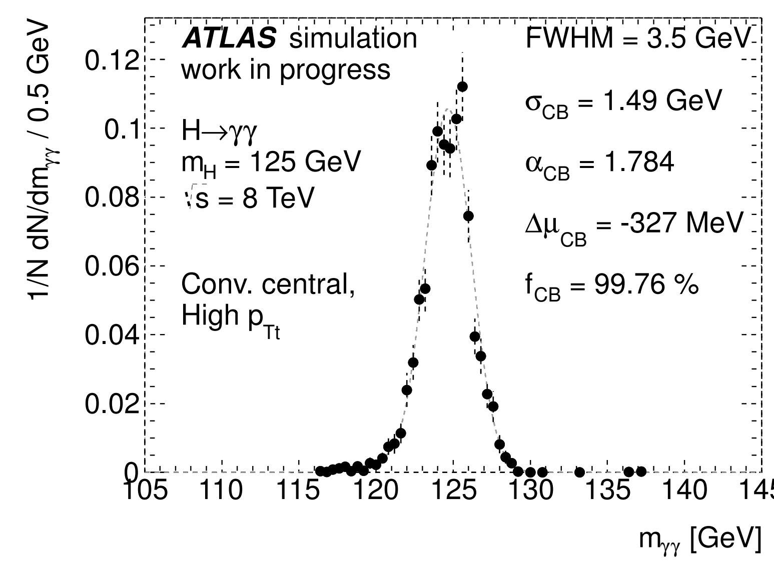
ATLAS simulation
work in progress
FWHM = 3.5 GeV
σ_{CB} = 1.49 GeV
α_{CB} = 1.784
$\Delta\mu_{CB}$ = -327 MeV
f_{CB} = 99.76 %
$H\rightarrow\gamma\gamma$
m_H = 125 GeV
$\sqrt{s}$ = 8 TeV
Conv. central,
High p_{Tt}
$1/N\ dN/dm_{\gamma\gamma}$ / 0.5 GeV
$m_{\gamma\gamma}$ [GeV]

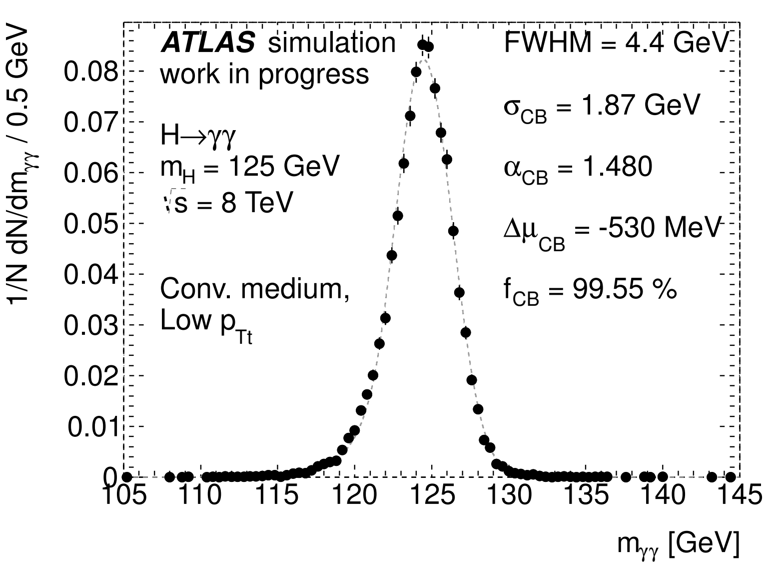
ATLAS simulation
work in progress
FWHM = 4.4 GeV
σ_{CB} = 1.87 GeV
α_{CB} = 1.480
$\Delta\mu_{CB}$ = -530 MeV
f_{CB} = 99.55 %
$H\rightarrow\gamma\gamma$
m_H = 125 GeV
$\sqrt{s}$ = 8 TeV
Conv. medium,
Low p_{Tt}
$1/N\ dN/dm_{\gamma\gamma}$ / 0.5 GeV
$m_{\gamma\gamma}$ [GeV]

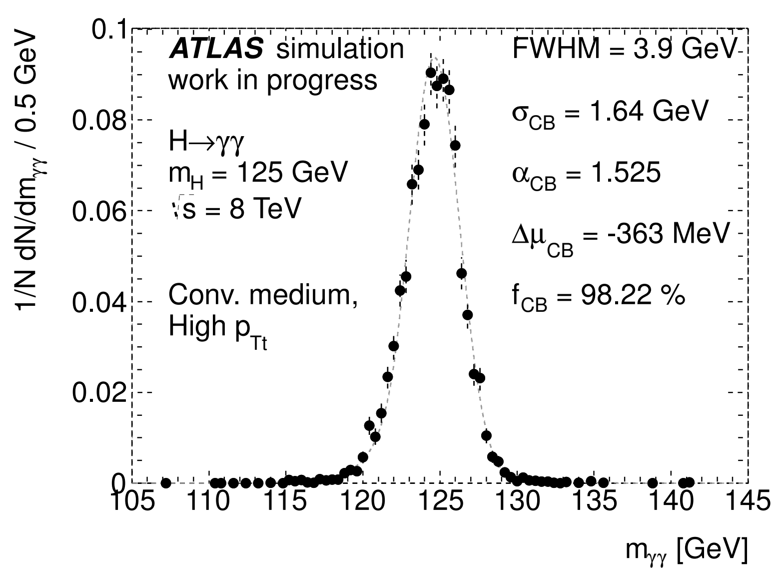
ATLAS simulation
work in progress
FWHM = 3.9 GeV
σ_{CB} = 1.64 GeV
α_{CB} = 1.525
$\Delta\mu_{CB}$ = -363 MeV
f_{CB} = 98.22 %
$H\rightarrow\gamma\gamma$
m_H = 125 GeV
$\sqrt{s}$ = 8 TeV
Conv. medium,
High p_{Tt}
$1/N\ dN/dm_{\gamma\gamma}$ / 0.5 GeV
$m_{\gamma\gamma}$ [GeV]

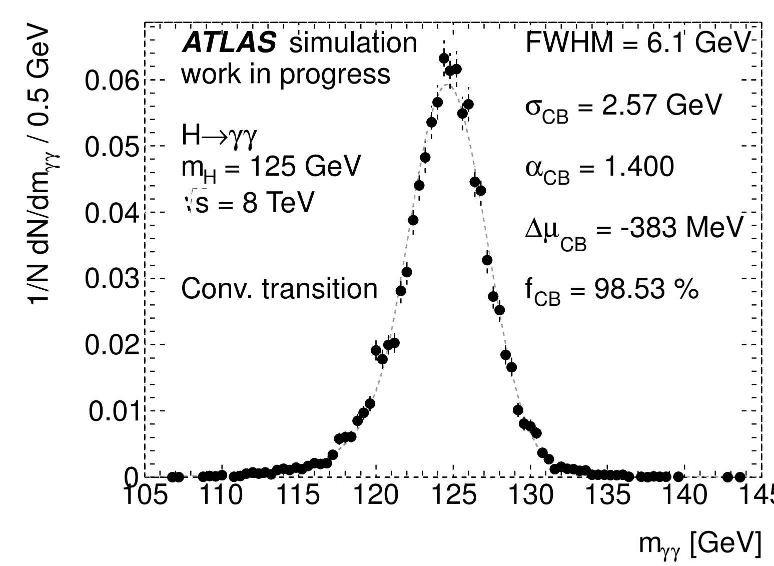
ATLAS simulation
work in progress
FWHM = 6.1 GeV
σ_{CB} = 2.57 GeV
α_{CB} = 1.400
$\Delta\mu_{CB}$ = -383 MeV
f_{CB} = 98.53 %
$H\rightarrow\gamma\gamma$
m_H = 125 GeV
$\sqrt{s}$ = 8 TeV
Conv. transition
$1/N\ dN/dm_{\gamma\gamma}$ / 0.5 GeV
$m_{\gamma\gamma}$ [GeV]

Background modeling

Category	Parametrisation	Uncertainty [N_{evt}] $\sqrt{s}=7$ TeV	$\sqrt{s}=8$TeV
Inclusive	4th order pol.	7.3	10.6
Unconverted central, low p_{Tt}	Exp. of 2nd order pol.	2.1	3.0
Unconverted central, high p_{Tt}	Exponential	0.2	0.3
Unconverted rest, low p_{Tt}	4th order pol.	2.2	3.3
Unconverted rest, high p_{Tt}	Exponential	0.5	0.8
Converted central, low p_{Tt}	Exp. of 2nd order pol.	1.6	2.3
Converted central, high p_{Tt}	Exponential	0.3	0.4
Converted rest, low p_{Tt}	4th order pol.	4.6	6.8
Converted rest, high p_{Tt}	Exponential	0.5	0.7
Converted transition	Exp. of 2nd order pol.	3.2	4.6
2-jets	Exponential	0.4	0.6

Observation of a new boson

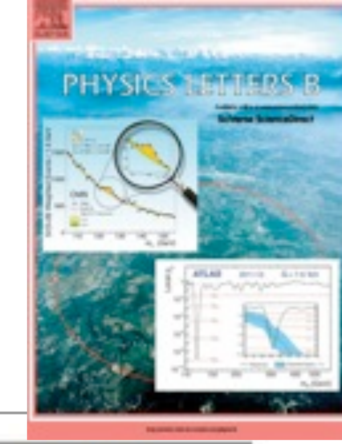

- **Systematic uncertainties of the analysis:**

Systematic uncertainties	$\sqrt{s}$ = 7 TeV [%]	$\sqrt{s}$ = 8 TeV [%]
Signal event yield		
Photon identification	±8.4	±10.8
Effect of pileup on photon rec/ID	±4	
Photon energy scale	±0.3	
Photon Isolation	±0.4	±0.5
Trigger	±1	
Higgs boson cross section (perturbative)	$gg \to H$: $^{+12}_{-8}$, VBF: ±0.3, WH: $^{+0.2}_{-0.8}$, ZH: $^{+1.4}_{-1.6}$, ttH: $^{+3}_{-9}$	$gg \to H$: $^{+7}_{-8}$, VBF: ±0.2, WH: $^{+0.2}_{-0.6}$, ZH: $^{+1.6}_{-1.5}$, ttH: $^{+4}_{-9}$
	$gg \to H + 2$ jets: ±25	
Higgs boson cross section (PDF+α_S)	$gg \to H$: $^{+8}_{-7}$, VBF: $^{+2.5}_{-2.1}$, VH: ±3.5, ttH: ±9	$gg \to H$: $^{+8}_{-7}$, VBF: $^{+2.6}_{-2.8}$, VH: ±3.5, ttH: ±8
Higgs boson branching ratio	±5	
Higgs boson p_T modeling	low p_{Tt}: ±1.1, high p_{Tt}: ∓12.5, 2-jets: ∓9	
Underlying Event (2-jets)	VBF: ±6, Others: ±30	
Luminosity	±1.8	±3.6
Signal category migration		
Material	Unconv: ±4, Conv: ∓3.5	
Effect of pileup on photon rec/ID	Unconv: ±3, Conv: ∓2, 2-jets: ±2	Unconv: ±2, Conv: ∓2, 2-jets: ±12
Jet energy scale	low p_{Tt}	
	$gg \to H$: ±0.1, VBF: ±2.6, Others: ±0.1	$gg \to H$: ±0.1, VBF: ±2.3, Others: ±0.1
	high p_{Tt}	
	$gg \to H$: ±0.1, VBF: ±4, Others: ±0.1	$gg \to H$: ±0.1, VBF: ±4, Others: ±0.1
	2-jets	
	$gg \to H$: ∓19, VBF: ∓8, Others: ∓15	$gg \to H$: ∓18, VBF: ∓9, Others: ∓13
Jet-vertex-fraction		2-jets: ±13, Others: ∓0.3
Primary vertex selection	negligible	
Signal mass resolution		
Calorimeter energy resolution	±12	
Electron to photon extrapolation	±6	
Effect of pileup on energy resolution	±4	
Primary vertex selection	negligible	
Signal mass position		
Photon energy scale	±0.6	

Observation of a new boson

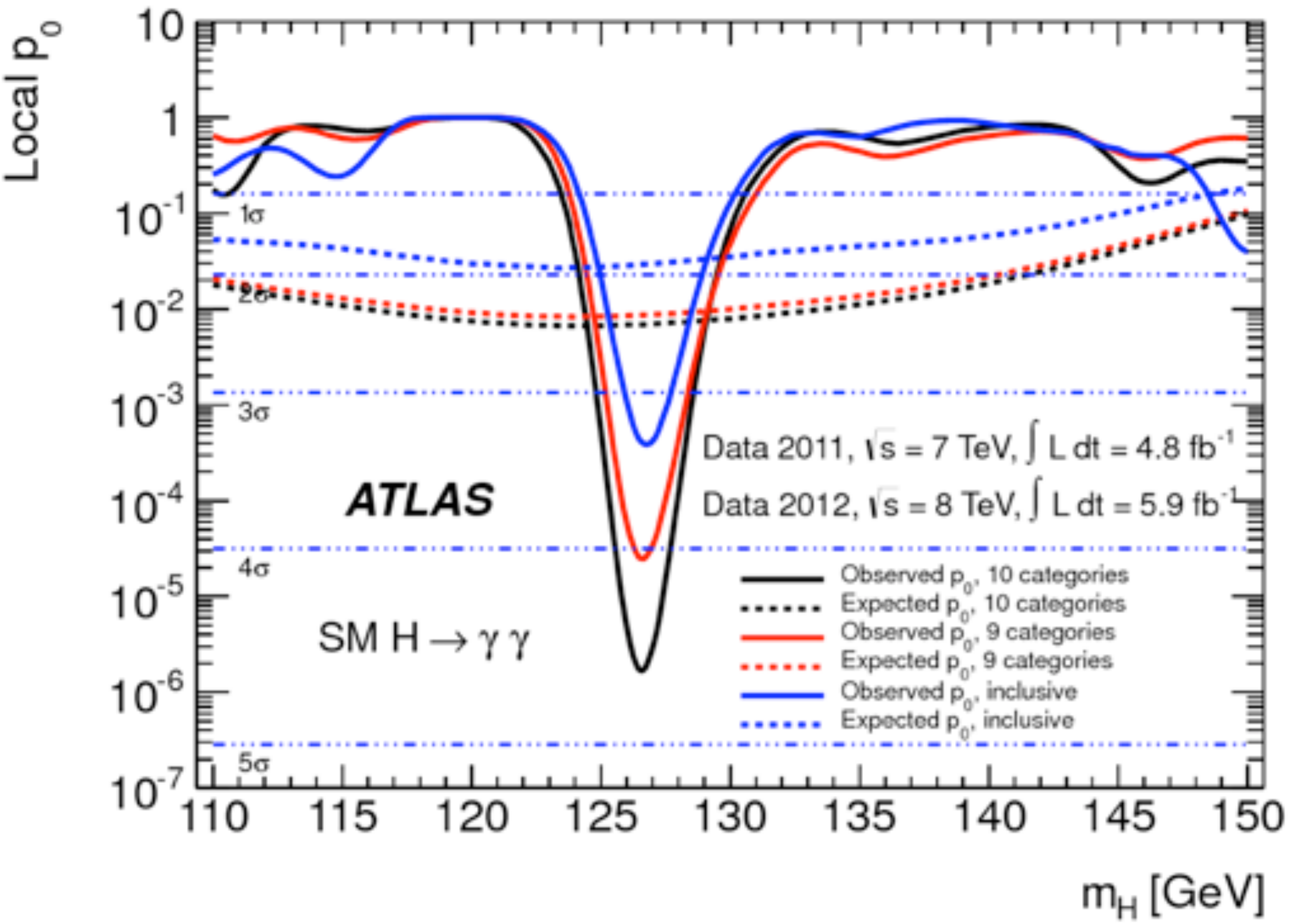

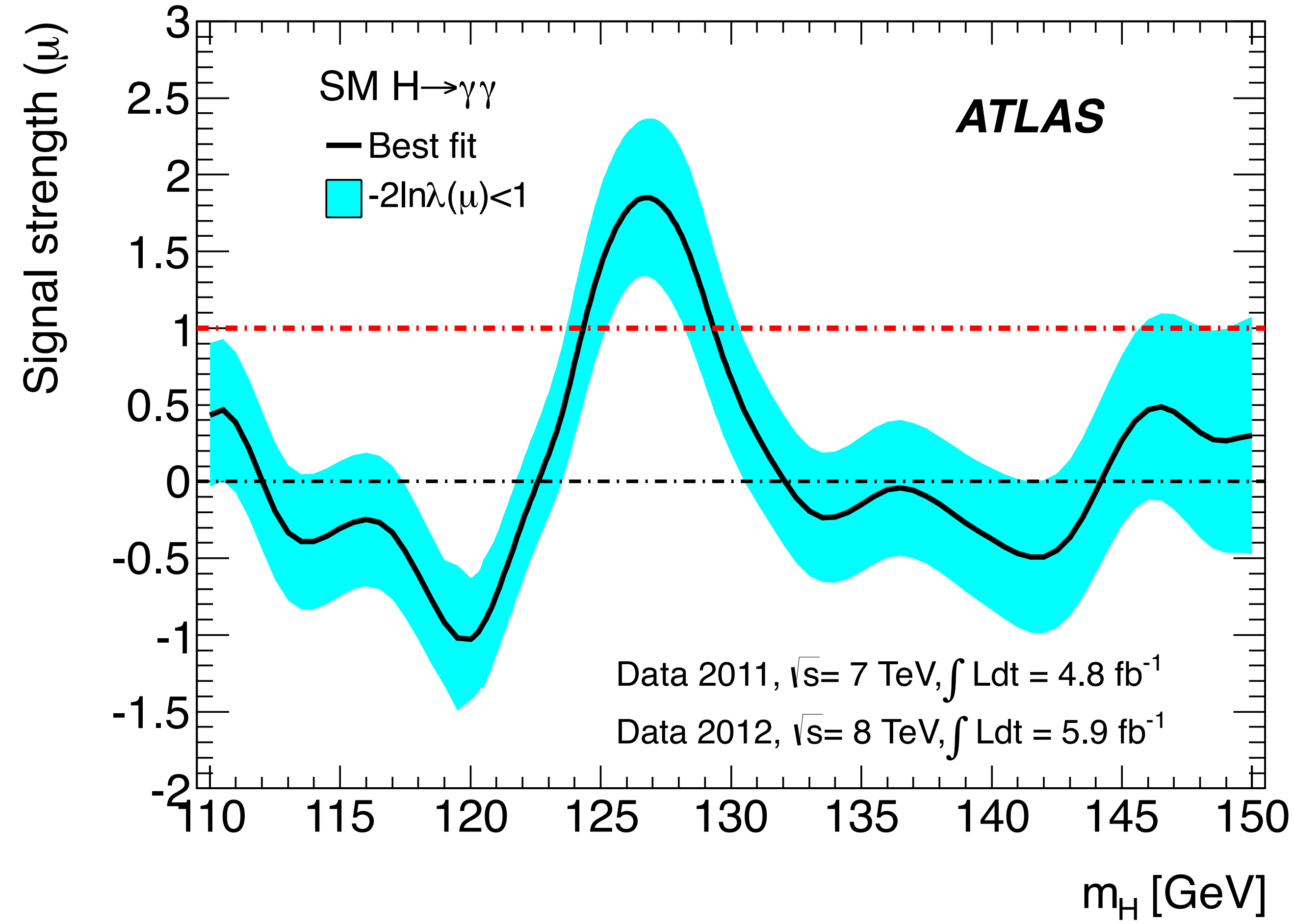

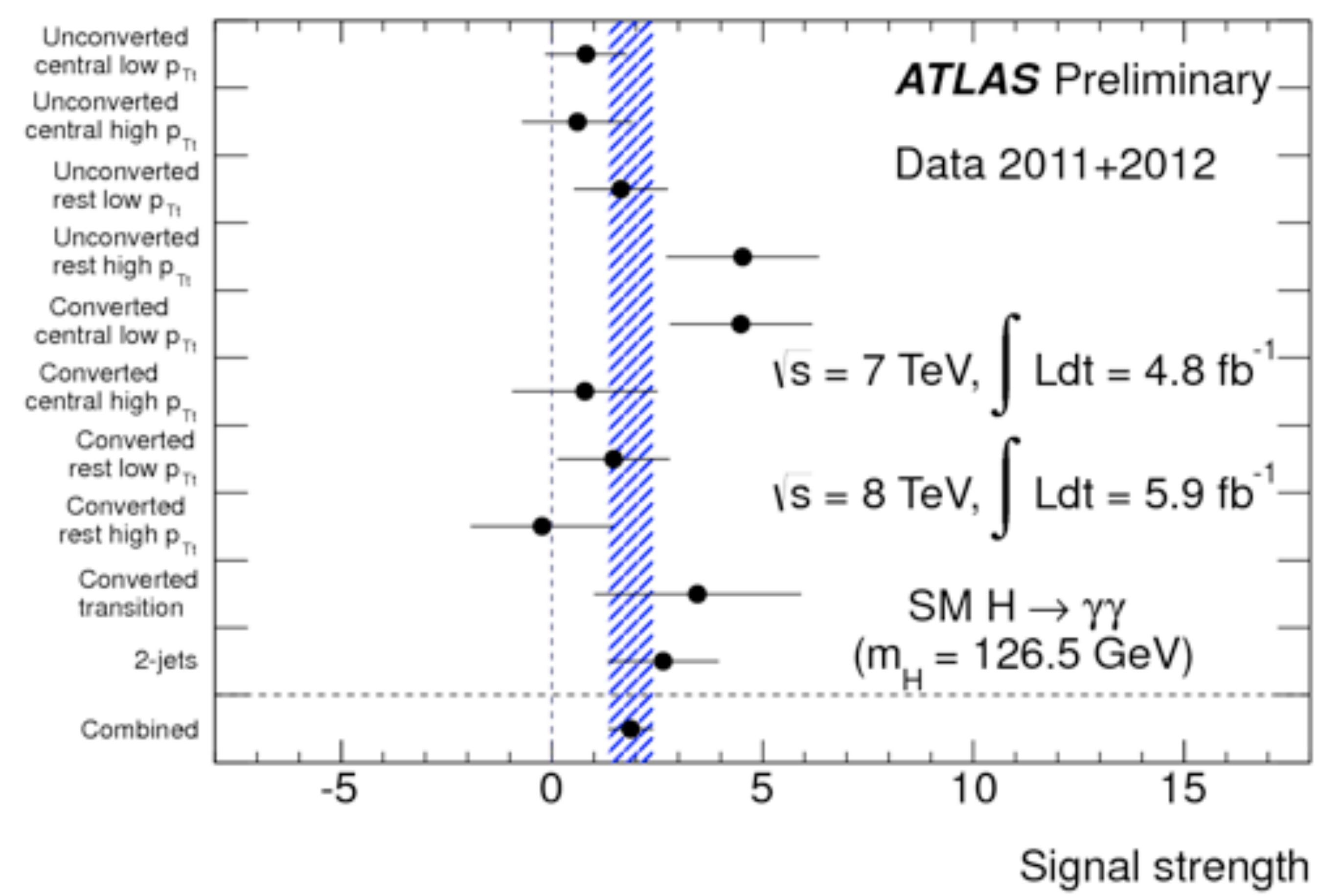

Analysis Update

ATLAS Preliminary

$H \rightarrow \gamma\gamma$

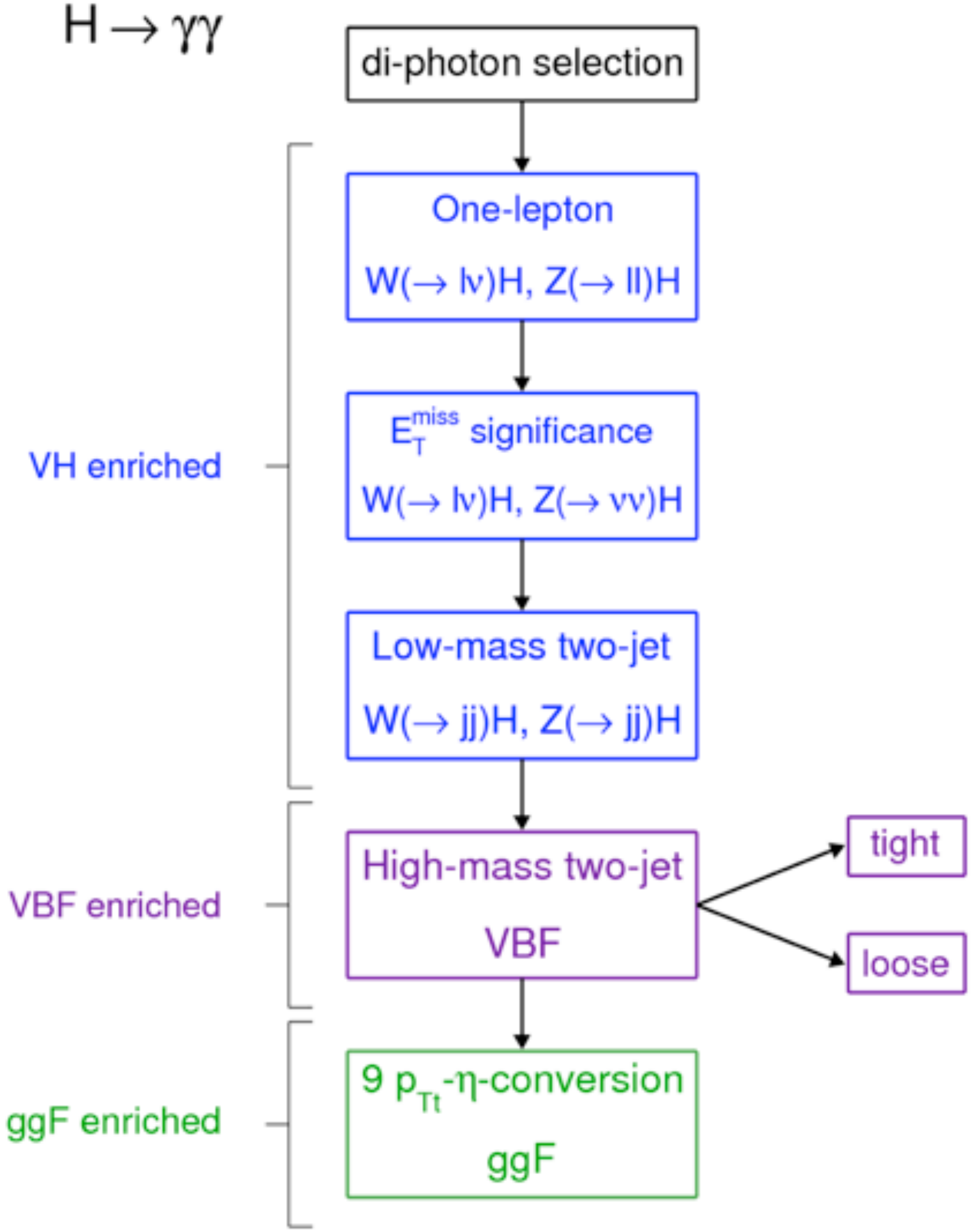

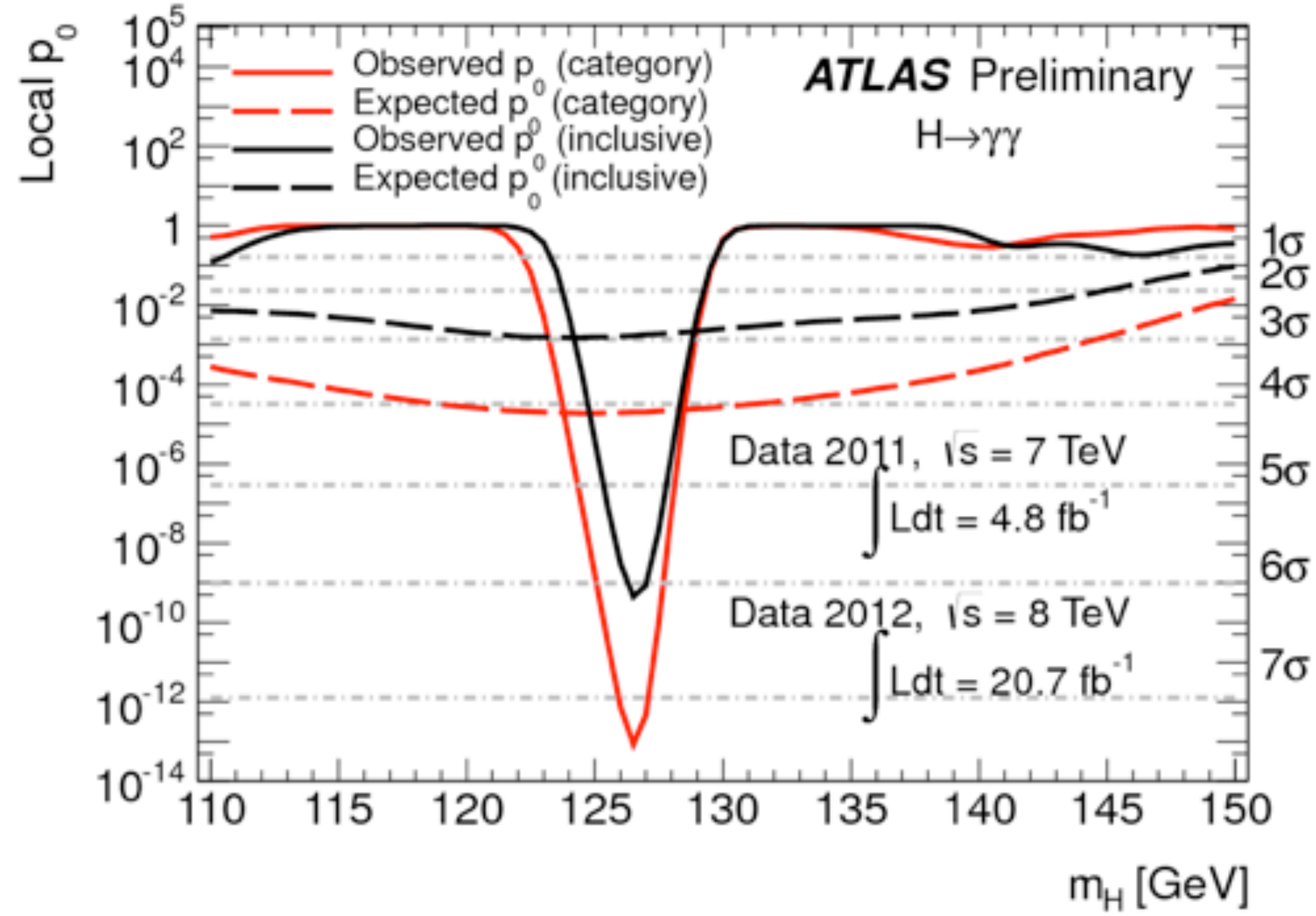

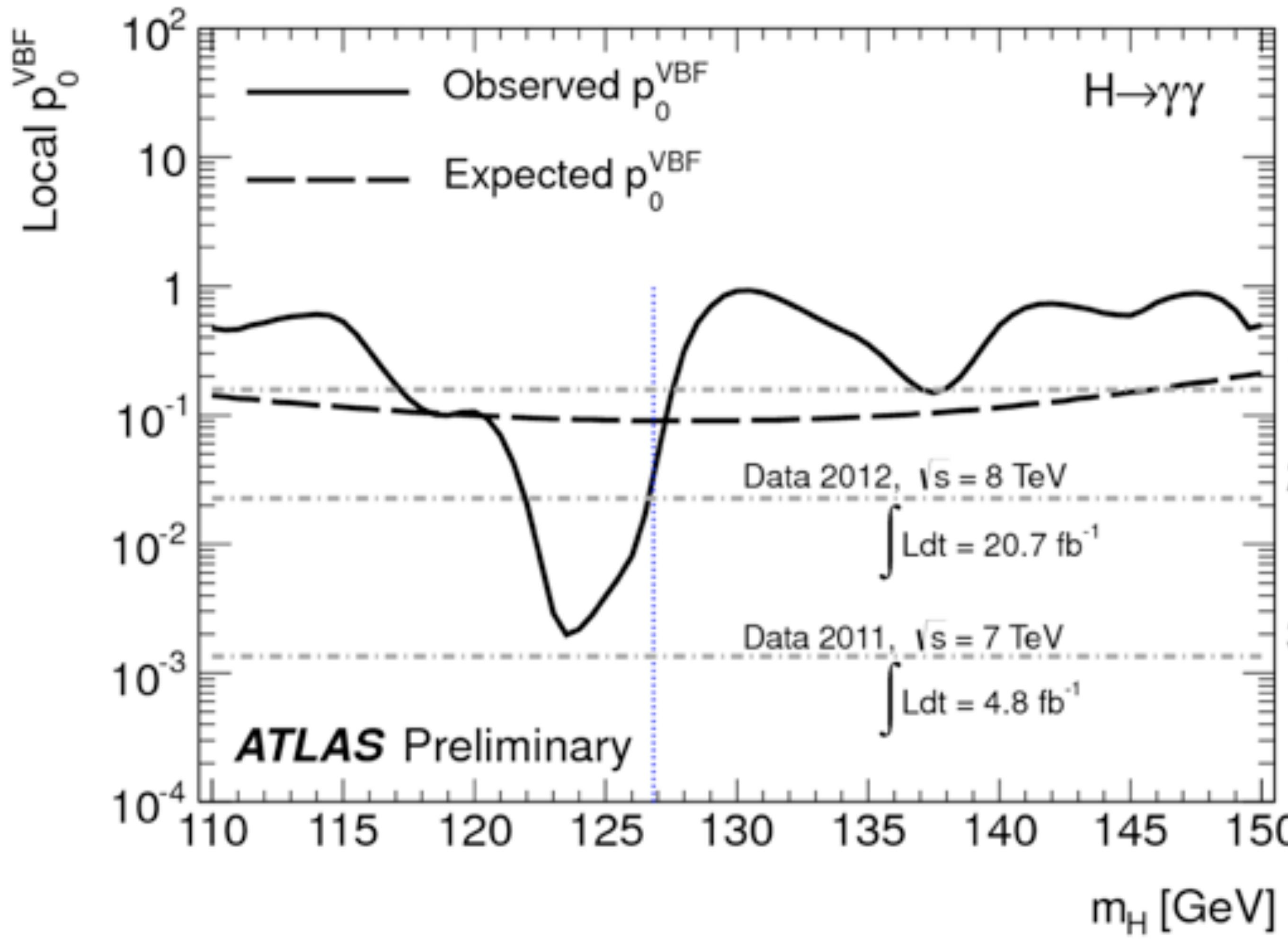

Differential cross section

Define a binning for a variable ($Pt_{\gamma\gamma}$, $|y_{\gamma\gamma}|$, cos(theta)*)

For each bin extract yield from fit to $m_{\gamma\gamma}$

For each bin, correct for acceptance, efficiency, resolution:
“unfolding”

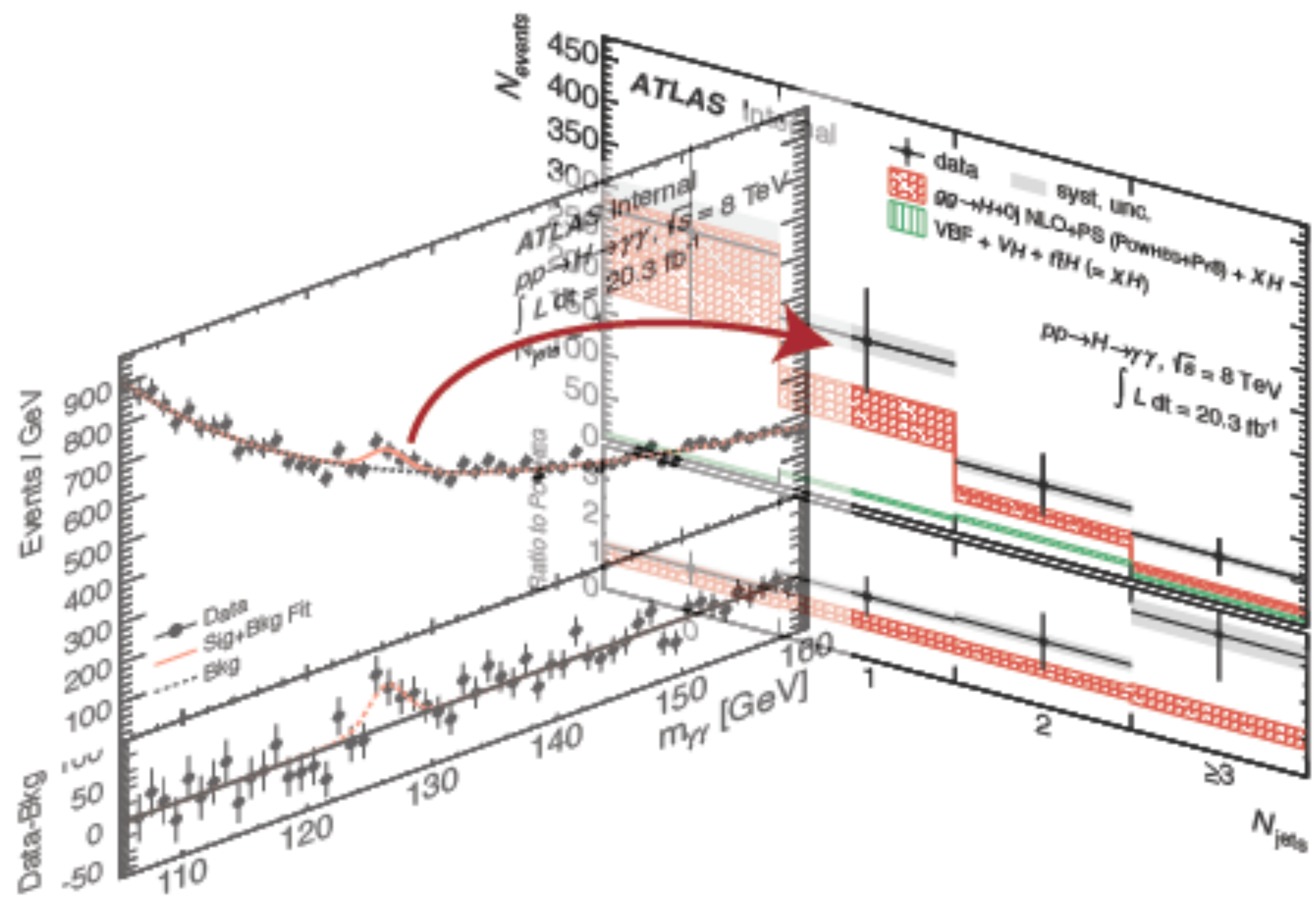

Properties measurements

Spin: Observed numbers of events in the signal region as a function of |cos theta*|, overlaid with the projection of the signal+background components obtained from the inclusive fit of the data in the nominal analysis under the spin-0 hypothesis.

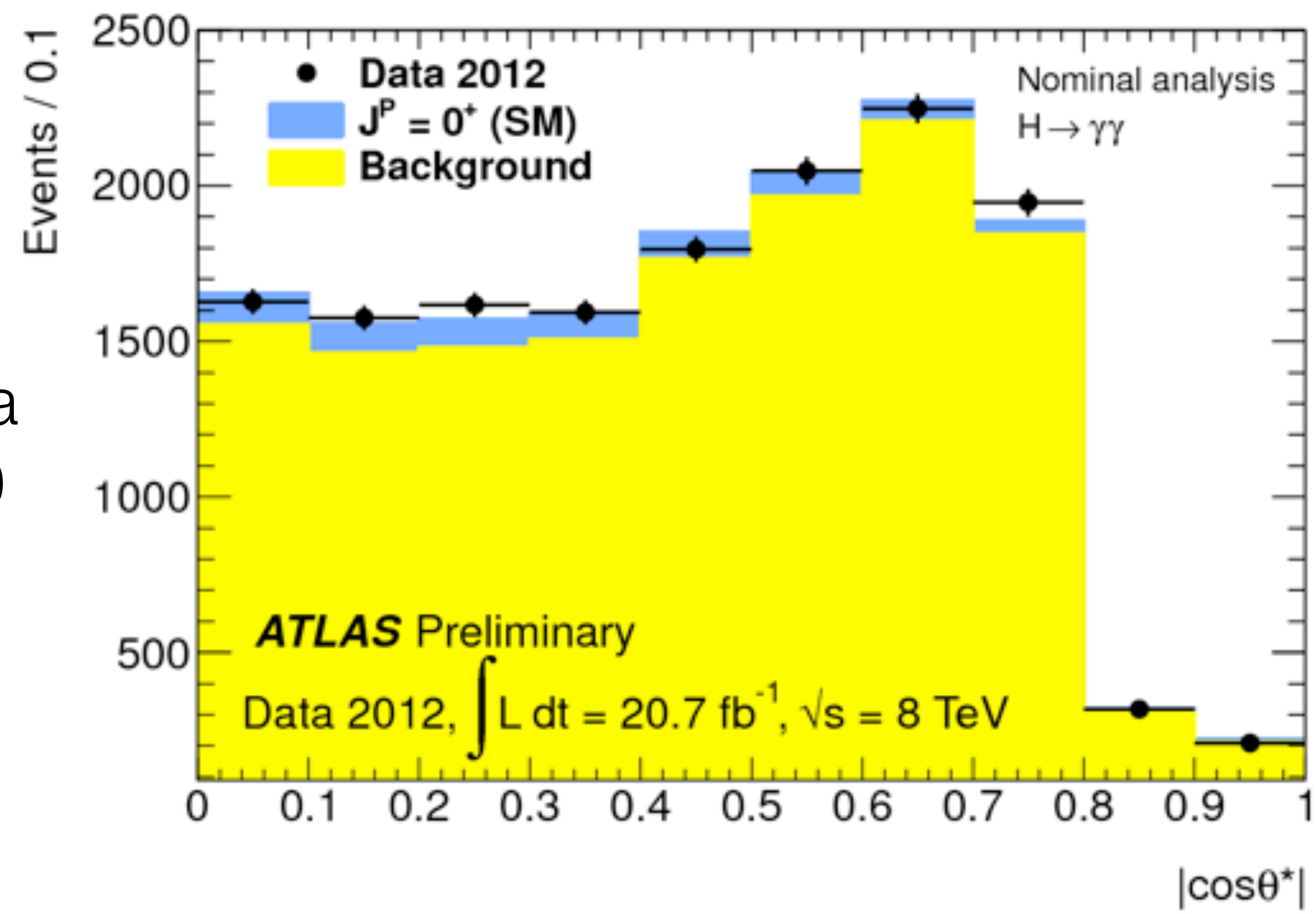

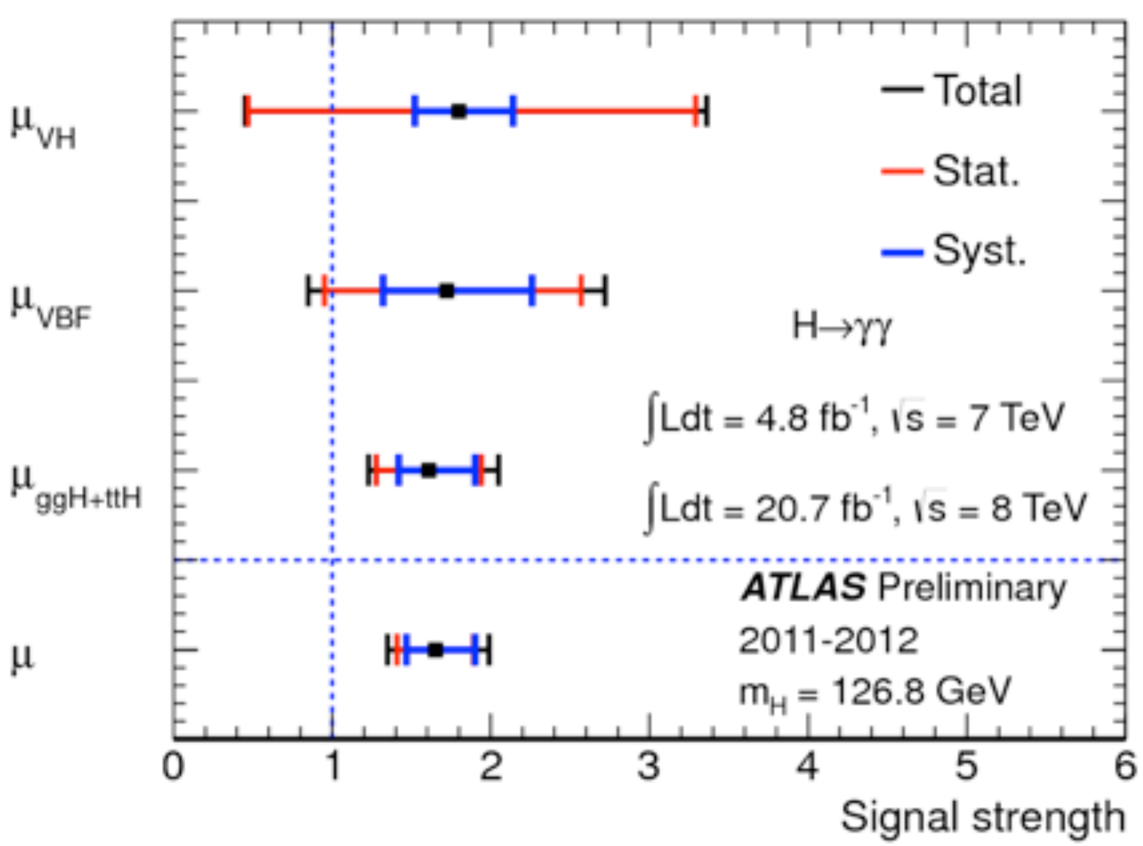

±0.08 (signal yield) ±0.09 (migration) ±0.10 (resolution)

Signal strength: Measured signal strengths $\mu_{ggF+ttH}$, μ_{VBF} and μ_{VH} for the different production modes.

CMS Higgs to diphoton

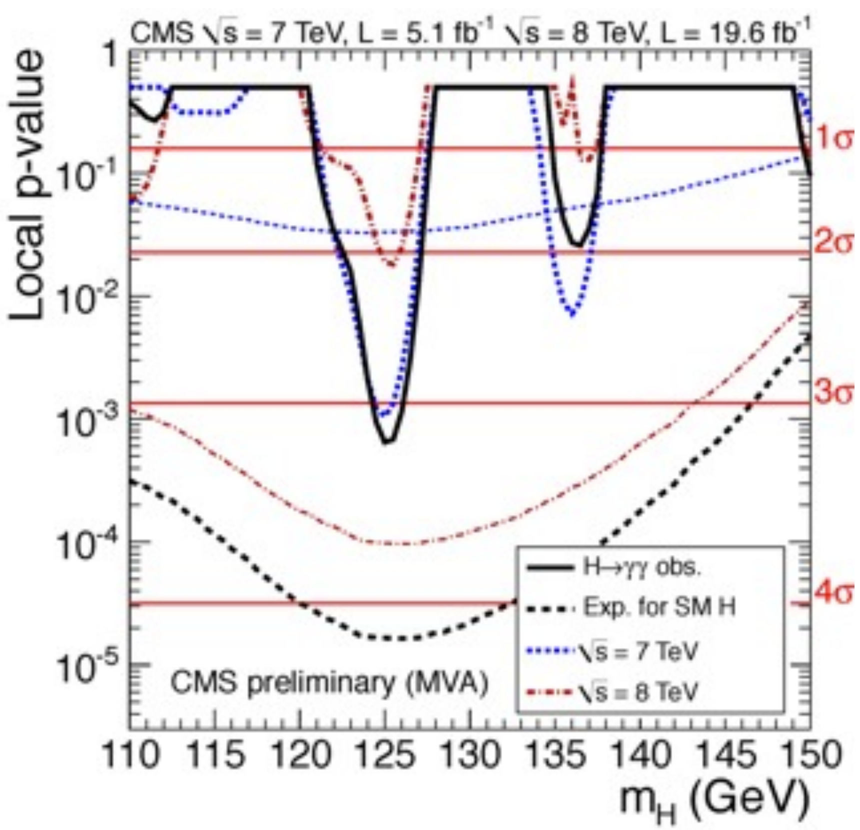

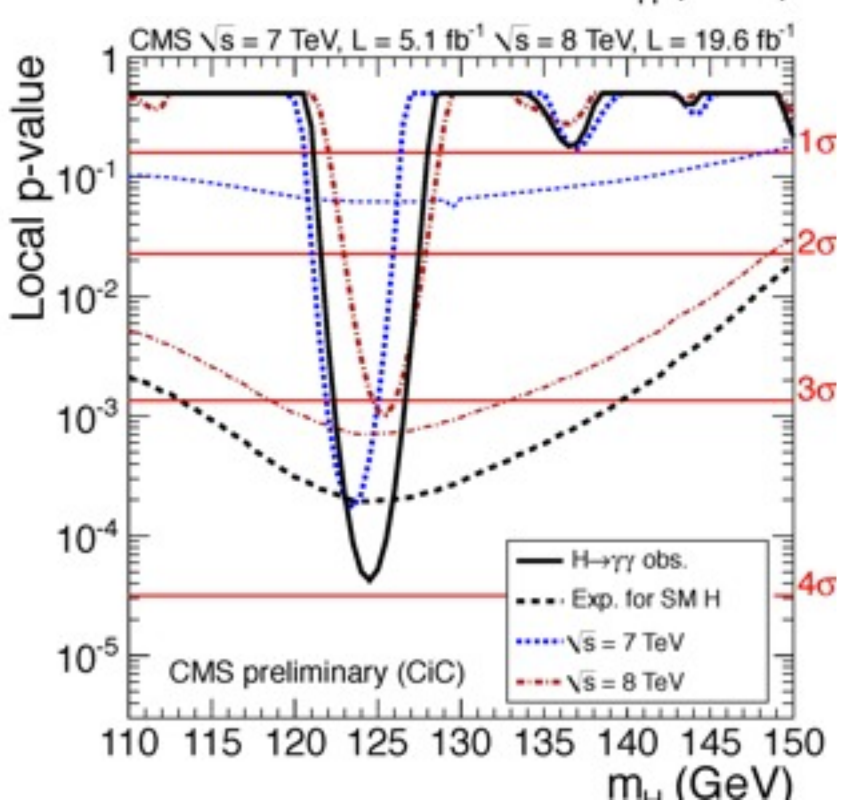

MVA and cut based analysis.

Expected signal and estimated background

Event classes		SM Higgs boson expected signal (m_H=125 GeV) Total	ggH	VBF	VH	ttH	σ_{eff} (GeV)	FWHM/2.35 (GeV)	Background $m_{\gamma\gamma}$ = 125 GeV (ev./GeV)
7 TeV 5.1 fb^{-1}	Untagged 0	3.2	61.4%	16.8%	18.7%	3.1%	1.21	1.14	3.3 ± 0.4
	Untagged 1	16.3	87.6%	6.2%	5.6%	0.5%	1.26	1.08	37.5 ± 1.3
	Untagged 2	21.5	91.3%	4.4%	3.9%	0.3%	1.59	1.32	74.8 ± 1.9
	Untagged 3	32.8	91.3%	4.4%	4.1%	0.2%	2.47	2.07	193.6 ± 3.0
	Dijet tag	2.9	26.8%	72.5%	0.6%	–	1.73	1.37	1.7 ± 0.2
8 TeV 19.6 fb^{-1}	Untagged 0	17.0	72.9%	11.6%	12.9%	2.6%	1.36	1.27	22.1 ± 0.5
	Untagged 1	37.8	83.5%	8.4%	7.1%	1.0%	1.50	1.39	94.3 ± 1.0
	Untagged 2	150.2	91.6%	4.5%	3.6%	0.4%	1.77	1.54	570.5 ± 2.6
	Untagged 3	159.9	92.5%	3.9%	3.3%	0.3%	2.61	2.14	1060.9 ± 3.5
	Dijet tight	9.2	20.7%	78.9%	0.3%	0.1%	1.79	1.50	3.4 ± 0.2
	Dijet loose	11.5	47.0%	50.9%	1.7%	0.5%	1.87	1.60	12.4 ± 0.4
	Muon tag	1.4	0.0%	0.2%	79.0%	20.8%	1.85	1.52	0.7 ± 0.1
	Electron tag	0.9	1.1%	0.4%	78.7%	19.8%	1.88	1.54	0.7 ± 0.1
	E_T^{miss} tag	1.7	22.0%	2.6%	63.7%	11.7%	1.79	1.64	1.8 ± 0.1

Photon scale determination χ² method

For each value of α the Χ² quantity is calculated using data and MC histograms of the three body invariant mass:

$$\chi^2 = \sum_{i}^{Nbins} \frac{\left(N_{ll\gamma_{Data},i} - N_{ll\gamma MC,i}\right)^2}{\sigma^2_{ll\gamma_{Data},i} + \sigma^2_{ll\gamma MC,i}} \longrightarrow$$

$i =$ bin label of the $M_{ll\gamma}$ histogram

$N_{ll\gamma,i} =$ number of events in each bin

$\sigma^2_{ll\gamma,i} = \left(N_{ll\gamma,i}\right)^{1/2}$

α is extracted of a parabolic interpolation to the ensemble of Χ² values:

$$\chi^2(\alpha) = \frac{(\alpha - \alpha_{\min})^2}{\sigma^2} + \chi^2_{\min}$$

$\alpha_{\min} =$ value of α that minimizes the function

$\sigma =$ error on α

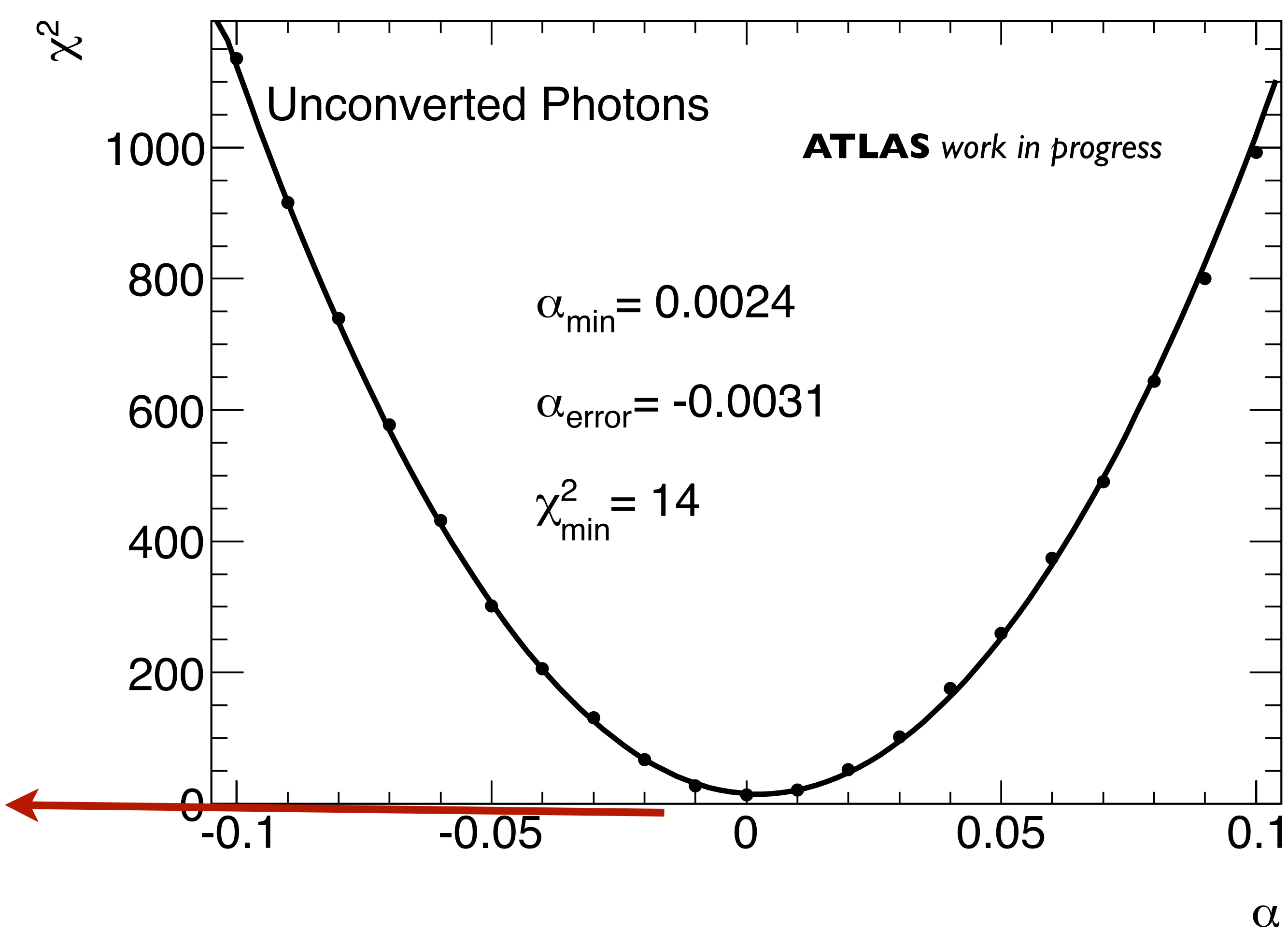

The α that minimizes the function is the energy scale

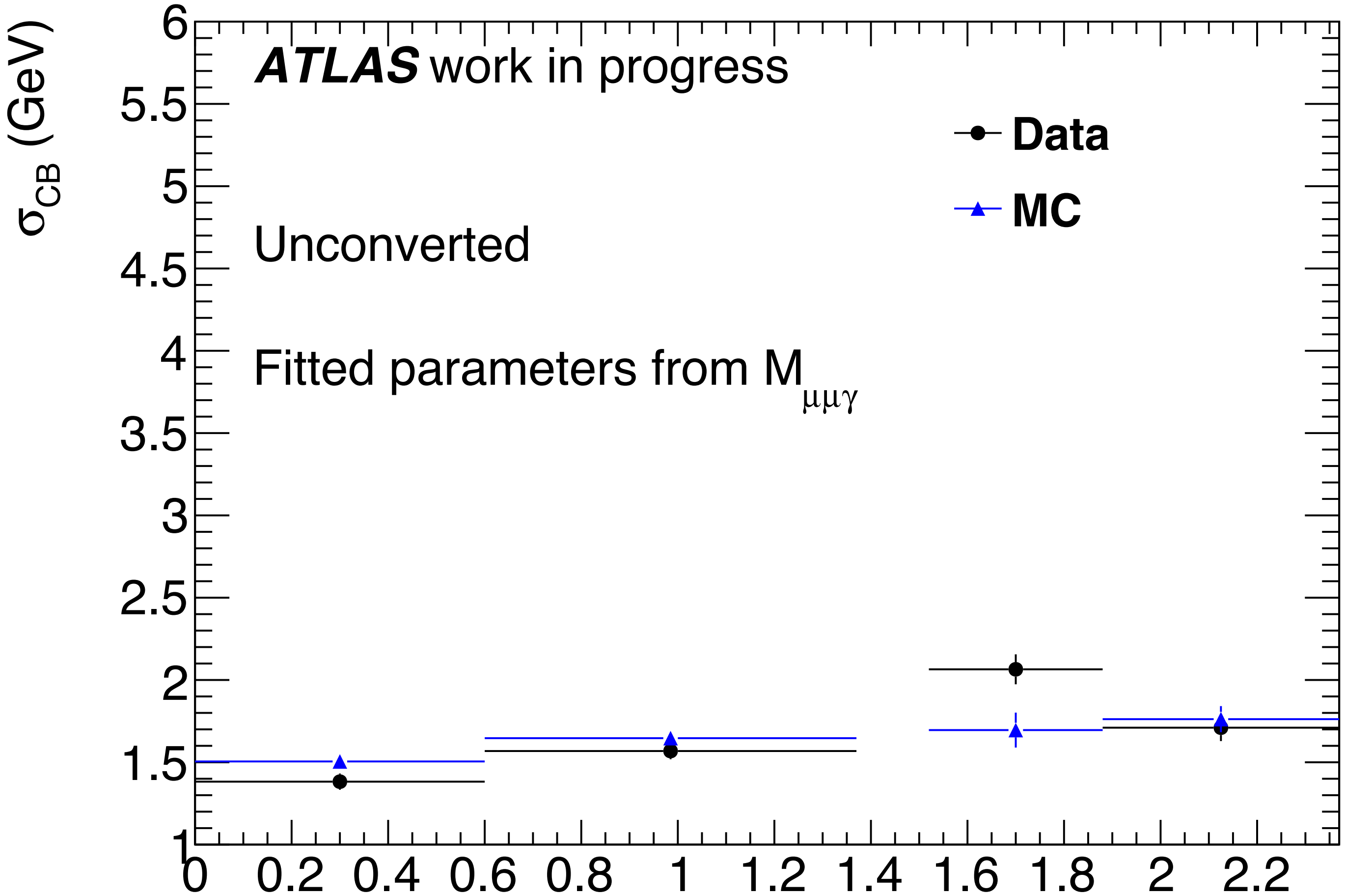
ATLAS work in progress
Data
MC
Unconverted
Fitted parameters from $M_{\mu\mu\gamma}$
σ_{CB} (GeV)

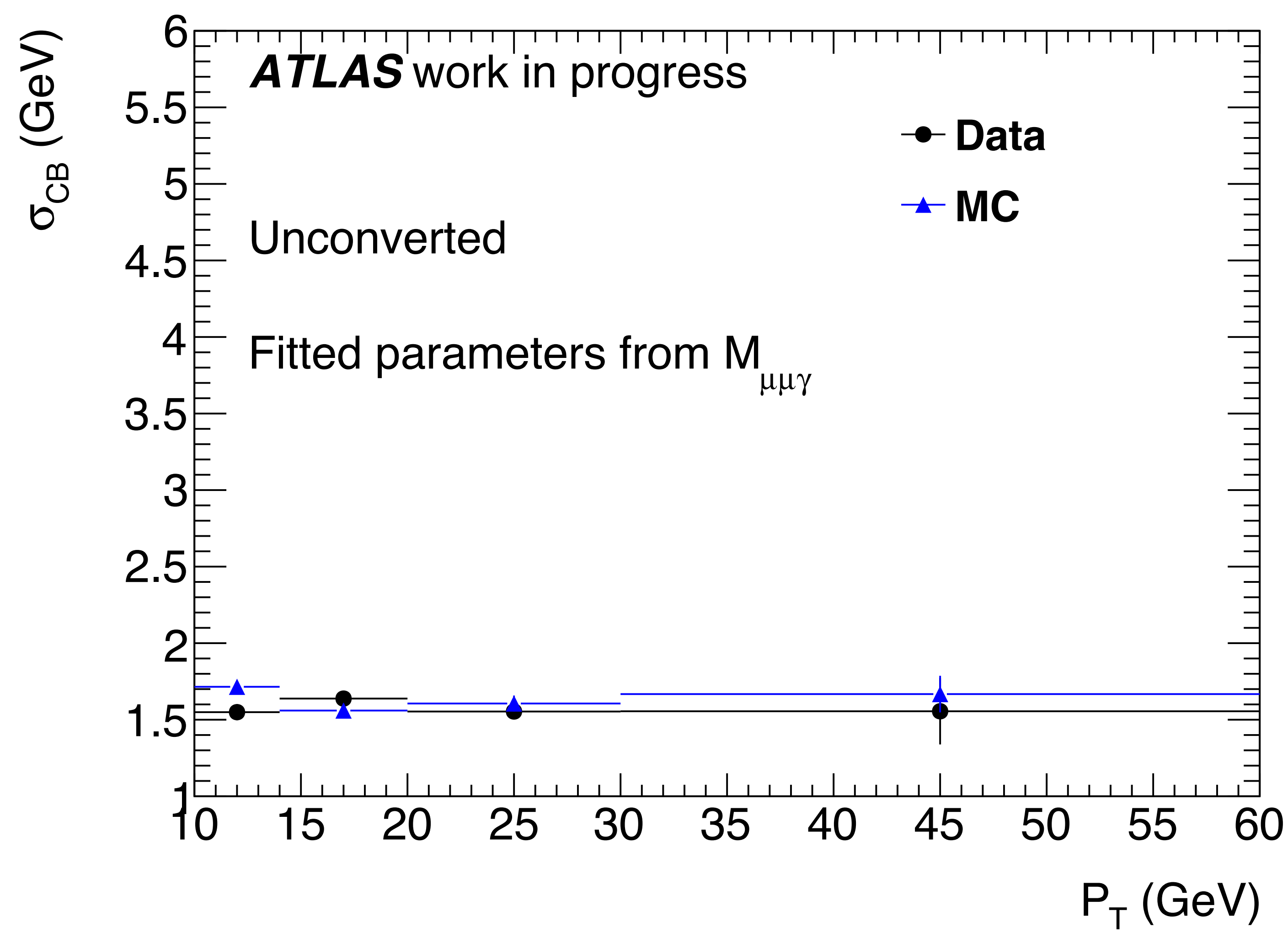
ATLAS work in progress
Data
MC
Unconverted
Fitted parameters from $M_{\mu\mu\gamma}$
σ_{CB} (GeV)
P_T (GeV)

Converted scales in eta:

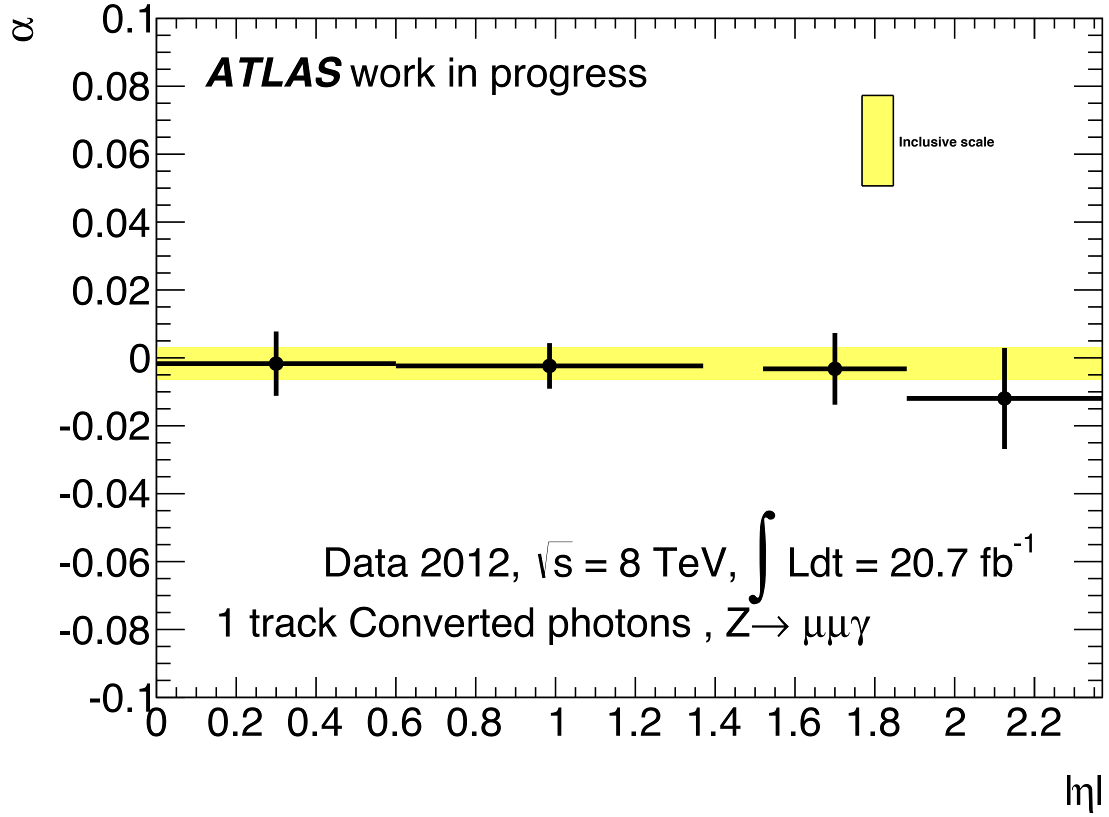

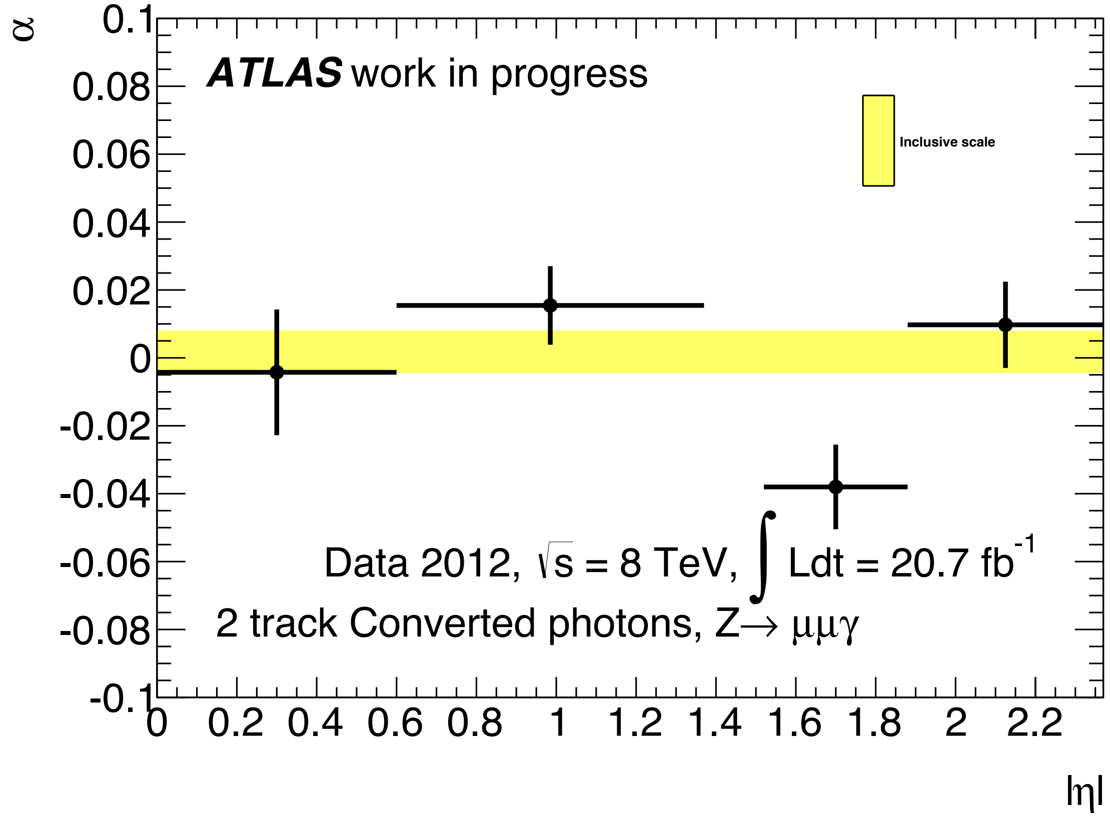

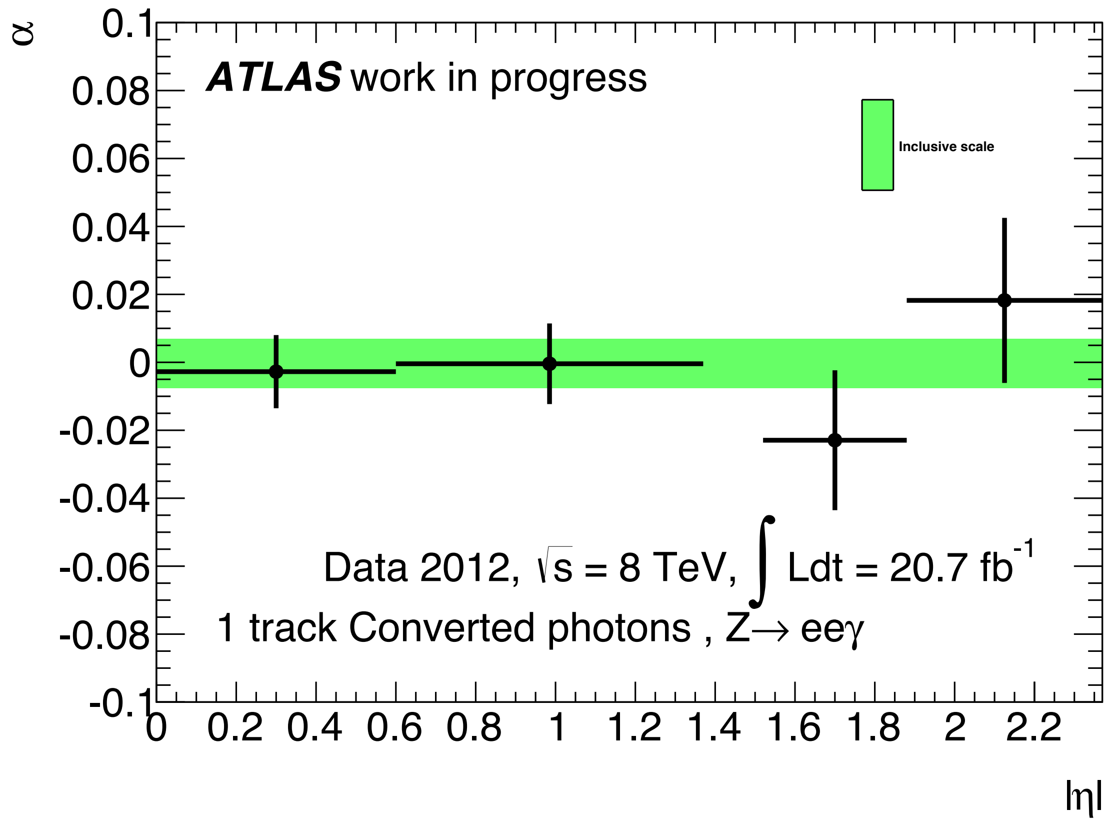

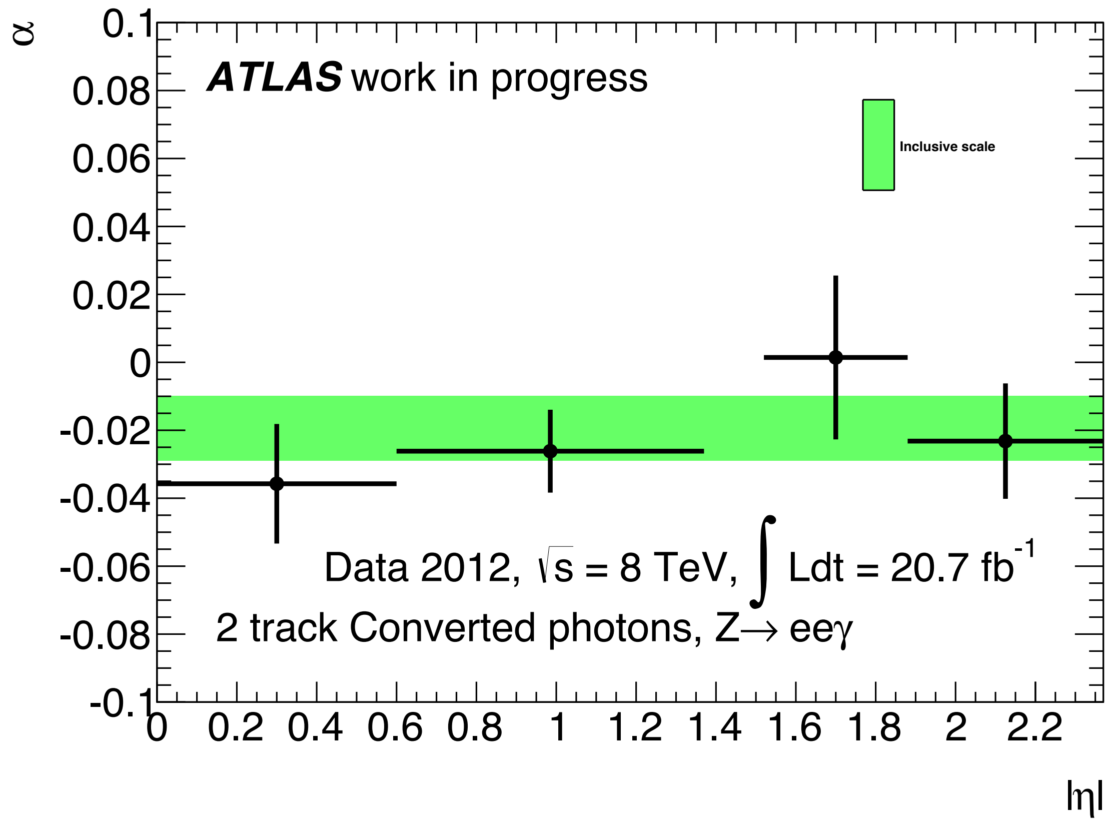

Converted scales in Pt:

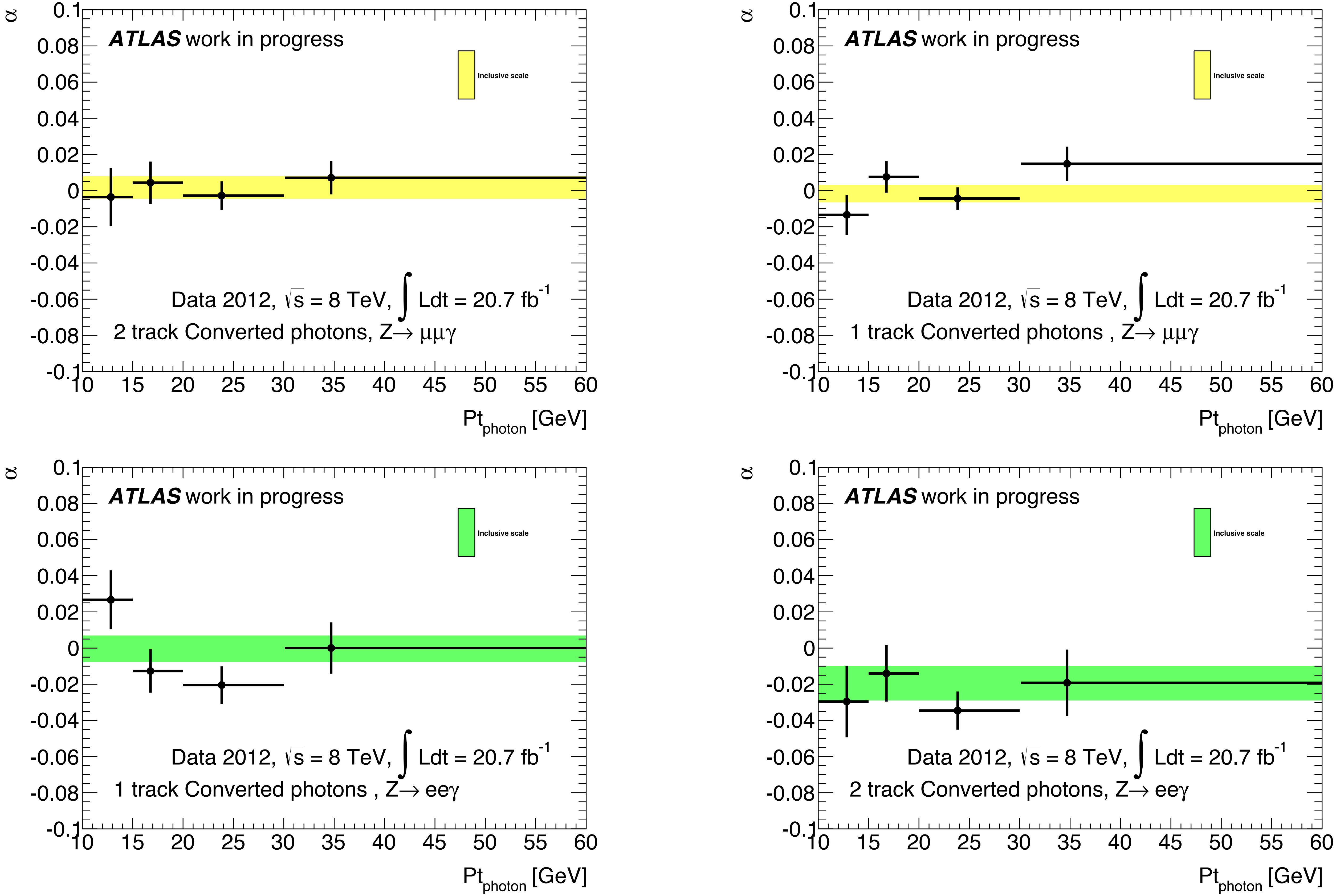

Photon scales with Z→μμγ in CMS

Sample based on the 2011 sample, photons with Et >25 GeV.

$$s = \frac{m^2_{\mu\mu\gamma} - m^2_{\mu\mu}}{m^2_{Z_0} - m^2_{\mu\mu}} - 1$$

Photon energy scale estimator, s.

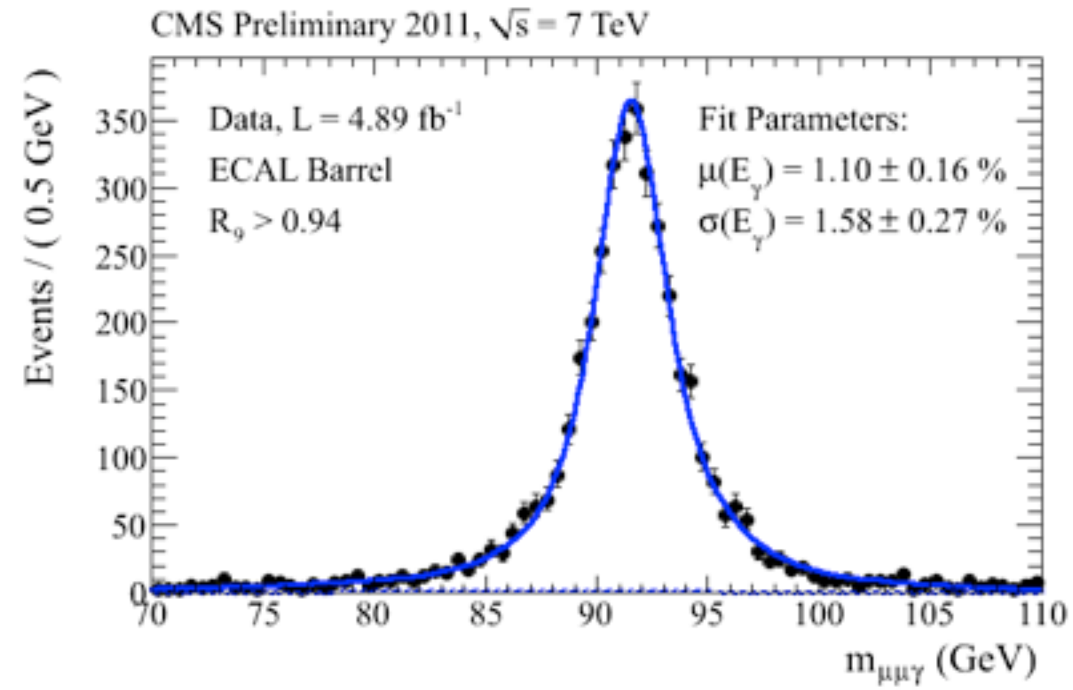

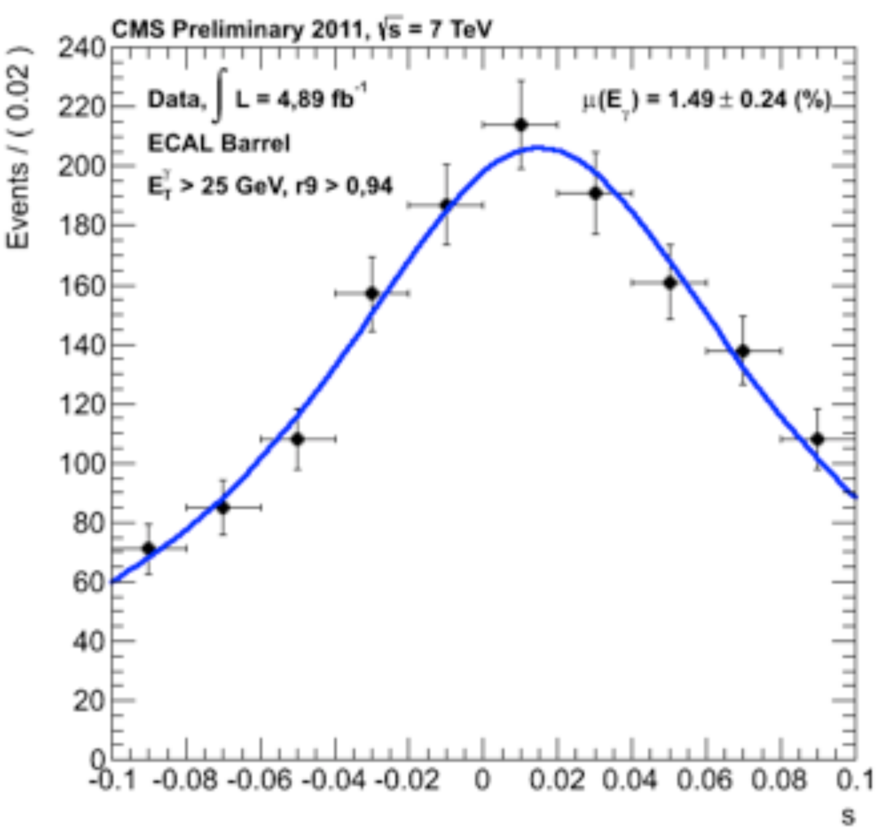

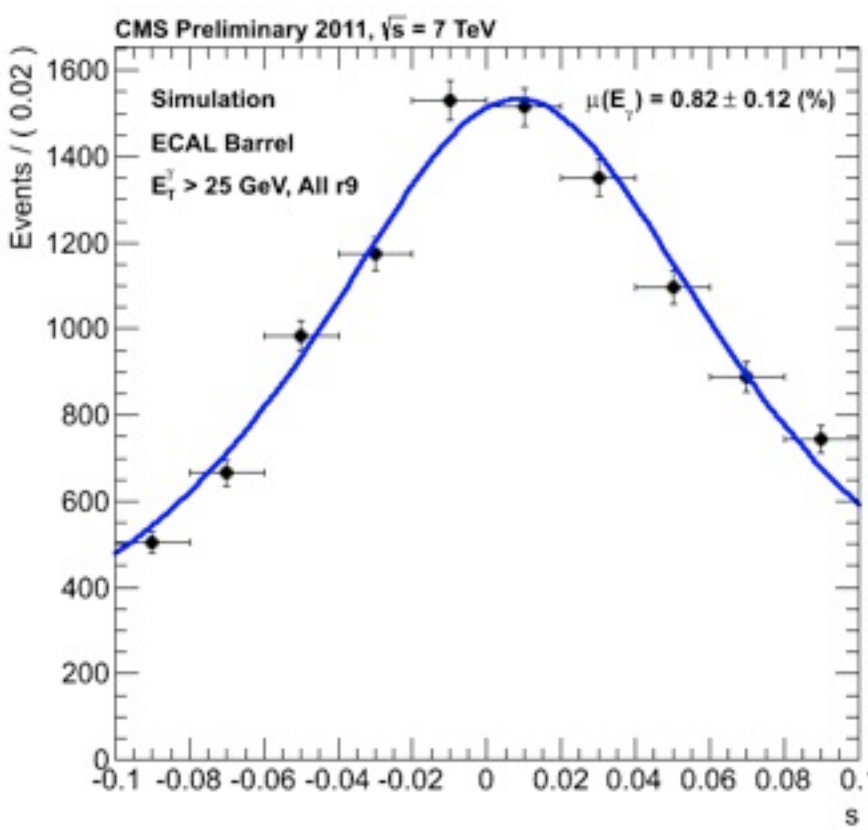

The photon energy scale agrees to within 0.5% with an independent method.

Reference :**CMS-DP-2012/024**

Systematics

Theory sys.

$\sqrt{s}$	Systematic uncertainty (%)										
	$\sigma(gg \to H)$		σ(VBF)		$\sigma(WH)$		$\sigma(ZH)$		$\sigma(t\bar{t}H)$		$B(H \to Z\gamma)$
	scale	PDF	scale	PDF	scale	PDF	scale	PDF	scale	PDF	
7 TeV	$^{+7.1}_{-7.8}$	$^{+7.6}_{-7.1}$	± 0.3	$^{+2.5}_{-2.1}$	$^{+0.2}_{-0.8}$	± 3.5	$^{+1.4}_{-1.6}$	± 3.5	$^{+3.3}_{-9.3}$	± 8.5	$^{+9.0}_{-8.8}$
8 TeV	$^{+7.3}_{-7.9}$	$^{+7.5}_{-6.9}$	± 0.2	$^{+2.6}_{-2.8}$	$^{+0.1}_{-0.6}$	± 3.4	$^{+1.5}_{-1.4}$	± 3.5	$^{+3.9}_{-9.3}$	± 7.8	$^{+9.0}_{-8.8}$

Systematic Uncertainty	$H \to Z(ee)\gamma(\%)$	$H \to Z(\mu\mu)\gamma(\%)$
Signal Yield		
Luminosity	3.6 (1.8)	3.6 (1.8)
Trigger efficiency	0.4 (0.2)	0.8 (0.7)
Acceptance of kinematic selection	4.0 (4.0)	4.0 (4.0)
γ identification efficiency	2.9 (2.9)	2.9 (2.9)
electron reconstruction and identification efficiency	2.7 (3.0)	
μ reconstruction and identification efficiency		0.6 (0.7)
e/γ energy scale	1.4 (0.3)	0.3 (0.2)
e/γ isolation	0.4 (0.3)	0.4 (0.2)
e/γ energy resolution	0.2 (0.2)	0.0 (0.0)
μ momentum scale		0.1 (0.1)
μ momentum resolution		0.0 (0.1)
Signal Δm resolution		
e/γ energy resolution	5.0 (5.0)	2.4 (2.4)
μ momentum resolution		0.0 (1.5)
Signal Δm peak position		
e/γ energy scale	0.2 (0.2) GeV	0.2 (0.2) GeV
μ momentum scale		negligible

Experimental sys.

H→Zγ first ATLAS result

At 125 GeV the expected and observed limits are 13.5 and 18.2 x SM, respectively. Statistical uncertainties are dominating: neglecting all systematic uncertainties, the observed (expected) 95% CL limit at 125 GeV is 17.4 (12.9) x SM.

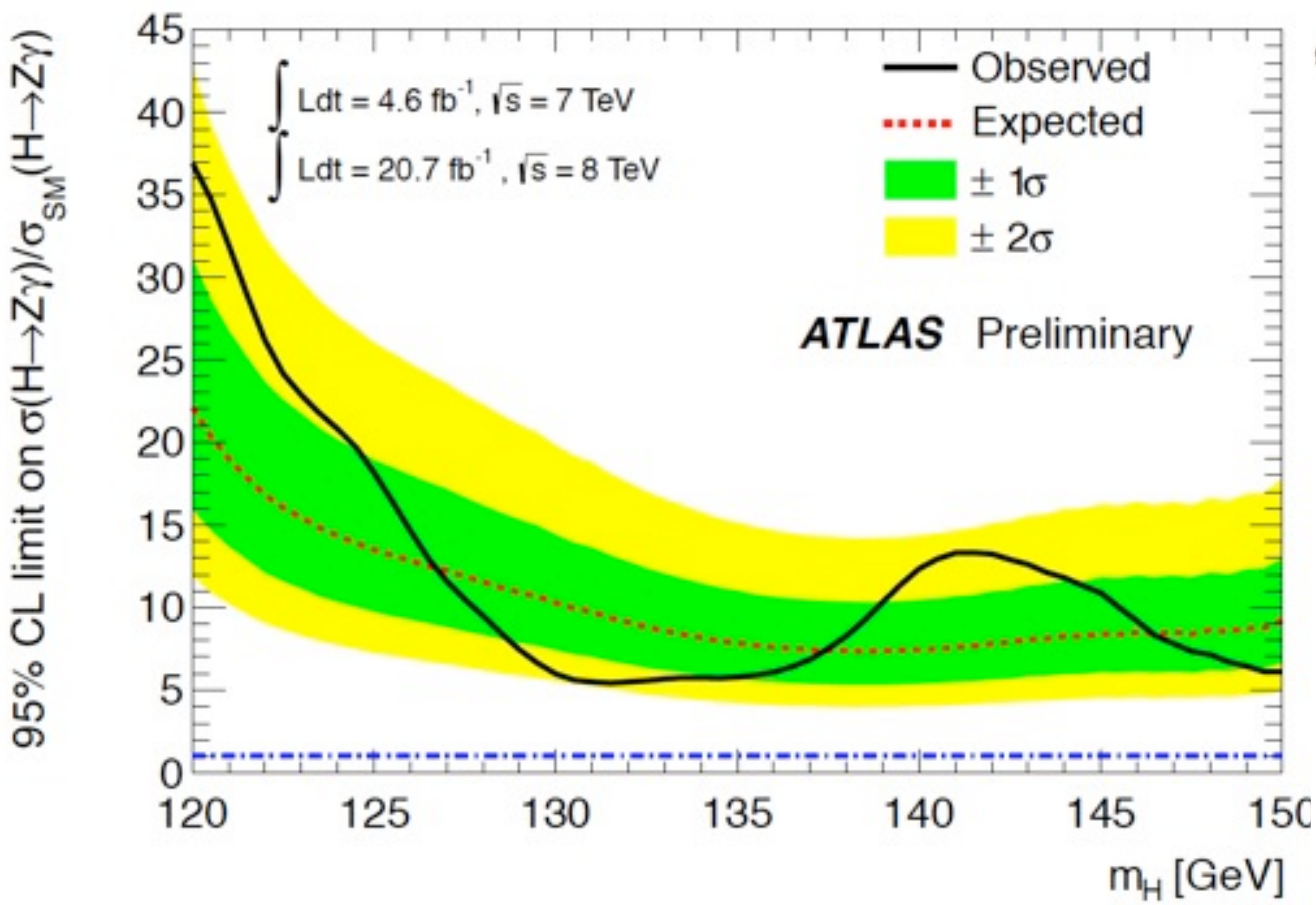

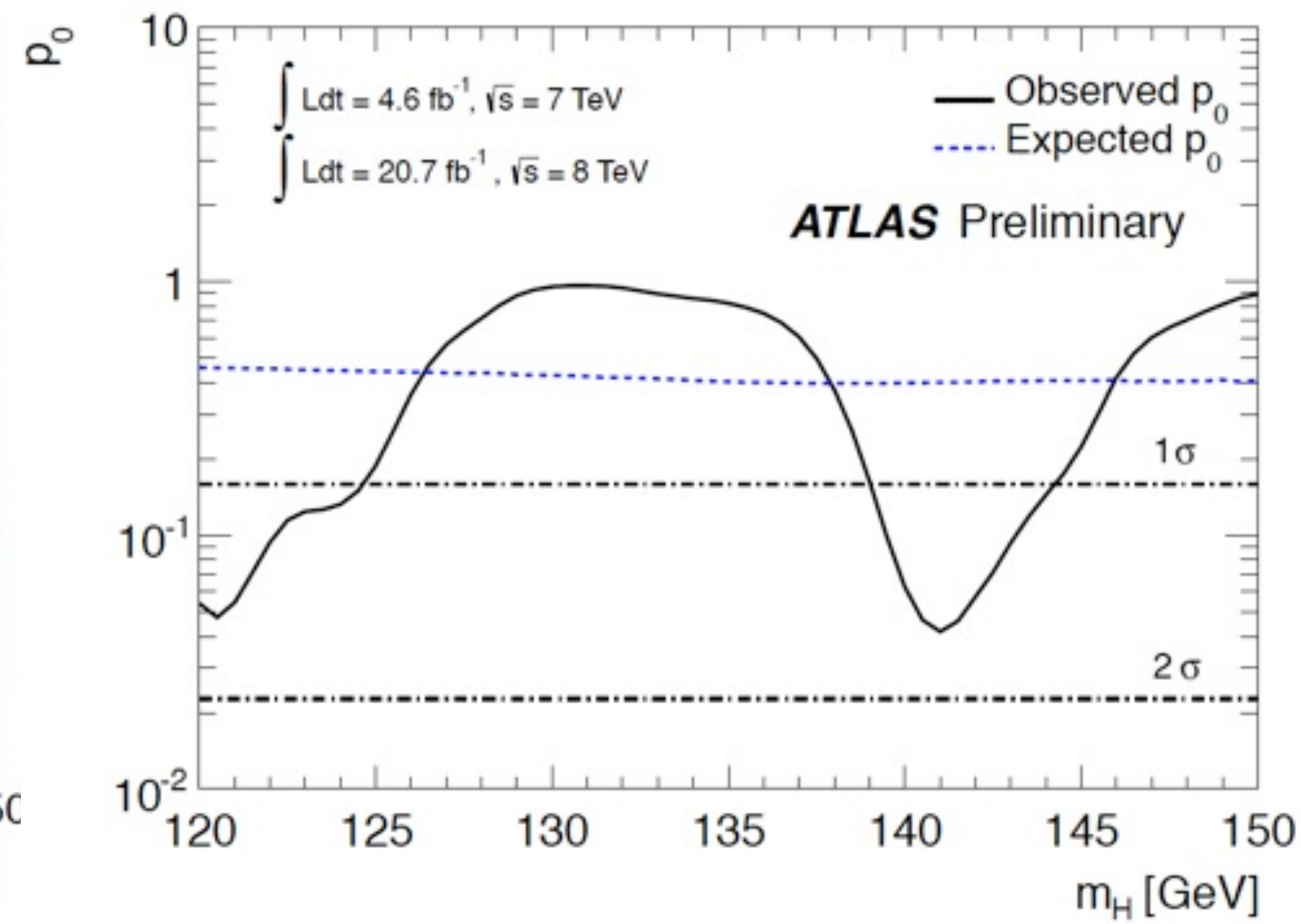

The expected p0 at mH = 125 GeV is 0.443, corresponding to a significance of 0.14 σ, while the observed one is 0.188 (0.89σ).

Table 2: Definition of the four untagged event classes and the dijet-tagged event class, the fraction of selected events for a signal with $m_{\mathrm{H}} = 125\,\mathrm{GeV}$ produced by gluon-gluon fusion at $\sqrt{s} = 8\,\mathrm{TeV}$, and data in a narrow bin centered at 125 GeV. The bin width is equal to two times the effective standard deviation (σ_{eff}). The expected full width at half maximum (FWHM) for the signal is also listed.

	$e^+e^-\gamma$	$\mu^+\mu^-\gamma$
	Event class 1	
	Photon $0 < \lvert\eta\rvert < 1.44$ Both leptons $0 < \lvert\eta\rvert < 1.44$ $R_9 > 0.94$	Photon $0 < \lvert\eta\rvert < 1.44$ Both leptons $0 < \lvert\eta\rvert < 2.1$ and one lepton $0 < \lvert\eta\rvert < 0.9$ $R_9 > 0.94$
Data	17%	20%
Signal	29%	33%
σ_{eff} (GeV)	1.9 GeV	1.6 GeV
FWHM (GeV)	4.5 GeV	3.7 GeV
	Event class 2	
	Photon $0 < \lvert\eta\rvert < 1.44$ Both leptons $0 < \lvert\eta\rvert < 1.44$ $R_9 < 0.94$	Photon $0 < \lvert\eta\rvert < 1.44$ Both leptons $0 < \lvert\eta\rvert < 2.1$ and one lepton $0 < \lvert\eta\rvert < 0.9$ $R_9 < 0.94$
Data	26%	31%
Signal	27%	30%
σ_{eff} (GeV)	2.1 GeV	1.9 GeV
FWHM (GeV)	5.0 GeV	4.6 GeV
	Event class 3	
	Photon $0 < \lvert\eta\rvert < 1.44$ At least one lepton $1.44 < \lvert\eta\rvert < 2.5$ No requirement on R_9	Photon $0 < \lvert\eta\rvert < 1.44$ Both leptons in $\lvert\eta\rvert > 0.9$ or one lepton in $2.1 < \lvert\eta\rvert < 2.4$ No requirement on R_9
Data	26%	20%
Signal	23%	18%
σ_{eff} (GeV)	3.1 GeV	2.1 GeV
FWHM (GeV)	7.3 GeV	5.0 GeV
	Event class 4	
	Photon $1.57 < \lvert\eta\rvert < 2.5$ Both leptons $0 < \lvert\eta\rvert < 2.5$ No requirement on R_9	Photon $1.57 < \lvert\eta\rvert < 2.5$ Both leptons $0 < \lvert\eta\rvert < 2.4$ No requirement on R_9
Data	31%	29%
Signal	19%	17%
σ_{eff} (GeV)	3.3 GeV	3.2 GeV
FWHM (GeV)	7.8 GeV	7.5 GeV
	VBF class	
	Photon $0 < \lvert\eta\rvert < 2.5$ Both leptons $0 < \lvert\eta\rvert < 2.5$ No requirement on R_9	Photon $0 < \lvert\eta\rvert < 2.5$ Both leptons $0 < \lvert\eta\rvert < 2.4$ No requirement on R_9
Data	0.1%	0.2%
Signal	1.8%	1.7%
σ_{eff} (GeV)	2.6 GeV	2.2 GeV
FWHM (GeV)	4.4 GeV	3.8 GeV

CMS Results

✓ Expecting about 16 events in 7 TeV + 8 TeV at 125 GeV.

Table 1: Observed and expected event yields for a 125 GeV SM Higgs boson.

Sample	Integrated luminosity (fb^{-1})	Observed event yield for $100 < m_{\ell\ell\gamma} < 190$ GeV	Expected number of signal events for $m_H = 125$ GeV
2011 ee	5.0	2353	1.2
2011 $\mu\mu$	5.1	2848	1.4
2012 ee	19.6	12899	6.3
2012 $\mu\mu$	19.6	13860	7.0

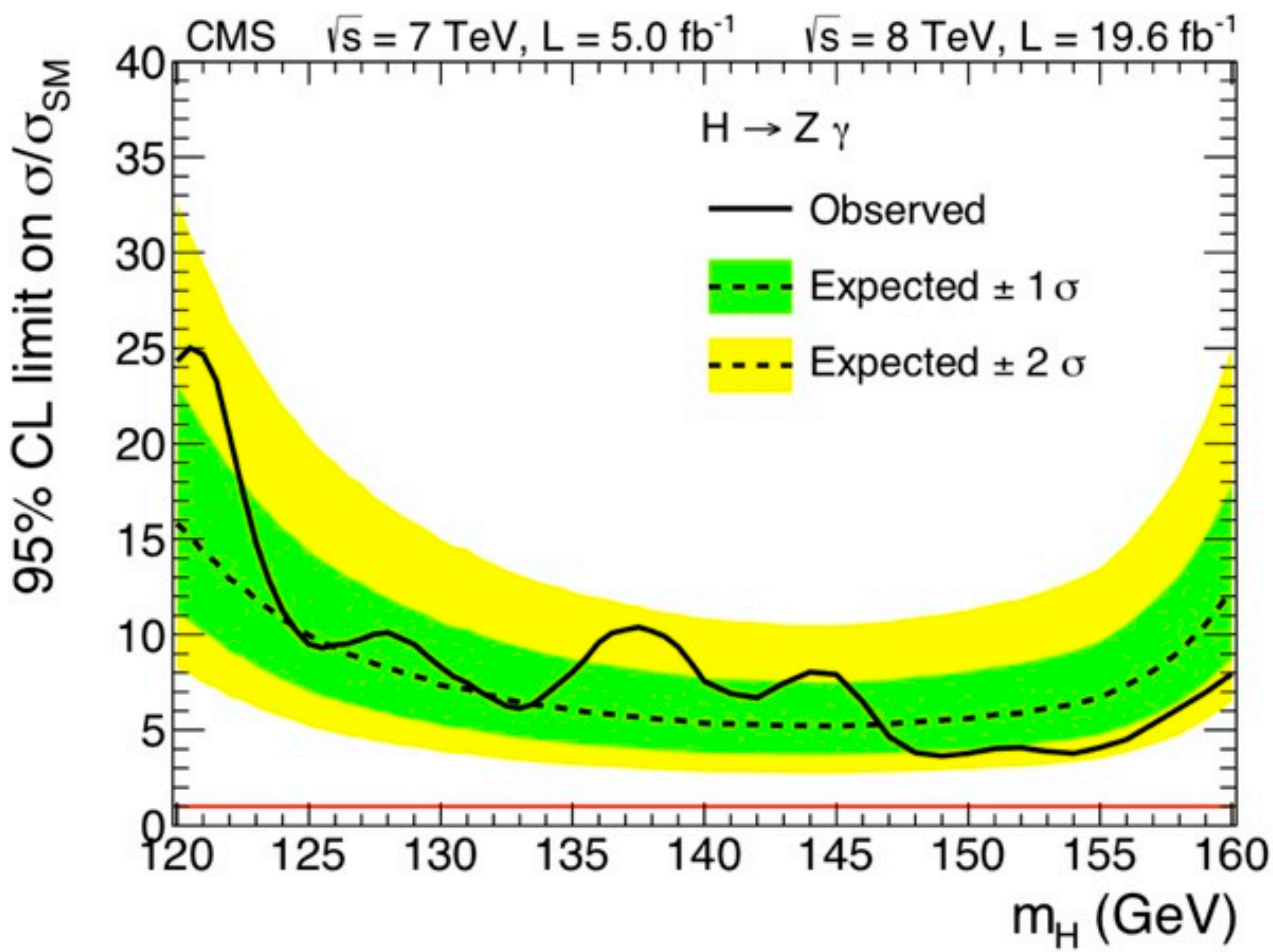

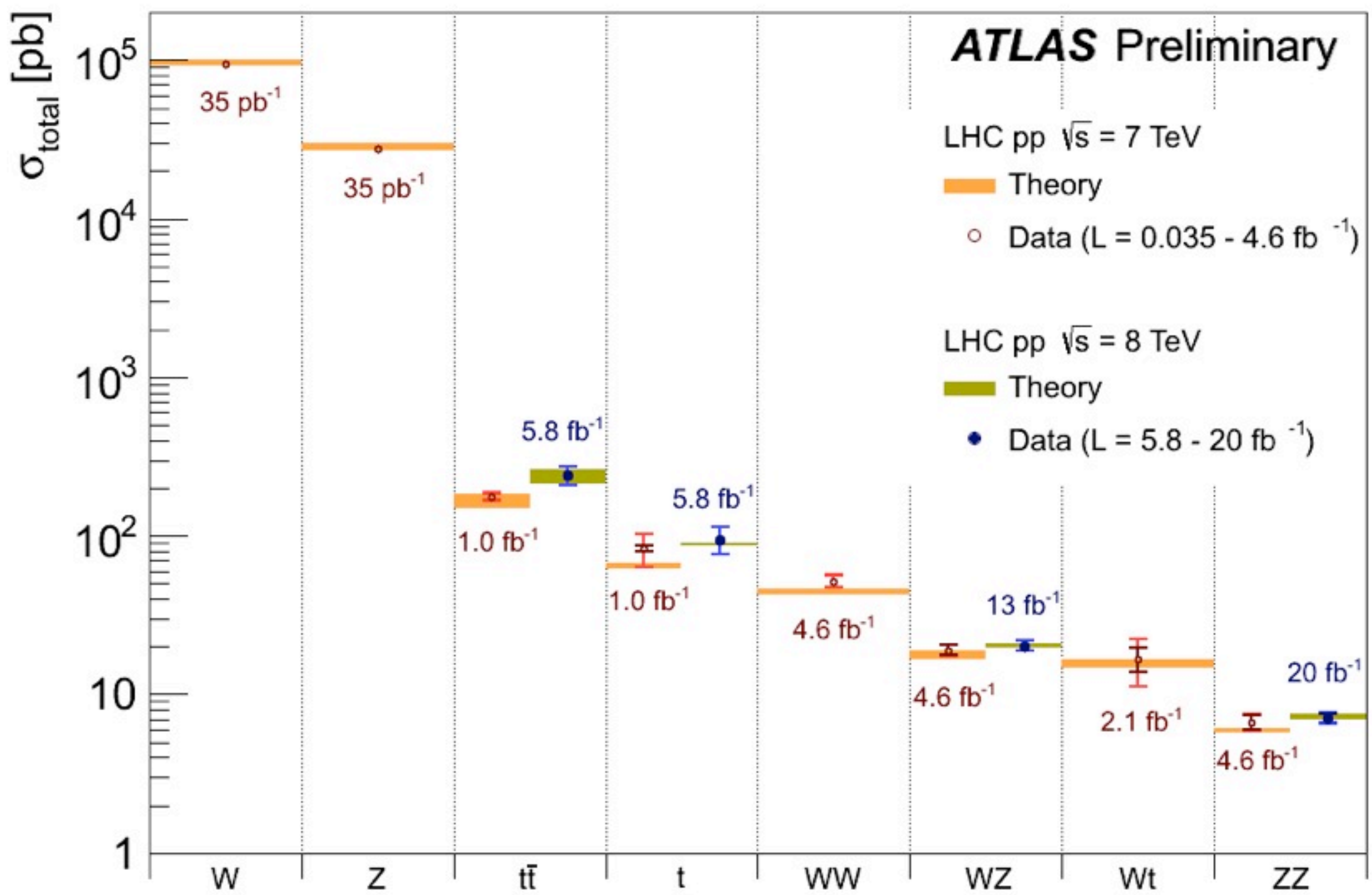

ATLAS Preliminary
σ_{total} [pb]
10^5
10^4
10^3
10^2
10
1
LHC pp $\sqrt{s}$ = 7 TeV
Theory
Data (L = 0.035 - 4.6 fb $^{-1}$)
LHC pp $\sqrt{s}$ = 8 TeV
Theory
Data (L = 5.8 - 20 fb $^{-1}$)
35 pb^{-1}
35 pb^{-1}
5.8 fb^{-1}
1.0 fb^{-1}
5.8 fb^{-1}
1.0 fb^{-1}
4.6 fb^{-1}
13 fb^{-1}
4.6 fb^{-1}
2.1 fb^{-1}
20 fb^{-1}
4.6 fb^{-1}
W
Z
$t\bar{t}$
t
WW
WZ
Wt
ZZ

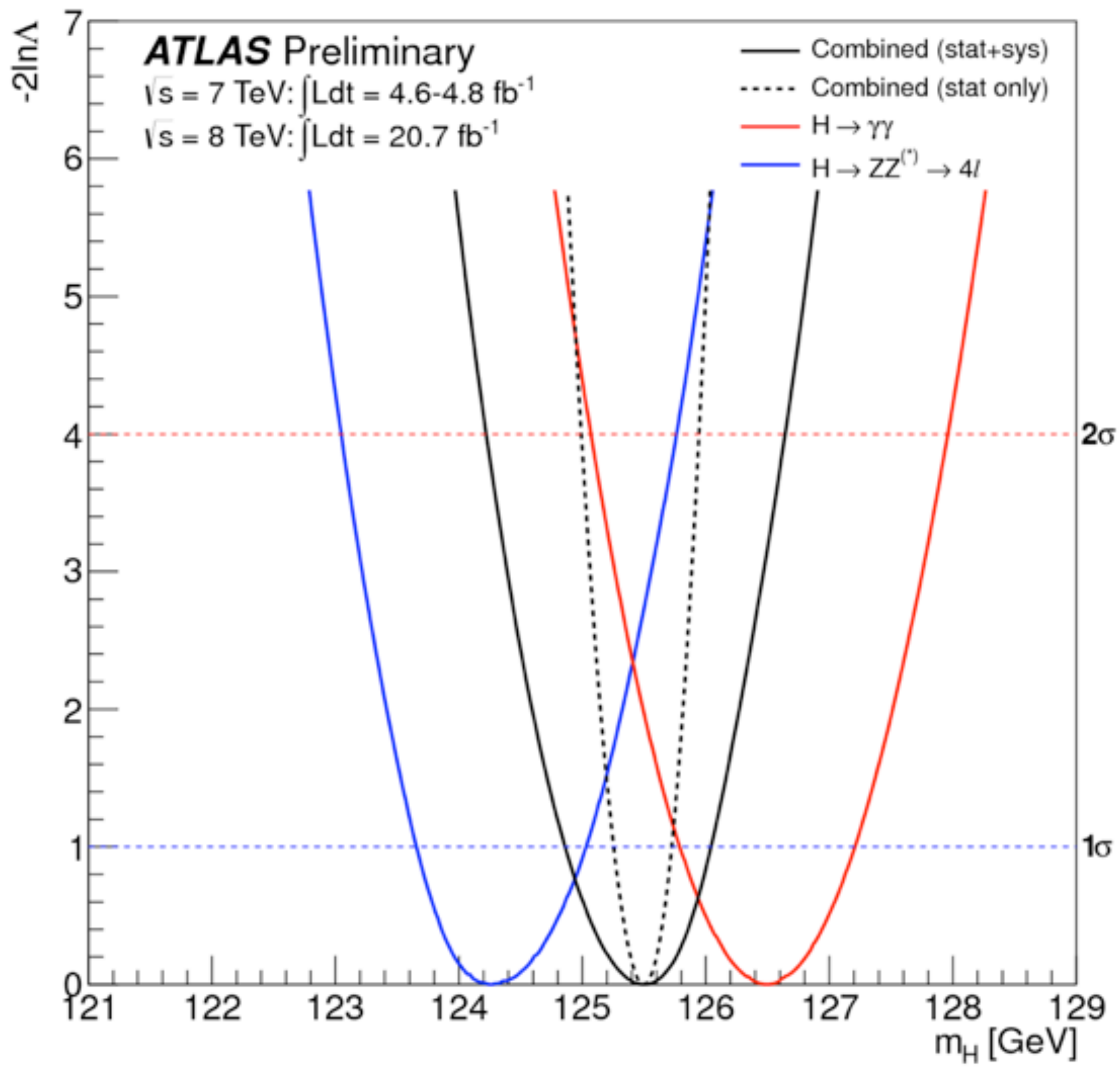

A mass of m_H = 126.8 ± 0.2(stat) ± 0.7(sys) GeV is found in the $H \rightarrow \gamma\gamma$ channel and a mass of m_H = 124.3 +0.6 -0.5 (stat) +0.5 -0.6 (sys) GeV in the $H \rightarrow ZZ^{(*)} \rightarrow$ 4l channel.

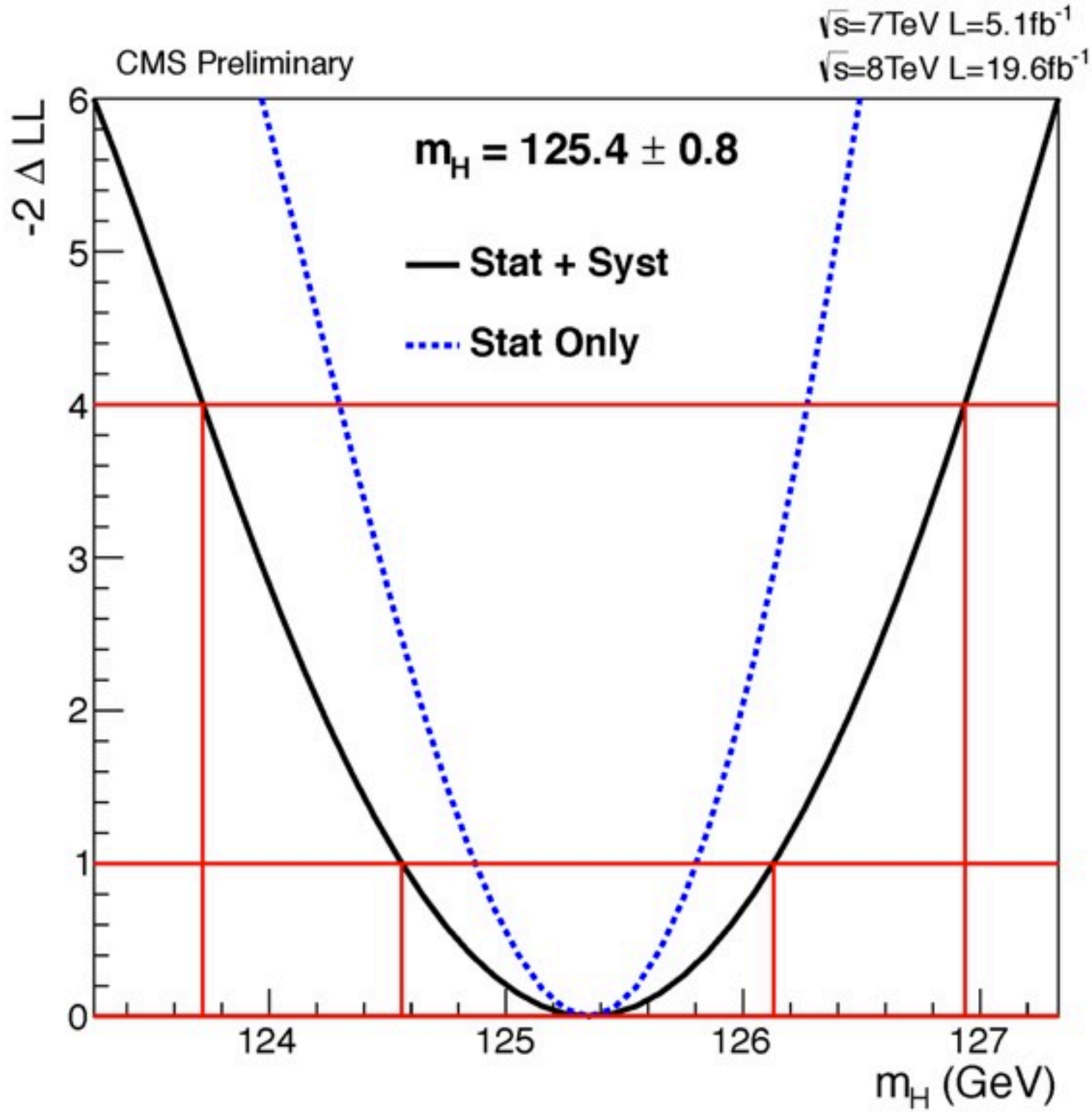

H to gamma=

125.4±0.5(*stat*.)±0.6(*syst*.)

H to ZZ to 4l=

125.8±0.5 (stat.) ±0.2(syst.)~GeV.